Kroenke, L. W., Berger, W. H., Janecek, T. R., et al., 1991
Proceedings of the Ocean Drilling Program, Initial Reports, Vol. 130

9. SITE 807[1]

Shipboard Scientific Party[2]

HOLE 807A

Date occupied: 26 February 1990

Date departed: 2 March 1990

Time on hole: 4 days, 4 hr, 52 min

Position: 3°36.42′N, 156°37.49′E

Bottom felt (rig floor; m, drill-pipe measurement): 2815.1

Distance between rig floor and sea level (m): 11.32

Water depth (drill-pipe measurement from sea level, m): 2803.8

Total depth (rig floor; m): 3638.00

Penetration (m): 822.90

Number of cores (including cores with no recovery): 86

Total length of cored section (m): 822.90 (APC, 254.4; XCB, 568.5)

Total core recovered (m): 716.74 (APC, 263.11; XCB, 453.63)

Core recovery (%): 87.1 (APC, 103.4; XCB, 79.8)

Oldest sediment cored:
Depth (mbsf): 822.90
Nature: nannofossil ooze with foraminifers
Youngest age: Quaternary
Oldest age: early Oligocene
Measured velocity (km/s): 1.9

HOLE 807B

Date occupied: 2 March 1990

Date departed: 4 March 1990

Time on hole: 1 day, 4 hr, 30 min

Position: 3°36.39′N, 156°37.49′E

Bottom felt (rig floor; m, drill-pipe measurement): 2817.4

Distance between rig floor and sea level (m): 11.32

Water depth (drill-pipe measurement from sea level, m): 2806.1

Total depth (rig floor; m): 3096.00

Penetration (m): 278.60

Number of cores (including cores with no recovery): 30

Total length of cored section (m): 278.60

Total core recovered (m): 280.18

Core recovery (%): 100.6

Oldest sediment cored:
Depth (mbsf): 278.60
Nature: nannofossil ooze with foraminifers
Youngest age: Quaternary
Oldest age: late Miocene
Measured velocity (km/s): 1.6

HOLE 807C

Date occupied: 4 March 1990

Date departed: 23 March 1990

Time on hole: 18 days, 22 hr

Position: 3°36.39′N, 156°37.48′E

Bottom felt (rig floor; m, drill-pipe measurement): 2817.0

Distance between rig floor and sea level (m): 11.32

Water depth (drill-pipe measurement from sea level, m): 2805.7

Total depth (rig floor; m): 4345.40

Penetration (m): 1528.40

Number of cores (including cores with no recovery): 93

Total length of cored section (m): 748.40

Total core recovered (m): 252.84

Core recovery (%): 33.8

Oldest sediment cored:
Depth (mbsf): 1379.70
Nature: limestone, claystone, radiolarian siltstone, and minor chert
Youngest age: lower Oligocene
Oldest age: Aptian-Albian
Measured velocity (km/s): 2.0

Basement:
Depth (mbsf): 1379.7
Nature: basalt
Measured velocity (km/s): 5.0

Principal results: Site 807 (proposed Site OJP-5A) is located on the northern rim of the Ontong Java Plateau (latitude 3°36.4′N, longitude 156←37.5′E) in 2805 m of water, roughly 475 km northwest of Deep Sea Drilling Project (DSDP) Sites 289/586. Site 807 was occupied with three major objectives: (1) to provide Paleogene and Cretaceous sediments for studies of pre-Neogene paleoceanography; (2) to obtain basement rock for studies of the origin of the Ontong Java Plateau; and (3) to provide a second shallow-water site, off the equator, for comparison with Sites 803 and 806 on the Neogene equatorial depth transect.

The site is located on a single-channel seismic (SCS) line acquired by the *Thomas Washington* during the EURYDICE Cruise 9 survey at 0255 UTC, 11 April 1975. The site was resurveyed on 26 January 1990 from 1117 to 1737 UTC and crossed again on 26 February during the approach to the site and before dropping the beacon. The beacon was dropped at 1608 UTC, 26 February 1990, in a location believed to be protected from bottom-current activity (i.e., within a shallow basement graben about 0.5 km from the footwall of the northern side of the graben).

Three holes were drilled at Site 807 between 1608 UTC, 26 February 1990, and 1800 UTC, 23 March 1990. Hole 807A was cored with the advanced hydraulic piston corer (APC) and the extended core barrel (XCB) to 822.9 mbsf with 87.1% recovery (103.4% in the section cored with the APC [0–254.4 mbsf], and 79.8% in the section cored with the XCB [254.4–822.9 mbsf]). The hole was successfully logged and a good suite of geophysical measurements was obtained. Hole 807B was cored with the APC to 278.6 mbsf, at which point 120,000-lb. of overpull was encountered on Core 130-807B-30H, forcing abandonment of the hole. Average recovery was 100.6%.

[1] Kroenke, L. W., Berger, W. H., Janecek, T. R., et al., 1991. *Proc. ODP, Init. Repts.,* 130: College Station, TX (Ocean Drilling Program).
[2] Shipboard Scientific Party is as given in the list of participants preceding the contents.

A reentry cone with about 58 m of 16.5-in. casing was set at Hole 807C and, after running in and cementing about 350 m of 11.75-in. casing, the hole was washed to 780.0 mbsf. Coring with the rotary core barrel (RCB) then began. Hole 807C was cored with the RCB to 1528.4 mbsf with 33.8% recovery. Hole 807C was also successfully logged to the total depth drilled, and a complete set of geophysical measurements, including formation microscanner (FMS) data, was obtained. Preliminary analyses of the shipboard data indicate that a complete, undisturbed record of the last 10 m.y. was recovered in the uppermost 280 m of sediment obtained from the two holes cored with the APC.

The Neogene section is around 591 m thick, and recovery in the Neogene and upper Oligocene sediments cored with the APC and the XCB (APC, 100.6% and 103.4%; XCB, 79.8%) was excellent. The Paleogene section is around 602 m thick, but recovery was significantly decreased in the lower Oligocene–Paleocene sediments cored with the RCB (averaging 26.8%). Recovery averaged 46.6% over the 186.5-m-thick Cretaceous section. Basalt was encountered at 1379.7 mbsf in Core 130-807C-74R. Total penetration into basement was 149.7 m, and 87.6 m of basalt (60% recovery) and 0.6 m of interbedded sediment were recovered.

The sedimentary sequence at Site 807 consists of three lithologic units, as follows:

Unit I (0–968.0 mbsf) is composed mainly of Pleistocene to upper/middle Eocene nannofossil ooze and chalk with foraminifers, with lesser amounts of foraminifer nannofossil ooze and chalk as well as nannofossil ooze and chalk. Unit I is divided into Subunits IA and IB, based on the depth of the ooze-chalk transition. The boundary between the two subunits is placed at 293 mbsf, which corresponds to an age of middle/late Miocene (ca. 10.4 Ma).

Unit II (968.0–1351.4 mbsf) is composed of upper/middle Eocene to upper Campanian limestone, chert, nannofossil chalk, and nannofossil chalk with foraminifers. Unit II is divided into Subunits IIA and IIB, based on the transition from chalk to limestone. The boundary between the two subunits is placed at 1098.0 mbsf, where a limestone lithology is indicated by the presence of over 50% nonbiogenic carbonate in smear slides. The transition is also reflected in the substantial increase in average core recovery, from about 7% in Subunit IIA to about 44% in Subunit IIB.

Unit III (1351.4–1379.7 mbsf) is composed of lower Cenomanian to upper Albian–Aptian claystone, siltstone with varying amounts of radiolarians, and limestone. Unit III is divided into Subunits IIIA and IIIB at the claystone/limestone boundary.

Unit IV (1379.7–1528.4 mbsf), comprising igneous basement at Site 807, is composed of Albian-Aptian basalt and interbedded limestone. Unit IV is further divided into seven subunits (IVA through IVG), five of which are igneous (IVA, IVC, IVE, IVF, and IVG), and two of which are sedimentary (IVB and IVD). All of the igneous subunits are composed of sightly altered tholeiitic basalts.

Subunit IVA (1379.7–1424.6 mbsf) consists of aphyric pillow lavas and thin (<2 m thick), massive flows with rare plagioclase phenocrysts up to 3 mm long, superficially similar to lavas at Site 803. Subunits IVC (1425.1–1441.9 mbsf), IVE (1442.0–1447.0 mbsf), IVF (1447.0–1475.0 mbsf), and IVG (1475.0–1528.4 mbsf) are also aphyric, but they contain sparse, euhedral to subhedral, olivine microphenocrysts (<1 mm long) as well, largely replaced by green and black clays. Like Subunit IVA, Subunits IVC, IVE, and IVG are successions of pillow lavas and thin (<3 m thick) massive flows. Subunit IVF, however, consists of a single massive flow, approximately 28 m thick. This flow documents the presence of thick flood basalt lavas on the Ontong Java Plateau.

The sedimentary interbeds, Subunits IVB (1424.6–1425.1 mbsf) and IVD (1441.9–1442.0 mbsf), are Albian-Aptian limestone interbedded with vitric tuff, and limestone containing quartz and illite/glauconite, respectively. Another sedimentary interbed, detected during logging at 1434 mbsf but unsampled in the coring, is located within Subunit IVC. Flecks of native copper were observed in several of the basalt cores below the sedimentary interbeds of Subunit IVB, particularly in vein material in Section 130-807C-82R-2 at 40 and 58 cm. Disseminated pyrite also was observed in glassy pillow rims and fractures.

The Albian-Aptian age of the sediments overlying the basalt suggests that the volcanic sequence will be useful in refining the Pacific Plate apparent polar-wander path. Three factors make the study of Unit IV basalts especially promising: (1) the presence of three sedimentary interbeds (which suggests that the sequence represents sufficient time to average a significant amount of secular variation in the paleofield direction); (2) the remarkably fresh state of many of the rocks; and (3) the occurrence of thick flows interbedded with pillows (which should permit recognition of tilting within the pillow basalts). The inclinations of natural remanent magnetizations (NRMs) of the basalts are dominantly steeper than 20°. If the NRM is dominated by a primary remanence, as suggested in accordance with the freshness of the rocks, the entire basalt sequence is of normal polarity.

Above the basalt and basal limestones, the overall interbedded pattern of the upper Albian to lower Cenomanian claystone/siltstone sequence may indicate the importance of periodic mass transport or cyclical deposition at Site 807. Much of the lower part of the Upper Cretaceous could be missing. The upper Campanian–Maestrichtian limestone apparently contains a signal of changing dissolution levels in the Cretaceous ocean, with good preservation of foraminifers observed in the Maestrichtian in places. The section is barren of radiolarians. Sedimentation rates decreased from 10 to 20 m/m.y. in the late Maestrichtian to less than 5 m/m.y. in the early Paleocene. The Cretaceous/Tertiary (K/T) boundary is located in Core 130-807C-54R. The sequence recovered is thought to be complete, with volcanic ash marking the transition.

Much of the Paleocene–middle Eocene is condensed, with the exception of part of the upper Paleocene (NP9) where sedimentation rates reach 30 m/m.y. Preservation of fossils below the upper Eocene generally is poor. The section is barren of diatoms, but radiolarians occur sporadically in the middle Eocene. After an initial low of 1 m/m.y. in the early middle Eocene (ca. 54–51 Ma), sedimentation rates increased again, peaking near 30 m/m.y. in the late middle Eocene (ca. 45–43 Ma). Hiatuses are present in the Paleogene section: two in the middle Eocene and one in the middle of the Oligocene. The latter hiatus immediately follows a jump in sedimentation rate to over 35 m/m.y. (ca. 30–32 Ma).

The Neogene section appears complete, albeit somewhat thinned in the upper part of the lower Miocene. Sedimentation rates range from near 30 m/m.y. across the Oligocene/Miocene boundary (ca. 28–22 Ma), to 15–20 m/m.y. in the early to early late Miocene (ca. 22–8 Ma), to more than 40 m/m.y. in the late Miocene (ca. 8–5 Ma), before dropping to about 15 m/m.y. in the Pleistocene. The overall sedimentation rate pattern for the Neogene is quite similar to those of Sites 805 and 806, with Site 807 having intermediate values. Surprisingly, the equatorial crossing of Site 807 (ca. 10–12 Ma) does not seem to affect the sedimentation rate greatly.

Hole 807C logging data, in conjunction with a detailed suite of physical properties measurements obtained from the split cores, confirm the depths of the ooze-chalk and chalk-limestone transitions based upon sediment descriptions and reveal the presence of local maxima and minima in velocity that correlate with chert or silicified chalk horizons and with the claystone/siltstone beds deep in the section. The logs allow an estimate of the amount of chert present in the section, which is thought to vary between 20% and 70% at any one interval, the higher values signifying the presence of massive cherts or beds of highly silicified limestone. The logs from different holes at Site 807 correlate well over intervals of 15 cm or less, instilling confidence in the interpretation of high-frequency events at Milankovitch time scales.

Gamma-ray logs and the FMS data confirm the presence of a single, massive flow in Subunit IVF and help identify the presence of sedimentary interbeds in the overlying pillowed-flow subunits, including one unsampled by the coring operation. Resistivity logs, moreover, indicate that another massive flow might be present at the bottom of the hole. The logs provide important constraints on the generation of synthetic seismograms. Duplication of logging runs in the paired Holes 807A and 807C allows assessment of the precision of the logging data.

A reasonably complete seismic stratigraphy is present at Site 807. Evidence for small-scale mass movement was observed at 0.14–0.24 s below seafloor (sbsf) and at 0.28–0.41 sbsf (4.7–6.7

and 7.5–12.5 Ma, respectively). Thickened wedges of sediment occur between 0.44 and 0.53 sbsf (14.5–20.5 Ma) and around 1.00–1.02 sbsf (about 50.4 Ma). Basement occurs at approximately 1.13 sbsf (1379.7 mbsf).

Magnetic susceptibility was measurable well into Pliocene sediments. These data will be useful for fine-scale correlation and for studies of Milankovitch-type cycles.

Results from interstitial water geochemistry at Site 807 are similar to the data obtained from Sites 803 and 804. The conservative gradients (Ca and Mg) compare favorably with those of Sites 288 and 289, suggesting similar basalt-alteration diffusion rates. These and other gradients reflect the dominance of biogenic sediments and the paucity of organic carbon. Calcium and magnesium depth gradients are the least pronounced at Site 807, however, and the magnesium profile at Site 807 is anomalous with the other Ontong Java sites in the lower part of the section where magnesium concentrations remain constant with increasing depth. Dissolved silica concentrations generally increase with depth down to 900 mbsf (ca. 36 Ma) and then decrease and level off at 1000 mbsf (ca. 42 Ma) in the silicified sediments of Unit II.

BACKGROUND AND OBJECTIVES

Overview

Site 807 (proposed Site OJP-5A) was the last of the Leg 130 sites to be drilled on the Ontong Java Plateau. It was scheduled as the primary site for deep penetration into basement. The site is located on the northern rim of the high plateau, in water shallow enough to ensure a high sedimentation rate, yet far enough away from Sites 288 and 289 to avoid the local hiatuses in the sedimentary sections at those sites. It was selected in a region of fairly smooth basement and sedimentary topography, away from such complicating features as seamounts, structural complexities, and canyons so as to maximize the chances of recovering little-disturbed sediment and basement sections. Also, the site was placed as far off the postulated isochron passing through Site 289 as possible to allow evaluation of the proposed north-south age progression across the Ontong Java Plateau. The goal was to drill a thick, well-preserved Cenozoic and Mesozoic sedimentary section before penetrating as deeply into basement as time allowed.

The maximum sedimentary thickness on the Ontong Java Plateau, which is more than 1200 m, occurs below the crest of the plateau in water depths greater than 2200 m. Site 807 was located on the northern rim of the high plateau to retain a thick sedimentary section yet avoid the problems of current-winnowing and bottom transport encountered at other drilling sites on the plateau, as well as the type of slope instability observed on the flanks of the plateau. Despite its shallow depth, the apparent thinning in the upper part of the section observed in the SCS reflection profile leading up to the site, as well as the apparent thickening observed in the lower part of the section, led us to expect the presence of a slightly thinner Neogene section and a slightly thicker Paleogene-Cretaceous section. The site was positioned in a shallow basement graben in the hope that the sediment laid down immediately following eruption of the final basement-capping flows was protected from erosion and thus preserved.

Site 807 was planned for drilling into basement, and our hope was to recover a complete section of Paleogene and Cretaceous sediments and as much basement rock as feasible, for pre-Neogene paleoceanography and for studies on the origin of the Ontong Java Plateau. We reached basement after penetrating 1379.7 m of sediment and continued to drill into basalt for 149 m. The Neogene is about 591 m thick, and recovery was excellent in the Neogene and upper Oligocene sediments (averaging 101%–103% in the 254- and 279-m sections cored with the APC, and 80% for the section cored with the XCB). The Paleogene is about 602 m thick, but recovery was significantly decreased in the lower Oligocene–Paleocene sediments (averaging 27.4% in the section cored with the RCB).

Background

The general background for all sites is contained in the "Introduction" chapter (this volume; also see Kroenke, 1972). The Ontong Java Plateau is a broad, shallow, mid-ocean highland in the western equatorial Pacific. Its shallowest regions lie above 2000 m, and its flanks reach depths in excess of 4500 m. With an area in excess of 1.5 million km^2, it is the largest of the "classic" Pacific plateaus. The plateau has a crustal thickness on the order of 40 km, yet it is in isostatic equilibrium, apparently maintaining its depth over much of its history. Crustal seismic velocities are in the range of oceanic crust (Hussong et al., 1979). Age estimates for basement have varied from Aptian (113–117 Ma) for the entire plateau to a succession of ages ranging from earliest Early Cretaceous (145 Ma) along the northernmost rim of the plateau to latest Late Cretaceous on Santa Isabel (see Fig. 1, "Introduction" chapter, this volume) along the southern margin of the plateau.

The oldest sediments overlying basalt are known to be Aptian at Site 289 and Aptian or older at Site 288. Paleontological dates of Albian or older were obtained for the oldest sediments overlying upraised plateau basement on Malaita, and dates of Eocene or older for the oldest sediments overlying plateau basement exposed on Santa Isabel. One radiometric date of 66 Ma has been obtained for a basement sample of uncertain affinity from Santa Isabel.

Leg 130 is the fourth drilling expedition to sample the sediment cover here; four DSDP sites were drilled earlier on the plateau. Three sites were rotary-drilled, with Site 64 spot cored during Leg 7 (Shipboard Scientific Party, 1971) and Sites 288 and 289 continuously cored during Leg 30 (Shipboard Scientific Party, 1975a, 1975b). Site 289, drilled in a water depth of 2206 m, terminated at 1271 mbsf in tholeiitic basalt overlain by Aptian sediments. Sediment thickness is 1262 m, of which the lowermost 293 m are mid-Cretaceous to upper Eocene radiolarian-bearing limestones, nannofossil foraminifer chalks, and nodular cherts. The upper 969 m consists of upper Eocene to Pleistocene nannofossil foraminifer chalks and oozes, with a continuous section down to the lower Oligocene. Semilithified chalk was first encountered near 250 m in the section (late Miocene age).

Site 586, drilled on Leg 89 next to Site 289, was piston cored to 305 mbsf and reached the lowermost upper Miocene (Shipboard Scientific Party, 1986a, 1986b). Well-preserved nannofossil ooze was recovered from the upper 300 m of the section, the first chalky layers appearing at 260 m (age, earliest late Miocene, ca. 10 Ma). Sedimentation rates in Site 586 vary between 13 and 39 m/m.y.

Objectives

Site 807 is located in 2805 m of water, roughly 475 km northwest of DSDP Sites 289/586 on the northern margin of the Ontong Java Plateau (Fig. 1). The site was originally positioned on a single-channel seismic (SCS) profile collected by the *Thomas Washington* during EURYDICE Cruise 9 at 0255 UTC, 11 April 1975 (Berger et al., 1977). It is located within a shallow basement graben about 0.5 km from the foot wall on the northern side of the graben (Fig. 2). The thickness of the sedimentary section at this site is roughly 1.20 s (two-way traveltime), approximately 7%–10% thicker than observed at Sites 289/586. The section is well stratified and appears to include most of the Neogene seismic reflection horizons that have been previously mapped on the Ontong Java Plateau and in other areas of the equatorial Pacific. The

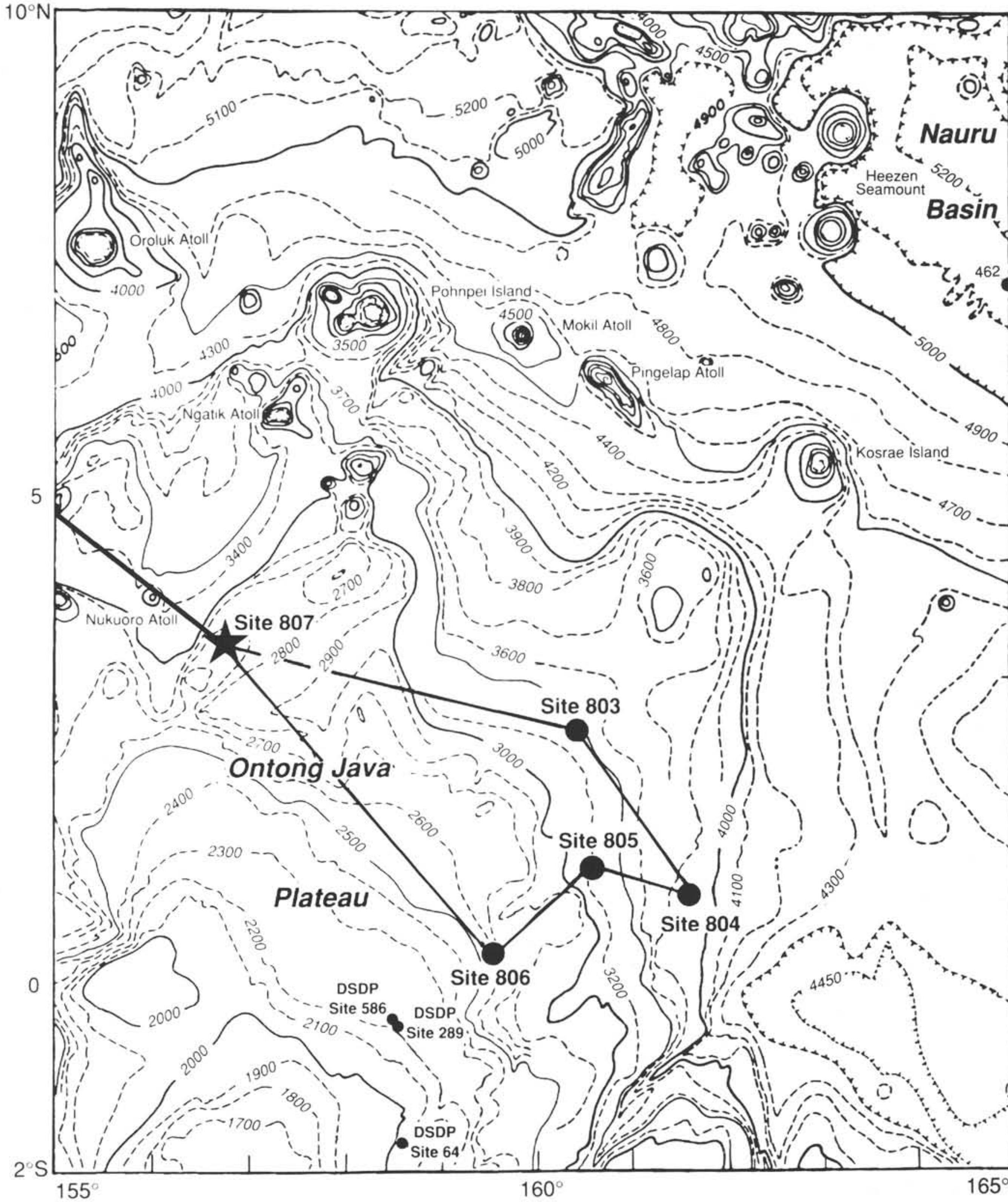

Figure 1. Bathymetry in meters of the northwestern part of the Ontong Java Plateau (after Mammerickx and Smith, 1985). The location of the Leg 130 sites together with those from DSDP Legs 7, 30, and 89 are shown for reference. Contour interval is 100 m.

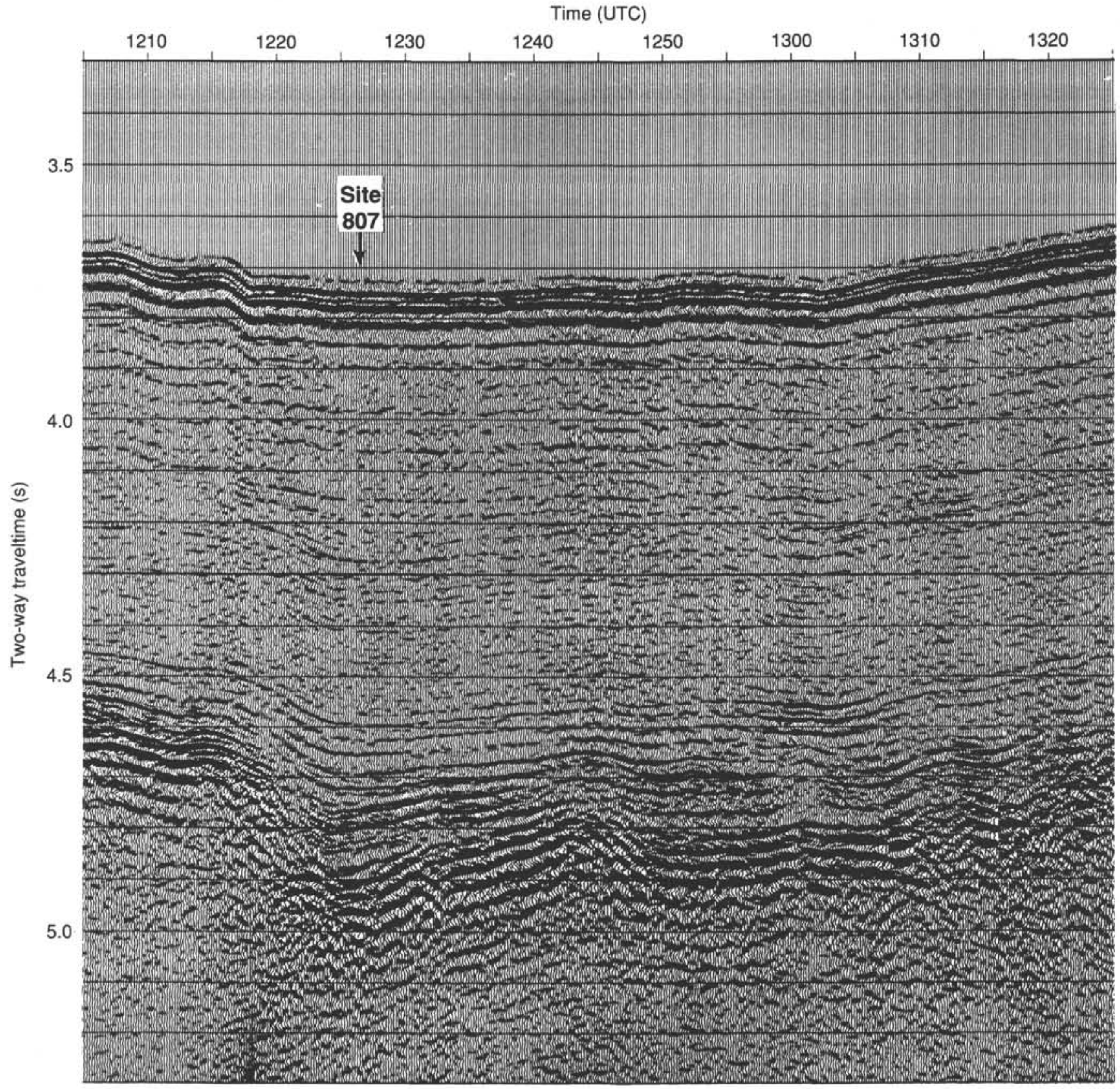

Figure 2. Site survey reflection profile across Site 807 (see "Underway Geophysics" chapter, this volume).

lower part of the section, preserved within a basement graben, has only minor sedimentary deformation, restricted for the most part to small compaction folds and subtle growth faults.

The site was planned to penetrate the entire sedimentary section and as far into basement as feasible. Drilling here was expected to provide a study in latitudinal contrasts between this site north of the equator and the other, more equatorial sites drilled across the northeastern flank of the Ontong Java Plateau on the Neogene depth transect. Water depth at Site 807 is intermediate between Sites 805 and 806, facilitating the comparison of changes in sedimentation caused by differences in latitude between the sites. The latitude of Site 807 is only slightly north of Site 803, however, facilitating comparison of depth-related paleoceanographic signals. Neogene objectives were to be achieved at Site 807 by double coring with the APC as deep as possible and then coring with the XCB to refusal.

Concerning Paleogene and Cretaceous sediments, the poor coverage in the Pacific leaves much to be desired. Substantial hiatuses exacerbate this situation. Major hiatuses were encountered in Upper Cretaceous to Paleogene sediments drilled at DSDP Sites 288 and 289, lowering our expectations with regard to finding complete sequences. However, many of the unconformities at Site 288 do not correlate with those at Site 289 (or the shallower, spot-cored Site 64), implying that they represent local events of limited areal extent (Shipboard Scientific Party, 1975a, 1975b). There was hope, therefore, that drilling at Site 807 could recover key sections missed earlier. There was also the expectation that we would find clues to the extent of Cretaceous anoxic events in the South Pacific and to the original basement depth of the plateau and subsequent bathymetric change.

If recovery were adequate, paleomagnetic investigations of Cretaceous sediments from the Ontong Java Plateau might also provide the opportunity to examine short polarity events within the Cretaceous normal polarity superchron (Tarduno, in press). Furthermore, if age estimates of early Aptian through Hauterivian for the basal sediments at Site 807 were correct, the basal sediments and basalt could be independently dated by magnetostratigraphy, complementing radiometric and isotopic studies.

Basement samples also were to be recovered at Site 807 for dating and geochemical/petrologic analyses. Previously, basement had been drilled at Site 289, recovering a scant 4.5 m of basalt of varying textures from a single flow. Recently, an $^{40}Ar/^{39}Ar$ date of 113 Ma was obtained on a sample of this basalt (R. Duncan, pers. comm., 1989). With a second suite of basaltic basement samples from Site 803, and a third and more comprehensive suite from Site 807, new light will be thrown on the question of the nature and origin of the Ontong Java Plateau. Problems to be addressed include whether the plateau formed at a hotspot during a short interval of time and over a single thermal plume (Mahoney, 1987); whether the plateau formed by ridge crest processes over a prolonged span of time and along a slowly spreading ridge system (Kroenke, 1984); or whether we have some combination of both processes, as in the example of the comparatively small Icelandic Plateau.

It was also hoped that a good paleolatitude might be obtained for the Ontong Java Plateau by sampling multiple flow units at Site 807. At present, the only absolute paleolatitudes for the Pacific Plate for the Early Cretaceous are based on marine magnetic anomaly skewness data (Gordon, in press). The reliability of these paleolatitudes is in doubt, however, because of possible systematic errors, as observed in other data sets (Petronotis and Gordon, 1989). Because only a single flow was sampled at Site 289, a biased estimate of the paleolatitude for the Ontong Java Plateau was obtained. By sampling multiple flows at Site 807, therefore, we hoped to obtain a benchmark Early Cretaceous paleolatitude for the Pacific Plate as well as the Ontong Java Plateau. Furthermore, if a viscous present-day overprint were to be present on the basalt, as has been observed in the western central Pacific (Tarduno et al., 1989), it might also be possible to construct a paleomagnetic pole for this period.

OPERATIONS

The transit from Sites 806 to 807 covered 251 nmi in 28.5 hr at an average speed of 8.81 kt. A 30-nmi seismic survey was run over the proposed site in 4.0 hr at 7.5 kt. The 200-in.^{3} water gun was used on the transit and site survey (see the "Underway Geophysics" chapter, this volume, for details of the surveys). The global positioning satellite (GPS) system was not available for the site survey but was available for the final positioning. The beacon was dropped at 1608 hr UTC, 26 February 1990, on the proposed site, initiating Site 807.

Hole 807A

The ship was positioned 30 m south-southwest of the beacon. Core 130-807A-1H was taken at 0005 hr, 27 February 1990 in a water depth of 2803.8 m. Cores 130-807A-1H through -27H were taken from 0 to 254.4 mbsf, with 254.4 m of sediment cored and 263.11 m recovered (103.4% recovery; see Table 1). Orientation surveys were taken during Cores 130-807A-3H through -27H. Coring with the APC ended at Core 130-807A-27H when overpull increased to 100,000 lb.

Cores 130-807A-28X through -86X were taken from 254.4 to 822.9 mbsf, with 568.5 m of sediment cored and 453.63 m recovered (79.8% recovery; see Table 1). Coring with the XCB ended when core recovery dropped below probable recovery with the RCB system. The sonic core monitor was run successfully on Cores 130-807A-74X, -76X, and -79X (recovery 5.46, 8.44, and 2.40 m, respectively). Problems with chalk jamming in the shoe were noted in Core 130-807A-69X (659.2 mbsf; 1.46-m recovery). The sinker bars were removed at that point, and a modified standard XCB shoe with a smaller inner diameter was used with good results.

Hole 807A Logging

Upon completion of coring at Hole 807A, the pipe was pulled to 100 mbsf and a high-viscosity mud sweep was made to clean the hole. The bit was pulled to 85.6 mbsf and logging operations began.

The following logs were completed:

Run No. 1: NGT/LSS/DIT/TLT; a successful logging run was made over the interval from 820.5 to 89.6 mbsf at 900 ft/hr. Approximately 2.4 m of fill was encountered at the base of the hole.

Run No. 2: NGT/ACT/HLDT; the log was run at 600 ft/hr from 821.1 to 323.4 mbsf, at which point problems with the heave compensator were encountered. The tool was lowered to 354.8 mbsf, the heave compensator turned back on, and logging data were collected to a depth of 75.6 mbsf.

At the end of logging operations, the pipe was pulled out of the hole, and the bottom hole assembly (BHA) cleared the seafloor at 2100 hr, 2 March 1990, ending Hole 807A.

Hole 807B

The ship was positioned 60 m south-southwest of the beacon. A jet-in test was conducted to a depth of 69 mbsf. The ship was then positioned 90 m south-southwest of the beacon. Core 130-807B-1H was taken at 2345 hr, 2 March 1990, in a water depth of 2806.1 m. Cores 130-807B-1H through -30H were taken from 0 to 278.6 mbsf, with 278.6 m of sediment cored and 280.18 m recovered (100.57% recovery).

Orientation surveys were taken during Cores 130-807B-3H- through -10H. Refusal of the APC was reached at Core 130-807B-30H (278.6 mbsf) when overpull reached 120,000 lb. At this point, the pipe was pulled out of the hole and the BHA cleared the rotary table at 0115 hr, 4 March 1990, ending Hole 807B.

Hole 807C

The ship was positioned 120 m south-southwest of the beacon. A new-style reentry cone was positioned under the rotary table; and a casing shoe, four joints of 16-in. casing, and the hanger were assembled and landed in the cone. The assembly was picked up and run slowly into the moonpool at 1000 hr, 4 March 1990. Seas were mild with 2–7 ft swells and 8-s periods. The cone was lowered about 3 m below the water surface when the driller observed the weight fluctuate between 36,000 and 15,000 lb, followed by a gradual loss of weight. A large surge was observed and a heavy dull thump was heard in the moonpool area. The cone had become unjayed and had sunk to the seafloor.

A second, new-style reentry cone was built, with the addition of two 10 × 10 in. holes in each of four mud-skirt plates and four 1 × 24 in. vertical slots in the reentry funnel to reduce surge effects while lowering the cone below the moonpool. An identical four-joint, 16-in. casing string and BHA were jayed into the cone. Entry into the water was smoother (the holes seemed to reduce the heave surge effect), and the cone was run to just above the seafloor 150 m from the beacon.

Hole 807C was spudded at 0700 hr, 5 March 1990, when the 16-in. casing was jetted-in to a sub-bottom depth of 58.1 mbsf. The bit was unjayed and a hole was drilled to 360.0 mbsf. A mud sweep was then made and the pipe pulled out of the hole.

Twenty-five joints of 11.75-in. casing were made up and run to the seafloor. The reentry cone was located with the televiewer (TV) camera after a 1.75-hr search, and the cone was reentered. The casing was run into the hole to 349.8 mbsf and cemented in place. The cementing string was pulled out, and an RCB bit with a 12 drill-collar BHA was run to the seafloor. The cone was reentered after a 1.5-hr TV camera search.

The casing shoe was drilled out in 2.25 hr, and a hole was drilled without coring to 780.0 mbsf in hard chalk in 5.0 hr. Coring with the RCB began at this point, and Cores 130-807C-1R through -56R (780.0–1216.3 mbsf) recovered 93.30 m of hard chalk (Cores 130-807C-1R through -24R), hard limestone (Cores 130-807C-25R through -41R), and chert (Cores 130-807C-42R through -56R). Poor recovery often resulted from the hard chalk fracturing and jamming in the bit throat. The bit deplugger was run three times. The bit was pulled after 44.65 hr of rotation time.

A four-cone insert bit was run to the seafloor and the reentry cone was entered after a short search. Cores 130-807C-57R through -79R (1216.3–1423.9 mbsf) were taken with 91.25 m of core recovered in hard limestone. Basalt was encountered at 1380 mbsf. The bit was pulled after rotating 42.0 hr, and two shanks were found to have broken welds.

A second four-cone insert bit was run to the seafloor, and the reentry cone was entered after a short search. Cores 130-807C-80R through -88R (1423.9–1503.0 mbsf) were cut, with 50.59 m of basalt recovered. The bit was pulled after 35.08 hr of rotation time, and one shank weld was found to have failed.

A third four-cone insert bit was run to the seafloor, and the reentry cone was entered after a short search. Cores 130-807C-89R through -93R (1503.0–1528.4 mbsf) were cut, with 13.10-m basalt recovered, and the bit was pulled after rotating 18.16 hr when it torqued up once again. The bit was examined with the TV camera at the seafloor and was found to have two shanks and cones missing; presumably they were left in Hole 807C. The bit was dropped on the seafloor by activating the mechanical bit release and the cone was reentered for logging. The pipe was set to 169 mbsf in preparation for logging.

Logs were run as follows:

Log No. 1: NGT/LSS/DIT/TLT; the log data were collected from 330.4 to 1492.9 mbsf and from 1528.3 to 348.7 mbsf at a rate of 900 ft/hr. Approximately 0.6 m of bottom fill were encountered.

Log No. 2: NGT/ACT/HLDT; the log was started at a depth of 1525.8 mbsf and run at a speed of 600 ft/hr. At 1467.9 mbsf, the caliper became jammed with debris and the logging run was stopped. The tool was lowered again to 1527.0 mbsf, and the logging run restarted. No further complications were encountered, and data were collected up to a depth of 348.7 mbsf.

Log No. 3: NGT/FMS/GPIT/TLT; the first log with this tool was made at 900 ft/hr over the interval from 1509.1 to 947.3 mbsf, at which point the hole was too wide for the FMS caliper. The tool was lowered again to the base of the hole, and a second log was collected from 1507.8 to 1095.5 mbsf.

After logging, the pipe was pulled out of the hole and the BHA cleared the rotary table at 0000 hr, 23 March 1990, ending Site 807.

Site 807 to Guam

The thrusters and hydrophones were pulled, and the ship began a post-site survey toward Guam at 0000 hr, 23 March 1990. A 203-nmi underway geophysics survey was conducted enroute to Guam.

The *JOIDES Resolution* arrived outside Apra Harbor, Guam, on 26 March 1990. The harbor pilot arrived on board at 1930 hr, 26 March. The first line ashore was at 2030 hr, 26 March 1990, ending Leg 130.

LITHOSTRATIGRAPHY

Introduction

The sedimentary sequence at Site 807 was divided into three lithologic units (Fig. 3 and Table 2). Unit I (0–968 mbsf) is composed predominantly of Pleistocene to upper Eocene nannofossil ooze and chalk with foraminifers, with lesser amounts of foraminifer nannofossil ooze and chalk and nannofossil ooze and chalk. This unit was divided into Subunits IA and IB, based on the degree of induration. The boundary between the two subunits was placed at 293 mbsf, the top of Core 130-807A-32X, which corresponds to a middle-late Miocene age of 10–11 Ma (see "Biostratigraphy" section, this chapter). The basal 30 m of Subunit IA contains a significant amount of chalk as isolated nodules and layers.

Unit II (968–1351.4 mbsf) is composed of Eocene to upper Campanian limestone, chert, nannofossil chalk, and nannofossil chalk with foraminifers. The boundary between Units I and II was placed at the level where chert becomes a significant component in the recovered sediment. Unit II was divided into Subunits IIA and IIB, based on the transition from chalk to limestone. The boundary between the two subunits was placed at 1098 mbsf, the top of Core 130-807C-41R, which corresponds to an early middle Eocene age of approximately 40 Ma (see "Biostratigraphy" section, this chapter). The transition in sediment induration is also reflected in a substantial increase in recovery, from 7% in Subunit IIA to 44% in Subunit IIB.

Unit III (1351.4–1379.7 mbsf) is composed of lower Cenomanian to upper Albian claystone and siltstone with varying amounts of radiolarians, and Albian to Aptian limestone. The unit was divided into Subunits IIIA and IIIB, at the transition from claystone to limestone. The boundary between the two subunits was placed at 1369.7 mbsf (Section 130-807C-73R-2, 82 cm). Limestone beds were also recovered as interlayers in the basalt at 1424.6–1425.1 mbsf (Section 130-807C-80R-1, 70–120 cm) and at 1439 mbsf (Section 130-807C-82R-3, 72–79 cm).

Description of Units

Unit I

Intervals: Hole 807A, Cores 130-807A-1H through -86X; Hole 807B, Cores 130-807B-1H through -30H; Hole 807C, Cores 130-807C-1R through -26R
Age: Pleistocene–late Eocene
Depth: 0–968 mbsf

Unit I consists predominantly of nannofossil ooze and chalk with foraminifers and lesser amounts of foraminifer nannofossil ooze and chalk and nannofossil ooze and chalk. Unit I was divided into two subunits. Subunit IA (0–293 mbsf) is primarily nannofossil ooze with foraminifers and foraminifer nannofossil ooze, but it grades to nannofossil ooze in some intervals. The basal 30 m of Subunit IA contains a significant percentage of chalk. Subunit IB (293–968 mbsf) grades downward from foraminifer nannofossil

Table 1. Coring summary, Site 807.

Core no.	Date (1990)	Time (UTC)	Depth (mbsf)	Cored (m)	Recovered (m)	Recovery (%)
130-807A-						
1H	Feb. 27	0005	0–7.4	7.4	7.37	99.6
2H	27	0050	7.4–16.9	9.5	9.90	104.0
3H	27	0125	16.9–26.4	9.5	9.91	104.0
4H	27	0215	26.4–35.9	9.5	9.94	104.0
5H	27	0250	35.9–45.4	9.5	9.85	103.0
6H	27	0345	45.4–54.9	9.5	9.93	104.0
7H	27	0420	54.9–64.4	9.5	9.96	105.0
8H	27	0500	64.4–73.9	9.5	9.95	105.0
9H	27	0535	73.9–83.4	9.5	9.70	102.0
10H	27	0615	83.4–92.9	9.5	9.87	104.0
11H	27	0655	92.9–102.4	9.5	9.85	103.0
12H	27	0730	102.4–111.9	9.5	9.74	102.0
13H	27	0820	111.9–121.4	9.5	9.66	101.0
14H	27	0845	121.4–130.9	9.5	9.84	103.0
15H	27	0930	130.9–140.4	9.5	9.93	104.0
16H	27	1005	140.4–149.9	9.5	9.97	105.0
17H	27	1045	149.9–159.4	9.5	9.92	104.0
18H	27	1125	159.4–168.9	9.5	9.73	102.0
19H	27	1210	168.9–178.4	9.5	9.92	104.0
20H	27	1250	178.4–187.9	9.5	9.71	102.0
21H	27	1325	187.9–197.4	9.5	9.40	98.9
22H	27	1405	197.4–206.9	9.5	9.89	104.0
23H	27	1455	206.9–216.4	9.5	9.98	105.0
24H	27	1540	216.4–225.9	9.5	9.80	103.0
25H	27	1625	225.9–235.4	9.5	9.90	104.0
26H	27	1715	235.4–244.9	9.5	9.89	104.0
27H	27	1810	244.9–254.4	9.5	9.60	101.0
28X	27	1900	254.4–264.1	9.7	9.04	93.2
29X	27	2000	264.1–273.8	9.7	9.58	98.7
30X	27	1945	273.8–283.5	9.7	9.30	95.9
31X	27	2130	283.5–292.7	9.2	8.12	88.2
32X	27	2215	292.7–302.3	9.6	8.02	83.5
33X	27	2245	302.3–312.0	9.7	9.41	97.0
34X	27	2335	312.0–321.2	9.2	9.71	105.0
35X	28	0010	321.2–330.9	9.7	8.56	88.2
36X	28	0055	330.9–340.6	9.7	9.48	97.7
37X	28	0125	340.6–350.2	9.6	9.77	102.0
38X	28	0210	350.2–359.9	9.7	9.13	94.1
39X	28	0250	359.9–369.7	9.8	8.51	86.8
40X	28	0325	369.7–379.5	9.8	9.62	98.1
41X	28	0400	379.5–389.2	9.7	9.02	93.0
42X	28	0452	389.2–398.9	9.7	8.33	85.9
43X	28	0530	398.9–408.6	9.7	8.76	90.3
44X	28	0600	408.6–418.3	9.7	8.14	83.9
45X	28	0635	418.3–427.8	9.5	9.87	104.0
46X	28	0715	427.8–437.5	9.7	8.97	92.5
47X	28	0750	437.5–447.1	9.6	9.05	94.3
48X	28	0830	447.1–456.8	9.7	9.66	99.6
49X	28	0905	456.8–466.4	9.6	7.93	82.6
50X	28	0950	466.4–476.1	9.7	9.45	97.4
51X	28	1030	476.1–485.8	9.7	8.94	92.1
52X	28	1110	485.8–495.4	9.6	8.59	89.5
53X	28	1150	495.4–505.1	9.7	8.50	87.6
54X	28	1225	505.1–514.8	9.7	8.74	90.1
55X	28	1305	514.8–524.0	9.2	9.23	100.0
56X	28	1340	524.0–533.7	9.7	8.58	88.4
57X	28	1420	533.7–543.4	9.7	8.42	86.8
58X	28	1500	543.4–553.0	9.6	7.85	81.8
59X	28	1540	553.0–562.6	9.6	7.01	73.0
60X	28	1620	562.6–572.3	9.7	7.48	77.1
61X	28	1700	572.3–581.9	9.6	8.84	92.1
62X	28	1740	581.9–591.6	9.7	7.93	81.7
63X	28	1820	591.6–601.3	9.7	6.92	71.3
64X	28	1905	601.3–611.0	9.7	7.55	77.8
65X	28	2000	611.0–620.6	9.6	7.36	76.6
66X	28	2045	620.6–630.3	9.7	6.65	68.5
67X	28	2120	630.3–639.9	9.6	5.15	53.6
68X	28	2215	639.9–649.6	9.7	6.88	70.9
69X	28	2335	649.6–659.2	9.6	1.46	15.2
70X	Mar. 1	0040	659.2–668.9	9.7	8.44	87.0
71X	1	0150	668.9–678.2	9.3	8.01	86.1
72X	1	0300	678.2–687.8	9.6	5.99	62.4
73X	1	0415	687.8–697.5	9.7	9.04	93.2
74X	1	0520	697.5–707.2	9.7	5.46	56.3
75X	1	0615	707.2–716.9	9.7	7.04	72.6
76X	1	0730	716.9–726.5	9.6	8.44	87.9

Table 1 (continued).

Core no.	Date (1990)	Time (UTC)	Depth (mbsf)	Cored (m)	Recovered (m)	Recovery (%)
77X	1	0820	726.5–736.2	9.7	8.21	84.6
78X	1	0930	736.2–745.5	9.3	8.08	86.9
79X	1	1035	745.5–755.2	9.7	2.40	24.7
80X	1	1155	755.2–764.9	9.7	4.11	42.4
81X	1	1305	764.9–774.5	9.6	1.09	11.3
82X	1	1430	774.5–784.2	9.7	5.91	60.9
83X	1	1540	784.2–793.9	9.7	6.29	64.8
84X	1	1700	793.9–803.6	9.7	9.65	99.5
85X	1	1820	803.6–813.2	9.6	3.48	36.2
86X	1	1940	813.2–822.9	9.7	2.48	25.5
Coring totals				822.9	716.74	87.1
130-807B-						
1H	Mar. 2	2345	0–3.1	3.1	3.04	98.0
2H	3	0020	3.1–12.6	9.5	9.75	102.0
3H	3	0100	12.6–22.1	9.5	9.64	101.0
4H	3	0145	22.1–31.6	9.5	9.59	101.0
5H	3	0220	31.6–41.1	9.5	9.73	102.0
6H	3	0300	41.1–50.6	9.5	9.83	103.0
7H	3	0350	50.6–60.1	9.5	9.79	103.0
8H	3	0430	60.1–69.6	9.5	9.88	104.0
9H	3	0505	69.6–79.1	9.5	9.72	102.0
10H	3	0550	79.1–88.6	9.5	9.78	103.0
11H	3	0630	88.6–98.1	9.5	10.06	105.9
12H	3	0705	98.1–107.6	9.5	9.76	103.0
13H	3	0745	107.6–117.1	9.5	9.87	104.0
14H	3	0805	117.1–126.6	9.5	9.33	98.2
15H	3	0845	126.6–136.1	9.5	9.23	97.1
16H	3	0920	136.1–145.6	9.5	9.91	104.0
17H	3	1000	145.6–155.1	9.5	9.97	105.0
18H	3	1030	155.1–164.6	9.5	9.67	102.0
19H	3	1135	164.6–174.1	9.5	7.33	77.1
20H	3	1215	174.1–183.6	9.5	5.67	59.7
21H	3	1255	183.6–193.1	9.5	9.79	103.0
22H	3	1325	193.1–202.6	9.5	9.82	103.0
23H	3	1400	202.6–212.1	9.5	9.95	105.0
24H	3	1440	212.1–221.6	9.5	9.93	104.0
25H	3	1520	221.6–231.1	9.5	9.91	104.0
26H	3	1555	231.1–240.6	9.5	9.93	104.0
27H	3	1635	240.6–250.1	9.5	9.84	103.0
28H	3	1720	250.1–259.6	9.5	9.94	104.0
29H	3	1820	259.6–269.1	9.5	9.72	102.0
30H	3	1900	269.1–278.6	9.5	9.80	103.0
Coring totals				278.6	280.18	100.6
130-807C-						
1R	Mar. 8	0930	780.0–789.7	9.7	0.20	2.1
2R	8	1030	789.7–799.3	9.6	2.52	26.2
3R	8	1140	799.3–809.0	9.7	0.04	0.4
4R	8	1300	809.0–818.6	9.6	2.68	27.9
5R	8	1400	818.6–828.3	9.7	0.02	0.2
6R	8	1525	828.3–838.0	9.7	7.59	78.2
7R	8	1650	838.0–847.7	9.7	0.19	2.0
8R	8	1805	847.7–857.4	9.7	0.01	0.1
9R	8	2000	857.4–867.1	9.7	0.62	6.4
10R	8	2200	867.1–872.3	5.2	0.00	0.0
11R	8	2300	872.3–876.6	4.3	0.00	0.0
12R	9	0145	876.6–881.9	5.3	0.59	11.1
13R	9	0300	881.9–888.9	7.0	0.22	3.1
14R	9	0400	888.9–893.9	5.0	0.15	3.0
15R	9	0500	893.9–898.9	5.0	0.72	14.4
16R	9	0600	898.9–903.9	5.0	1.36	27.2
17R	9	0700	903.9–908.9	5.0	3.47	69.4
18R	9	0800	908.9–913.9	5.0	0.23	4.6
19R	9	0900	913.9–918.9	5.0	0.67	13.4
20R	9	1000	918.9–923.9	5.0	0.23	4.6
21R	9	1220	923.9–933.7	9.8	0.39	4.0
22R	9	1415	933.7–938.7	5.0	0.36	7.2
23R	9	1520	938.7–943.7	5.0	5.21	104.0
24R	9	1630	943.7–948.4	4.7	2.94	62.5
25R	9	1745	948.4–958.1	9.7	1.29	13.3
26R	9	1900	958.1–967.8	9.7	1.53	15.8
27R	9	2015	967.8–977.5	9.7	0.09	0.9
28R	9	2130	977.5–987.1	9.6	0.15	1.6
29R	9	2300	987.1–996.8	9.7	0.32	3.3

Table 1 (continued).

Core no.	Date (1990)	Time (UTC)	Depth (mbsf)	Cored (m)	Recovered (m)	Recovery (%)
30R	10	0200	996.8–1006.5	9.7	1.52	15.7
31R	10	0345	1006.5–1016.1	9.6	0.78	8.1
32R	10	0500	1016.1–1025.4	9.3	0.22	2.4
33R	10	0620	1025.4–1034.6	9.2	0.40	4.4
34R	10	0740	1034.6–1044.3	9.7	0.47	4.8
35R	10	0850	1044.3–1054.0	9.7	0.82	8.5
36R	10	1010	1054.0–1063.7	9.7	0.41	4.2
37R	10	1135	1063.7–1073.2	9.5	0.31	3.3
38R	10	1250	1073.2–1082.4	9.2	0.68	7.4
39R	10	1415	1082.4–1092.0	9.6	0.42	4.4
40R	10	1520	1092.0–1097.7	5.7	1.72	30.2
41R	10	1700	1097.7–1102.4	4.7	0.94	20.0
42R	10	1845	1102.4–1106.4	4.0	1.65	41.2
43R	10	2100	1106.4–1116.0	9.6	1.20	12.5
44R	10	2340	1116.0–1125.6	9.6	1.08	11.2
45R	11	0220	1125.6–1135.2	9.6	2.84	29.6
46R	11	0500	1135.2–1140.2	5.0	3.86	77.2
47R	11	0725	1140.2–1145.2	5.0	2.51	50.2
48R	11	0940	1145.2–1150.2	5.0	3.19	63.8
49R	11	1220	1150.2–1155.2	5.0	1.23	24.6
50R	11	1420	1155.2–1160.2	5.0	1.97	39.4
51R	11	1800	1160.2–1169.8	9.6	5.11	53.2
52R	11	2300	1169.8–1179.4	9.6	4.58	47.7
53R	12	0400	1179.4–1188.8	9.4	5.75	61.2
54R	12	0845	1188.8–1196.9	8.1	6.00	74.1
55R	12	1450	1196.9–1206.6	9.7	6.05	62.4
56R	12	1915	1206.6–1216.3	9.7	3.80	39.2
57R	13	1600	1216.3–1222.5	6.2	2.87	46.3
58R	13	1900	1222.5–1232.2	9.7	0.57	5.9
59R	13	2215	1232.2–1241.8	9.6	3.34	34.8
60R	13	0115	1241.8–1251.5	9.7	0.22	2.3
61R	14	0400	1251.5–1261.2	9.7	2.84	29.3
62R	14	0645	1261.2–1270.8	9.6	4.72	49.1
63R	14	0920	1270.8–1280.5	9.7	5.49	56.6
64R	14	1210	1280.5–1290.1	9.6	3.75	39.0
65R	14	1515	1290.1–1299.8	9.7	3.34	34.4
66R	14	1800	1299.8–1309.5	9.7	4.60	47.4
67R	14	2100	1309.5–1319.1	9.6	6.93	72.2
68R	14	2335	1319.1–1328.8	9.7	3.64	37.5
69R	15	0230	1328.8–1338.4	9.6	7.08	73.7
70R	15	0520	1338.4–1348.0	9.6	6.37	66.3
71R	15	0800	1348.0–1357.7	9.7	9.31	96.0
72R	15	0945	1357.7–1367.4	9.7	3.31	34.1
73R	15	1145	1367.4–1375.4	8.0	2.71	33.9
74R	15	1545	1375.4–1385.2	9.8	5.67	57.8
75R	15	2045	1385.2–1394.8	9.6	6.02	62.7
76R	16	0050	1394.8–1404.5	9.7	1.45	14.9
77R	16	0300	1404.5–1409.5	5.0	2.70	54.0
78R	16	0600	1409.5–1414.5	5.0	3.56	71.2
79R	16	1030	1414.5–1423.9	9.4	5.36	57.0
80R	17	1050	1423.9–1433.6	9.7	4.43	45.7
81R	17	1405	1433.6–1438.2	4.6	3.72	80.8
82R	17	1850	1438.2–1447.2	9.0	6.95	77.2
83R	18	0145	1447.2–1455.9	8.7	8.51	97.8
84R	18	0825	1455.9–1465.6	9.7	7.03	72.5
85R	18	1355	1465.6–1475.3	9.7	8.84	91.1
86R	18	1905	1475.3–1485.0	9.7	3.91	40.3
87R	18	2345	1485.0–1494.7	9.7	2.28	23.5
88R	19	0515	1494.7–1503.0	8.3	4.92	59.3
89R	20	0400	1503.0–1509.1	6.1	3.25	53.3
90R	20	0845	1509.1–1515.3	6.2	3.90	62.9
91R	20	1115	1515.3–1516.8	1.5	0.44	29.3
92R	20	1415	1516.8–1518.8	2.0	2.40	120.0
93R	20	2130	1518.8–1528.4	9.6	3.11	32.4
Coring totals				748.4	252.84	33.8

chalk to nannofossil chalk with foraminifers and, at greater depth, to nannofossil chalk.

Subunit IA

Intervals: Hole 807A, Cores 130-807A-1H through -31X; Hole 807B, Cores 130-807B-1H through -30H
Age: Pleistocene–middle/late Miocene boundary
Depth: 0–293 mbsf

Subunit IA consists of 293 m of foraminifer nannofossil ooze, nannofossil ooze with foraminifers, and minor amounts of nannofossil ooze. Smear slide data indicate that nannofossil content in the ooze averages about 75% (Fig. 4A). Foraminifer abundance averages approximately 23% (Table 3) and ranges between 8% and 40%. Maxima in foraminifer abundance were noted in both Holes 807A and 807B from 20 to 40 mbsf (1.0–2.0 Ma), from 60 to 90 mbsf (ca. 2.5 Ma), from 155 to 170 mbsf (ca. 6 Ma), and from 220 to 250 mbsf (ca. 8 Ma). Foraminifer abundances are low in both holes at approximately 50 (2.0–2.5 Ma), 135 (ca. 5.2 Ma), and 190–210 mbsf (ca. 7.5 Ma). Constituents present in trace amounts include radiolarians, diatoms, siliceous sponge spicules, silicoflagellates, volcanic glass, quartz, accessory minerals, and clay.

Texturally, Subunit IA is composed of silts that range from sandy silt to rare clayey silt (Table 3).The high proportion of silt reflects the abundance of nannofossils. Mean grain size averages 28 μm (medium silt) throughout Subunit IA and exhibits crude positive covariation with the estimates of foraminifer abundance based on smear slides (Figs. 4 and 5; Tables 3 and 4). For instance, both mean grain size and foraminifer abundance are high between 60 and 90 mbsf and between 220 and 250 mbsf. Fluctuations in the relative abundance of foraminifers can be further illustrated by analysis of the coarse (>125 μm) and intermediate (63–125 μm) size fractions, which are dominated by foraminifers (Fig. 5B). The size fraction data and smear slide data correlate well with foraminifer abundance.

Calcium carbonate contents in Subunit IA range between 88% and 94% and average 92% (Fig. 6A). The top 30 m of the subunit, representing the Pleistocene (see "Paleomagnetics" section, this chapter), have the lowest carbonate contents of the subunit; below that level, carbonate contents gradually increase to a maximum at 165–210 mbsf. The carbonate contents then decrease over the interval from 210 mbsf to the base of the subunit. X-ray diffraction (XRD) analyses indicate that the relative abundances of terrigenous components, including clays, quartz, and feldspar, are higher in the upper portion of the subunit and decrease below approximately 70 mbsf. Long-term changes in carbonate content and in the abundances of the coarse- and intermediate-size fractions generally correspond throughout Subunit IA. Mean carbonate contents and coarse/intermediate fraction abundances are low above 60 mbsf and high between 60 and 130 mbsf. Between 210 and 260 mbsf, carbonate content is low and coarse/intermediate fraction abundances are high.

Colors in Subunit IA grade from pale brown (10YR 6/3) in the top 50 cm to light gray (10YR 7/2) from 0.5 to 3 mbsf, to predominantly white (2.5Y 8/0, 5Y 8/1, 7.5YR 8/1, and 10YR 8/1) below 3 mbsf. As at Sites 803, 804, 805 and 806, color bands are pervasive. The colors of the bands are either various shades of green, such as light greenish gray (5G 7/1) and pale yellowish green (10GY 7/2), or purple, including reddish gray (5R 6/1), grayish blue (5PB 5/2), and pale purple (5P 6/2). The bands are horizontal, up to 2 cm thick, and commonly occur as green and purple pairs separated by white ooze. The bands first appear at about 9 mbsf and increase in frequency downhole to a maximum at approximately 200 mbsf, corresponding to the upper Miocene. The abundance of bands decreases over the interval from 200 mbsf to the base of Subunit IA (Fig. 7).

Subunit IA is extensively bioturbated. The evidence includes burrows, cylindrical pyrite concretions, and abundant trace fossils. Burrows are commonly surrounded by pale purple (5P 6/2) elliptical halos. In some instances, halo diameters are as large as 20 cm. As a result, it is possible that many of the dipping and horizontal color streaks and bands observed in Subunit IA are fragments of large halos. Color bands were observed to pass through burrows but to be overprinted by the burrow-ringing halo (Fig. 8). These relationships indicate that the color bands and halos reflect different generations of diagenesis.

Other noteworthy features in Subunit IA are the presence of microfaults and a nodule of porcellanite. The porcellanite nodule that was found at 252 mbsf (Core 130-807B-27X-5, 110 cm) is 2–3 cm in diameter and microcrystalline in texture. Similar concretions were found at Site 806 as shallow as 240 mbsf (see "Lithostratigraphy" section, "Site 806" chapter, this volume). Microfaults are present below 49 mbsf as offsets of up to 5 cm in color bands. Several microfaults were also observed between 101 and 107 mbsf (Sections 130-807B-12H-2 and -6); between 132 and 133 mbsf (Core 130-807B-15H); between 191 and 198 mbsf (Sections 130-807A-21H-3 and -4 and Sections 130-807B-22H-1 and -3); and between 242 and 246 mbsf (Sections 130-807A-26H-5 and -6 and Section 130-807B-27H-4).

At a depth of approximately 253 mbsf, 40 m above the base of Subunit IA, the increased induration of ooze is indicated by the first recovery of chalk biscuits. Between 253 and 264 mbsf, the proportion of indurated layers and chalk nodules increases to approximately 10% of the sediment. The abundance of chalk nodules increases throughout the basal 30 m of Subunit IA, and the sediment is predominantly chalk at 294 mbsf.

Support for the division of Unit I into subunits based on induration also comes from the logging results (see "Logging" section, this chapter). Log stratigraphic Unit A2 was chosen with upper and lower boundaries at 254 and 306 mbsf, depths that correspond closely to those chosen from visual examination. Log stratigraphic Unit A2 is characterized by velocities intermediate between those in overlying and underlying sediments. Sonic velocities measured onboard ship increase markedly for samples recovered below 290 m, probably reflecting the change from ooze to chalk (see "Physical Properties" section, this chapter).

Subunit IB

Intervals: Hole 807A, Cores 130-807A-32X through -86X; Hole 807C, Cores 130-807C-1R through -26R
Age: late middle Miocene–late Eocene
Depth: 293–968 mbsf

Subunit IB is composed primarily of nannofossil chalk with foraminifers, foraminifer nannofossil chalk, and nannofossil chalk (Fig. 3). Smear slide analyses indicate that nannofossils compose approximately 80% of Subunit IB (Fig. 4B). Foraminifer abundances are high, approximately 20%, from 350 to 500 mbsf (13–21 Ma) and from 690 to 840 mbsf (middle Oligocene). Foraminifer content is low from 300 to 350 mbsf (11–13 Ma), from 525 to 675 mbsf (22–27 Ma), and from 915 to 968 mbsf (upper Eocene).

Nine ash layers, composed of altered glass and opaque minerals, are present in Subunit IB between 639 and 759 mbsf (ca. 26–32 Ma) (Table 5). The ash layers are dark gray (2.5Y 4/0) and strongly bioturbated (Fig. 9). Other components in Subunit IB, such as radiolarians and diatoms, are present in trace quantities. One chert nodule, 2–3 cm in diameter, was found at 494 mbsf (Section 130-807A-52X-6) and another at 543 mbsf (Section 130-807A-58X-1). Four layers or nodules of chert, each 3–7 cm thick, were found between 959 and 961 mbsf; each contained a partially silicified exterior of chalk (Fig. 10).

Carbonate contents are less than approximately 91% above 415 mbsf (Fig. 7), increase to approximately 95% from 415 to 460 mbsf (14–17 Ma), and decrease below 575 mbsf. In Subunit IB carbonate contents vary inversely with the large shifts in foraminifer abundance estimated from smear slide analyses.

Subunit IB is predominantly white (2.5Y 8/0, 5Y 8/0, 7.5YR 8/0, and 10YR 8/1), but it grades in color to intervals (20–30 cm thick) of pale pink (5RP 8/2) and pale blue (5PB 7/2). Alternate faint and distinct color bands in various shades of green (5G 7/1 and 5GY 7/2) are apparent at the top of Subunit IB (Fig. 8), but they disappear almost completely below 300 mbsf. Purple (5P 6/2) and gray bands fluctuate in abundance throughout the subunit but are concentrated at approximately 350 and 760 mbsf. The color bands become thinner with depth

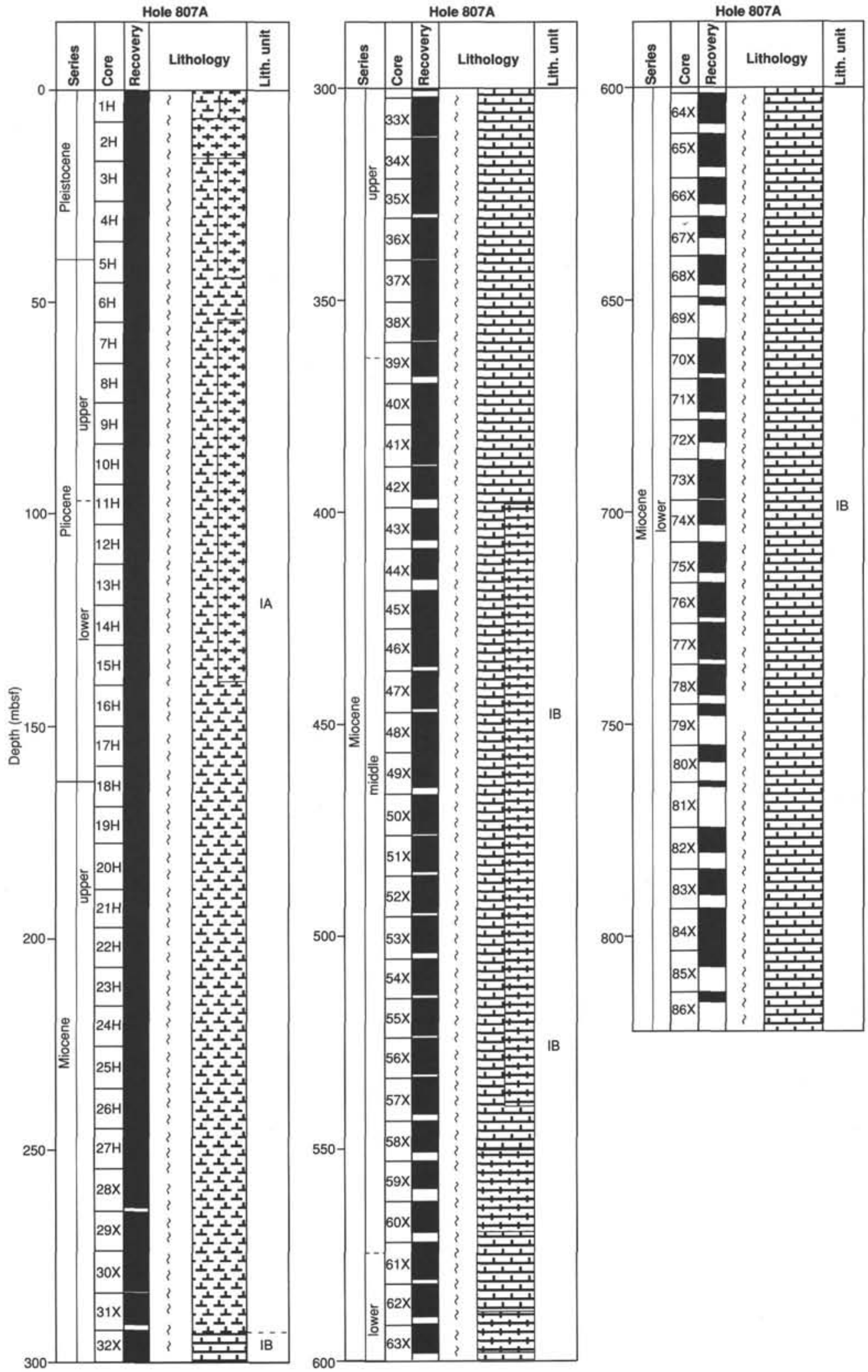

Figure 3. Lithologic summary, Site 807.

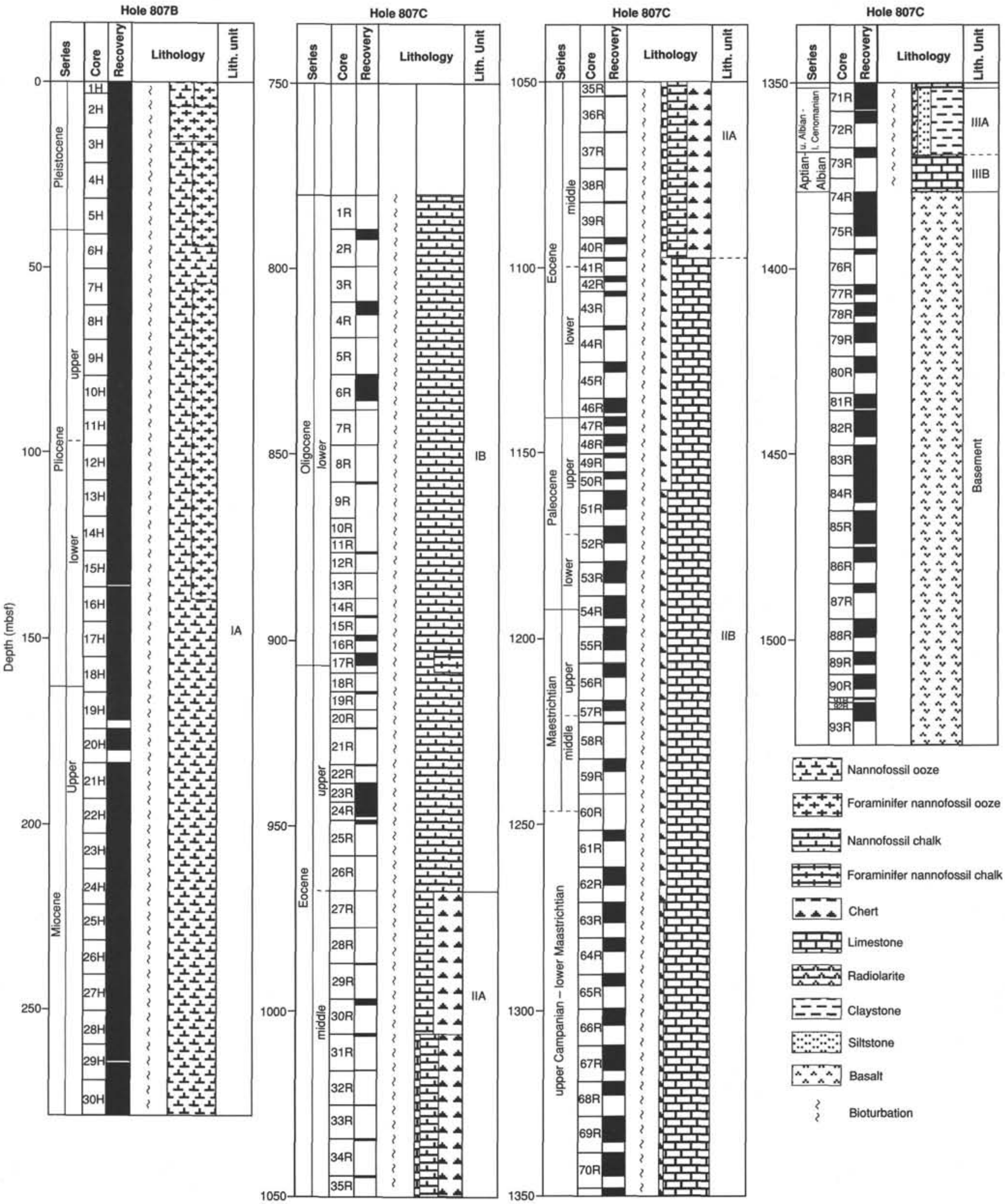

Figure 3 (continued).

Table 2. Lithologic summary, Site 807.

Lithologic unit	Cores	Depth (mbsf)	Age	Lithology
IA	807A-1H to -31X 807B-1H to -30H	0–293	Pleistocene to middle/late Miocene	Foraminifer nannofossil ooze to nannofossil ooze with foraminifers
IB	807A-32X to -86X 807C-1R to -26R	293–968	middle/late Miocene to late Eocene	Nannofossil chalk to foraminifer nannofossil chalk
IIA	807C-27R to -40R	968–1098	middle Eocene	Chert, nannofossil chalk to nannofossil chalk with foraminifers, limestone
IIB	807C-41R to -71R, 45 cm	1098–1351.4	Eocene to late Campanian	Limestone
IIIA	807C-71R-3, 45 cm, to -73R-2, 82 cm	1351.4–1369.7	early Cenomanian to late Albian	Claystone, radiolarian siltstone
IIIB	807C-73R-2, 82 cm, to -74R-1, 25 cm	1369.7–1379.7	Early Cretaceous (Albian/Aptian)	Limestone

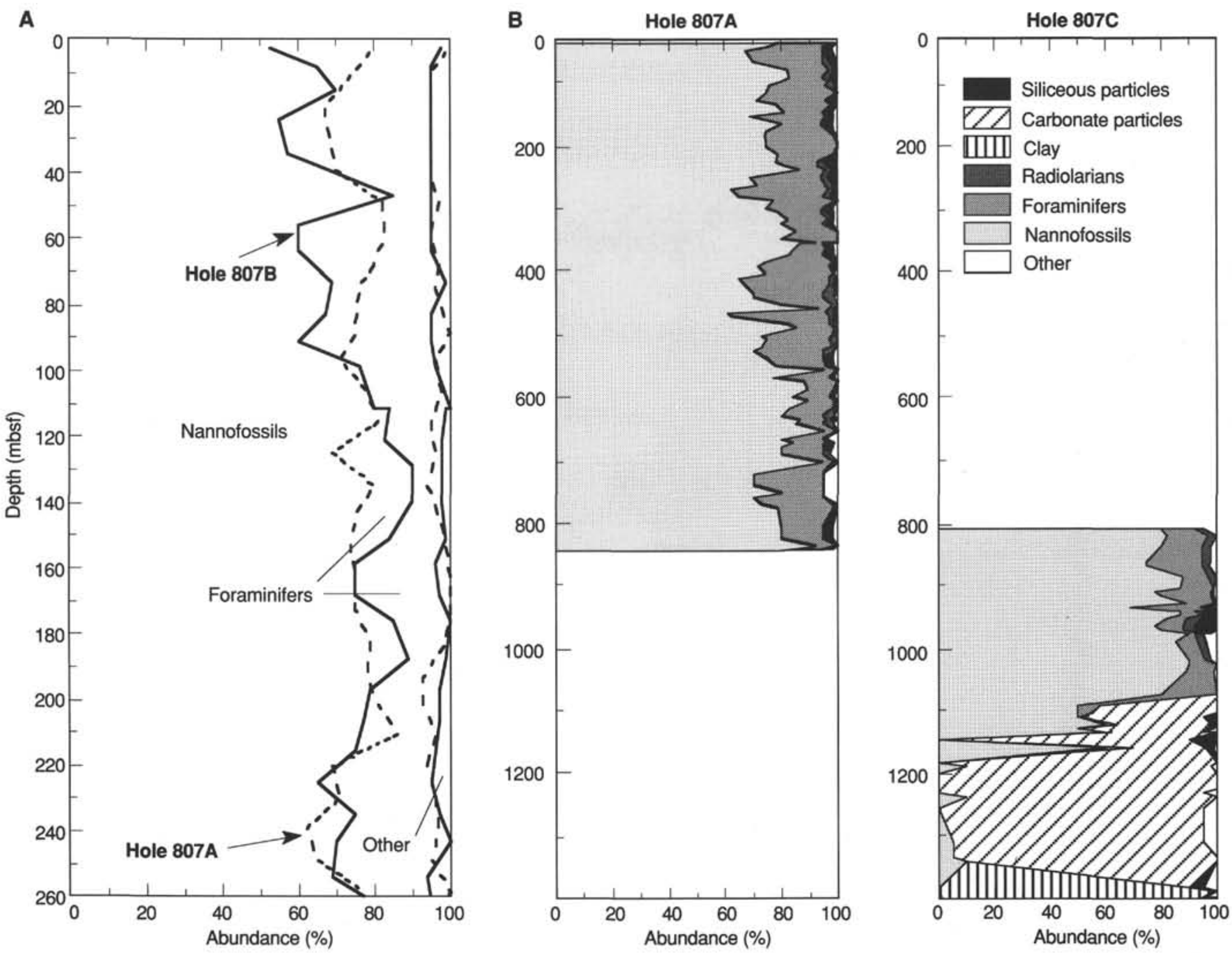

Figure 4. Abundances of major sediment components estimated from smear slides. A. Subunit IA, Hole 807A (dashed lines) and Hole 807B (solid lines) (0–260 mbsf). B. All units, Holes 807A and 807C.

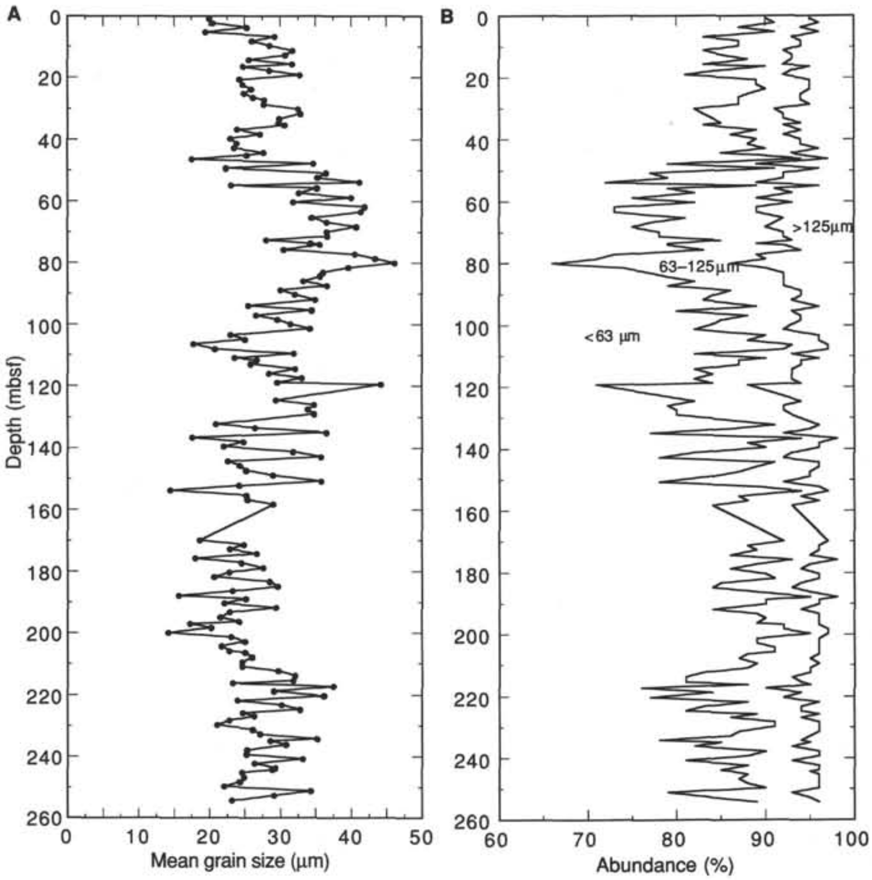

Figure 5. **A.** Mean grain size of Subunit IA sediments, Hole 807A. **B.** Coarse (>125 μm), intermediate (63–125 μm), and fine (<63 μm) fraction abundances, Subunit IA, Hole 807A.

and average 1–2 mm in thickness. In the upper part of Subunit IB, the bands have planar outlines and are closely spaced (Fig. 11). Below 700 mbsf, however, the color bands are developed either as gray microstylolitic swarms or as wavy, braided patterns of thin bands that grade to diagenetic flaser structures (Fig. 12) or dissolution seams (Fig. 13).

Bioturbation is pervasive in Subunit IB. The evidence includes mottling in shades of white, trace fossils (e.g., *Zoophycos*) (Fig. 14), disseminated pyrite, and rare pyritized burrow linings. Burrows commonly become more flattened with increasing depth. Where thin color bands and bioturbation structures intersect, color bands are continuous throughout (and so postdate) the bioturbation structures (Fig. 15).

Unit II

Intervals: Hole 807C, Core 130-807C-27R through Section 130-807C-71R-3, 45 cm
Age: middle Eocene–late Campanian
Depth: 968–1351.4 mbsf

Unit II is dominated by limestone and chert but also contains nannofossil chalk and nannofossil chalk with foraminifers. Unit II was divided into two subunits. Subunit IIA (968–1098 mbsf) was primarily recovered as chert and nannofossil chalk to nannofossil chalk with foraminifers, but limestone and silicified limestone are present as minor constituents below 1006 mbsf. Subunit IIB (1098–1351.4 mbsf) is predominantly limestone,

Table 3. Summary statistics for sedimentary parameters, Site 807.

Subunit	Mean size	Sand (%)	Silt (%)	Clay (%)	>125 μm (%)	63–125 μm (%)	Foraminifers (%)	$CaCO_3$ (%)
IA:								
Mean	28.3	14.9	79.9	5.1	6.0	9.0	22	92
Sigma	6.2	5.4	5.8	2.9	2.2	3.5	8	1.7
N	170	170	170	170	170	170	59	170
IB:								
Mean							17	93
Sigma							8	23
N							54	223

Notes: Mean grain size is reported in microns. Mean size and sand, silt, and clay (>125 and 63–125 μm fraction) abundances are from shipboard grain-size analyses. Foraminifer contents are from smear slide estimates. Carbonated contents are from shipboard carbonate analyses. *N* = number of analyses.

Table 4. Grain-size data for sediments in Subunit IA, Hole 807A.

Core, section, interval (cm)	Depth (mbsf)	Mean	Sand (%)	Silt (%)	Clay (%)	>125 μm (%)
130-807A-						
1H-1, 95	0.95	20.0	10	78	13	95
1H-2, 95	2.45	20.5	9	81	9	96
1H-3, 95	3.95	25.3	13	79	8	94
1H-4, 95	5.45	19.5	9	87	5	96
1H-5, 95	6.95	29.2	17	78	6	93
2H-1, 95	8.35	26.0	13	80	7	94
2H-2, 95	9.85	28.5	13	85	1	94
2H-3, 95	11.35	31.7	17	77	6	92
2H-4, 95	12.85	30.7	15	78	7	93
2H-5, 95	14.35	25.6	12	88	2	93
2H-6, 95	15.85	31.7	17	78	6	92
2H-7, 18	16.58	24.8	10	83	6	95
3H-1, 95	17.85	28.5	15	81	6	93
3H-2, 95	19.35	32.8	19	77	5	92
3H-3, 95	20.85	24.3	11	80	8	95
3H-4, 95	22.35	24.7	11	81	7	95
3H-5, 95	23.85	25.9	10	87	2	95
3H-6, 95	25.35	24.9	12	81	8	94
3H-7, 64	26.54	26.2	13	80	7	94
4H-1, 95	27.35	27.8	13	81	6	94
4H-2, 95	28.85	27.7	13	87	1	95
4H-3, 95	30.35	32.5	18	76	6	91
4H-4, 95	31.85	32.9	17	76	7	92
4H-5, 95	33.35	29.9	16	78	7	92
4H-6, 95	34.85	29.8	15	83	1	94
4H-7, 10	35.50	30.6	17	76	6	92
5H-1, 109	36.99	23.9	11	86	3	94
5H-2, 110	38.50	27.1	14	85	1	92
5H-3, 109	39.99	23.0	11	86	4	94
5H-4, 109	41.49	23.9	11	87	1	94
5H-5, 109	42.99	23.5	10	82	8	96
5H-6, 109	44.49	27.7	15	78	7	93
5H-7, 30	45.20	25.3	11	86	3	94
6H-1, 109	46.49	17.6	6	92	2	97
6H-2, 112	48.02	34.7	21	70	10	89
6H-3, 111	49.51	22.4	9	90	1	96
6H-4, 110	51.00	36.5	23	71	6	92
6H-5, 111	52.51	35.3	21	78	1	92
6H-6, 111	54.01	41.2	28	68	3	89
6H-7, 70	55.10	23.1	11	87	2	96
7H-1, 110	56.00	35.2	21	76	2	91
7H-2, 110	57.50	32.6	18	78	3	93
7H-3, 110	59.00	40.0	25	69	5	89
7H-4, 110	60.50	31.8	18	75	7	93
7H-5, 110	62.00	41.9	27	68	5	89
7H-6, 110	63.50	41.4	27	67	6	89
8H-1, 110	65.50	34.5	19	78	2	92
8H-2, 110	67.00	36.6	23	72	6	91
8H-3, 110	68.50	40.8	25	68	6	90
8H-4, 110	70.00	36.6	22	76	1	92
8H-5, 110	71.50	36.7	22	76	1	92
8H-6, 85	72.75	28.0	15	74	10	93
8H-7, 45	73.85	34.3	21	70	10	89
9H-1, 35	74.25	35.6	21	72	6	92
9H-2, 35	75.75	30.5	17	81	2	94
9H-3, 35	77.25	40.6	27	67	6	89
9H-4, 35	78.75	43.4	29	66	5	90
9H-5, 35	80.25	46.2	34	63	4	86
9H-6, 35	81.75	39.6	26	69	6	90
9H-7, 35	83.25	36.1	23	71	6	92
10H-1, 109	84.49	35.6	21	74	4	92
10H-2, 109	85.99	33.3	18	77	5	92
10H-3, 109	87.49	36.6	21	79	0	92
10H-4, 109	88.99	30.0	14	79	6	94
10H-5, 109	90.49	32.1	16	82	0	94
10H-6, 109	91.99	35.0	17	76	6	93
11H-1, 109	93.99	25.5	11	85	3	96
11H-2, 108	95.48	34.5	20	74	6	93
11H-3, 108	96.98	26.6	12	81	7	94
11H-4, 107	98.47	29.6	15	85	1	94
11H-5, 107	99.97	31.5	16	78	6	93
11H-6, 107	101.47	34.2	18	78	5	92
12H-1, 106	103.46	23.0	10	89	1	96
12H-2, 107	104.97	25.0	12	86	2	96
12H-3, 107	106.47	17.8	7	92	2	97
12H-4, 116	108.06	20.8	8	91	1	97

Table 4 (continued).

Core, section, interval (cm)	Depth (mbsf)	Mean	Sand (%)	Silt (%)	Clay (%)	>125 μm (%)
12H-5, 110	109.50	31.9	18	82	1	93
12H-6, 106	110.96	23.5	10	89	0	96
12H-7, 22	111.62	26.7	13	82	4	94
13H-1, 107	112.97	25.8	13	78	9	94
13H-2, 107	114.47	32.1	18	74	6	93
13H-3, 107	115.97	28.4	16	77	7	93
13H-4, 107	117.47	33.1	18	81	1	93
13H-5, 107	118.97	29.6	16	79	5	94
13H-6, 10	119.50	44.2	29	68	3	88
14H-3, 31	124.71	29.4	18	75	4	94
14H-4, 31	126.21	34.8	21	73	6	92
14H-5, 31	127.71	33.9	20	75	5	92
14H-6, 31	129.21	34.8	20	76	3	93
15H-2, 121	132.36	20.9	9	86	5	96
15H-3, 109	133.74	26.4	14	80	7	95
15H-4, 109	135.24	36.5	23	72	4	92
15H-5, 109	136.74	17.6	6	87	6	98
15H-6, 109	138.24	24.8	12	82	7	96
15H-7, 109	139.74	22.0	10	82	8	96
16H-1, 108	141.48	31.8	18	81	1	93
16H-2, 108	142.98	35.8	22	71	7	92
16H-3, 108	144.48	22.6	9	83	8	96
16H-4, 108	145.98	24.3	11	81	8	96
16H-5, 108	147.48	25.2	13	80	7	95
16H-6, 123	149.13	29.0	16	76	7	95
17H-1, 100	150.90	35.8	22	71	7	92
17H-2, 100	152.40	24.2	11	80	8	96
17H-3, 100	153.90	14.5	6	94	0	97
17H-4, 100	155.40	25.2	13	79	8	94
17H-5, 100	156.90	25.4	12	81	7	96
17H-6, 100	158.40	29.0	16	78	7	93
19H-1, 103	169.93	18.7	8	84	8	97
19H-2, 103	171.43	24.9	12	80	7	96
19H-3, 103	172.93	22.9	11	82	8	96
19H-4, 103	174.43	26.7	14	79	7	95
19H-5, 103	175.93	18.0	7	83	9	98
19H-6, 103	177.43	24.5	11	82	7	95
20H-1, 55	178.95	27.6	14	79	6	94
20H-2, 55	180.45	22.8	10	89	0	96
20H-3, 55	181.95	20.7	9	85	7	96
20H-4, 55	183.45	28.5	15	80	5	94
20H-5, 55	184.95	29.6	16	82	2	93
20H-6, 55	186.45	23.3	11	83	6	95
20H-7, 55	187.95	15.7	5	85	11	98
21H-1, 100	188.90	25.1	10	88	1	96
21H-2, 100	190.40	22.1	10	87	3	96
21H-3, 100	191.90	29.4	16	78	6	94
21H-4, 100	193.40	22.9	11	79	10	96
21H-5, 100	194.90	21.6	10	81	10	96
21H-6, 100	196.40	24.2	11	89	0	96
21H-7, 10	197.00	17.3	8	79	13	96
22H-1, 100	198.40	20.3	8	91	1	97
22H-2, 100	199.90	14.2	5	83	13	97
22H-3, 100	201.40	23.1	11	81	9	96
22H-4, 100	202.90	25.0	11	82	6	96
22H-5, 100	204.40	21.7	9	81	10	96
22H-6, 100	205.90	22.8	9	86	5	96
22H-7, 10	206.50	25.0	12	86	2	96
23H-1, 106	207.96	26.0	13	88	1	95
23H-2, 110	209.50	24.6	11	88	1	96
23H-4, 111	212.51	29.7	17	76	6	95
23H-3, 108	210.98	24.6	12	81	8	95
23H-5, 109	213.99	32.1	19	81	1	93
23H-6, 110	215.50	31.8	19	74	6	94
23H-7, 50	216.40	23.3	12	76	11	95
24H-1, 109	217.49	37.5	24	71	6	90
24H-2, 109	218.99	29.1	16	77	7	94
24H-3, 109	220.49	36.2	23	76	1	92
24H-4, 109	221.99	24.0	12	81	7	96
24H-5, 109	223.49	30.2	17	82	1	94
24H-6, 109	224.99	32.8	19	76	5	94
24H-7, 50	225.90	24.7	11	86	3	96
25H-1, 105	226.95	26.3	14	81	6	94
25H-2, 105	228.45	22.8	9	84	7	96
25H-3, 105	229.95	21.1	9	89	3	96
25H-4, 105	231.45	26.1	13	81	6	96
25H-5, 105	232.95	27.1	14	79	7	95

Table 4 (continued).

Core, section, interval (cm)	Depth (mbsf)	Mean	Sand (%)	Silt (%)	Clay (%)	>125 μm (%)
25H-6, 105	234.45	35.2	22	73	4	94
25H-7, 15	235.05	28.6	15	84	1	95
26H-1, 105	236.45	30.8	18	76	7	93
26H-2, 105	237.95	25.3	10	84	6	96
26H-3, 105	239.45	25.2	12	87	2	96
26H-4, 105	240.95	33.2	19	81	1	93
26H-5, 105	242.45	26.3	12	81	7	96
26H-6, 105	243.95	29.3	15	79	5	96
26H-7, 10	244.50	28.9	14	81	5	95
27H-1, 43	245.33	24.6	12	82	6	96
27H-2, 43	246.83	24.9	13	83	5	96
27H-3, 43	248.33	24.3	12	84	5	96
27H-4, 43	249.83	22.1	10	82	7	96
27H-5, 43	251.33	34.3	21	76	4	93
27H-6, 43	252.83	29.1	16	80	6	95
27H-7, 43	254.33	23.2	11	84	6	96

although chert is presented as a minor constituent throughout. The boundary between the two subunits is placed at 1098 mbsf, below which limestone dominates.

Subunit IIA

Intervals: Hole 807C, Core 130-807C-27R through -40R
Age: middle Eocene
Depth: 968–1098 mbsf

Recovery from Subunit IIA was low, ranging from 1% to 30%. Approximately 50% of the recovered sediment was chert, but the low recovery hinders an evaluation of the actual abundance of each lithology in the cored interval (Fig. 3). Estimates from the wireline log velocity data indicate a chert content of approximately 20% through Subunit IIA. The chert is gray (N5/ and 5Y 6/1) and apparently nodular, as demonstrated by chalk coatings on outer surfaces and by chalk inclusions, 1 mm to 1 cm in size (Fig. 16). The remainder of the recovered material was approximately 40% nannofossil chalk to nannofossil chalk with foraminifers and 10% limestone.

The chalk is commonly brecciated by drilling, but larger pieces were recovered from 997.0 to 998.1 mbsf (Core 130-807C-30R), from 1006.5 to 1007.1 mbsf (Core 130-807C-31R), from 1044.0 to 1045.0 mbsf (Core 130-807C-35R), from 1063.7 to 1064.0 mbsf (Core 130-807C-37R), and from 1073.2 to 1073.7 mbsf (Core 130-807C-38R). The chalk is white (2.5Y 8/0) and moderately bioturbated. Burrows are commonly flattened and subhorizontal in orientation. Isolated greenish gray (5GY 6/1) and gray (N7/) microstylolitic braided patterns are present, occasionally grading to diagenetic flaser structures.

A few single stylolites, with amplitudes of less than 1 mm, were observed. The white (2.5Y 8/0) limestone and silicified limestone were recovered only as drilling rubble. The chalks, limestones, and silicified limestones are interlayered. XRD analyses indicate that zones of pure calcite, <20 m thick, alternate with zones that are dominated by calcite but also contain cristobalite, quartz, and clay. Carbonate contents indicate a similar pattern of fluctuation through this subunit (Fig. 6C). Evidence for the silicification of chalk by cementation or replacement of microfossils and for calcite cementation and recrystallization is seen in thin section (Figs. 17 and 18).

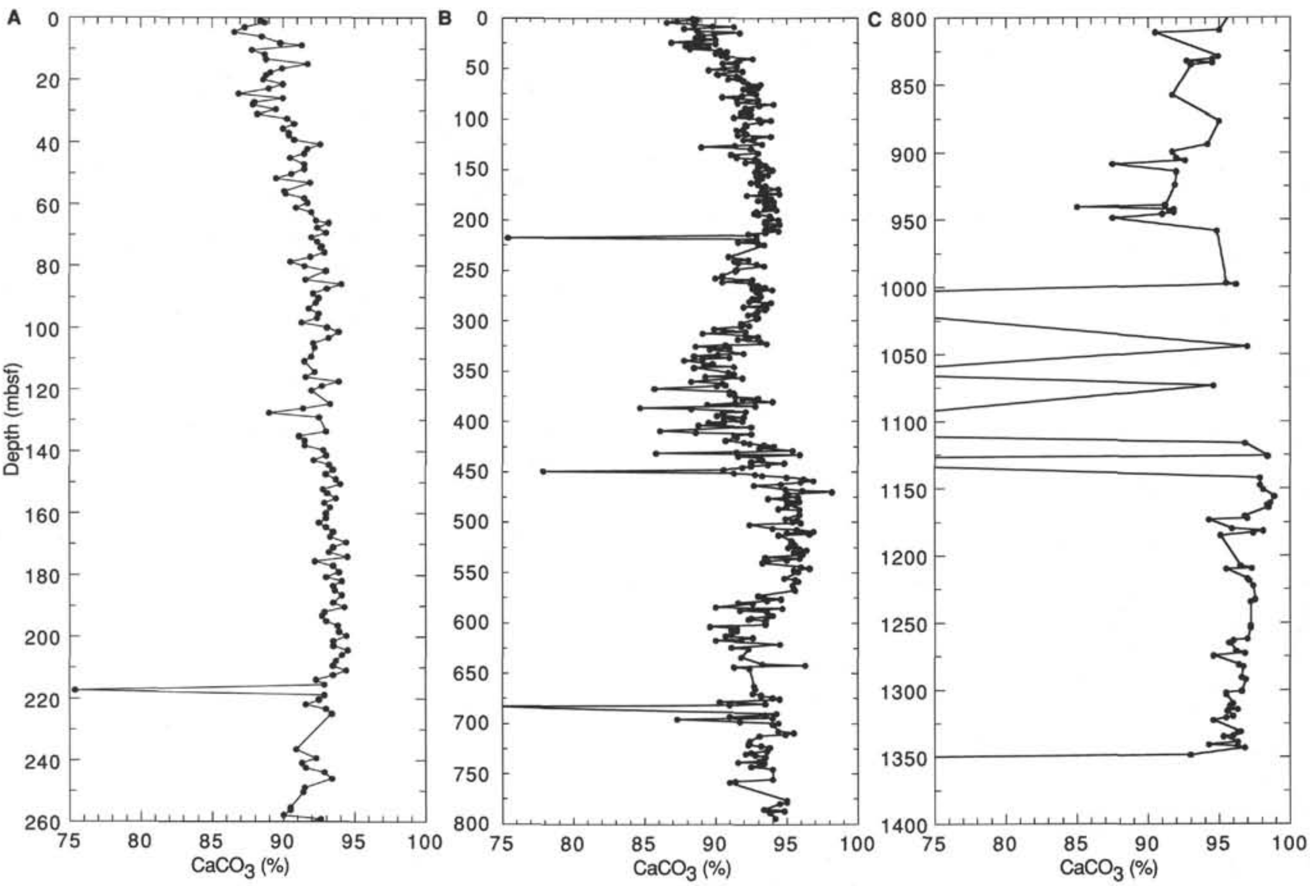

Figure 6. Carbonate contents, Site 807. **A.** Subunit IA, Hole 807A. **B.** Unit I, Hole 807A. **C.** Hole 807C.

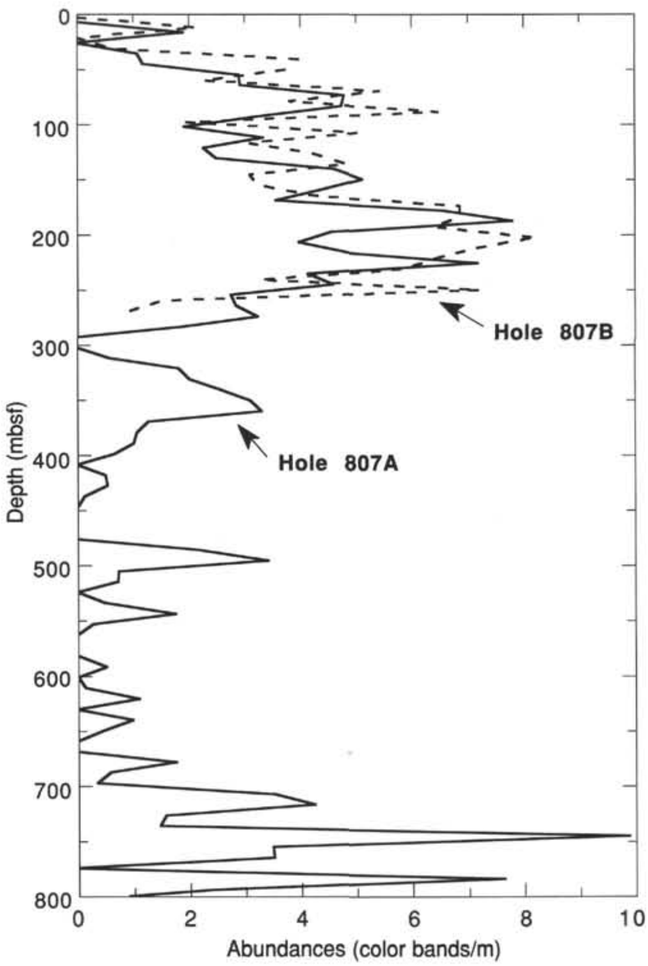

Figure 7. Abundances of color bands, Holes 807A and 807B. The number of color bands has been estimated from core photographs.

Subunit IIB

Intervals: Hole 807C, Core 130-807C-41R through Section 130-807C-71R-3, 45 cm
Age: Eocene to late Campanian
Depth: 1098–1351.4 mbsf

Subunit IIB is composed primarily of limestone (Fig. 3). Smear slide data indicate a transition from material dominated by nannofossils to material dominated by carbonate particles between 1060 and 1140 mbsf (Fig. 4). Silicified limestone is present to a depth of 1140 mbsf and contains abundant cristobalite (and quartz), as indicated by XRD traces. Carbonate contents are low episodically through Subunit IIB, superimposed on a general decrease downhole (Fig. 6C). Only minor clay and quartz are seen in XRD traces of samples taken below 1140 mbsf.

Chert is present as nodules or in layers, up to 7 cm thick, in all cores of Subunit IIB. Chert abundance rarely exceeds 10% of the recovered material, however, and constitutes <5% of the recovered sediment below 1270 mbsf. The chert exhibits various shades of gray and red, including light gray (N6/ and N7/), gray (5Y 5/1, 2.5Y 5/0, and N5/), dark gray (5YR 4/1), reddish gray (5YR 4/2 and 5YR 5/2), weak red (2.5YR 4/2), dusky red (10R 3/3), reddish brown (4YR 4/2 and 5YR 4/3), dark brown (10YR 4/3 and 7.5YR 4/2), brownish gray (10YR 6/2 and 5YR 6/1), grayish blue (5PB 5/2), and dusky blue (5PB 3/2).

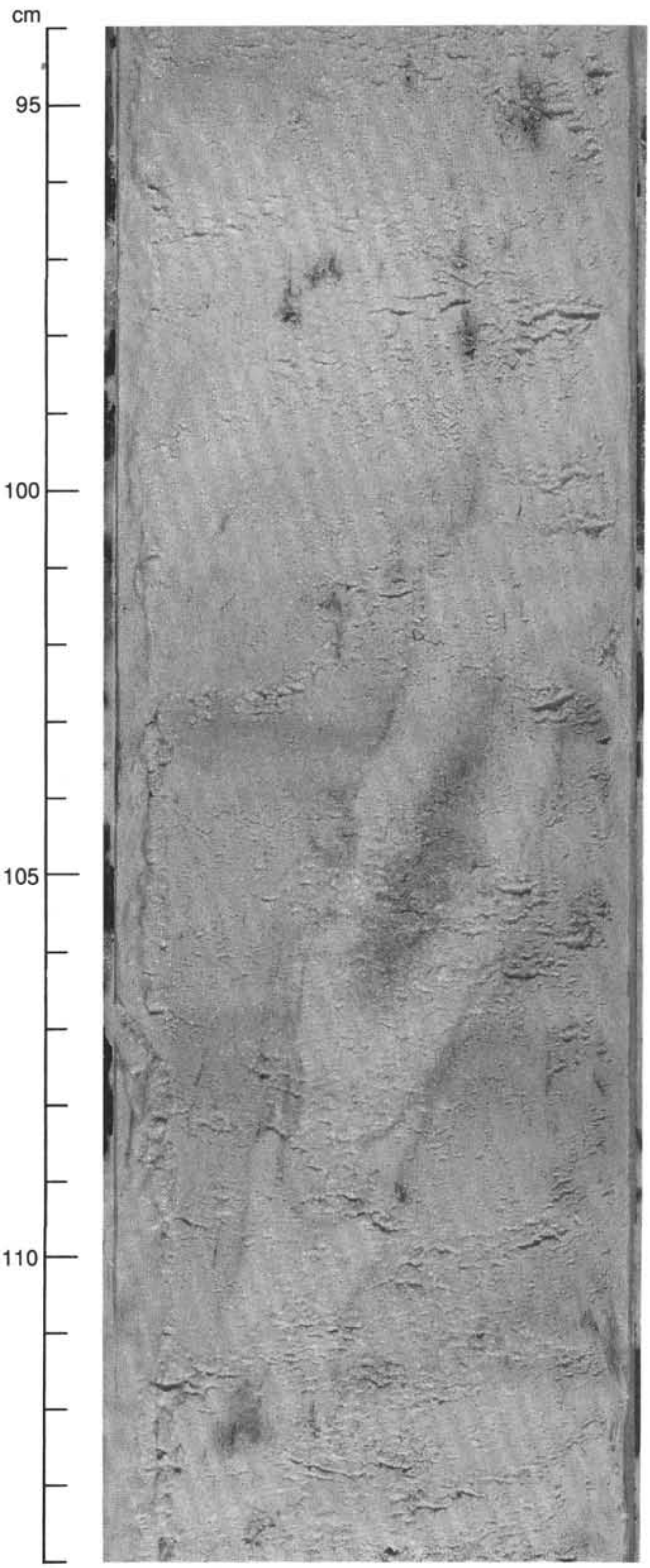

Figure 8. Photograph of color band passing through burrow, Hole 807A (Section 130-807A-25H-2, 94–114 cm; 228 mbsf). Note that redox haloes around the burrow overprint the color bands.

Table 5. Inventory of ash layers, Site 807.

Core, section, interval (cm)	Depth (mbsf)
130-807A-	
67X-CC, 20–23	639.70
70X-5, 110–116	666.33
71X-5, 63–70	675.57
72X-4, 66–69	683.32
72X-4, 94–98	683.66
73X-CC, 56–61	697.50
77X-4, 56–61	731.60
78X-5, 45–47	742.67
80X-3, 48–50	758.71
130-807C-	
47R-1, 40–41	1140.60
50R-1, 14–17	1155.34
52R-3, 67–100	1173.64
54R-1, 40–41	1189.20
54R-1, 63–64	1189.43
54R-1, 138–139	1190.18
54R-2, 13–14	1190.43
54R-2, 16–17	1190.46
54R-2, 60–61	1190.90
54R-2, 70–71	1191.00
54R-2, 83–84	1191.13
54R-2, 115–116	1191.45
54R-3, 27–28	1192.07
54R-3, 134–135	1193.14
55R-1, 27–28	1197.17
55R-1, 87–88	1197.77
66R-1, 102–103	1300.82

At least 15 layers of gray (N4/, N5/, and N5/1) ash are present between 1140 and 1200 mbsf (Table 5). One layer, located at 1156.6 mbsf, is 3 cm thick whereas the other layers are <1 cm thick. Several bioturbated ash layers are present at 1174 mbsf (Core 130-807C-52R; Fig. 19). Diagenesis may have produced flaserlike structures in the ash. At least 10 dark gray (N3/1, 10YR4/1, and 5Y 4/1), brown (7.5YR 3/3), and grayish brown (10YR 4/2) layers of ash and clay, which may be altered volcanic ash, are located between 1300 and 1351 mbsf. Only the layers composed obviously of volcanic glass layers are included in Table 5.

Subunit IIB is predominantly white (2.5Y 8/0, 5Y 8/1, 5YR 8/0, 5YR 8/1, 7.5YR 8/0, 10YR 8/0, and 10YR 8/1) in color with isolated light gray (5Y 7/1) intervals. In the interval between 1116 and 1135 mbsf (Cores 130-807C-44R and -45R), white limestone clasts up to 5 mm in diameter were found. Nannofossils from one such clast at 1127 mbsf are of Late Cretaceous age, whereas nannofossils in the surrounding matrix are a mixture of Paleocene and Cretaceous species. The clasts, therefore, are reworked, older sediments. At approximately the same level, a 5-cm-thick finely laminated bed was composed of only lower Eocene nannofossils. Between 1197 and 1232 mbsf (Cores 130-807C-55R to -58R), 1-mm- to 1-cm-scale bands or pseudolaminae of well-sorted carbonate particles exhibit low-angle truncation surfaces (Fig. 20). Clasts 1–5 cm in diameter are common below 1232 mbsf (Cores 130-807C-59R to -70R). Most of the clasts are white limestone (Fig. 21), but gray limestone clasts become more abundant below 1271 mbsf, and angular green, noncalcareous, clay-rich clasts are present below 1290 mbsf (Fig. 22). Dark brown claystone clasts are common below 1321 mbsf. The clast-bearing intervals alternate with clast-free intervals at a scale of 1 to 5 m. A fold overlying a microfault at 1264 mbsf (Core 130-807C-62R; Fig. 23) underlies a 1-m-thick, graded, clast-bearing interval.

Figure 9. Photograph of bioturbated ash layer, Hole 807A (Section 130-807A-78X-5, 43–48 cm; 743 mbsf).

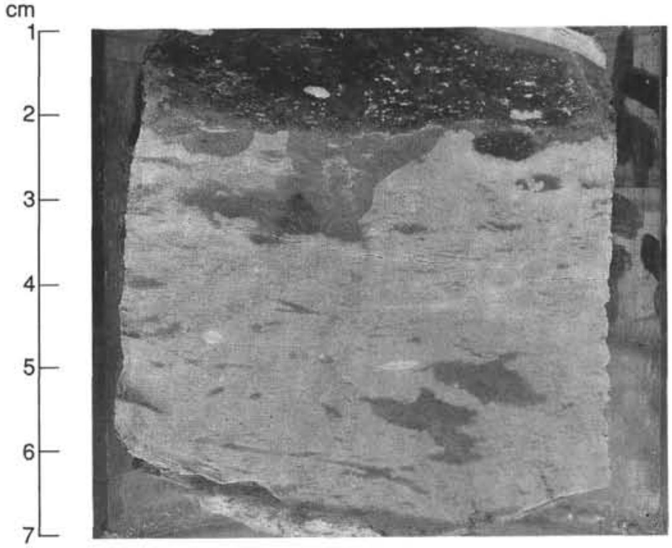

Figure 10. Photograph of chert, probably of nodular origin, Subunit IB, Hole 807C (Section 130-807C-26R-1, 1–7 cm; 960 mbsf).

Stylolites, with up to 5-mm amplitude and dark greenish gray (5G 4/1) or gray (N5/) drapes, are present throughout Subunit IIB (Fig. 24). Differential compaction, possibly of chemical origin, is evident at 1184 mbsf (Section 130-807C-53R-3), where burrows exist as uncompacted lenses in the more heavily compacted, clay-rich matrix (Fig. 25).

An apparently complete K/T boundary section was recovered at approximately 1193.14 mbsf (Section 130-807C-54R-3, 135 cm). This section is composed of limestone and silicified limestone with minor chert, similar to the rest of Subunit IIB; however, the section is notable for the presence of a 0.5-cm-thick ash at the actual position of the K/T boundary (Fig. 26 and Table 5).

Unit III

Intervals: Hole 807C, Section 130-807C-71R-3, 45 cm, through -74R-1, 25 cm
Age: early Cenomanian to Albian-Aptian
Depth: 1351.4–1379.7 mbsf

Unit III consists of upper Albian to lower Cenomanian claystone and siltstone with varying amounts of radiolarians, and Aptian to Albian limestone. The unit is divided into two subunits on the basis of claystone and limestone abundances. Subunit IIIA (1351.4–1369.7 mbsf) contains claystone inter-

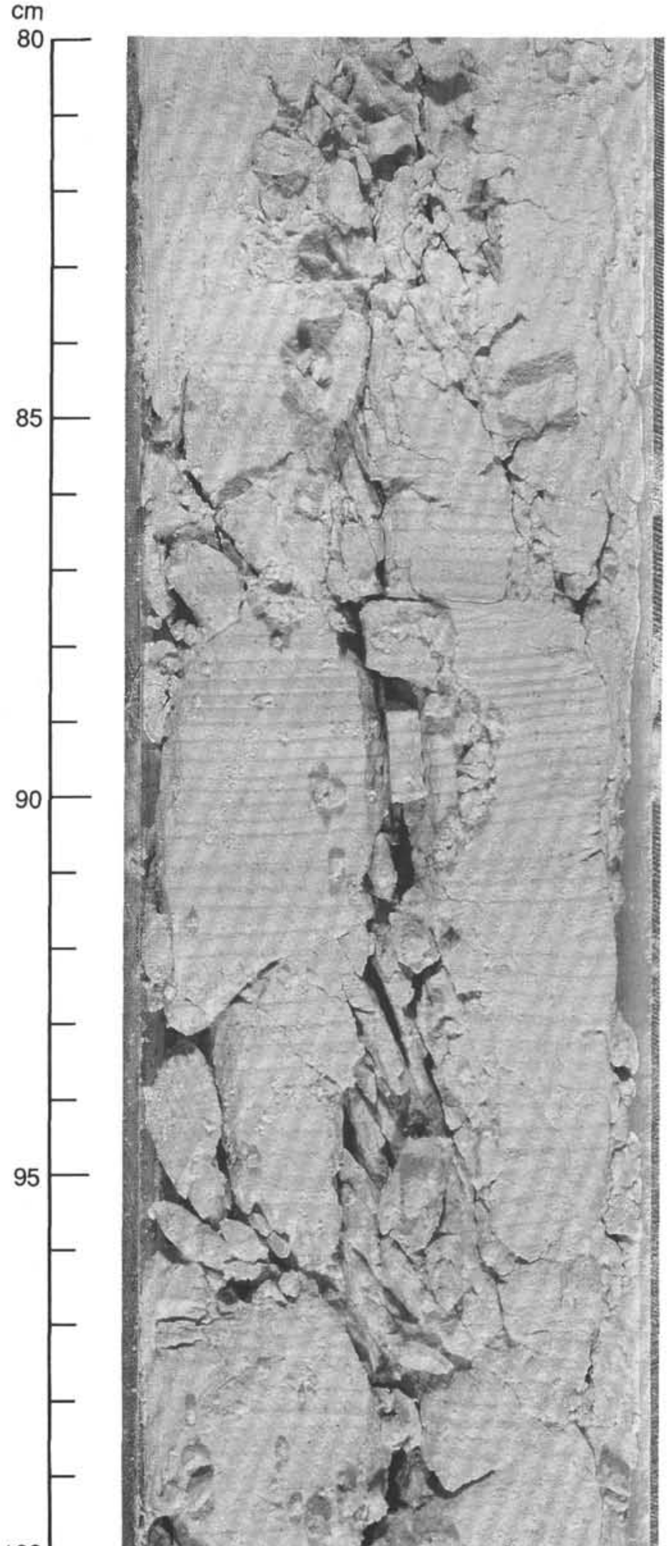

Figure 11. Photograph of thin color bands, Hole 807A (Section 130-807A-34X-6, 80–100 cm; 318 mbsf).

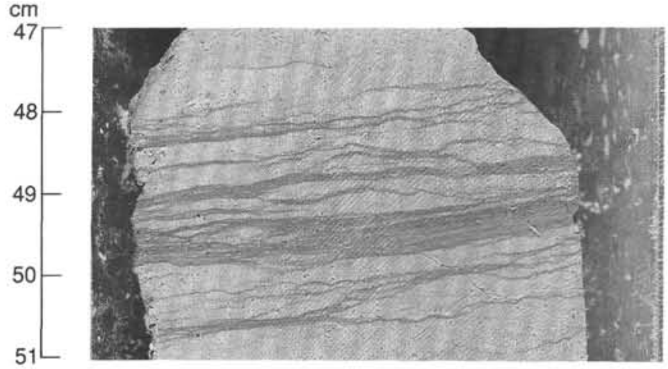

Figure 12. Photograph of a braided swarm of microstylolites in chalk, Subunit IB, Hole 807C (Section 130-807C-12R-1, 47–51 cm, 877 mbsf). These bands exhibit flaser-type structures caused by their wavy, braided appearance and are interpreted as a product of chemical compaction.

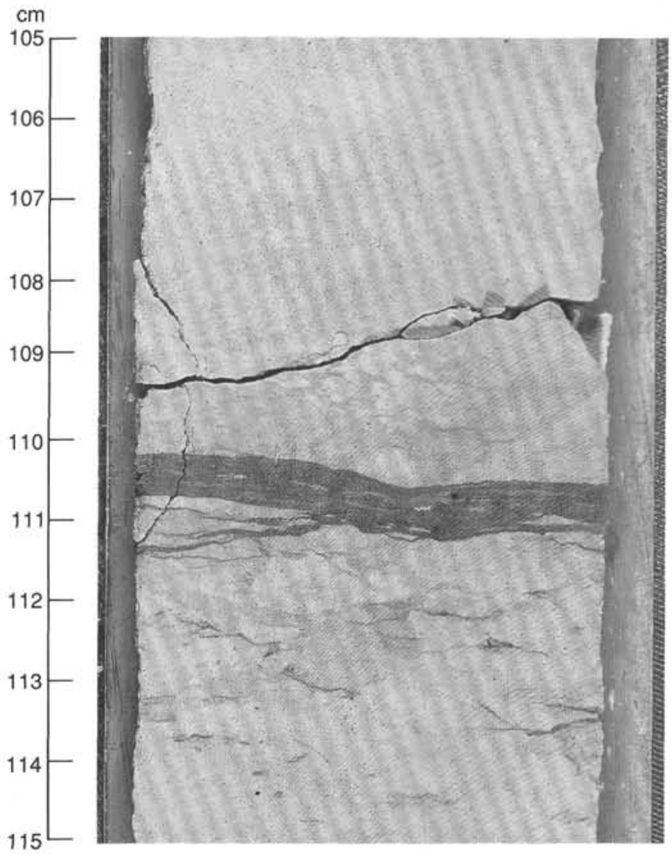

Figure 13. Photograph of microstylolitic dissolution seam, Hole 807C (Section 130-807C-6R-4, 105–115 cm; 834 mbsf). Burrows in the chalk matrix are truncated by dissolution at the seam boundaries.

bedded with siltstone; Subunit IIIB (1369.7–1379.7 mbsf) consists of limestone.

Subunit IIIA

Intervals: Hole 807C, Section 130-807C-71R-3, 45 cm, through -73R-2, 82 cm
Age: early Cenomanian to late Albian
Depth: 1351.4-1369.7 mbsf

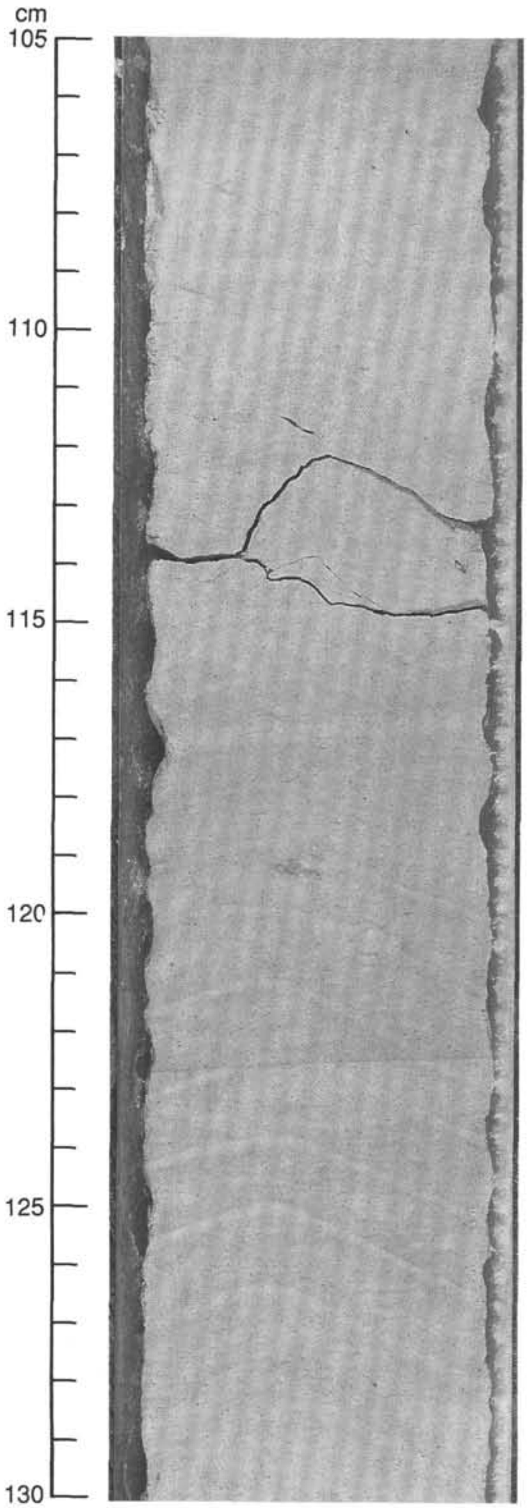

Figure 14. *Zoophycos* burrow, Hole 807C (Section 130-807C-2R-1, 105–130 cm; 791 mbsf). The helical burrow structure is demonstrated by the presence of small traces near the top and wider/thicker traces near the base.

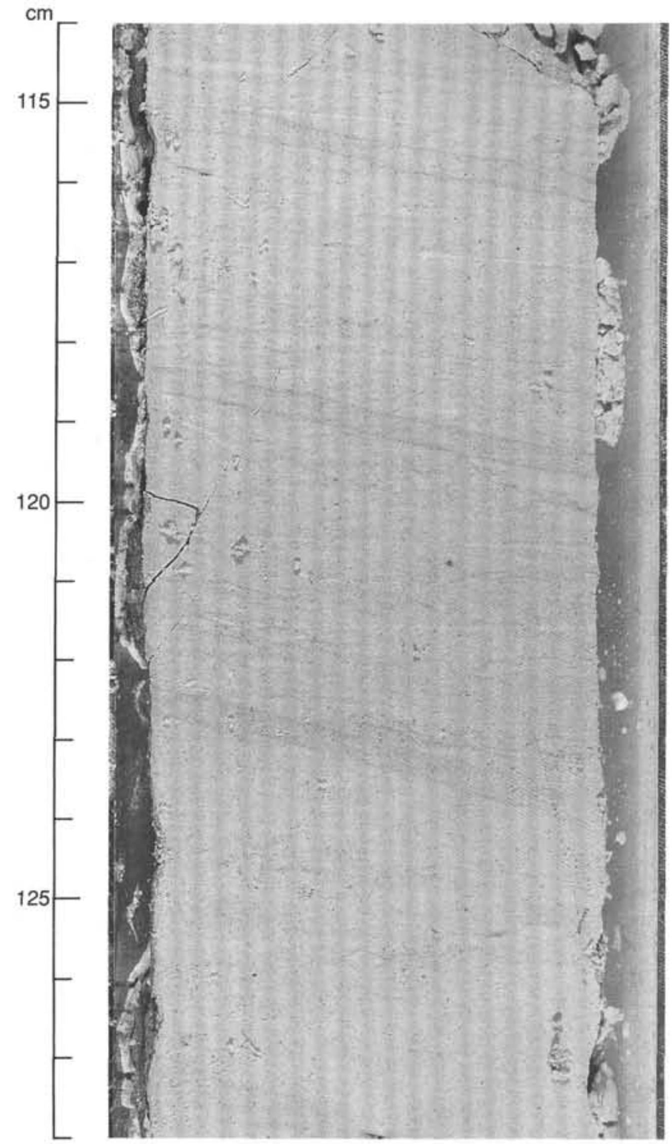

Figure 15. Photograph of very thin (1 mm) horizontal color bands passing through inclined trace fossils, Hole 807A (Section 130-807A-71X-3, 114–128 cm, 659 mbsf).

Subunit IIIA contains claystone, siltstone with radiolarians, radiolarian siltstone, and radiolarian sandy siltstone. The claystone is predominantly very dark grayish brown (10YR 3/2), but reddish brown (5YR 4/4) and black (10YR 2/1, 10YR 3/1) intervals are also present. Isolated heavily bioturbated intervals are indicated by mottling and burrows as large as 2 cm in diameter. XRD analyses indicate the presence of quartz, illite, and feldspar in the claystones.

The siltstone interbeds are pale blue green (5BG 7/2), reddish brown (5YR 4/4), pink (7.5YR 7/4), pinkish gray (7.5YR 7/2), light gray (N7/), grayish brown (10YR 5/2), gray (10YR 6/1), and light brownish gray (10YR 6/2). The radiolarian content of the siltstones increases downcore. XRD analyses indicate that quartz is the major component of the siltstones and that cristobalite is present. Siltstone beds are rare at the top of Subunit IIIA and become more abundant with depth. The downcore increase in siltstone frequency produces an overall upward-fining sequence in Subunit IIIA. The contacts between the claystone and siltstone intervals are pre-

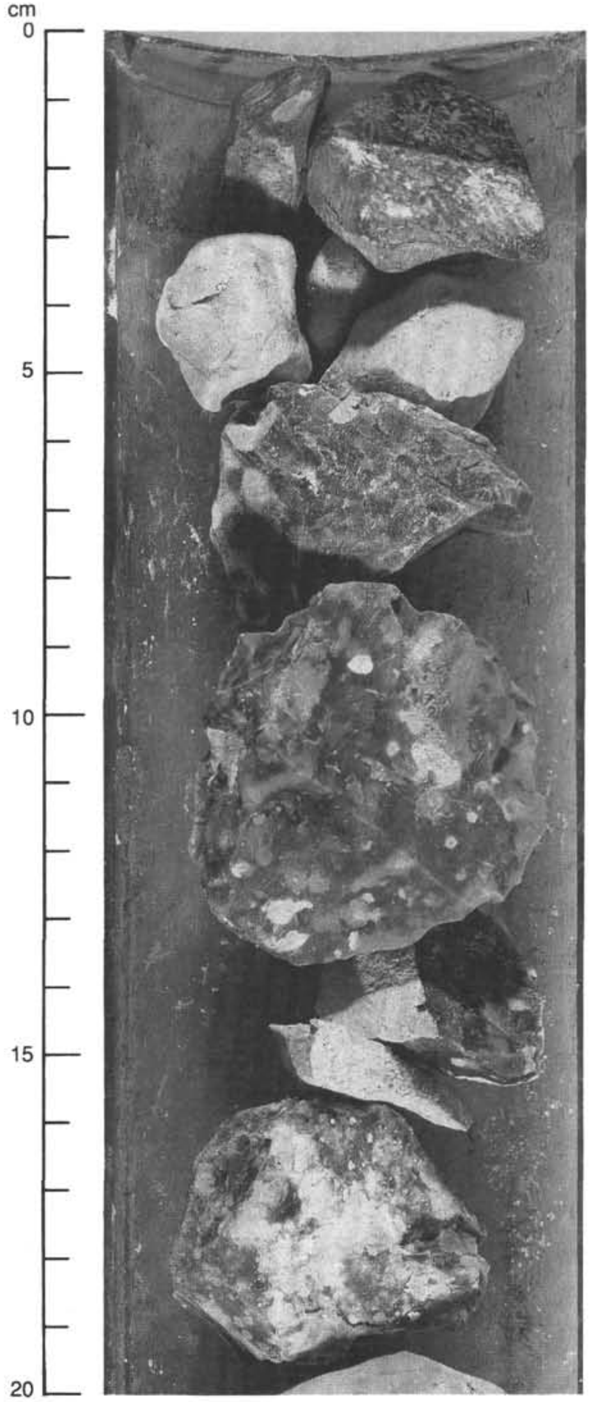

Figure 16. Photograph of chert, probably of nodular origin, Subunit IIA, Hole 807C (Section 130-807C-33R-1, 0–20 cm, 1026 mbsf).

dominantly gradational, but sharp contacts and graded bedding also are present. Wavy contacts are common, producing wavy, lenticular, and flaser bedding. Limited evidence of scouring or loading was observed (Figs. 27 and 28).

Subunit IIIB

Intervals: Hole 807C, Section 130-807-73R-2, 82 cm, through -74R-1, 25 cm
Age: Early Cretaceous, Albian-Aptian
Depth: 1369.7–1379.7 mbsf

Subunit IIIB is composed of bioturbated limestone. Limestone was recovered in the interval from 1369.7 to 1375.7 mbsf, but a distinct decrease in drilling rate at 1379.7 mbsf suggests that the latter depth is the contact between limestone and basalt. The limestone is gray (10YR 6/1) to light gray (10YR 7/2) in color. The upper part of the recovered section contains vertical, very fine, anastomosing fractures, whereas the lower part of the section contains pervasive wavy and lenticular bedding on a scale of 0.5 to 3 cm, as well as microfaults and abundant healed tensional cracks (Fig. 28). Both intervals contain black (2.5Y 2.5/0) to dark gray (N/5) chert, apparently of nodular origin.

Two limestone beds were recovered as interlayers in the basalt. The upper bed (Section 130-807C-80R-1, 70–120 cm) is white (10YR 8/1 to 10YR 8/2) interbedded with dark reddish brown (5YR 3/3) to reddish brown (5YR 4/3) vitric tuff, and contains numerous healed fractures. XRD analyses indicate that the lower, olive brown (2.5Y 4/4) clayey limestone (Section 130-807C-82R-3, 72–79 cm) also contains quartz and illite/glauconite.

Discussion

The sediments overlying basalt at Site 807 consist of 10 m of limestone (Subunit IIIB), overlain by 18 m of siliciclastic sediments (Subunit IIIA) and 1351 m of carbonate sediments (Units II and I). The basal limestone of Early Cretaceous age overlies basalt directly without a metalliferous interbed, indicating a hiatus of unknown duration. The wavy and lenticular bedding of the limestone (Fig. 28) may be primary depositional structures, but diagenetic alteration of burrowed pelagic sediment can produce similar structures.

The radiolarian-bearing nature of the upper Albian to lower Cenomanian claystone and interbedded siltstones that directly overlie the limestone indicates the marine origin of these siliciclastics. The upward fining of these sediments, their interbedded pattern, and the sedimentary structures seen (Figs. 27 and 28) indicate the importance of repeated mass transport events during the deposition of these sediments.

The overlying carbonates span the period from the late Campanian to the present. At Site 803, the early Late Cretaceous to middle Eocene is represented by a 4.5-m-thick siliciclastic interval at a depth of 621.8–626.3 mbsf, corresponding to a depth of approximately 4020 m below the present sea level. At Site 807, the same time interval is represented by more than 200 m of carbonate sediments, the base of which is approximately 4150 m below the present sea level. At Site 807, the K/T boundary is located in carbonate sediments that are 4000 m below the present sea level, whereas at Site 803 the K/T boundary is present in siliclastic sediments that are 4020 m below the present sea level. The apparent difference in the late Campanian to Maestrichtian carbonate-compensation depth (CCD) deduced from these depth values may be explained by post-Cretaceous tectonic movement of Site 807 relative to Site 803. On seismic sections, Site 807 is seen to be located on down-dropped basement, so that Site 807 may have been shallower than Site 803 for part of the time since the late Campanian.

The carbonate sediments of Site 807 were divided into two units based on the degree of diagenesis. Limestone and chert dominate Unit II, whereas only minor chert and porcellanite were found in the chalks and oozes of Unit I. The transition from chert-rich Unit II to chert-poor Unit I at 968 mbsf is also reflected in a marked upsection increase in dissolved silica in the pore water (see "Inorganic Geochemistry" section, this chapter; Fig. 47). An equivalent lithologic boundary was defined at approximately the same depth at nearby Site 289 (Shipboard Scientific Party, 1975b). Unit II is further subdi-

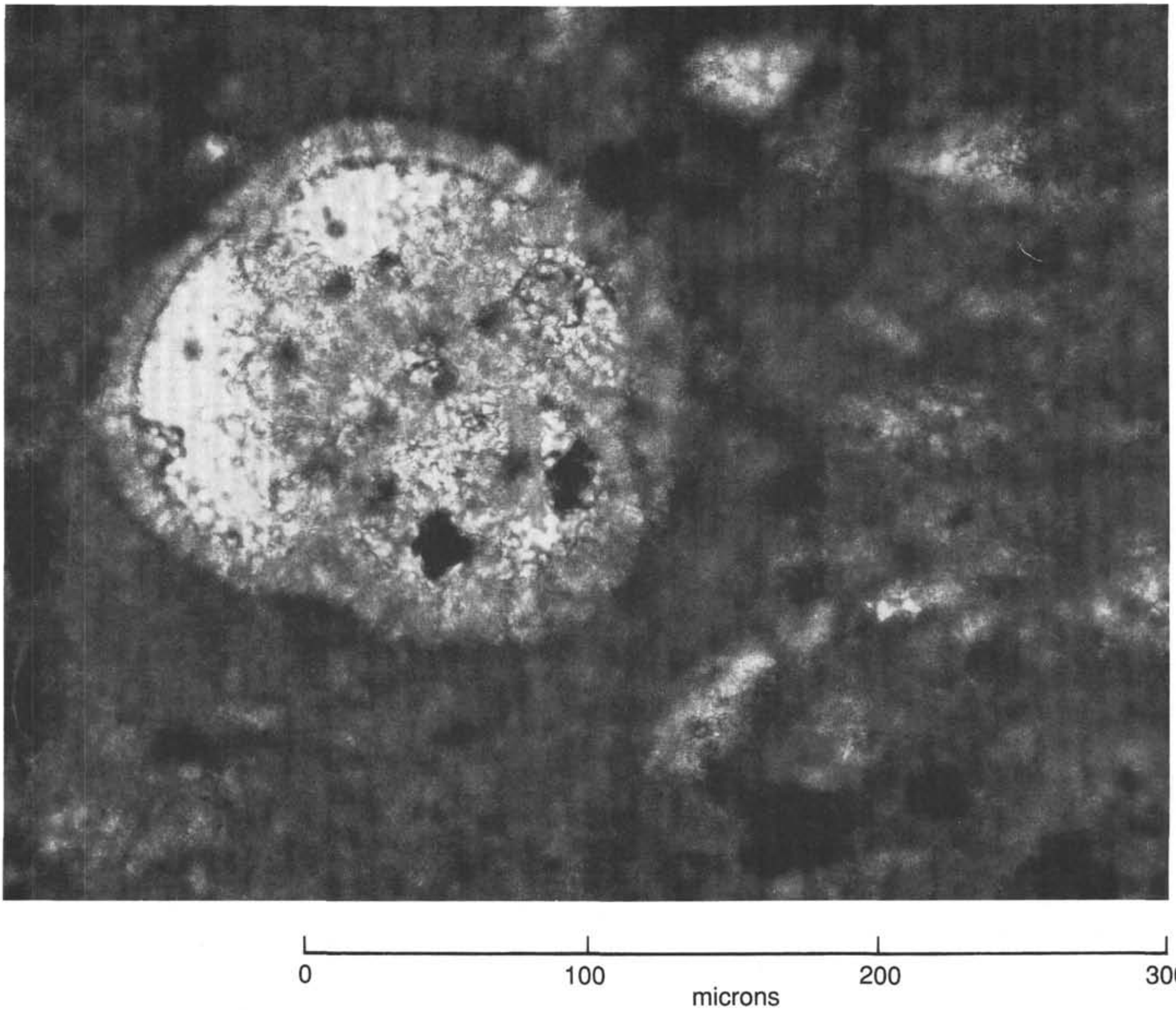

Figure 17. Photomicrograph of silicified chalk, illustrating cementation and/or replacement of microfossils by silica, Hole 807C (Section 130-807C-41R-1, 47 cm; 1098 mbsf).

vided into the 253-m-thick Subunit IIB, which consists of limestone with a low chert content, and the 130-m-thick Subunit IIA, which is composed predominantly of chert and chalk. The extent of carbonate recrystallization decreases upsection.

The interbedded and graded clast-bearing intervals in the lower 120 m of Subunit IIB and the presence of a fold at 1264 mbsf beneath a 1-m-thick, graded, clast-bearing interval indicate mass movement events and deposition. The claystone clasts, which are common in the lower 30 m, may have been derived from deposits equivalent to the siliciclastic rocks of Subunit IIIA. The angular green clasts in the lower 60 m are probably altered fragments of basalt. The presence of these mass-flow deposits may indicate that Site 807 was already partially downfaulted in the late Campanian. The overlying, 35-m-thick limestone interval contains laminae of well-sorted carbonate particles; those laminae may be primary sedimentary structures. Some of the bands include low-angle truncation surfaces and may have been produced by winnowing during deposition. The upper 100 m of Subunit IIB is composed of bioturbated limestone, which probably originated as pelagic carbonate sediment with isolated interbeds of mass-flow deposited material.

The low recovery in the overlying 130 m of middle Eocene Subunit IIA complicates the interpretation of its depositional history. The interval may be a sequence of pelagic carbonates with a generally high initial content of siliceous material that subsequently acted as the source material for chert formation.

Unit I is an apparently continuous, 968-m-thick sequence of well-preserved biogenic carbonate deposited from the late Eocene to the Pleistocene. The principal lithologic characteristics of Unit I, such as mean grain size, foraminifer abundance, and carbonate content, reflect changes in carbonate productivity, dissolution, winnowing, dilution, and climate change. Detailed shore-based study is required to resolve the relative influences of these processes. A further influence on the long-term changes in Unit I composition is the plate-tectonic drift of Site 807 northwestward through the equatorial

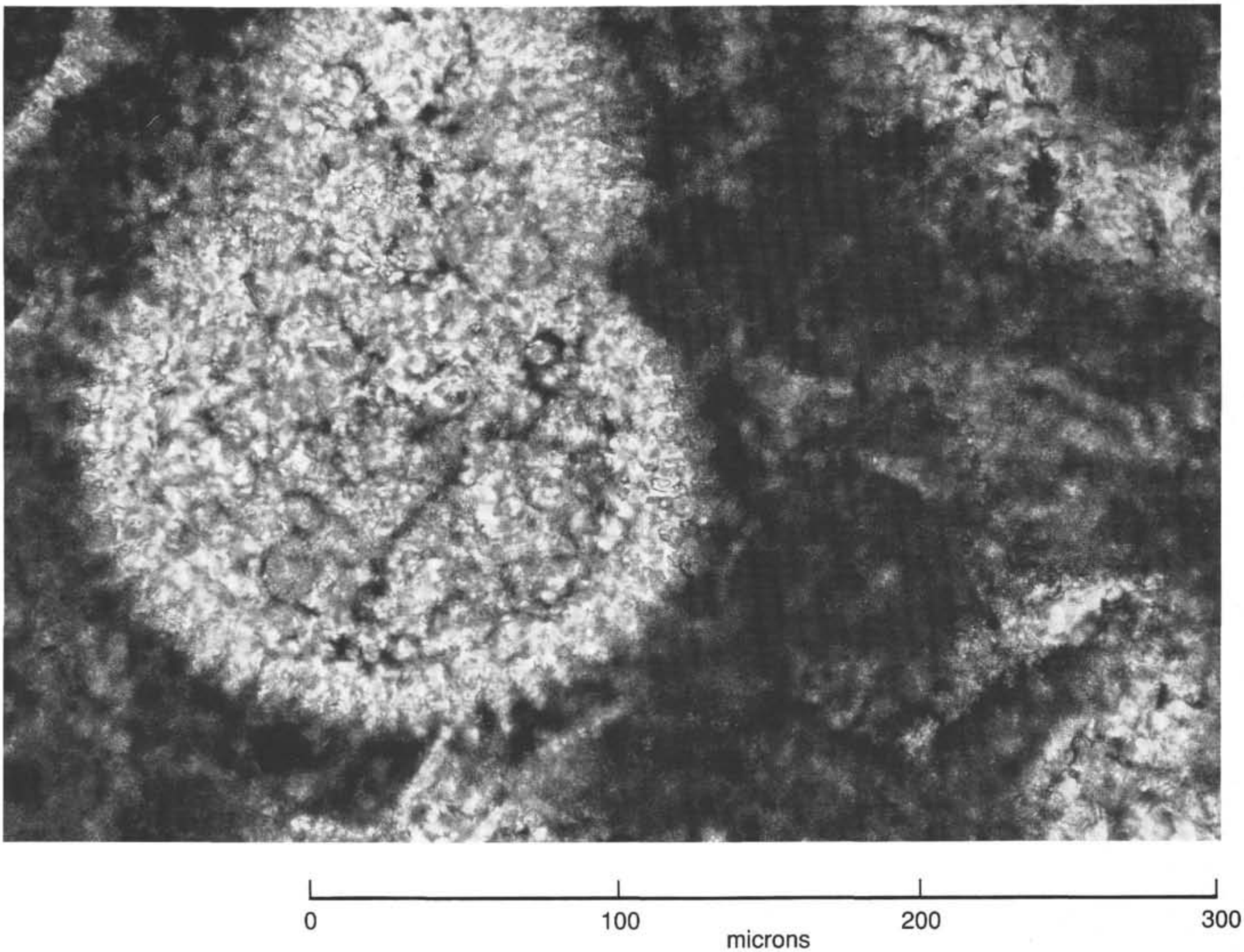

Figure 18. Photomicrograph of material from the chalk-limestone transition zone, Hole 807C, illustrating the effects of calcite cementation and/or recrystallization (Section 130-807C-45R-1, 45 cm; 1126 mbsf).

high-productivity zone, which is presently confined within 1° of the equator.

The lithologic characteristics of Subunit IA at the Leg 130 sites provide preliminary evidence for long-term changes in the depth-related carbonate dissolution gradient, as well as the latitude-related productivity gradient, in the western tropical Pacific Ocean. The decrease in mean grain size from Sites 806 and 807, which are well above the lysocline, to Site 805, at a lysoclinal water depth of 3188 m, probably reflects an increase in carbonate dissolution with depth (Fig. 29). The effects of dissolution also explain some of the decrease in sedimentation rates with increasing water depth (see "Sedimentation Rates" section, this chapter, as well as in the chapters for Sites 803 through 806, this volume). As a result, temporal changes in the gradient of mean grain size with water depth may record temporal changes in the carbonate dissolution gradient.

At the same time, contrasts between sedimentation rates at Sites 806 and 807 hold promise for resolving changes in productivity in the western equatorial Pacific upwelling zone. For example, foraminifer abundances, mean grain sizes, and carbonate contents in Subunit IA at Sites 806 and 807 are very similar (Fig. 29), suggesting that carbonate dissolution at Site 807 is not significantly greater than at Site 806. The sedimentation rates for Subunit IA at Site 807 are only 70% of those at Site 806, however. Because the decrease in sedimentation rate cannot be explained by a significant dissolution gradient between Sites 806 and 807, the difference in sedimentation rate may be driven predominantly by greater productivity at Site 806. This hypothesis is consistent with present productivity patterns in the western equatorial Pacific Ocean, which show that Site 806 is located within a narrow belt of high productivity whereas Site 807 is located just north of this belt (Berger, 1989). A further complication is that the two sites, which are widely separated on the Ontong Java Plateau, may have different winnowing histories.

A comparison of the ooze-chalk transformation at Site 807 with the ooze-chalk transformations at the other Leg 130 sites provides insight into the carbonate lithification process (Fig. 30). The ooze-chalk transition at Site 807 is evident over a 60-m interval, from 252 to 312 mbsf, with the critical change placed at 293 mbsf (near the middle/late Miocene boundary). This pattern is consistent with a trend established from Sites 803 to 806, which shows that the depth of the ooze-chalk transition decreases and the age of the transition increases as

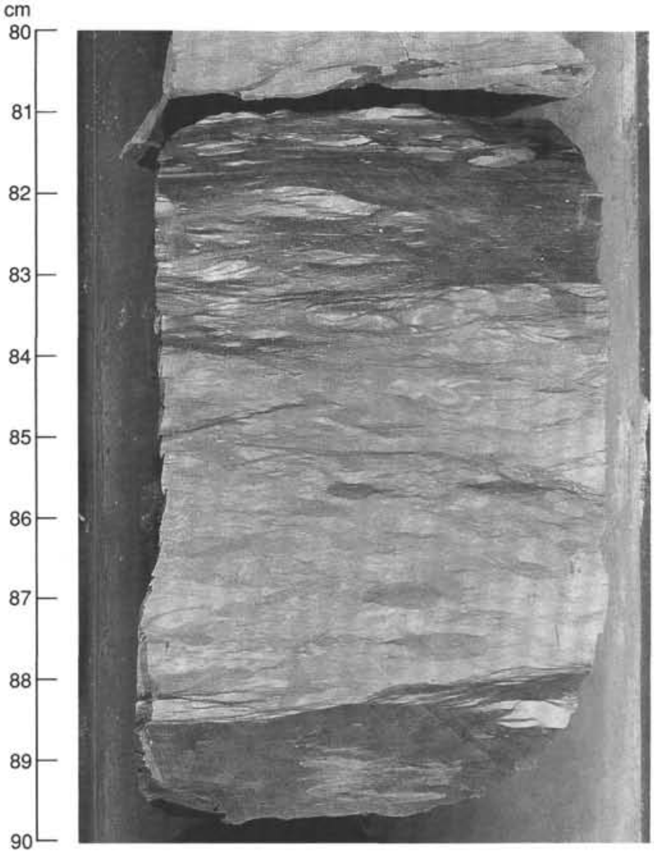

Figure 19. Bioturbated ash(?) layers, Hole 807C (Section 130-807C-52R-3, 80–90 cm, 1174 mbsf). The wispy ("flaser") structures suggest recrystallization and possible chemical compaction.

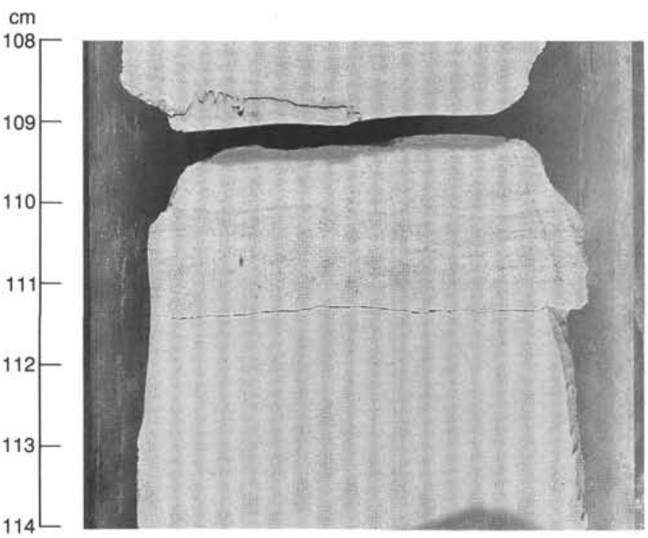

Figure 20. Zone with wispy laminae of well-sorted carbonate particles, Hole 807C (Section 130-807C-56R-2, 108–114 cm; 1209 mbsf).

water depth increases. In general, this suggests that the depth of the transition is strongly influenced by burial depth and age, and that a decrease in the depth of burial can be overcome by the increased time allowed for the diagenetic process. More detailed comparisons between these sites should identify other factors that affect the rate of conversion from ooze to chalk. These factors may include the increasing effects of carbonate dissolution at increasing water depth, as well as variations in the mass wasting and winnowing histories with water depth.

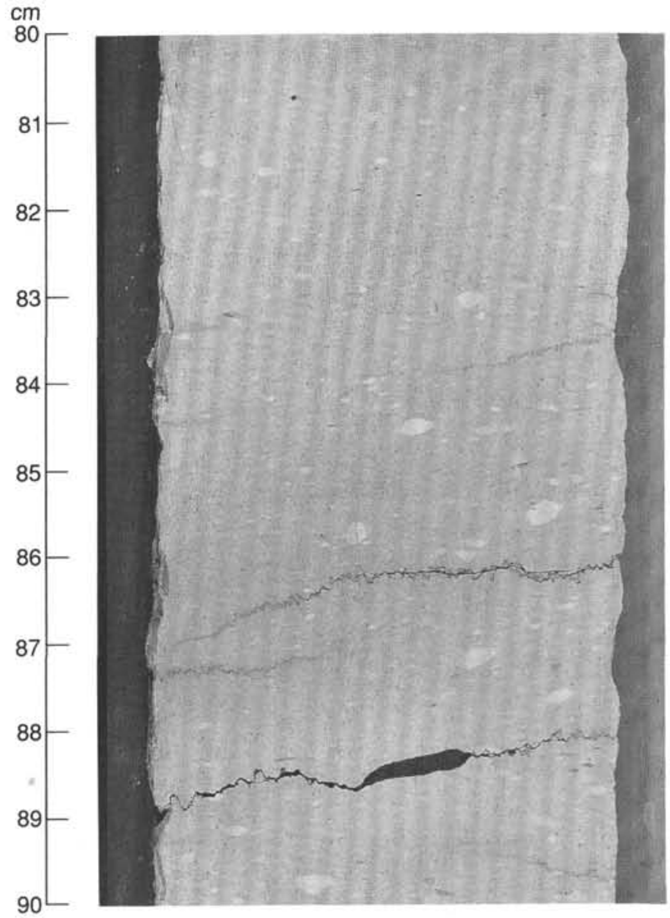

Figure 21. Clast-bearing limestone, Hole 807C (Section 130-807C-59R-2, 80–90 cm; 1235 mbsf). White limestone clasts are dominant, but a single flattened claystone clast is present in the middle of the stylolite at 89 cm.

BIOSTRATIGRAPHY

Introduction

The Neogene section at Site 807 (lithologic Subunit IA and part of Subunit IB) is virtually complete, based on the shipboard analyses of calcareous nannofossils, planktonic foraminifers, diatoms, and radiolarians from core-catcher samples (Fig. 31). However, the sequence is somewhat condensed in the upper part of the lower Miocene. This same interval is absent at Sites 803 and 804 and likewise is thin at Site 805. Microfossil preservation is good to moderate throughout the Neogene for all groups studied, except in the interval from the middle part of the middle Miocene through the lower Miocene where diatom preservation is poor.

All fossil groups are well represented in the Oligocene and upper Eocene chalk (part of lithologic Subunit IB). In contrast to the Neogene, the Paleogene section contains several hiatuses and condensed intervals (see "Sedimentation Rates" section, this chapter). A hiatus or condensed interval is present in the lower part of the upper Oligocene. Two hiatuses are recognized in the middle Eocene. Much of the middle Eocene through Paleocene section is condensed with the

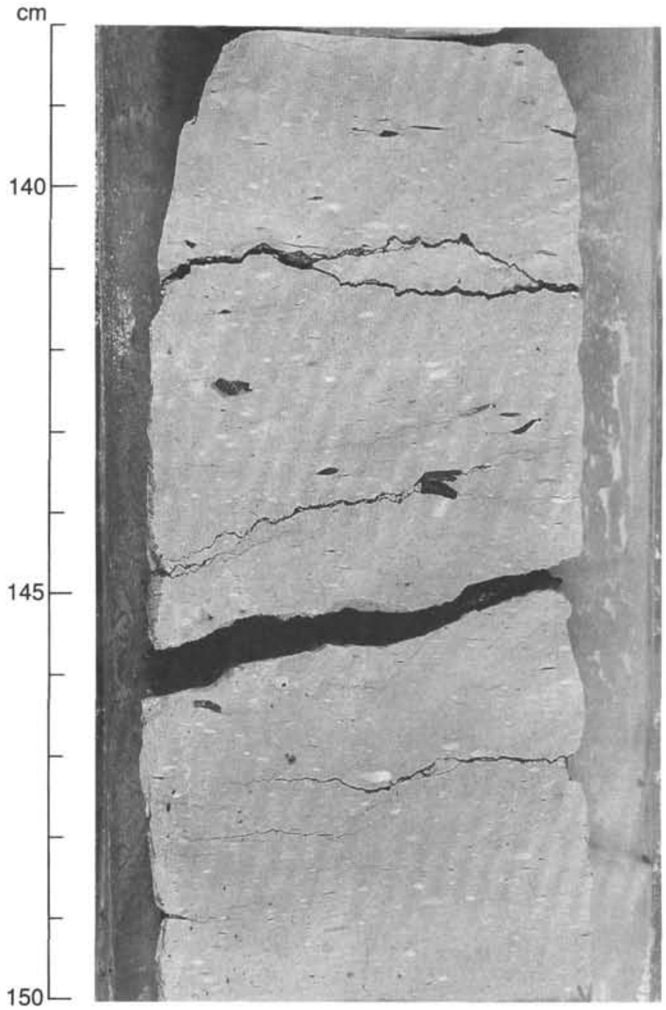

Figure 22. Clast-bearing limestone, Hole 807C (Section 130-807C-68R-2, 138–150 cm; 1322 mbsf). The dark angular fragments are green and probably of basaltic origin.

exception of part of the upper Paleocene (nannofossil Zone NP9). The transition from chalk (lithologic Subunit IB) to chalk and siliceous limestone with chert (lithologic Subunit IIA) occurs at the base of the upper Eocene. Limestones (lithologic Subunit IIB) dominate the lithology of the lower Eocene and Paleocene. As a consequence, the extraction of planktonic foraminifers for shipboard analyses became difficult in sediments older than the late Eocene. Sediments older than latest Eocene are barren of diatoms. Radiolarians occur sporadically through the middle Eocene but are absent in lower Eocene and Paleocene strata at Site 807. Calcareous nannofossils provided the most consistent and reliable shipboard age determinations for the middle Eocene–Paleocene interval.

An apparently complete K/T boundary sequence is preserved in Core 130-807C-54R. The boundary interval is recognized principally on an acme of the calcareous dinoflagellate *Thoracosphaera* in the lower part of Section 130-807C-54R-3 (Table 6). Upper Campanian and Maestrichtian limestones of Site 807 (lithologic Subunit IIB) are barren of siliceous microfossils but generally contain common to abundant populations of poorly preserved calcareous nannofossils. Planktonic foraminifers were successfully extracted from part of the Maestrichtian limestones. Radiolarians provide age controls throughout the sequence of

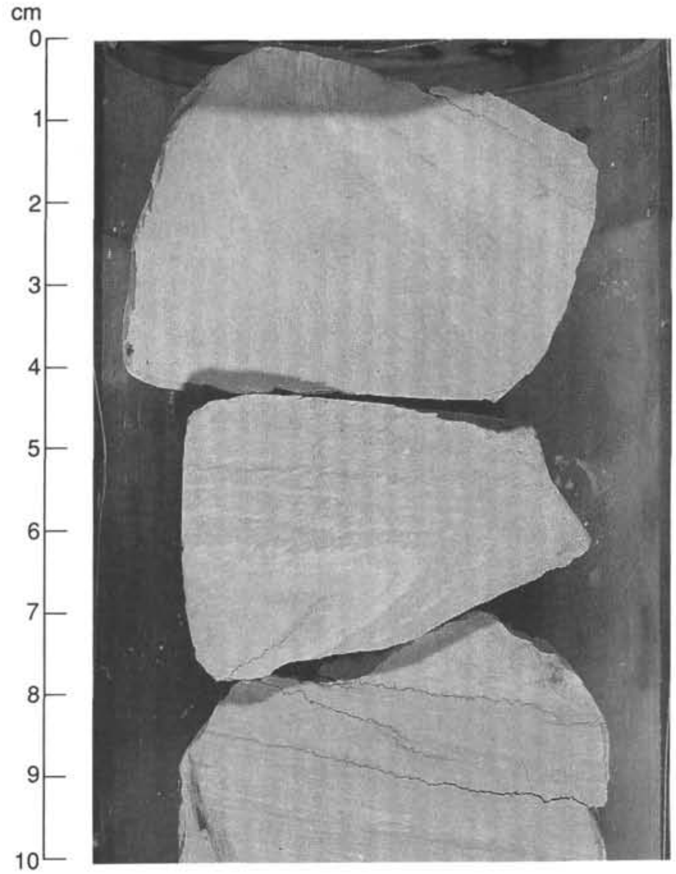

Figure 23. Folded limestone, Hole 807C (Section 130-807C-62R-3, 0–10 cm; 1264 mbsf).

lower Cenomanian–upper Albian brown mudstones (lithologic Subunit IIIA). A hiatus of unknown duration separates the limestones and mudstones. A thin sequence of limestones (lithologic Subunit IIIB) overlies basalt and yields a loosely defined Albian-Aptian age on the basis of calcareous nannofossils and radiolarians.

Calcareous Nannofossils

Hole 807A

The section recovered from this hole ranges in age from late Pleistocene to early Oligocene. Calcareous nannofossils are abundant throughout the core. Preservation is good in the Pleistocene and generally moderate in the remainder of the section, the chief problem being overgrowth of calcite on many discoaster specimens.

Pleistocene

The youngest calcareous nannofossil flora in this hole was observed in Sample 130-807A-1H-CC and belongs to Zones NN21–NN20, where abundant gephyrocapsid specimens occur together with *Calcidiscus leptoporus, Helicosphaera carteri, Syracosphaera pulchra,* and *Umbilicosphaera mirabilis*. Trace amounts of reworked *Calcidiscus macintyrei, Cyclicargolithus floridanus,* and *Discoaster* spp. were also observed in Sample 130-807A-1H-CC. The presence of abundant *Pseudoemiliania lacunosa* and the absence of discoasters place Samples 130-807A-2H-CC and -3H-CC in Zone NN19. The former sample contains comparatively abundant *Reticulofenestra asanoi,* but no *Gephyrocapsa parallela,* suggesting an age of this sample that is between 0.83 and 1.06 Ma. The

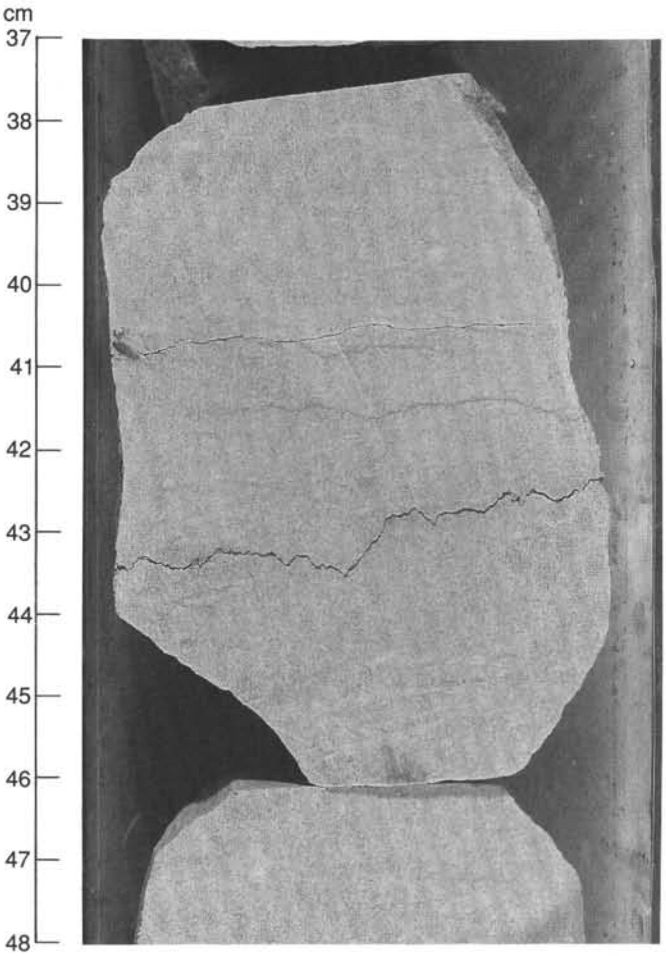

Figure 24. Well-developed stylolite in limestone, Hole 807C (Section 130-807C-48R-1, 37–48 cm; 1146 mbsf).

latter sample contains both *Helicosphaera sellii* and *Calcidiscus macintyrei* and therefore corresponds to the lower part of Zone NN19.

Pliocene

Sample 130-807A-4H-CC contains *Discoaster brouweri* and rare *Discoaster triradiatus* and is assigned to latest Pliocene Zone NN18. The Pliocene/Pleistocene boundary lies within Core 130-807A-4H. The assemblages in the next lower four samples, Samples 130-807A-5H-CC through -8H-CC, are characterized by the occurrences of *Discoaster brouweri, Discoaster pentaradiatus,* and *Discoaster surculus,* which place these samples in the upper Pliocene Zone NN16. The long sample intervals used did not permit recognition of the short Zone NN17 in Hole 807A. Sample 130-807A-6H-CC is older than 2.65 Ma because of the presence of *Discoaster tamalis*. Similarly, because of the presence of *Sphenolithus abies* and the absence of *Reticulofenestra pseudoumbilica,* Sample 130-807A-8H-CC was referred to the basal part of Zone NN16, which approximates the lower/upper Pliocene boundary. Sample 130-807A-9H-CC contains *Reticulofenestra pseudoumbilica, Sphenolithus abies, Amaurolithus delicatus,* and rare *Discoaster asymmetricus,* together with abundant small placoliths. This sample was placed in Zones NN13–NN14.

Samples 130-807A-10H-CC through -13H-CC do not contain *Discoaster quinqueramus*. *Ceratolithus acutus* was observed in Samples 130-807A-10H-CC and -12H-CC, placing

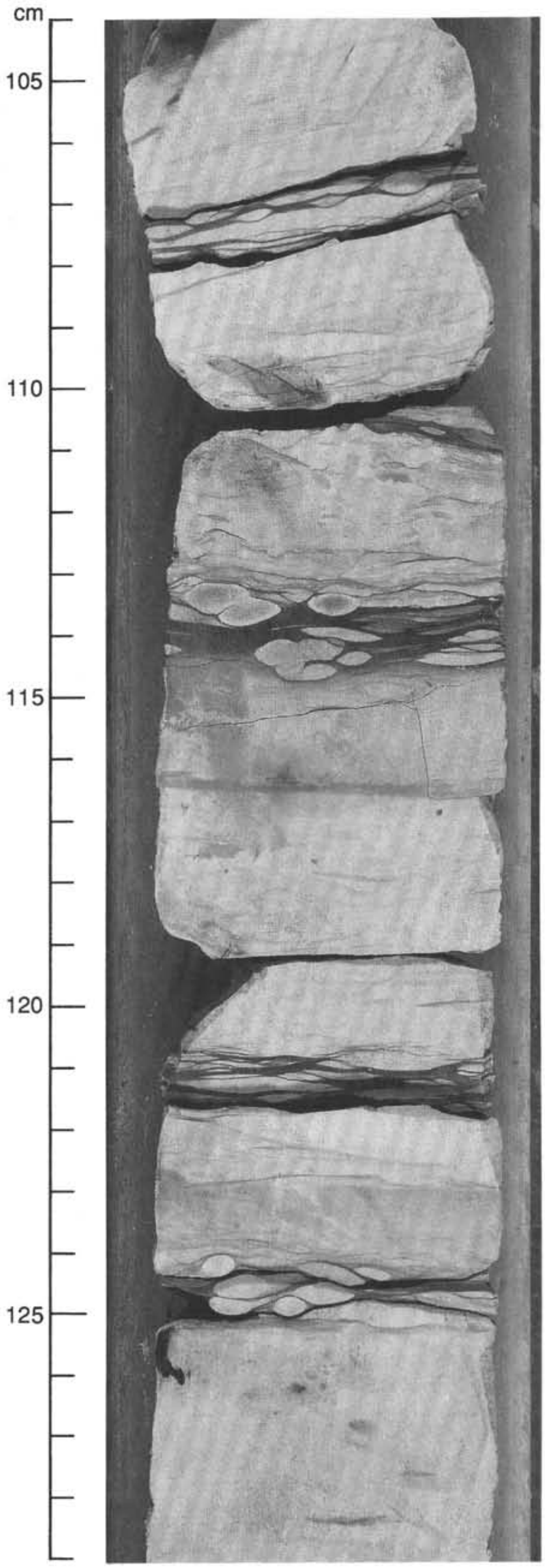

Figure 25. Illustration of the effects of differential compaction between more compacted clay-rich matrix, possibly caused by chemical compaction, and less compacted limestone lenses, which probably represent burrows, Hole 807C (Section 130-807C-53R-3, 104–129 cm; 1184 mbsf).

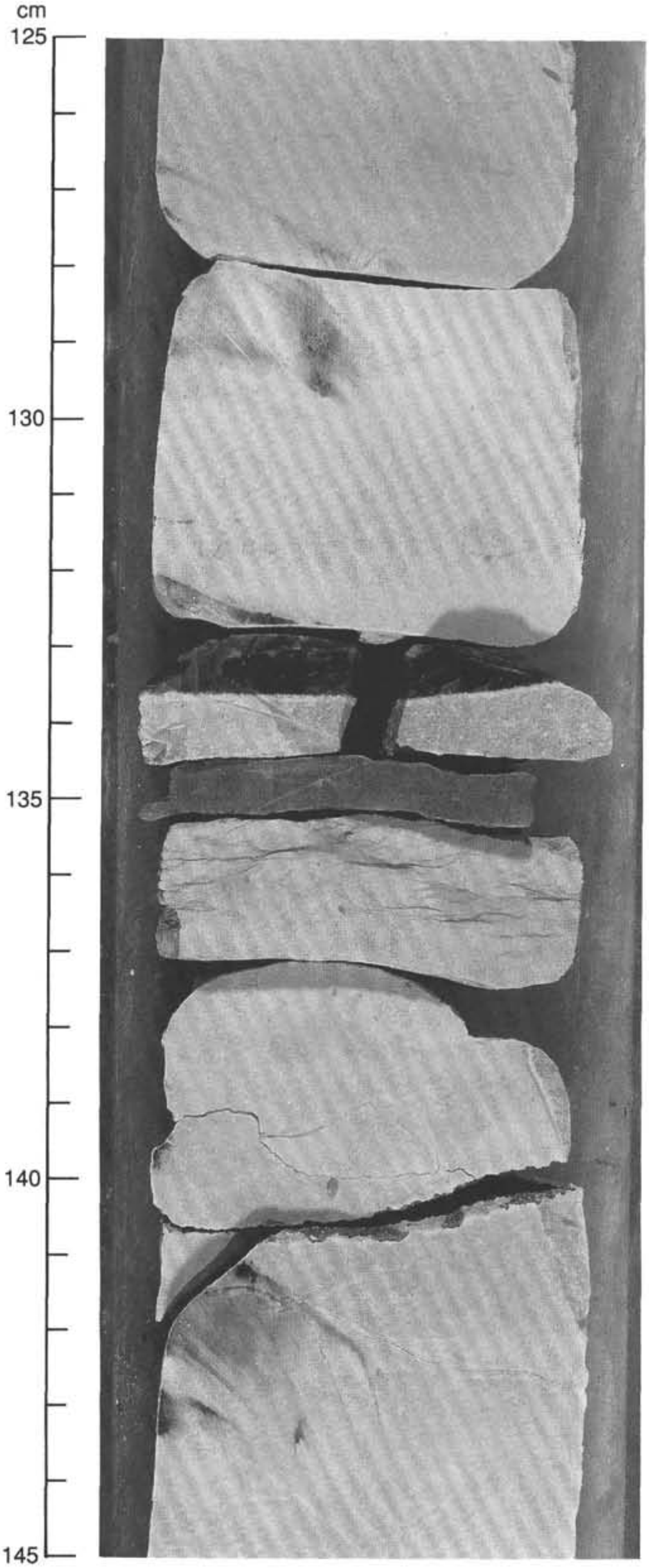

Figure 26. Photograph of Cretaceous/Tertiary boundary interval, Hole 807C. Biostratigraphic data place the actual boundary at the volcanic ash layer in Section 130-807C-54R-3 at 135 cm (1193.14 mbsf).

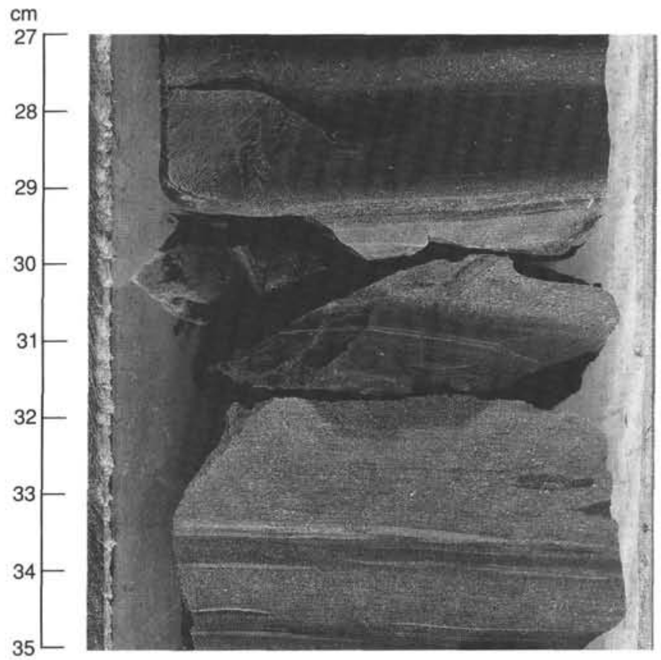

Figure 27. Graded and lenticular bedding in claystone and radiolarian siltstone, Subunit IIIA, Hole 807C (Section 130-807C-72R-2, 27–35 cm; 1360 mbsf).

them in Zone NN12. The absence of *Triquetrorhabdulus rugosus* and *Discoaster quinqueramus* in Sample 130-807A-13H-CC suggests that this sample also belongs to Zone NN12.

Miocene

Discoaster quinqueramus is considered to be present in Sample 130-807A-14H-CC, although the central knob is not as prominent as in Sample 130-807A-15H-CC and below. *Discoaster quinqueramus* was observed down through Sample 130-807A-25H-CC, indicating Zone NN11. Samples 130-807A-17H-CC through -19H-CC contain *Amaurolithus amplificus*. Samples 130-807A-17H-CC and -18H-CC contain fairly abundant sphenoliths and small placoliths. A couple of large specimens of *Discoaster neorectus* that were nearly 25 mm in diameter were observed in Sample 130-807A-21H-CC. Samples 130-807A-26H-CC through -30X-CC contain neither *Discoaster quinqueramus* nor *D. hamatus* and were placed in upper Miocene Zone NN10. The sediments around the Zone NN9/NN10 boundary (Samples 130-807A-24H-CC through -26H-CC) are characterized by bloomlike abundances of small *Sphenolithus abies* and *S. neoabies*. This distinct acme event has been observed at the identical stratigraphic level in all Leg 130 sites.

The occurrence of *Discoaster hamatus* places Samples 130-807A-31X-CC and -32X-CC in Zone NN9. The former sample contains *Discoaster neohamatus,* whereas the latter sample contains fairly common *Catinaster coalitus*. Thus, Core 130-807A-32X contains the middle/upper Miocene boundary. The next lower four samples, Samples 130-807A-33X-CC through -36X-CC, contain neither *Discoaster hamatus* nor *Sphenolithus heteromorphus*. *Coronocyclus nitescens* occurs in and below Sample 130-807A-37X-CC. The last occurrence (LO) of *Coronocyclus nitescens* is supposed to fall near the first occurrence (FO) event of *Discoaster kugleri,* which defines the Zone NN6/NN7 boundary. In the absence of *Discoaster kugleri* in the Leg 130 sediments, the former event has been used as a substitute marker that approximates

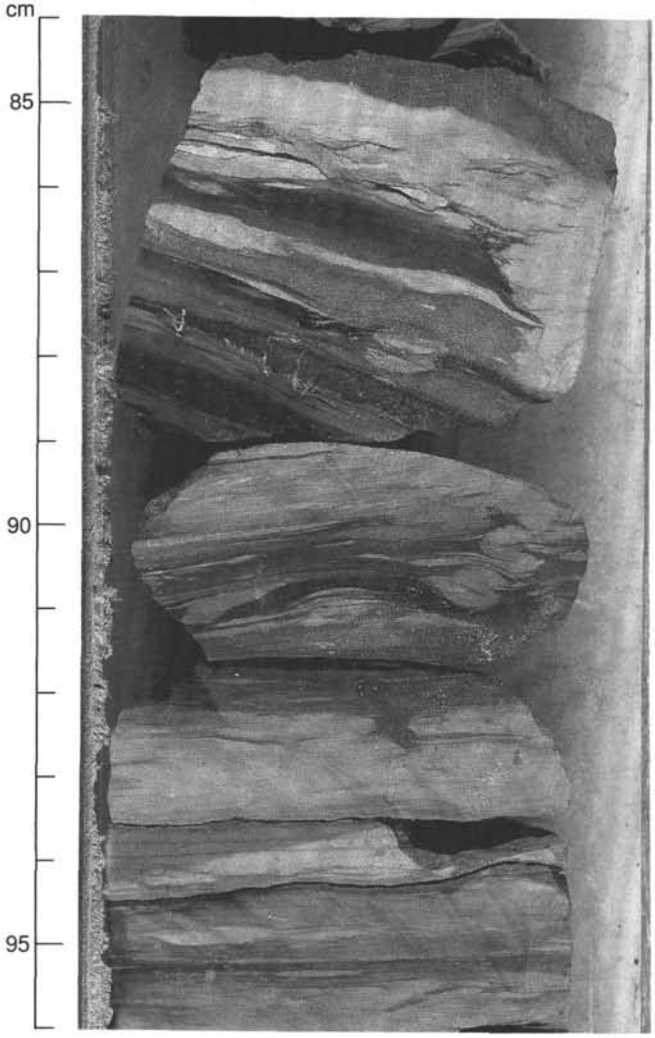

Figure 28. Wavy and lenticular bedding in limestone, Subunit IIIB, Hole 807C (Section 130-807C-73R-2, 84–96 cm, 1370 mbsf).

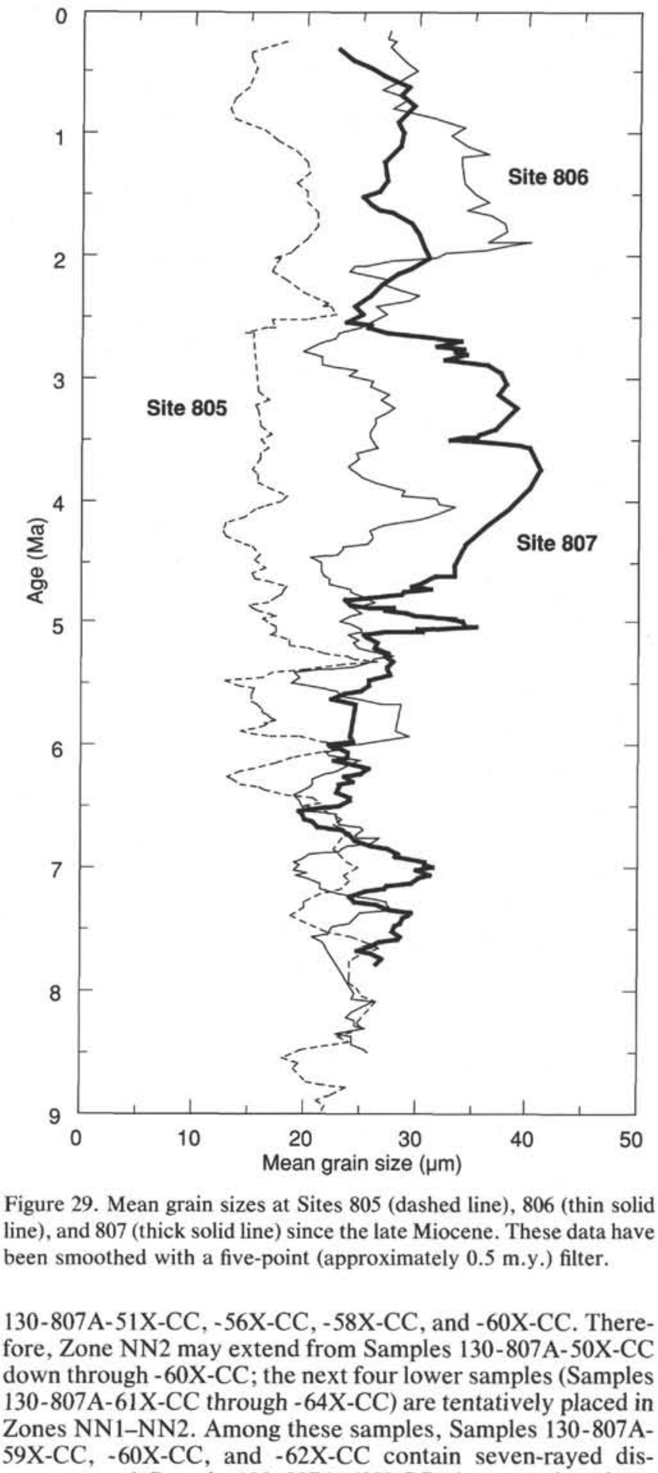

Figure 29. Mean grain sizes at Sites 805 (dashed line), 806 (thin solid line), and 807 (thick solid line) since the late Miocene. These data have been smoothed with a five-point (approximately 0.5 m.y.) filter.

the NN6–NN7 boundary. Samples 130-807A-37X-CC through -39X-CC were referred to Zone NN6 because of the presence of *Coronocyclus nitescens* and the absence of *Sphenolithus heteromorphus*. *Reticulofenestra pseudoumbilica* and *Reticulofenestra gelida* are fairly large in size in Sample 130-807A-34X-CC. Samples 130-807A-40X-CC through -48X-CC contain *Sphenolithus heteromorphus* together with *Cyclicargolithus floridanus*, indicating Zone NN5.

The LO of *Helicosphaera ampliaperta*, which marks the Zone NN4/NN5 boundary, is also lacking at Site 807. The top of the acme of *Discoaster deflandrei*, however, was observed between Samples 130-807A-45X-CC and -46X-CC. The interval from Samples 130-807A-40X-CC through -45X-CC was placed in Zone NN5, whereas the interval from Samples 130-807A-46X-CC through -48X-CC was placed in Zone NN4. The calcareous nannofossil assemblages are poorly preserved in Samples 130-807A-45X-CC and -46X-CC.

A short-range sphenolith species, *Sphenolithus milanetti*, was observed in Sample 130-807A-47X-CC. The presence of *Sphenolithus belemnos* and the absence of *Sphenolithus heteromorphus* and *Triquetrorhabdulus carinatus* place Sample 130-807A-49X-CC in Zone NN3. The latter species was observed up through Sample 130-807A-50X-CC. *Discoaster druggii* occurs only occasionally in small numbers in Samples 130-807A-51X-CC, -56X-CC, -58X-CC, and -60X-CC. Therefore, Zone NN2 may extend from Samples 130-807A-50X-CC down through -60X-CC; the next four lower samples (Samples 130-807A-61X-CC through -64X-CC) are tentatively placed in Zones NN1–NN2. Among these samples, Samples 130-807A-59X-CC, -60X-CC, and -62X-CC contain seven-rayed discoasters and Sample 130-807A-62X-CC also contains abundant *Sphenolithus delphix*. The highest occurrence of *Cyclicargolithus abisectus* was recognized in Sample 130-807A-64X-CC.

Oligocene

The LO of the upper Oligocene species *Sphenolithus ciperoensis* between Samples 130-807A-64X-CC and -65X-CC, and the fact that *Sphenolithus delphix* is common in Core 130-807A-62X, indicates that the Oligocene/Miocene boundary probably lies within Core 130-807A-63X. *Sphenolithus ciperoensis* was observed in Samples 130-807A-

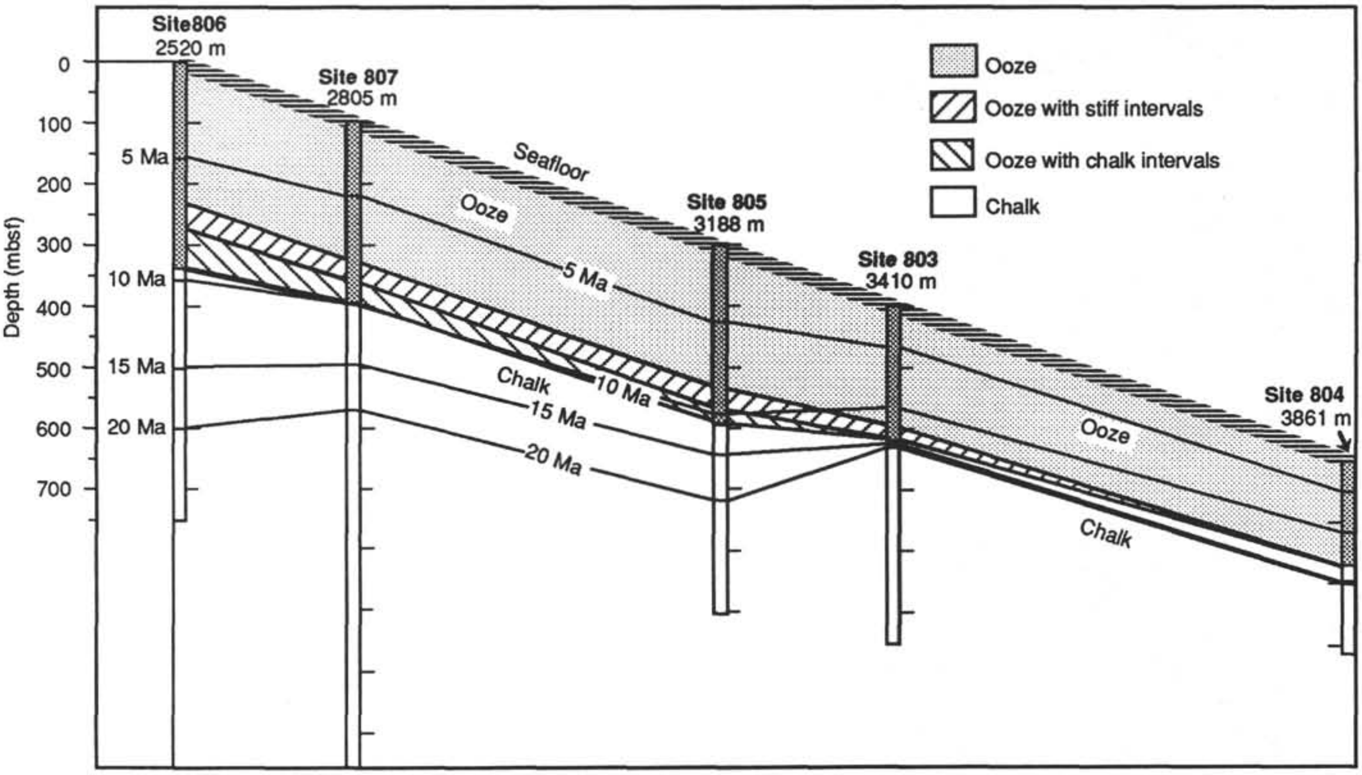

Figure 30. Summary of the bathymetry, ages, and sub-bottom depths of the ooze-chalk transition at the sites drilled on Leg 130.

65X-CC through -72X-CC. *Sphenolithus distentus* occurs together with *S. ciperoensis* in Sample 130-807A-72X-CC. Samples 130-807A-65X-CC through -71X-CC were placed in Zone NP25, and Sample 130-807A-72X-CC in Zone NP24. Throughout Zone NP25, *Cyclicargolithus abisectus* occurs occasionally.

The highest occurrence of *Coccolithus eopelagicus* was observed in Sample 130-807A-68X-CC. Sample 130-807A-73X-CC contains several specimens of transitional forms between *Sphenolithus distentus* and *Sphenolithus ciperoensis* and must lie close to the Zone NP23–NP24 boundary. This implies that Zone NP24 is exceptionally thin relative to surrounding Zones NP25 (above) and NP23 (below). Nevertheless, the lower/upper Oligocene boundary probably lies within Core 130-807A-73X. The interval from Sample 130-807A-74X-CC down to the bottom of the hole was assigned to lower Oligocene Zone NP23 because of the absence of *Sphenolithus ciperoensis* and *Reticulofenestra umbilica*. *Sphenolithus distentus* was observed in Samples 130-807A-74X-CC through -81X-CC. The highest occurrence of *Sphenolithus pseudoradians* was observed in Sample 130-807A-80X-CC. The interval from Sample 130-807A-82X-CC down to the bottom of the hole contains *Dictyococcites bisectus* and *Zygrhablithus bijugatus*. *Coccolithus eopelagicus* occurs sporadically in the upper part of Zone NP23, but continuously in and below Sample 130-807A-83X-CC. *Helicosphaera bramlettei* was observed in Sample 130-807A-79X-CC, and *Helicosphaera compacta* was observed in Samples 130-807A-84X-CC and -86X-CC.

Hole 807B

Hole 807B was cored continuously with the APC to refusal at 278.6 mbsf (Core 130-807B-30H). The nannofossil assemblages in Hole 807B are similar to those observed in the corresponding interval in Hole 807A, and the biostratigraphic relationships of these two holes are shown in Figure 31. The sediments obtained from the bottom of this hole contain *Calcidiscus leptoporus, Calcidiscus macintyrei, Catinaster calyculus, Coccolithus pelagicus,* various discoasters (such as *D. bellus, D. brouweri, D. challengeri,* and *D. variabilis*), *Helicosphaera carteri, Reticulofenestra* spp., *Sphenolithus abies,* and *Triquetrorhabdulus rugosus*. This assemblage is characterized by the absence of *Discoaster quinqueramus* and *Discoaster hamatus,* which places these sediments in upper Miocene Zone NN10. This zone extended over five cores in Hole 807A. The deepest core of Hole 807B (Core 130-807B-30H) is the fifth core representing Zone NN10, implying that Hole 807B probably ended shortly above the Zone NN9/NN10 boundary.

Hole 807C

Oligocene

The nannofossil assemblages in depth correlative Samples 130-807A-86X-CC and 130-807C-1R-CC are similar in composition and abundance: *Cyclicargolithus floridanus* and *Sphenolithus moriformis* are abundant, whereas *Coccolithus pelagicus, Coccolithus eopelagicus, Dictyococcites bisectus, Dictyococcites hesslandii, Helicosphaera compacta, Sphenolithus predistentus,* and *Zygrhablithus bijugatus* range in abundance between common and rare. This basic composition of the nannofossil assemblages, representing Zone NP23, continues down through Core 130-807C-8R, although the proportions between species change between samples. Lower Oligocene species such as *Discoaster tanii, Ericsonia fenestratus, Ericsonia obruta, Helicosphaera reticulata,* and *Rhabdosphaera tenuis* were observed in several samples from Zone NP23. Moreover, a sphenolith species that resembles *Sphenolithus distentus* but has its entire range below the continuous range of *Sphenolithus distentus* s.s. was observed in

Cores 130-807C-7R through -15R. These two morphotypes, therefore, do not overlap stratigraphically. Okada (1990) recently observed this morphotype from the identical stratigraphic interval in the equatorial Indian Ocean. For the time being, we follow Okada's designation of this species as *Sphenolithus* aff. *distentus*.

The LO of the *Reticulofenestra umbilica–Reticulofenestra hillae* complex, and hence the Zones NP22/NP23 boundary, was observed in Core 130-807C-9R. There was no recovery in Cores 130-807C-10R and -11R, although they also must lie in the Zone NP22 interval as the underlying Core 130-807C-12R belongs to that zone. The LO of *Ericsonia formosa* was observed in Core 130-807C-13R. The *Dictyococcites bisectus–Dictyococcites hesslandii* complex has its first continuous occurrence in the lower Oligocene. This group increases in abundance, together with *Bramlettius serraculoides,* through the lower Oligocene.

Eocene

Discoaster preservation is consistently poor throughout the lower Oligocene and Eocene, making a precise determination of the LO of *Discoaster saipanensis* difficult. Thus, the NP20/NP21 boundary, which approximates the Eocene/Oligocene boundary, is difficult to determine precisely. We consider, however, that rare *Discoaster saipanensis* is present as high as Sample 130-807C-18R-CC. Typical *Discoaster barbadiensis* was observed up to Sample 130-807C-19R-CC. This upper Eocene sample also yields abundant *Bramlettius serraculoides, Coccolithus pelagicus, Cyclicargolithus floridanus,* and common *Reticulofenestra umbilica–Reticulofenestra hillae*. Common discoasters belonging to the six-rayed *Discoaster deflandrei* group and the five-rayed *Discoaster tanii* group were also observed. A few helicosphaerid species and *Ericsonia formosa* formed the less abundant members of this upper Eocene assemblage.

The LO of *Cribrocentrum reticulatum* was observed in Core 130-807C-22R, whereas the last "*Calcidiscus*" *protoannulus* was observed in Core 130-807C-24R. Rare *Chiasmolithus solitus* was observed in Sample 130-807C-29R-CC, suggesting a position within Zone NP16. This sample also contains the LO of *Chiasmolithus grandis,* the extinction of which closely approximates the middle Eocene/upper Eocene boundary. The LO of *Campylosphaera dela* was observed in Core 130-807C-30R. The taxonomic diversity increased through the upper Eocene down through the middle Eocene, and the upper middle Eocene assemblages cored at Site 807 typically contain about 20 easily recognizable species, a number that would increase had preservation been better.

The biostratigraphically important *Dictyococcites bisectus–Dictyococcites hesslandii* complex has its first evolutionary appearance in Core 130-807C-31R. Large reticulofenestrids (i.e., *Reticulofenestra umbilica*), appeared in Core 130-807C-36R. *Sphenolithus furcatolithoides* was observed in Core 130-807C-37R, whereas the LO of *Nannotetrina alata* falls in Core 130-807C-38R. This core is also characterized by the presence of abundant *Coccolithus pelagicus* and *Pseudotriquetrorhabdulus inversus,* common (relatively small) chiasmoliths and *Reticulofenestra dictyoda,* and few to rare *Chiasmolithus grandis, Coccolithus eopelagicus, Ericsonia formosa,* and *Sphenolithus radians*. The smaller nannotetrinas were not recognized because of severe calcite overgrowth. Rare and poorly preserved *Chiasmolithus gigas* were added to this general assemblage in Sample 130-807C-39R-CC, thus providing an important biostratigraphic control point within the middle Eocene Zone NP15. This sample also contains *Nannotetrina alata*.

Poor preservation and severe calcite overgrowth prevents confident identification of the nannotetrinas, including *Nannotetrina alata,* in Sample 130-807C-40R-CC. The presence of *Discoaster sublodoensis,* however, places this sample in Zone NP14 or lowermost Zone NP15. *Discoaster lodoensis* co-occurred with *Discoaster sublodoensis* in Sample 130-807C-41R-CC, indicating Zone NP14. Hence, the lower Eocene/middle Eocene boundary must be located in Core 130-807C-41R. This is also the deepest core containing representatives of the genus *Reticulofenestra,* a genus that is considered to appear within Zone NP13 (Romein, 1979).

Sample 130-807C-42R-CC, therefore, lacks reticulofenestrids, but severely overgrown specimens of *Tribrachiatus orthostylus* were observed together with *Discoaster lodoensis,* implying that the sample belongs to Zone NP12 and that Zone NP13 is condensed and lies within Core 130-807C-42R. The diversity in this sample is low, which partly is caused by poor preservation. Sample 130-807C-43R-CC was taken from a silicified limestone and is virtually barren of nannofossils. The co-occurrence of typical *Discoaster diastypus, Discoaster keupperi, Discoaster lodoensis,* and overgrown *Tribrachiatus orthostylus,* places Sample 130-807C- 44R-CC in Zone NP12.

Core 130-807C-45R has biostratigraphic relationships that indicate the influence of turbiditic or debris-flow deposition. Sample 130-807C-45R-1, 10 cm, yielded an upper Paleocene assemblage (Zone NP9; including the only *Ellipsolithus macellus* specimens observed from Site 807), intermixed with Cretaceous forms (e.g., *Micula* spp. and *Watznaueria barnesae*). Investigation of a small white clast (Sample 130-807C-45R-1, 34 cm) yielded an assemblage composed almost exclusively of Cretaceous forms, whereas the surrounding grayish matrix at the same level contains a predominantly Zone NP9 flora with little Cretaceous representation. Sample 130-807C-45R-1, 114–116 cm, however, represents the lower Eocene Zone NP12 (*Discoaster lodoensis* and *Tribrachiatus orthostylus* are both present). The presence of *Discoaster diastypus* and *Tribrachiatus orthostylus* in Core 130-807C-46R indicates Zone NP11.

Paleocene

Discoaster multiradiatus was observed in Samples 130-807C-47R-CC and -48R-CC, together with representatives of the genera *Toweius* and, possibly, *Rhomboaster*. Poor preservation prevents a reliable identification of rhomboasters, which share a tendency with the descendant *Tribrachiatus* lineage to being prone to secondary calcite overgrowth. The biostratigraphic assignment of these two samples into upper Zone NP9, therefore, must rely also on the absence of *Discoaster diastypus,* which indicates a position below Zone NP10, and the absence of fasciculiths, which indicates a position in uppermost Zone NP9 when, as here, *Discoaster multiradiatus* is present. It follows that Zone NP10 probably is condensed, and that both this zone and the Paleocene/Eocene boundary lie within Core 130-807C-47R.

Cores 130-807C-49R and -50R were also assigned to Zone NP9 because of the co-occurrences of abundant and diverse fasciculiths, including *Fasciculithus tympaniformis* and *Discoaster multiradiatus*. One of the best preserved samples in that depth interval consisted of an easily disintegrated chalk clast taken from within a chert layer. This sample (130-807C-50R-1, 116 cm) contained abundant fasciculiths; common *Coccolithus pelagicus, Discoaster multiradiatus, Toweius* spp., and *Sphenolithus moriformis;* and few to rare *Discoaster nobilis,* chiasmoliths, thoracosphaerids, and one of the few observations of *Neochiastozygus*.

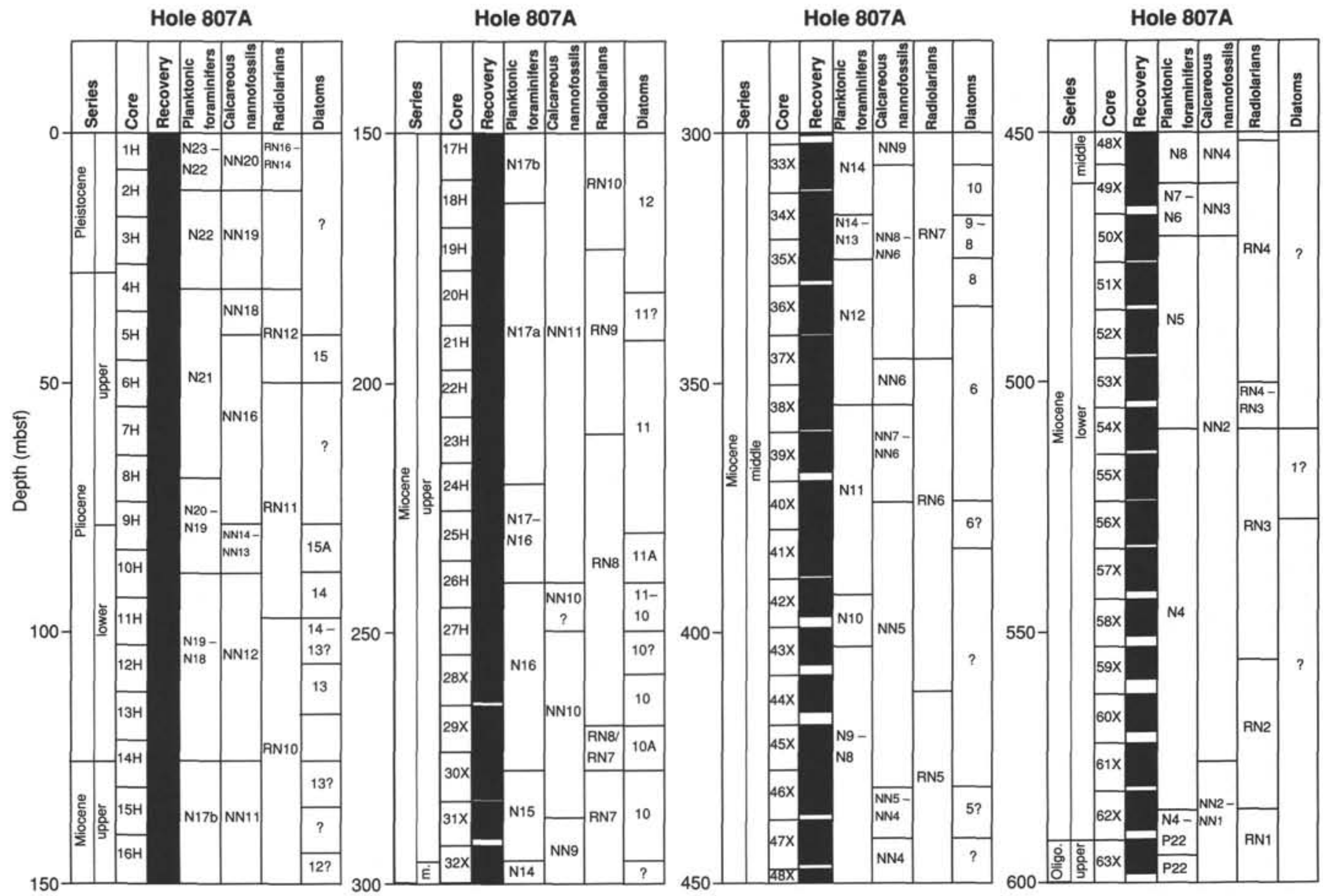

Figure 31. Biostratigraphic hole summaries, Site 807. RN = radiolarian Neogene zone, NTD = Neogene tropical diatom zone, RP = radiolarian Paleogene zone, and NN = nannofossil Neogene zone.

The LO of *Ericsonia robusta* was observed between Samples 130-807C-51R-1, 90 cm, and -2, 88 cm. *Discoaster multiradiatus* is common and fasciculiths are abundant in these samples, indicating a position in lower Zone NP9. Rare *Heliolithus riedelii* were observed in Sample 130-807C-51R-CC; a long search for *Discoaster multiradiatus* in this sample yielded one possible specimen. This sample, therefore, is considered to lie close to the NP8/NP9 boundary.

Core 130-807C-52R contained the NP5–NP7 zonal interval. The lowermost occurrence of *Discoaster mohleri,* the FO of which defines the NP6/NP7 boundary, was observed through Sample 130-807C-52R-3, 20–22 cm. This sample contained rare, fairly small, *Heliolithus kleinpellii,* a species that was observed also at a level 10 cm further downcore; its ancestor, *Heliolithus cantabriae,* was present in Sample 130-807C-52R-3, 75 cm. Thus, the NP6/NP7 and NP5/NP6 boundaries both lie in the upper half of Section 130-807C-52R-3. Abundant fasciculiths, including rare *Fasciculithus pileatus,* were observed in Sample 130-807C-52R-CC, indicating Zone NP5.

Sample 130-807C-53R-2, 130 cm, contained an evolutionary young fasciculith association, including *Fasciculithus bitectus, Fasciculithus magnicordis,* and *Fasciculithus ulii.* This association lacks *Fasciculithus tympaniformis,* thus indicating Zone NP4. The next lower sample (Sample 130-807C-53R-3, 23 cm) lies below the ranges of both fasciculiths and sphenoliths, but contains rare specimens of Danian (lower Paleocene) species, such as *Cruciplacolithus primus, Cruciplacolithus tenuis,* and *Prinsius bisulcus.*

The abundance of nannofossils decreases markedly through Core 130-807C-53R from "abundant" to "few" or "rare"; preservation is consistently poor and diversity is low. Nevertheless, characteristic lower Paleocene species (i.e., *Cruciplacolithus primus*) were observed in several samples from the lower part of this core, and one would expect, therefore, to find abundant small placoliths (e.g., *Biscutum* spp.) in these lower Paleocene limestones. Their absence is interpreted to represent diagenetic destruction and reduction of the original assemblage. Despite the fact that the lower Paleocene forms are rare, their presence indicates that the observed Cretaceous species must be reworked.

General conditions of low abundance, low diversity, and poor preservation also characterized Core 130-807C-54R, in which an apparently continuous K/T boundary transition was recovered.

The Cretaceous/Tertiary Boundary

The wealth of small Tertiary placolith taxa (i.e., *Biscutum, Cruciplacolithus,* and *Toweius*) emerging immediately after the mass extinction of Cretaceous forms (e.g., Romein, 1979; Thierstein and Okada, 1979; Manivit and Feinberg, 1984; Monechi, 1985) essentially have been dissolved in the nearest 8 m above the assigned K/T boundary horizon at Site 807. Trace amounts of such Danian placoliths, however, are con-

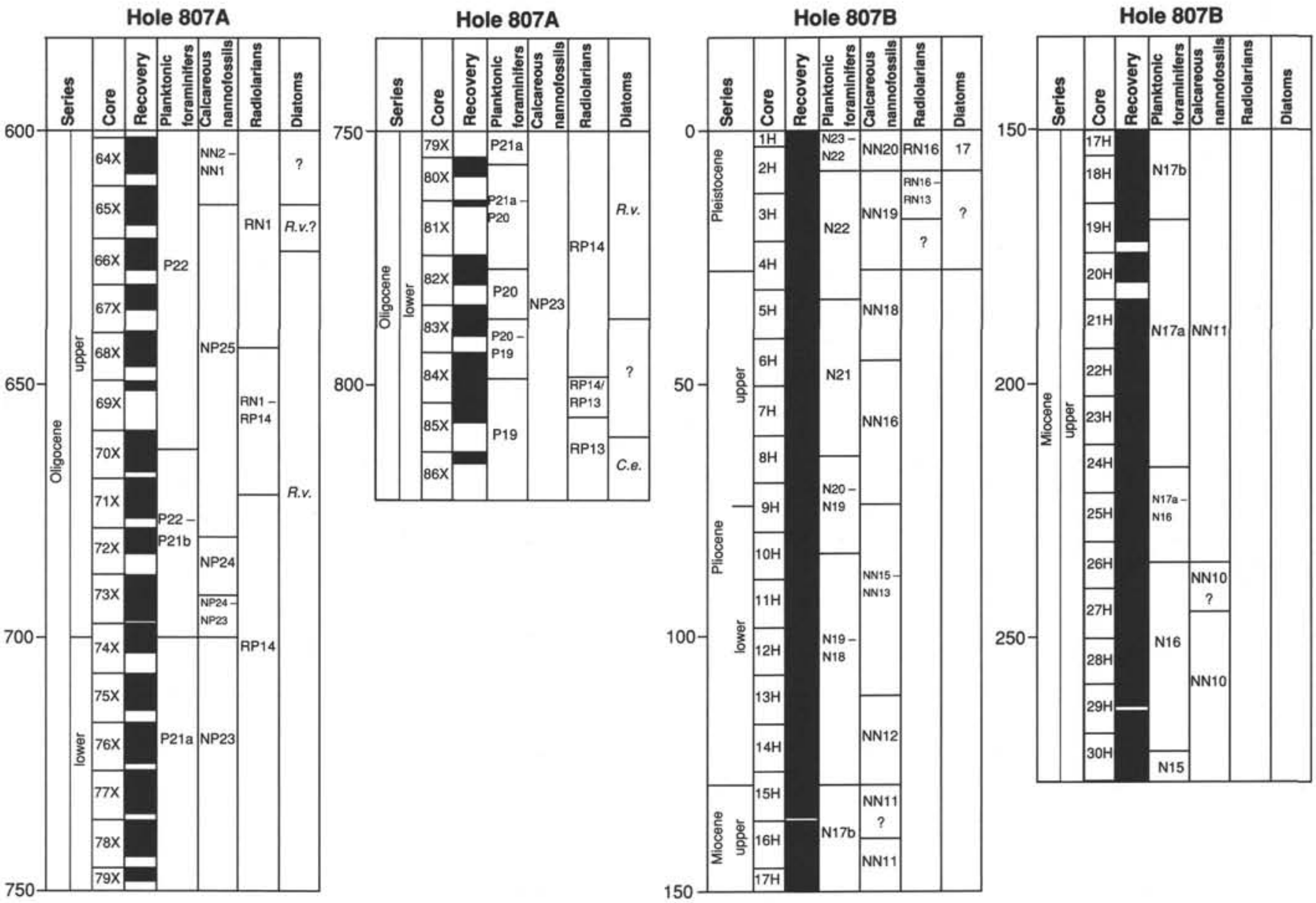

Figure 31 (continued).

sistently present from 1.1 m above the boundary horizon. The boundary was placed within a 16-cm interval at the base of Section 130-807C-54R-3 because of the FO, rapid rise, and subsequent rapid decline in abundance (acme) of the calcareous dinoflagellate *Thoracosphaera* (Table 6). Only fragments of these dissolution-resistant morphotypes were preserved in the deeply buried (1193 mbsf) K/T sequence at Site 807. Moreover, the lowermost Danian sediments contain abundant Cretaceous specimens, in comparison with the low abundance of indigenous species, reflecting the fact that the Cretaceous-source sediments are rich in such dissolution-resistant morphotypes as *Watznaueria* and *Micula* (Thierstein, 1981).

Cretaceous

The abundance of Upper Cretaceous assemblages varies from few to common, whereas the preservation varies between poor and moderate. Cores 130-807C-55R through -57R contain *Micula murus* and hence belong to the upper Maestrichtian; Sample 130-807C-55R-1, 86 cm, yielded a few specimens of *Micula prinsii*, indicating a position immediately below the K/T boundary. Other typical forms in these poorly preserved upper Maestrichtian assemblages include *Arkhangelskiella cymbiformis, Cretarhabdus crenulatus, Cribrosphaerella ehrenbergii, Lithraphidites quadratus*, and the ubiquitous *Watznaueria barnesae*. *Microrhabdulus decoratus, Prediscosphaera cretacea*, and *Ceratolithoides aculeus* were observed occasionally in the Maestrichtian cores. The latter species, however, is a fairly regular member of assemblages from Samples 130-807C-60R-CC to -70R-CC, whereas *Parhabdolithus embergeri* was observed in Core 130-807C-61R and downhole.

Quadrum trifidium has its LO in Core 130-807C-61R. This important marker species is consistently present throughout its observed range; its FO level was observed between Samples 130-807C-70R-CC and -71R-1, 37–38 cm. *Quadrum gothicum* occurs consistently from Sample 130-807C-59R-CC through the continuous carbonate-bearing sediments, to the sharp red clay contact in Section 130-807C-71R-3. Thus, the age range of this interval is limited to the early Maestrichtian–late Campanian.

A short interval of nannofossil-bearing limestones in basal Core 130-807C-73R and topmost Core 130-807C-74R separates the barren red and brown zeolitic clays above from the igneous basement below. The nannofossils in this limestone are abundant but poorly preserved, and *Watznaueria barnesae* appears to occupy over 90% of the total assemblage. The presence of a few specimens of *Rucinolithus irregularis*, which had a stratigraphic range restricted to the Aptian and Albian, places Sample 130-807C-73R-CC in the Lower Cretaceous. Therefore, it appears reasonable to assume that the red clay interval, which separates these Aptian- Albian limestones from the overlying upper Campanian limestones in Core 130-807C-71R, is associated with hiatus(es) of considerable duration (on the order of 10^7 yr). *Parhabdolithus embergeri* and, possibly, *Watznaueria britannica* are rare members of the assemblage in Sample 130-807C-73R-CC. If the latter species, indeed, is a member of this assemblage, its presence supports the Lower Cretaceous assignment.

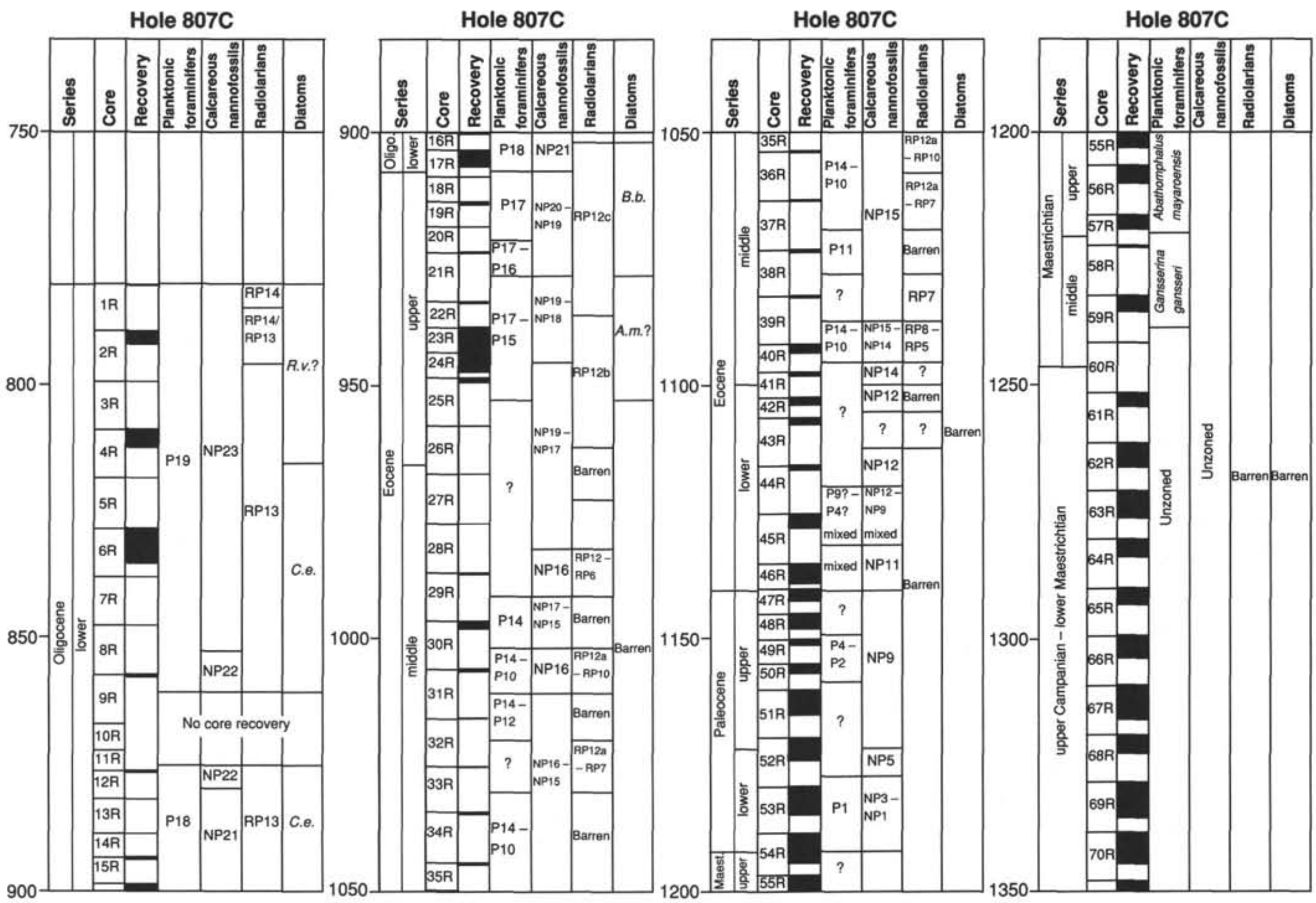

Figure 31 (continued).

Basement was reached about 20 cm below Sample 130-807C-73R-CC, and the Aptian-Albian age assignment for the overlying limestone presumably also applies for the basalt. The basal sedimentary sequence cored in Hole 807C has some interesting characteristics in common with the sequence cored at neighboring Site 289 (see Shipboard Scientific Party, 1975b). A fairly extended Maestrichtian through upper Campanian carbonate-rich sequence ends in a short interval of red clays (described as a vitric tuff bed). The tuff bed is underlain by a short interval of limestones, which, in turn, rests on basaltic basement. The age of these lower limestones is uncertain. They are referred to as being "... probably Aptian ..." (Shafik, 1975, p. 598), or upper Albian (Shafik, 1975, p. 583), because "... only the *Eiffellithus turriseiffeli* Zone from the Lower Cretaceous has been identified among Leg 30 material" (implying that the sediments cannot be older than late Albian). Nevertheless, both estimates are coherent with the less precise Aptian-Albian assignment suggested for the basal limestones in Hole 807C.

A few pieces of limestone were retrieved from within the basalt sequence. The limestones from Section 130-807C-80R-1 yielded poorly preserved nannofossils, although the presence of both *Watznaueria barnesae* and some distinct specimens of *Watznaueria britannica* indicate an Early Cretaceous age for these limestone pieces, as well as the adjacent basalts. It appears likely that this estimate can be considerably refined.

Planktonic Foraminifers

Neogene

Neogene sediments are present to a depth of approximately 592 mbsf in Hole 807A. The Oligocene/Miocene boundary (P22/N4) can probably be placed in the upper part of Core 130-807A-63X. Hole 807B ended in basal upper Miocene sediments (Zone N15). Planktonic foraminifers are generally abundant and well to moderately well preserved through the Neogene section at Site 807. The sequence appears to be complete except in the upper part of the lower Miocene (Zones N6 and N7) where the section is thin either because of reduced sediment accumulation or gaps in the sediment record (Fig. 31).

Pleistocene–uppermost Pliocene Zones N22–N23 are characterized by the presence of *Globorotalia truncatulinoides*, although the occurrence of this taxon is often sporadic in the holes drilled during Leg 130. The LO of *Globigerinoides fistulosus* marks the Pliocene/Pleistocene boundary. The co-occurrence of *G. truncatulinoides* and *G. fistulosus* defines the uppermost Pliocene part of Zone N22 (e.g., Sample 130-807B-4H- CC). Upper Pliocene Zone N21 is characterized by the presence of *G. fistulosus* and *Sphaeroidinella dehiscens*. The FO of *Globorotalia tosaensis* defines the base of Zone N21, but this taxon occurs only sporadically at this site; therefore, the FO of *S. dehiscens* s.s. is used as a proxy for the base of the zone. The LO of *Globoquadrina altispira* and the LO of

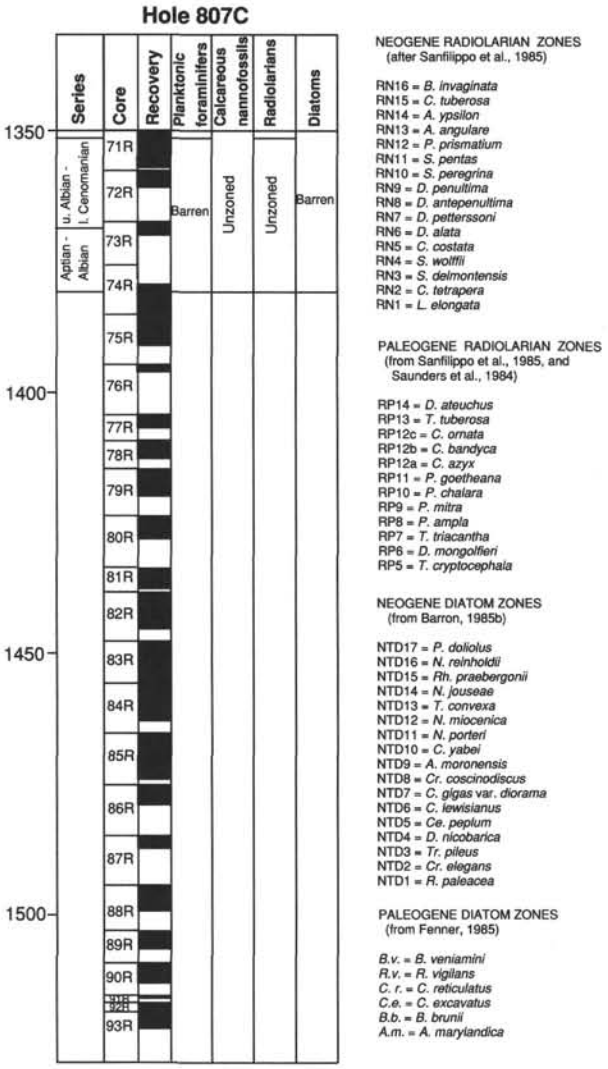

Figure 31 (continued).

Sphaeroidinellopsis spp. are present in the lower part of Zone N21.

The mid-Pliocene interval (Zones N19–N20) is characterized by the presence of right-coiled *Pulleniatina*. The LO of *Globorotalia margaritae* is in this zone. *Sphaeroidinella dehiscens* s.l. (*S. dehiscens immaturus*) would normally be used to differentiate Zones N18 and N19. However, this taxon is very rare in the lower Pliocene of Site 807. The coiling change in *Pulleniatina* is used to mark the boundary between Zones N19–N20 and Zones N18–N19 (undifferentiated) at this site. Characteristic taxa of Zones N18–N19 include *Globorotalia margaritae, G. tumida, G. plesiotumida, G. menardii, Globoquadrina altispira, Sphaeroidinellopsis seminulina, S. paenedehiscens, Globigerinoides extremus, G. conglobatus*, and left-coiled *Pulleniatina primalis, P. praecursor*, and *P. spectabilis*. The FO of *Globorotalia tumida* marks the Miocene/Pliocene boundary at this site.

Upper Miocene Zone N17 is divided into Subzones N17a and N17b based on the FO of *Pulleniatina primalis*, which is restricted to Subzone N17b. The faunal composition of Subzones N17a and N17b is otherwise similar and includes *Globorotalia menardii, G. plesiotumida, G. merotumida, Globoquadrina dehiscens, G. altispira, Globigerinoides* spp., *Sphaeroidinellopsis* spp., *Neogloboquadrina humerosa*, and *N. acostaensis*. The FO of *Globorotalia plesiotumida* was used to define the base of Subzone N17a. However, the presence of forms transitional to *G. merotumida* make the exact placement of this boundary tenuous. Coiling changes in the *Globorotalia menardii* group in Subzone N17a and the FO of *Neogloboquadrina humerosa* in Zone N16 (Berggren et al., 1985) help to bracket the boundary. The composition of the Zone N16 assemblage is similar to that of Subzone N17a with the exception of the FOs noted above. The FO of *Neogloboquadrina acostaensis* marks the N15/N16 zonal boundary. The interval with neither *N. acostaensis* nor *Globorotalia siakensis* corresponds to basal upper Miocene Zone N15. The LO of *Globorotalia continuosa* is in Zone N15. *Streptochilus* occurs commonly throughout the upper Miocene of this site.

Table 6. Relative abundances of Tertiary and Cretaceous calcareous nannofossils and the calcareous dinoflagellate *Thoracosphaera* in Core 130-807C-54R.

Core, section, interval (cm)	Depth (mbsf)	Cretaceous	Thoracosphaera	Tertiary
130-807C-				
54R-2, 12	1190.42	Common	—	Trace
54R-2, 29	1190.59	Common	—	Trace
54R-2, 115	1191.45	Common	Rare	Trace
54R-2, 120	1191.50	Common	Rare	Trace
54R-3, 27	1192.07	Common	Rare	Trace
54R-3, 51	1192.31	Rare	Rare	—
54R-3, 56	1192.36	Rare	Rare	—
54R-3, 84	1192.39	—	Common	Trace
54R-3, 116	1192.64	Few	Rare	—
54R-3, 127	1193.07	Common	Abundant	—
54R-3, 134	1193.14	Rare	Rare	—
54R-3, 135.5	1193.16	Rare	Rare	—
54R-3, 137	1193.17	Common	Rare	—
54R-3, 150	1193.30	Abundant	Rare	—
54R-4, 3	1193.33	Few	—	—
54R-4, 29	1193.59	Few	—	—
54R-4, 60	1193.90	Common	—	—
54R-4, 101	1194.31	—	—	—
54R-CC	1196.90	Common	—	—
55R-1, 86	1197.76	Rare	—	—

Note: The Cretaceous/Tertiary boundary interval is recognized by the first occurrence and the rapid rise of *Thoracosphaera*.

The uppermost zone of the middle Miocene (N14) is recognized by the LO of *Globorotalia siakensis*. Other characteristic taxa of this zone include *Globorotalia continuosa, G. menardii, G. praemenardii, G. lenguaensis, Globoquadrina dehiscens, G. altispira, Globigerinoides sacculifer, G. trilobus, G. subquadratus, Globigerina woodi*, and rare *G. nepenthes*. The FO of *Globigerina nepenthes* differentiates Zones N13 and N14. *Globorotalia fohsi, G. fohsi lobata*, and *G. fohsi robusta* are diagnostic of middle Miocene Zone N12. The FO of the *G. fohsi* group marks the base of the zone. Zone N11 is characterized by the presence of *Globorotalia praefohsi*, whereas *Globorotalia peripheroacuta* in the absence of *G. praefohsi* characterizes Zone N10. The FO of *G. peripheroacuta* marks the base of Zone N10. Other taxa present in Zones N10–N12 include *Globorotalia siakensis, G. praemenardii, G. lenguaensis, Globoquadrina dehiscens, G. altispira, Sphaeroidinellopsis seminulina, S. kochii, Globigerinoides trilobus, G. subquadratus*, and *Globigerina woodi*. The LO of *Globorotalia peripheroronda* is present within Zone N10. The lowest zones of the middle Miocene (N8 and N9) could not be differentiated at Site 807 because of the general absence of species of the *Praeorbulina-Orbulina* lineage. However, *Praeorbulina sicanus* is present and its FO marks the base of Zone N8.

The upper part of the lower Miocene is thin at Site 807. Only one core-catcher sample contains a fauna indicative of either Zone N7 or N6 (Sample 130-807A-49X-CC). This sample contains *Globorotalia birnageae*, *G. peripheroronda*, *G. siakensis*, *Catapsydrax stainforthi*, and *C. dissimilis*. This part of the section could represent a condensed interval with a mixed fauna, as evidenced by the co-occurrence of *G. birnageae* (FO in Zone N7) and *C. dissimilis* (LO at the top of Zone N6). The remainder of the lower Miocene, including most of Zone N5 and all of Zone N4, is thick and apparently complete. Zone N5 is recognized by the presence of *Globoquadrina binaiensis* in the absence of *Globorotalia kugleri*. Zone N4 is defined by the total range of *G. kugleri* s.s. Other taxa found within Zones N4 and N5 include *Catapsydrax dissimilis*, *C. unicavus*, and *Globorotalia siakensis*. *Globigerinoides altiaperturus* occurs in Zone N5, and the LO of *Globorotalia nana* is in Zone N4. The base of the Miocene probably occurs within Core 130-807A-63X.

Paleogene

Upper Oligocene Zone P22 is recognized by the absence of *Globorotalia kugleri* and *G. opima*. Taxa present throughout the zone include *Globorotalia nana*, *G. siakensis*, *Catapsydrax* spp., *Globigerina angustiumbilicata*, and *Cassigerinella chipolensis*. *Globorotalia pseudokugleri* is present in the upper part of the zone. The top of Zone P21 is defined by the LO of *Globorotalia opima*. Zone P21 is subdivided into upper Oligocene Subzone P21b and lower Oligocene Subzone P21a based on the LO of *Chiloguembelina*, which is restricted to Subzone P21a. Core-catcher samples from Cores 130-807A-70X to -73X contain specimens transitional between *G. nana* and *G. opima*. Because these samples apparently do not contain *G. opima* s.s., it is not clear whether they belong to Zone P22 or Subzone P21b. Other taxa present in this interval, including *Globigerina angulisuturalis* and *G. ciperoensis*, do not help to resolve the uncertainty. Sample 130-807A-74X-CC contains both *G. opima* s.s. and *Chiloguembelina*, indicative of Subzone P21a. A hiatus within the lower part of the upper Oligocene sequence is one interpretation of the data (see "Sedimentation Rates" section, this chapter).

The base of lower Oligocene Subzone P21a is defined by the FO of *Globigerina angulisuturalis*, which is a rare component of these Oligocene sediments. Zone P20 is recognized by the presence of *Globorotalia opima* in the absence of *G. angulisuturalis* and *Globigerina ampliapertura*. The LO of *G. ampliapertura* defines the top of Zone P19. Other taxa present in Zone P19 include *Chiloguembelina*, *Cassigerinella chipolensis*, *Catapsydrax* spp., *Globigerina yeguaensis*, *G. tripartita*, and *Globorotalia nana*. The lowest zone of the Oligocene (Zone P18) is characterized by the presence of *Pseudohastigerina micra* in the absence of late Eocene taxa. Additional taxa noted in Zone P18 include *Globorotalia increbescens*, *Cassigerinella chipolensis*, *Catapsydrax* spp., *Globigerina ampliapertura*, *G. gortanii*, and *G. yeguaensis*. The upper Eocene (Zones P15–P17) is recognized by the co-occurrence of *Globorotalia cerroazulensis*, *Hantkenina* spp. (primarily observed as spines), and *Globigerina angiporoides*.

Chert with little surrounding matrix dominates the recovered sediment through the middle Eocene (Zones P10–P14) (Fig. 31). The matrix consists mostly of chalky limestone that becomes more siliceous adjacent to cherts. It is very difficult to extract planktonic foraminifers from this material, but rare specimens in most samples provide a crude age determination. Some samples appear to be barren. This, however, may largely be an artifact of the harsh mechanical treatment needed to extract foraminifer tests, including grinding with a mortar and pestel and ultrasonic vibration. Thin-section analyses would probably permit resolution of the planktonic foraminifer zones through this interval and the underlying limestones.

Taxa indicative of middle Eocene Zone P14 in Sample 130-807C-30R-CC include *Truncorotaloides rohri*, *Morozovella spinulosa*, *Acarinina bullbrooki*, *Globigerinatheka* spp., spines of *Hantkenina*, and *Subbotina eocaena*. An assemblage indicative of middle Eocene Zone P11 was found in Sample 130-807C-38R-CC that includes *Morozovella aragonensis*, *Acarinina bullbrooki*, *Globigerinatheka index*, and *G. subconglobatus*. Other core-catcher samples in the middle Eocene are mostly characterized by the presence of robust, indeterminate species of *Subbotina* and *Globigerinatheka*.

The zones of the lower Eocene were not clearly recognized on the basis of planktonic foraminifers. This interval contains evidence of slumping and/or reworking based on nannofossil and foraminifer evidence. Mixed floras and faunas were noted in several samples. For example, Sample 130-807C-45R-1, 30–32 cm, contains a mixed foraminifer assemblage that indicates a late Paleocene (P4–P6a) to early Eocene (P6b–P9) age based on the presence of *Planorotalites pseudomenardii*, *P. chapmani*, *Morozovella velascoensis*, *M. angulata*, *M. aequa*, and *M. quetra*. This sample also contains about 5%–10% reworked, middle Maestrichtian species, including *Globotruncana esnehensis*, *G. mariei*, *G. arca*, *G. rosetta*, *Rugoglobigerina* sp., *Pseudoguembelina costulata*, and *Pseudotextularia elegans*. A thin-section sample from Sample 130-807C-46R-CC similarly contains a mixed Paleocene–lower Eocene assemblage, including such lower Paleocene species as *Morozovella trinidadensis*. No Cretaceous taxa were noted in this sample.

Foraminifers provided spotty age controls in the Paleocene strata of Site 807. To facilitate the extraction of planktonic foraminifers from the limestone matrix, the core-catcher samples were first crushed with a Carver hydraulic press and then crushed again with a mortar and pestel. This method was particularly successful where the limestone contains wispy gray horizons of volcanic ash or clay. The more homogeneous white limestones yielded the fewest specimens with the crushing method. Thin-section analyses would undoubtedly yield the best results for zoning these rocks with planktonic foraminifers. Sample 130-807C-49R-CC contains *Morozovella* cf. *M. conicotruncata*, indicating Zone P3 or P4. The presence of *Planorotalites pseudomenardii* and *Morozovella* cf. *M. angulata* in Sample 130-807C-50R-CC indicates Zone P4. Subzone P1b was suggested by the presence of *Subbotina pseudobulloides* and *S. triloculinoides* in Sample 130-807C-53R-4, 97–98 cm, whereas the presence of *Eoglobigerina fringa* in Sample 130-807C-54R-2, 120–122 cm, suggests Subzone P1a.

According to calcareous nannofossil data, the K/T boundary is present in the lower 16 cm of Core 130-807C-54R-3. A foraminifer assemblage from Sample 130-807C-54R-3, 56–58 cm, is composed of small indeterminate planktonic foraminifers along with a couple of small specimens of indeterminate Upper Cretaceous globotruncanids. This may represent a basal Tertiary Pα assemblage with recycled(?) Upper Cretaceous elements. Thin-section analyses through Core 130-807C-54R are needed to define the boundary more clearly, relative to the interval of elevated Thoracosphaera abundance recognized in the microflora (Table 6).

Cretaceous

Shipboard analyses of Cretaceous planktonic foraminifers were problematic because of the indurated nature of the limestones. However, specimens were extracted from part of the Maestrichtian section by the crushing technique outlined above. Sample 130-807C-57R-CC contains *Abathomphalus* *mayaroensis, Rosita contusa* s.l., and *Pseudoguembelina costulata* of the upper Maestrichtian *Abathomphalus mayaroensis* Zone (lower part). The mid-Maestrichtian *Gansserina gansseri* Zone was indicated by the presence of *Gansserina wiedenmayeri*, the *Globotruncana orientalis-falsostuarti* plexus, *Globotruncanita stuartiformis, Rugoglobigerina hexacamerata, Rosita fornicata, Globigerinelloides* sp., *Pseudotextularia elegans*, and *Pseudoguembelina costulata* in Sample 130-807C-59R-CC. Sample 130-807C-60R-CC contains a similar assemblage with the addition of *Globotruncanita subspinosa*. Samples 130-807C-59R-CC and -60R-CC are indicative of the lower to mid-Maestrichtian.

Very few foraminifers were extracted from the lower Maestrichtian–upper Campanian limestones in Cores 130-807C-61R to -71R, as dated by calcareous nannofossils. Cut slabs of limestone in this interval contain fewer tests of planktonic foraminifers than are present in higher stratigraphic levels, as observed by means of a stereo-zoom microscope. The greater relative abundance of planktonic foraminifers in part of the Maestrichtian may record a primary signal of changing dissolution levels in the Cretaceous ocean. The CCD was elevated from Aptian through Campanian time (Thierstein, 1979; Tucholke and Vogt, 1979). The increase in planktonic foraminifer preservation in the Maestrichtian of Site 807 may record the rapid depression of the Maestrichtian CCD observed in the Atlantic (Tucholke and Vogt, 1979). Diagenetic factors, including the clay content of limestones, may also be responsible for the apparent changes in relative abundances of planktonic foraminifers.

The lower Cenomanian–upper Albian red mudstones of Cores 130-807C-71R, -72R, and -73R, as dated by radiolarians, are barren of foraminifers. Aptian-Albian carbonates overlying basalt in Core 130-807C-74R, dated by calcareous nannofossils and radiolarians, are likewise barren of planktonic foraminifers. Sample 130-807C-73R-CC contains a few calcareous benthic foraminifers that are overgrown with calcite. A thin limestone between basalt flows in Core 130-807C-80R also contains only a few poorly preserved, overgrown calcareous benthic foraminifers.

Benthic Foraminifers

All core-catcher samples from Hole 807A (Samples 130-807A-1H-CC through -86X-CC) and those from Hole 807C in which the chalks could be readily disaggregated (Samples 130-807C-1R-CC through -38R-CC) contain benthic foraminifers. Some of the lower Eocene, Paleocene, and Cretaceous limestones below Core 130-807C-38R probably contain small numbers of benthic specimens, but they were not seen in cursory examinations of the surfaces of the siliceous limestones. Two sectional samples from the claystone above the basalt basement (130-807C-71R-3, 74–76 cm, and -71R-5, 127–129 cm) were barren of foraminifers.

Benthic specimens comprise <1% of the foraminifers in the sand fraction of almost all of the samples examined, except for small percentage increases in intervals of moderate dissolution (Samples 130-807A-4H-CC, -5H-CC, -30X-CC, -49X-CC, and -63X-CC) and high percentages of benthic specimens in intervals of strong dissolution of planktonic foraminifers (Samples 130-807C-32R-CC and -34R-CC) in the middle Eocene section. Few foraminifers are present in a part of the upper Eocene section that contains abundant radiolarians (Samples 130-807C-24R-CC and -25R-CC). A comparison with Sites 803 and 805 shows a general increase with depth of site in the percentage of benthic specimens, reflecting selective dissolution of planktonic components through time. Exceptions are the lower Oligocene and upper Miocene samples, in which benthic foraminifers are well preserved at all three sites.

The benthic specimens are well preserved down to the lower Oligocene, at which time they begin to appear in a recrystallized form. This deterioration in preservation corresponds with an increase in radiolarians. The frequency of breakage also increases in the lower Oligocene through middle Eocene part of the section. Some of this breakage is probably a result of sample processing.

The stratigraphic distribution of taxa is comparable with that of Sites 803 and 805, in which lower bathyal to abyssal assemblages characteristic of the upper Eocene–lower Oligocene, upper Oligocene–lower Miocene transition, and middle Miocene–Quaternary transitions were recognized. Just as at Site 803, *Alabamina dissonata*, but not *Nuttallides truempyi*, is present in the latest Eocene sample. However, *N. truempyi* was noted lower in the section at both sites. Prominent Eocene species that continue into the Oligocene include *Cibicidoides grimsdalei, Anomalinoides spissiformis, Nonion havanense, Gyroidinoides girardanus*, and *Cibicidoides praemundulus*. All three sites analyzed (803, 805, and 807) are characterized by *Linaresia* (= *Anomalinoides*) *pseudogrosserugosa* in the lower Miocene and *Brizalina pusilla* in the middle Miocene, high percentages of *Nuttallides umbonifera* from the lower Miocene through the lower Pliocene, and rare uvigerinids from the Oligocene through the middle Miocene. Uvigerinids decrease in frequency away from the equator in Quaternary and upper Miocene samples, presumably related to upwelling and organic flux of the sediments. The lower Pliocene sample at Site 807, however, contains more uvigerinids than comparable samples at the two deeper sites, perhaps a reflection of shifts in water mass boundaries or in the equatorial divergence zone.

Listed in Table 7 are the most frequent species present in sand-fraction (63 μm) samples representative of the various time-stratigraphic units. Their percent frequencies among the benthic fauna are given, as well as the names of some less frequent members of the assemblages. The following data are also given: B = the percent representation of benthic specimens relative to total foraminifer content; N = the number of specimens counted for the percent frequency data; and T = the total number of benthic specimens in each approximately 20-cc core-catcher sample, calculated from the sample split used for the census data.

Diatoms

Diatoms were examined in Holes 807A and 807C. The assignment of Site 807 samples to low-latitude diatom zonations is summarized in Figure 31.

Hole 807A

Above 83.4 mbsf (Pleistocene to upper Pliocene, Cores 130-807A-1H to -9H), diatoms are rare and poorly preserved. An exception was found in Sample 130-807A-5H-CC, in which diatoms are abundant and moderately preserved. This sample was assigned to the NTD 15 *Rhizosolenia praebergonii* Zone; it is characterized by a diverse flora dominated by *Coscinodiscus nodulifer* and *Nitzschia marina. Rhizosolenia praebergonii, Asteromphalus elegans, Hemidiscus cuneiformis, Thalassiosira convexa* var. *aspinosa, T. oestrupii, T. leptopus, T. eccentrica, Nitzschia fossilis, N. reinholdii*, and *Thalassionema nitzschioides* are also characteristic of NTD 15. Diatoms increase sharply in abundance and preservation from Samples 130-807A-9H-CC (middle Pliocene NTD 15A *R. praebergonii* Zone) through -40X-CC (middle Miocene NTD 6 *Coscinodiscus lewisianus* Zone). The poor preservation of diatoms between 389.2 mbsf (middle Miocene, Sample 130-807A-41X-CC) and 620.6 mbsf (upper Oligocene, Sample 130-807A-65X-CC) and the lack of age-diagnostic fossils

Table 7. Benthic foraminifers as a percentage of total foraminifers, Site 807.

Age and sample data	Species name	Sample (%)
Quaternary (N22)	*Pullenia bulloides*	18%
Sample 130-807A-2H-CC	*Globocassidulina subglobosa*	12%
B = <1%	*Pseudoparrella exigua*	10%
N = 197	*Oridorsalis umbonatus*	7%
T = 3,152	*Melonis affinis*	6%
	Pacinonion novozealandicum	5%
	(Others: *Fontbotia wuellerstorfi*, *Nuttallides umbonifera*)	
lower Pliocene (N18)	*Globocassidulina subglobosa*	13%
Sample 130-807A-13H-CC	*Nuttallides umbonifera*	13%
B = <1%	*Siphouvigerina* sp.	9%
N = 152	*Pullenia bulloides*	7%
T = 2,432	*Cibicidoides mundulus*	6%
	(Others: *Fontbotia wuellerstorfi*, *Parrelloides bradyi*)	
upper Miocene (N17a)	*Globocassidulina* sp.	9%
Sample 130-807A-23H-CC	*Globocassidulina subglobosa*	7%
B = <1%	*Favocassidulina favus*	7%
N = 236	*Cibicidoides mundulus*	6%
T = 1,888	*Oridorsalis umbonatus*	6%
	Siphonodosaria sp.	6%
	(Others: *Siphouvigerina* sp., *Uvigerina bradyana*, *Nuttallides umbonifera*)	
middle Miocene (N11)	*Nuttallides umbonifera*	10%
Sample 130-807A-40X-CC	*Globocassidulina subglobosa*	9%
B = <1%	*Fontbotia wuellerstorfi*	6%
N = 133	*Globocassidulina* sp.	5%
T = 2,128	*Brizalina pusilla*	5%
	Oridorsalis umbonatus	5%
	(Others: *Uvigerina gracilliformis*, *Parrelloides bradyi*)	
lower Miocene (N4)	*Globocassidulina subglobosa*	14%
Sample 130-807A-56X-CC	*Nuttallides umbonifera*	8%
B = <1%	*Linaresia pseudogrosserugosa*	7%
N = 134	*Stilostomella* sp.	7%
T = 536	*Gyroidinoides zealandicus*	6%
	Pyrulinoides sp.	6%
	Pullenia bulloides	5%
	(Others: *Parrelloides bradyi*, *Cibicidoides* sp., *Nonion havanense*, *Uvigerina gracilliformis*)	
upper Oligocene (P22)	*Cibicidoides praemundulus*	14%
Sample 130-807A-65X-CC	*Globocassidulina subglobosa*	13%
B = <1%	*Eggerella bradyi*	9%
N = 109	*Gyroidinoides lamarckianus*	7%
T = 436	*Pleurostomella subnodosa*	6%
	Oridorsalis umbonatus	5%
	(Others: *Parrelloides bradyi*, *Anomalinoides spissiformis*, *Uvigerina gracilliformis*, *Cassidulina spinifera*, *Bulimina glomarchallengeri*)	
lower Oligocene (P19)	*Globocassidulina subglobosa*	22%
Sample 130-807A-85X-CC	*Cibicidoides praemundulus*	8%
B = <1%	*Pacinonion* sp.	8%
N = 129	*Gyroidinoides girardanus*	7%
T = 516	*Oridorsalis umbonatus*	6%
	Pleurostomella sp.	6%
	Parrelloides bradyi	5%
	Bulimina cf. *microcostata*	5%
	(Others: *Cibicidoides grimsdalei*, *Anomalinoides spissiformis*)	
upper Eocene (P17)	*Anomalinoides spissiformis*	11%
Sample 130-807C-18R-CC	*Gyroidinoides girardanus*	10%
B = <1%	*Globocassidulina subglobosa*	10%
N = 209	*Cibicidoides praemundulus*	9%
T = 209	*Oridorsalis umbonatus*	8%
	Alabamina dissonata	5%
	Cibicidoides grimsdalei	5%
	Pleurostomella sp.	5%
	(Others: *Nonion havanense*, *Uvigerina havanensis*, *Cibicidoides eocaenus*)	

Notes: B = the percentage of representation of benthic specimens relative to total foraminifer content; N = the number of specimens counted for the percent frequency data; and T = the total number of benthic specimens in each approximately 20-cm^3 core-catcher sample, calculated from the sample split used for the census data.

precludes an age assignment for this rather large interval. Samples 130-807A-66X-CC through -81X-CC were assigned to the *Rocella vigilans* Zone. The LO of *Coscinodiscus excavatus* was found in Sample 130-807A-86X-CC (early Oligocene *C. excavatus* Zone).

Hole 807C

The diatom assemblages of Samples 130-807A-82X-CC through -86X-CC and Samples 130-807C-1R-CC through -5R-CC are very similar in composition and abundance. The LO of *C. excavatus* was found in Sample 130-807C-5R-CC at 828.3 mbsf.

Diatoms are common to abundant and moderately to well preserved from the Oligocene (Sample 130-807C-1R-CC) to the upper middle Eocene (Sample 130-807C-24R-CC). The following diatom zones were recognized (Fig. 31): *C. excavatus* Zone (Samples 130-807C-5R-CC through -16R-CC), *Baxteriopsis brunii* Zone (Samples 130-807C-17R-CC to -21R-CC), and *Asterolampra marylandica*(?) Zone (Samples 130-807C-22R-CC through -25R-CC). For the purposes of this report, the *C. excavatus* Range Zone of Barron (1985) was used here without recognition of Fenner's (1984) *Cestodiscus reticulatus* Zone. *Cestodiscus reticulatus* seems to be absent in Hole 807C, or this species may have been confused with *Cestodiscus robustus* (see comments in Barron, 1985).

A sharp decrease in abundance and preservation was seen in Sample 130-807C-25R-CC, below which the stratigraphic section is barren of diatoms.

Radiolarians

At Site 807, radiolarians were recovered from essentially all (except for several Pleistocene samples) of the section down to the middle Eocene, but generally none (or only trace amounts) were recovered from limestones below the upper middle Eocene. The radiolarians in the oozes (Pleistocene to middle Miocene) and chalks (middle Miocene to middle Eocene) are well to poorly preserved, and they provide useful age information in most cases. Radiolarian preservation in Neogene sediments at Site 807 is generally the worst of all the sites drilled during Leg 130. Nevertheless, zonal assignments for the Oligocene to lower Miocene were best accomplished at Site 807, among all sites of Leg 130, because of the presence of key taxa and high sedimentation rates, despite the poor preservation of radiolarians during this time interval.

Radiolarian-barren intervals become common downcore in the middle Eocene. Essentially all of the limestone samples are barren of radiolarians, including those from the Cretaceous/Tertiary boundary (see "Calcareous Nannofossil" section, this chapter). Below the Maestrichtian and Campanian limestones, the lithology changed into radiolarian siltstones and radiolarian sandy siltstones, just above the basement basalts. In these siltstones, abundant radiolarians were recovered that provided important zonal information.

Core-catcher samples from Hole 807A were examined throughout the interval drilled, down to the base of the hole (822.9 mbsf). Three core-catcher samples recovered from Hole 807B were also examined and used to make a stratigraphic composite, as the uppermost three core-catcher samples from Hole 807A did not provide well-defined age information because of the dissolution. In Hole 807C, sediments were washed to 780.0 mbsf and cores were recovered thereafter; core-catcher samples throughout the hole (from 789.7 to 1375.4 mbsf) were examined. In addition, samples from within Cretaceous cores were examined to determine ages otherwise not obtainable because of the absence of all other microfossil groups. Zonal assignments (Saunders et al., 1984; Sanfilippo and Riedel, 1985; Sanfilippo et al., 1985) of the samples with stratigraphically important taxa are discussed below. The radiolarian datums with absolute ages cited in this discussion are taken from those listed by Nigrini in the "Explanatory Notes" chapter of Leg 117 (Shipboard Scientific Party, 1989). Figure 31 summarizes the radiolarian zonation of the Holes 807A, 807B, and 807C as well as provides correlation with zones of other taxa. The radiolarian zones are continuous from at least the lower Pleistocene to the base of the upper Eocene. No evidence for significant sediment reworking was found at this site.

Quaternary

Sample 130-807B-1H-CC was placed in the *Buccinosphaera invaginata* Zone of the Quaternary based on the presence of *B. invaginata*. Sample 130-807B-2H-CC contains *Theocorythium trachelium,* suggesting that it is in the *Anthocyrtidium angulare* Zone or younger. Neither Sample 130-807A-3H-CC nor 130-807B-3H-CC contains enough radiolarians (thus lacking key taxa) to assign ages.

Pliocene

Sample 130-807A-4H-CC belongs to the *Pterocanium prismatium* Zone, which contains *Lamprocyrtis heteroporos* and the LO of *Theocalyptra davisiana*. Sample 130-807A-5H-CC was also placed in the same zone and contains the LO of *P. prismatium* (1.52–1.56 Ma). This datum level, however, may be in one or two shallower cores as dissolution has affected the assemblages. Thus, this datum level, which may not be reliable, was not used in the sedimentation rate estimates (see "Sedimentation Rates" section, this chapter). Samples 130-807A-6H-CC through -10H-CC contain assemblages that place them in the *Spongaster pentas* Zone. This zone contains the following radiolarian events: the LO of *Stichocorys peregrina* (2.62–2.64 Ma) in Sample 130-807A-6H-CC; the FO of *Amphirhopalum ypsilon* (3.77–3.79 Ma) in Sample 130-807A-8H-CC; the LO of *Phormostichoartus fistula* in Sample 130-807A-8H-CC; the LO of *S. pentas* (3.74–3.82 Ma) in Sample 130-807A-9H-CC; the FO of *Spongaster tetras* (3.83–3.85 Ma) in Sample 130-807A-9H-CC; and the LO of *Phormostichoartus doliolum* (3.53–3.55 Ma) in Sample 130-807A-10H-CC. Samples 130-807A-11H-CC through -18H-CC were placed in the *S. peregrina* Zone. Radiolarian events found in this zone include the following: the LO of *Spongaster berminghami* (3.85–3.87 Ma) in Sample 130-807A-11H-CC; the LO of *Solenosphaera omnitubus* (4.7–4.8 Ma) in Sample 130-807A-11H-CC; the FO of *S. pentas* (4.2–4.3 Ma) in Sample 130-807A-13H-CC; and the LO of *Acrobotrys tritubus* (5.3–5.4 Ma) in Sample 130-807A-16H-CC.

Upper Miocene

Samples 130-807A-19H-CC through -22H-CC were assigned to the *Didymocyrtis penultima* Zone. Radiolarian events found in these samples include the LO of *Stichocorys delmontensis* (5 Ma) in Sample 130-807A-19H-CC; the LO of *Siphostichartus corona* (5.0–5.1 Ma) in Sample 130-807A-20H-CC; the LO of *Calocycletta caepa* (6.2–6.6 Ma) in Sample 130-807A-21H-CC; and the FO of *Solenosphaera omnitubus* (6.3–6.5 Ma) in Sample 130-807A-21H-CC. Samples 130-807A-23H-CC through -28H-CC were placed in the *Didymocyrtis antepenultima* Zone. The LOs of the following six taxa were found in this zone: *Diartus hughesi* (7.1–7.2 Ma) in Sample 130-807A-23H-CC; *Dictyocoryne ontogenesis* (7.2–7.7 Ma) in Sample 130-807A-23H-CC; *Didymocyrtis laticonus* (8.1–8.2 Ma) in Sample 130-807A-25H-CC; *Botryostrobus miralestensis* (8.1–8.2 Ma) in Sample 130-807A-27H-CC; *Diartus petterssoni* (8.1–8.2 Ma) in Sample 130-807A-29H-CC; and *Stichocorys wolffii* (8.1–8.2 Ma) in Sample 130-807A-28H-CC. The FOs of two taxa were also found in this zone: *A. tritubus* (7.7–7.78 Ma) in Sample 130-807A-24H-CC and *S. berminghami* (7.9–8.0 Ma) in Sample 130-807A-28H-CC. Sample 130-807A-29X-CC was placed at the boundary (8.3–8.5 Ma) between the *D. petterssoni* and *D. antepenultima* zones, as this sample is located one core below the FO of *S. berminghami* (7.9–8.0 Ma) and the LO of *D. petterssoni* (8.1–8.2 Ma) and contains both *D. hughesi* and *D. petterssoni.* This boundary, therefore, was defined as the evolutionary transition from *D. petterssoni* to *D. hughesi* (Sanfilippo et al., 1985).

Middle Miocene

Samples 130-807A-29H-CC through -36X-CC were placed in the *D. petterssoni* Zone. The FO of *D. hughesi* (8.7–8.8 Ma) in Sample 130-807A-30H-CC and the LOs of *Lithopera thornburgi* (10.3–11.6 Ma) in Sample 130-807A-32H-CC, *Cyrtocapsella japonica* (10.0–10.3 Ma) in Sample 130-807A-33H-CC, and *Cyrtocapsella cornuta* (11.6–11.9 Ma) in Sample 130-807A-36X-CC were found in this zone. Samples 130-807A-37X-CC through -43X-CC were placed in the *Dorcadospyris alata* Zone. Several FOs and LOs of *Dorcadospyris* species are in this zone, but exact datum levels are yet to be determined.

Lower Miocene

Samples 130-807A-44X-CC through -47X-CC were placed in the *Calocycletta costata* Zone. Samples 130-807A-48X-CC through -52X-CC were placed in the *Stichocorys wolffii* Zone. Sample 130-807A-53X-CC was assigned to either the *Stichocorys delmontensis* Zone or the *S. wolffii* Zone, which could not be differentiated because of the lack of key taxa. Diagnostic taxa found in this sample include *Cyrtocapsella tetrapera, Cyrtocapsella japonica, Dorcadospyris ateuchus,* and *Dorcadospyris simplex*. Samples 130-807A-54X-CC through -58X-CC were placed in the *S. delmontensis* Zone, followed by the *Cyrtocapsella tetrapera* Zone in which Samples 130-807A-59X-CC through -61X-CC were placed. Samples 130-807A-62X-CC through -67X-CC were placed in the *Lychnocanoma elongata* Zone. Zonal assignment for the earliest lower Miocene was best accomplished at Site 807, among all sites of Leg 130, because of the presence of key taxa and high sedimentation rates, despite the generally poor radiolarian preservation. At this site, *Dorcadospyris riedeli* appears just above the occurrence of *Dorcadospyris papilio*. This has been a consistent occurence at all sites drilled during Leg 130. The range of *D. riedeli* on the Ontong Java Plateau appears within the duration of *L. elongata* Zone. This will serve as a useful time marker near the Oligocene/Miocene boundary in future studies.

Oligocene

Samples 130-807A-68X-CC through -70X-CC belong to either the *Dorcadospyris ateuchus* Zone or the *L. elongata* Zone, which also could not be differentiated because of the lack of key taxa. Samples 130-807A-71X-CC through -82X-CC and 130-807C-1R-CC (789.7 mbsf) were assigned to the *D. ateuchus* Zone of the upper Oligocene. These samples usually contain the following key taxa: *Dorcadospyris forcipata, D. ateuchus, Theocyrtis annosa, Lithocyclia angusta,* and *Artophormis gracilis*. Samples 130-807A-84X-CC (803.6 mbsf) and 130-807C-2R-CC (799.3 mbsf) were placed at the boundary between the *Theocyrtis tuberosa* Zone and the *D. ateuchus* Zone as both contained *Dorcadospyris circulus* and *Dorcadospyris quadripes* (Moore, 1971), together with *A. gracilis* and *L. angusta*. The match between Holes 807A and 807C is very good as documented by the boundary depths indicated above. Samples 130-807A-85X-CC and -86X-CC and 130-807C-3R-CC through -16R-CC belong to the *T. tuberosa* Zone of the lower Oligocene; diagnostic taxa include *Artophormis gracilis, Centrobotrys gravida, Cyclampterium milowi, Tristylospyris triceros, Lithocyclia crux,* and *L. angusta.*

Upper Eocene

Samples 130-807C-17R-CC through -22R-CC, all of which contain *Cryptoprora ornata,* were placed in the *C. ornata* Zone (= upper *Thyrsocyrtis bromia* Zone of Sanfilippo et al., 1985) of the uppermost Eocene (Saunders et al., 1984). Samples from the upper part of this zone contain *L. aristotelis* group (varieties with three and four wide arms). Samples 130-807C-23R-CC through -26R-CC, bearing *Calocyclas bandyca,* are placed in the *C. bandyca* Zone. Other age-diagnostic taxa co-occurring with *C. bandyca* include *Calocyclas turris, Artophormis balbadensis, Lophocyrtis jacchia, Thyrsocyrtis tetracantha, T. bromia,* and *Thyrsocyrtis rhizodon.* In Core 130-807C-26R the first chert nodules were found (for more details, see the "Lithostratigraphy" section, this chapter). Below this core, the occurrence of cherts generally increased.

Middle Eocene

Coincidental with the occurrence of cherts and silicified chalk, radiolarian abundance decreased with depth; apparently the result of the dissolution of biogenic opal and the remobilization of silica during chert formation. Cores 130-807C-27R through -39R, containing chalk or a mixture of chalk and limestone, have poorly preserved radiolarians or are barren. Thus, zonal assignments were possible only for the following samples. Sample 130-807C-28R-CC was placed in the *Dictyoprora mongolfieri* Zone to the *Cryptoprora ornata* Zone of the middle Eocene to the upper Eocene, which could not be resolved because only *D. mongolfieri, Dictyoprora armadillo,* and *Lithochytris vespertilio* were present. Samples 130-807C-31R-CC and -36R-CC belong to the *Podocyrtis chalara* Zone of the middle Eocene up to the *Carpocanistrum azyx* Zone of the basal late Eocene, which also could not be resolved further, as only *P. chalara, T. rhizodon, L. vespertilio, Eusyringium fistuligerum,* and members of the *Sethochytris babylonis* group were present. Samples 130-807C-33R-CC and -37R-CC were placed in the *T. triacantha* Zone up to the *C. azyx* Zone as they contain *E. fistuligerum.* Sample 130-807C-39R-CC belongs to the *T. triacantha* Zone as *T. triacantha, Theocotyle venezuelensis,* and *Podocyrtis sinuosa* were present. Sample 130-807C-40R-CC was assigned to a range from the *Theocotyle cryptecephala* Zone to the *Pterocodon ampla* Zone, based on the presence of *P. sinuosa.* Samples 130-807C-27R-CC, -30R-CC, -32R-CC, -34R-CC, -35R-CC, and -38R-CC were barren of radiolarians.

Cores 130-807C-40R through -70R are limestones with intermittent occurrences of cherts, especially in the Tertiary. Core-catcher samples in this long interval were usually devoid of radiolarians and only occasionally contained trace amounts of radiolarian fragments or radiolarian casts. Thus, no age information was obtained from these cores or from Core 130-807C-54R, which was examined in several sectional samples.

Cretaceous

Radiolarian abundance increased with a drastic change in lithology from limestone to brown siltstone. Samples 130-807C-71R-CC; -72R-1, 89–91 and 144–146 cm; -72R-2, 121–123 cm; and -73R-1, 100–102 cm, were placed in the upper *Acaeniotyle umbilicata* Zone of the upper Albian to the lower *Abesacapsula sophedia* Zone of the lower Cenomanian (103–95 Ma) (Sanfilippo and Riedel, 1985). They contain opal CT or quartz-filled (e.g., inside of shells) radiolarians of the following taxa: *Pseudodictyomitra pseudomacrocephala, Thanarla veneta, T. elegantissima, T. pulchra* (of Sanfilippo and Riedel, 1985), *Thanarla* sp., *Archaeodictyomitra* cf. *vulgaris, Archaeodictyomitra* sp. A (of Thurow, 1988), and *Novixitus*[00a0]sp. Although the range of *T. pulchra* (of Sanfilippo and Riedel, 1985) was illustrated as Berriasian to Barremian by Sanfilippo and Riedel (1985), Thurow (1988, p. 407) points out that ". . . their text figure 8 (2d) shows Pessagno's (1977) type specimen, which is from the lower Cenomanian . . . ." Thus, the above co-occurrence of the two taxa presents no problem, and zonal assignment from the upper Albian to the lower Cenomanian is justified. Specimens of the two species of *Thanarla* showed distensions both greater than and less than 25% (see Sanfilippo and Riedel, 1985), so they were placed into *T. pulchra* and *T. elegantissima,* according to the definitions of Sanfilippo and Riedel (1985). Thurow's (1988) definition of this species is slightly different: both forms of the genus observed here fall into Thurow's *T. elegantissima.* In either case, specimens with distensions greater than 25% (i.e., *T. pulchra* or *T. elegantissima*) are Albian-Cenomanian in age.

Basalt was recovered in Core 130-807C-74R, and a thin layer of limestone occurred at the top of the core. Sample 130-807C-74R-1, 0–2 cm, contains a small number of poorly preserved radiolarians and was tentatively given an Aptian to Cenomanian age based on the presence of the following taxa and the evolutionary changes mentioned below: *Thanarla* sp. A aff. *T. conica* (Thurow, 1988, pl. 7, figs. 7 and 8), *Thanarla* sp. B aff. *T. conica* (Thurow, 1988, pl. 7, fig. 12), ?*Archaeodictyomitra vulgaris,* and *Cyrtocapsa* sp. cf. *C. grutterinki.* All the taxa mentioned in this sample are illustrated in plates 7 and 8 of Thurow (1988), which are characteristic of the Hauterivian to the lower Aptian. With increasing depth, changes in the morphology of the genus *Thanarla* from a *T. elegantissima* type to a *Thanarla conica* type were noticed. Sample 130-807C-73R-1, 100–102 cm, contains *Thanarla conica.* It appears that we are seeing a gradual evolutionary change in *Thanarla* morphology: among the five samples assigned from the upper Albian to the lower Cenomanian, Sample 130-807C-73R-1, 100–102 cm (the deepest one) is slightly older than the rest of the four. By the same token, Sample 130-807C-74R-1, 0–2 cm, is slightly older (but not substantially) than the five samples from Cores 130-807C-71R through -73R.

Two sedimentary layers composed of limestones were found in Sections 130-807C-80R-1 and -82R-3 between pillow basalts. Sample 130-807C-80R-1, 70–72 cm, contains rare, poorly preserved, non-age-diagnostic spumellarians. Sample 130-807C-80R-1, 74–75 cm, is barren of radiolarians, and spherical cavities in rock matrices were found during standard acidified slide procedures. Nonacidified foraminifer preparation of this sample yielded spherical spumellarian-like specimens. Thus, we consider that the specimens were replaced by calcium carbonate. Sample 130-807C-82R-1, 75–76 cm, is also barren of radiolarians. No age information, therefore, can be given to any of the three samples interbedded in the basalt layers.

PALEOMAGNETISM

Introduction

Pass-through magnetometer measurements were taken on the split-archive sections cored with the APC in Hole 807A, all of which were oriented except Cores 130-807A-1H and -2H. A sharp drop in magnetic intensity, similar to that seen at the other Leg 130 sites, was observed at approximately 32 mbsf.

Below that depth, magnetic intensities were close to the noise level of the pass-through cryogenic magnetometer, and the paleomagnetic directional information useful for polarity determination was lost. In response to this behavior, only Cores 130-807B-1H through -10H were measured from Hole 807B.

All XCB and RCB cores from Hole 807C were measured, except those lacking a substantial number of sufficiently long pieces that were likely to have remained aligned in the core. Certain intervals cored with the RCB had exceptional recovery, and both inclination and relative declination information were available. Unlike Site 803, basalts recovered from Site 807 commonly contained numerous continuous pieces in a given section. Therefore, split archive sections were measured rather than representative pieces from a section. These sections were measured after the individual section pieces had been numbered for curatorial purposes. Measurement intervals for Site 807 paleomagnetic analyses varied between 1, 3, 5 and 10 cm. Basalt sections generally were measured at 1-cm sampling intervals. This detailed sampling interval should allow the examination of individual numbered pieces in the data.

Sediments

Pleistocene

The loss of an interpretable paleomagnetic polarity signal appears to be related in a simple fashion to the drop in magnetic remanence at Site 807. Loss of signal and decrease of remanence coincide at approximately 32 mbsf. Above the decrease in intensity, the Brunhes/Matuyama boundary as well as the Jaramillo and Olduvai subchrons were recognized (Fig. 32). Sedimentation rates, based on an age control provided by these polarity boundaries, average 15.6 m/m.y. (Hole 807B) over the interval from 1.88 Ma to the present (Fig. 33).

Sulfate Reduction and Magnetization

By analogy with other studies with detailed supporting rock magnetic data (e.g., Karlin and Levi, 1985), we think that the drop in magnetic intensity displayed in the Site 807 data is a result of the dissolution of magnetite by postdepositional reduction diagenesis. As at Site 806, there also appears to be a relationship between sulfate concentration measured by means of interstitial water geochemistry and the point at which magnetic intensity is lost (Fig. 34). Sulfate reduction increases more slowly with depth at Site 807 than at Site 806 (see "Inorganic Geochemistry" section, this chapter), but the sudden decrease in magnetization intensity and the accompanying loss of an interpretable polarity signal occurs at a similar sulfate concentration at both sites (about 26.6 mM at Hole 806B and about 26.8 mM at Hole 807A) (Fig. 34). Over the interval from approximately 18 to 27 mbsf, the natural remanent magnetization (NRM) inclination record is steeply negative (Fig. 32A), perhaps caused by the acquisition of a drill-string remanence. After 15-mT demagnetization, the inclination of this interval remains anomalously high (Fig. 32B). This may indicate the presence of a diagenetic mineral phase related to reduction.

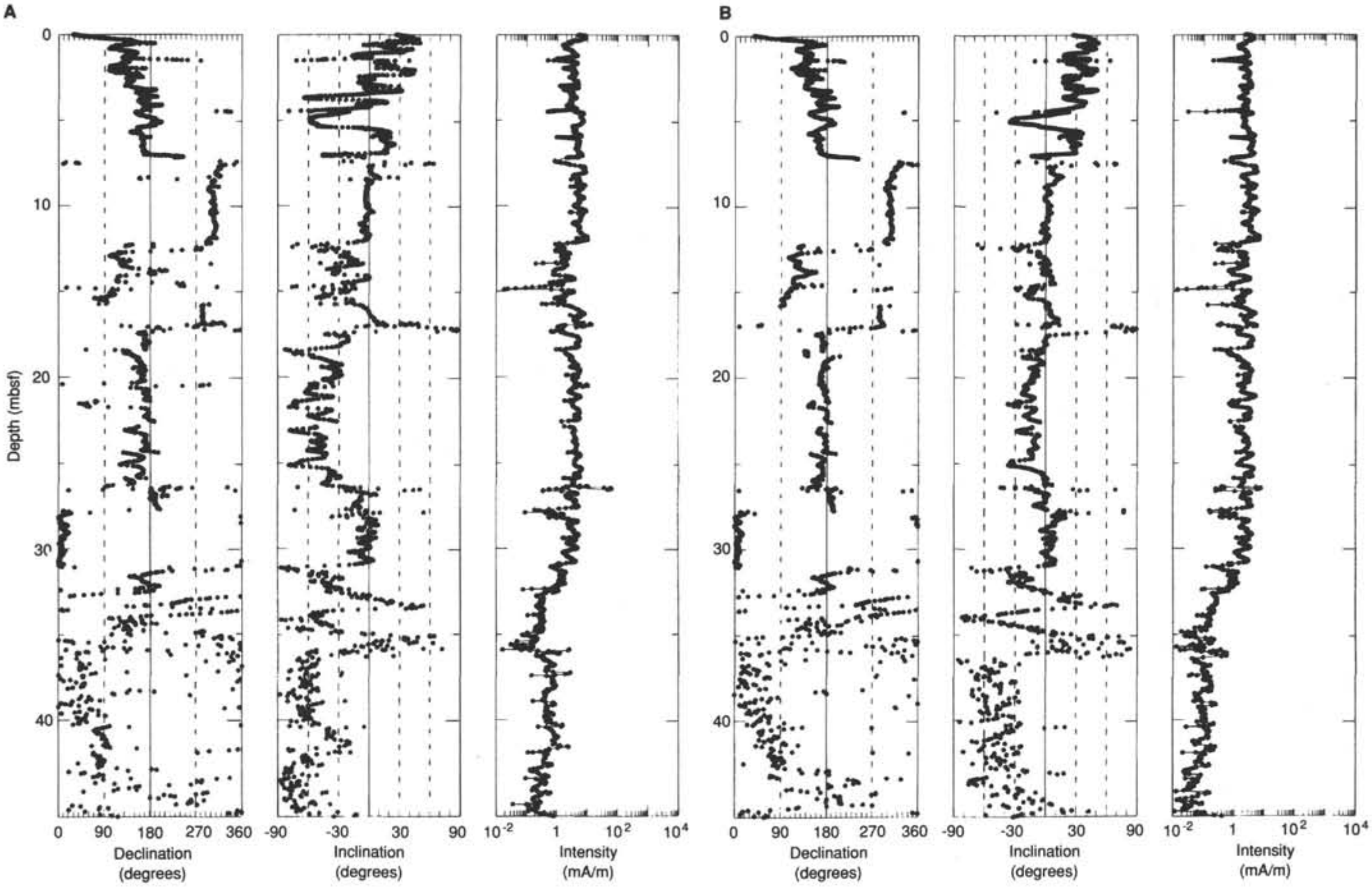

Figure 32. NRM (A) and AF-demagnetized (B) declination, inclination, and intensity record for Cores 130-807A-1H through -5H. Cores 130-807A-1H and -2H (0–16.9 mbsf) have not been oriented.

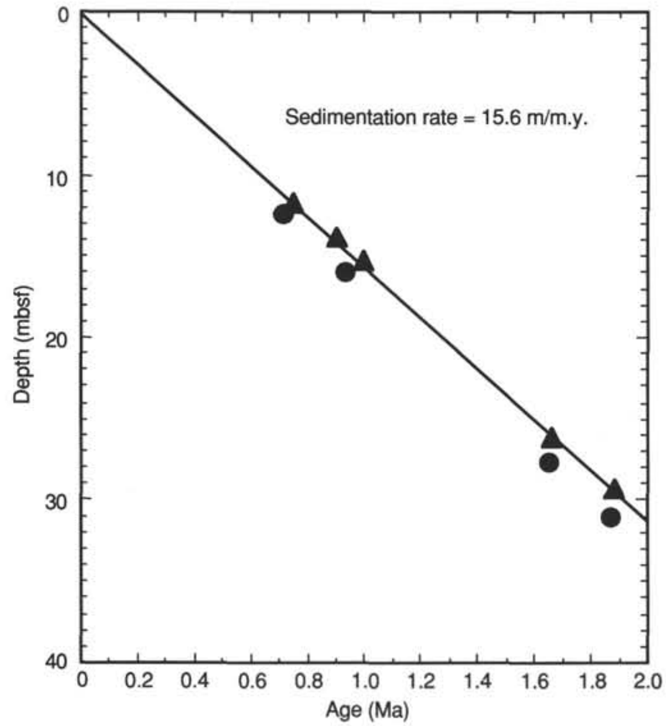

Figure 33. Depth vs. age plot derived from magnetostratigraphic data, Holes 807A (dots) and 807B (triangles). See discussion in text for details of magnetostratigraphic boundaries.

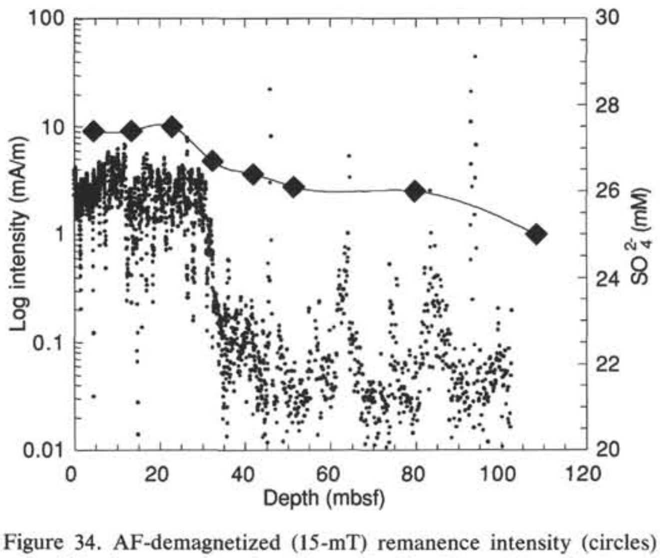

Figure 34. AF-demagnetized (15-mT) remanence intensity (circles) and sulfate ion concentration (diamonds, fitted by cubic splines) as a function of sub-bottom depth, Hole 807A.

The paleomagnetic record at Site 807, like the other sites of the Ontong Java Plateau, indicates a loss of magnetic intensity and polarity information at the same sub-bottom depth for the different APC holes, but at a different depth when comparing sites (Fig. 35). In general, decreasing water depth and latitude (i.e., proximity to the equatorial zone of upwelling) coincide with a decrease in the length of the paleomagnetic record. Differences in reduction are most likely ultimately caused by the supply of organic carbon: the greater the supply, the lesser the chance of retaining a magnetic signature.

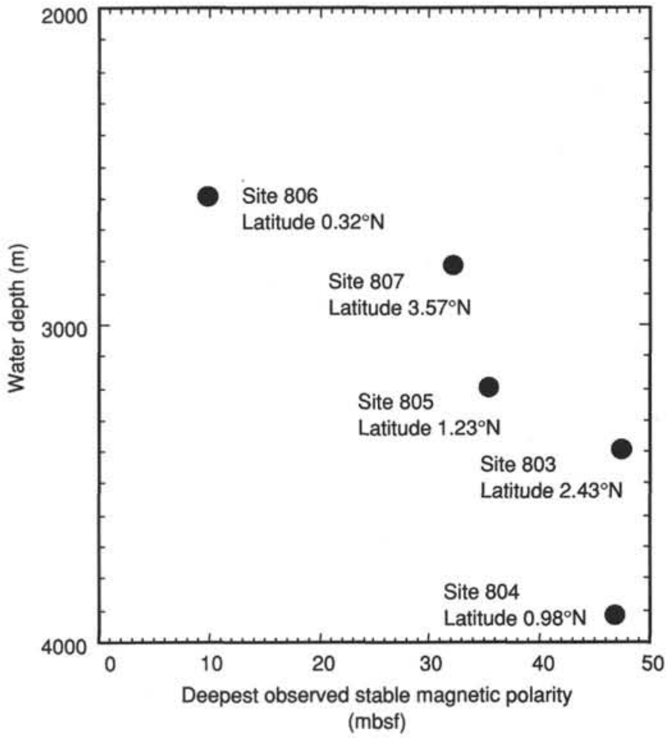

Figure 35. Depth at which paleomagnetic polarity information is lost vs. site water depth and latitude.

Miocene, Oligocene, and Eocene

Several intervals of consistent inclination were seen in the Miocene and Oligocene sequence in Hole 807A and in the Oligocene and Eocene sequence in Hole 807C. Inclination records after 15-mT demagnetization from Cores 130-807A-46X to -49X, 130-807A-64X to -71X, and 130-807C-4R, -6R, -17R, -23R, -24R, and- 26R all appear to record a consistent, stable magnetization. Rotary-drilled Cores 130-807C-4R, -6R, -17R, and -23R consist of continuous pieces as long as 3 m (two sections). Declination records following 15-mT demagnetization in these cores are continuous over these unbroken pieces (Fig. 36).

Paleolatitudes over the period represented by Cores 130-807A-46X to -49X, which date to early to middle Miocene nannofossil Zones NN5–NN3, are likely to have been very low, and the magnetostratigraphy was not determined on the inclination data alone. The frequency of 1° intervals of AF-cleaned inclination summed over these four cores peaks between +2° and −10° (Fig. 37A). Extrapolation of the 39-Ma point on the Pacific apparent polar wander path (APWP) (Gordon, 1983; Sager, 1987) predicts a paleolatitude of about 1.7°S for Site 807 at Zone NN4 time, corresponding to an inclination of ±3.4°. The frequency analyses suggest that the distribution of inclinations is shifted with respect to these values toward slightly steeper negative values. This could be a result of either an unremoved drill-string remanence or a sampling of more normal polarity samples than reversed.

Cores 130-807A-64X to -72X span the interval in the late Oligocene from foraminifer Subzone P21b to P22. Interpolation from the Pacific APWP places Site 807 from 4°S to 5.7° over this interval, corresponding to paleo-inclinations of ±8° to ±11.3°. The frequency distribution of 1° intervals of AF-cleaned inclination for this set of cores (Fig. 37B) has a broader maximum than that for the Miocene cores, perhaps reflecting the increased separation between normal and re-

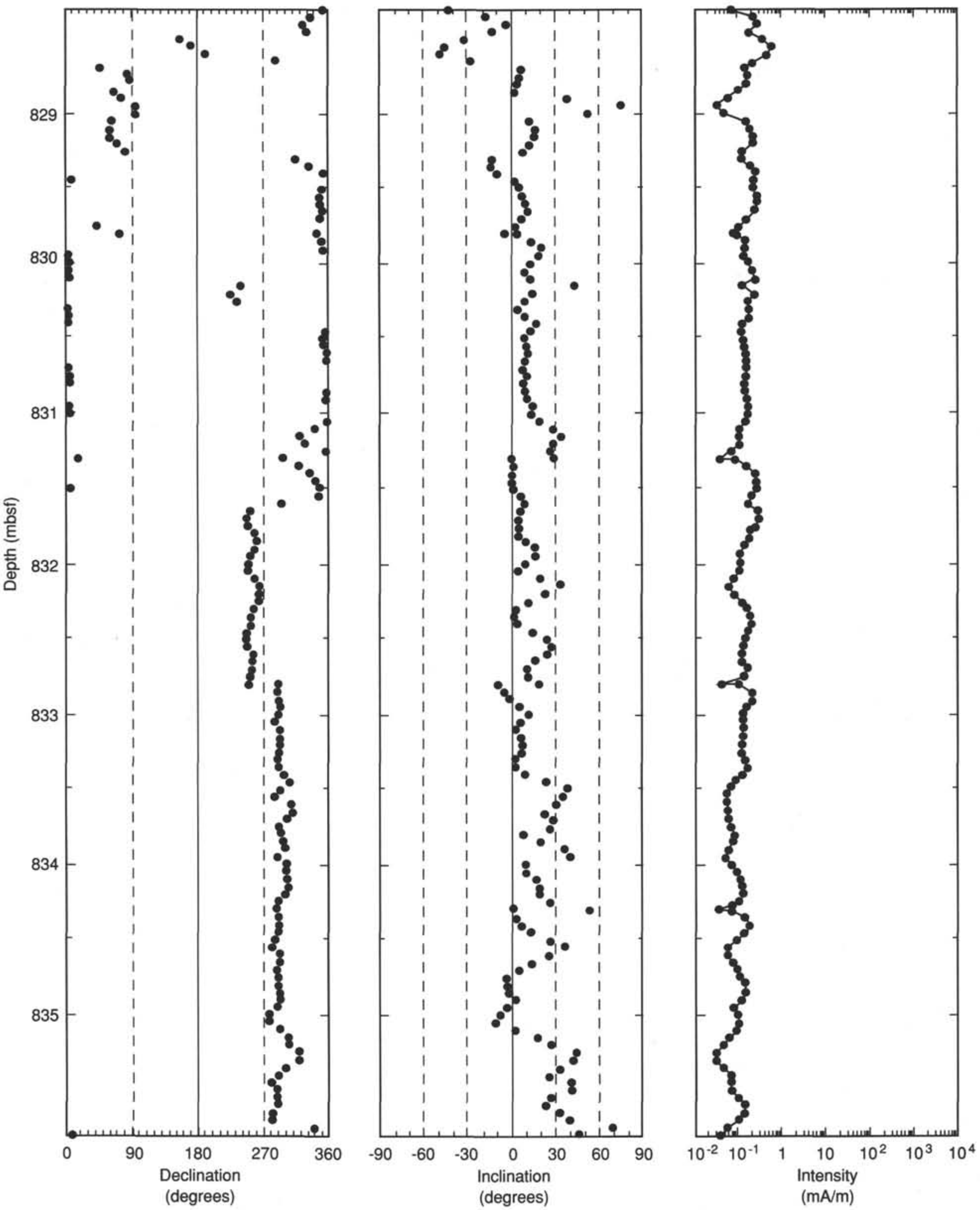

Figure 36. Declination, inclination, and intensity from unoriented Core 130-807C-6R. Note the long sections of continuous declination marking unbroken intervals within the core.

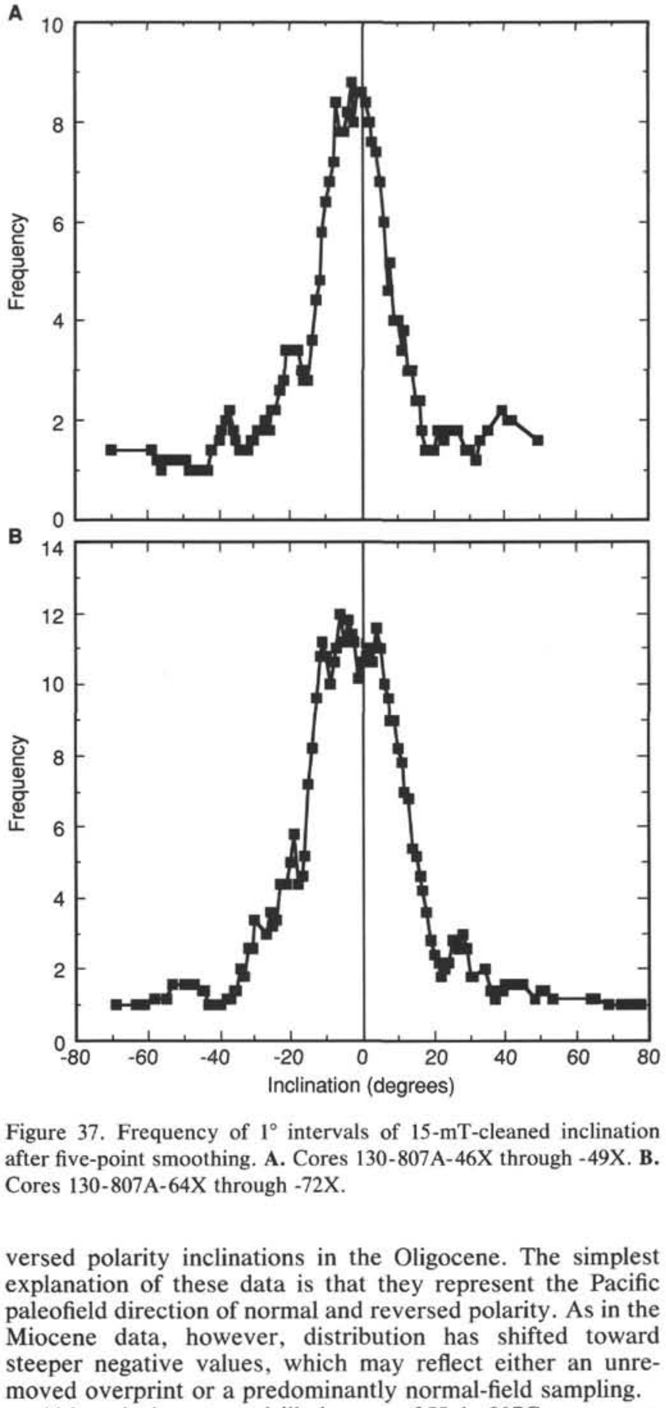

Figure 37. Frequency of 1° intervals of 15-mT-cleaned inclination after five-point smoothing. **A.** Cores 130-807A-46X through -49X. **B.** Cores 130-807A-64X through -72X.

versed polarity inclinations in the Oligocene. The simplest explanation of these data is that they represent the Pacific paleofield direction of normal and reversed polarity. As in the Miocene data, however, distribution has shifted toward steeper negative values, which may reflect either an unremoved overprint or a predominantly normal-field sampling.

Although the rotary-drilled cores of Hole 807C preserve a continuous record of both inclination and declination in many instances, inclinations are commonly variable within cores as well as between closely adjacent cores (Fig. 38). Combining data from all of the early Oligocene cores from Hole 807C for which there was sufficient recovery to enable processing through the cryogenic magnetometer (Cores 130-807C-2R, -4R, -6R, -9R, -12R, -15R, and -17R) yields the graph of frequency vs. 1° intervals of inclination shown in Figure 39A. Extrapolation of the Pacific APWP indicates a latitude of 6° to 7° for Site 807 during the early Oligocene, equating to an inclination of about ±12° to ±14°. The major peak of the inclination frequency graph occurs at +6°, essentially the inclination expected for a viscous remanent magnetization (VRM) acquired over the Brunhes Chron. Although a minor peak does occur at +14° AF-cleaned magnetizations in this set of cores appear to have recorded a present-day field overprint that can probably be removed with higher peak-field demagnetization.

The 15-mT-cleaned magnetizations of Eocene cores from Hole 807C with sufficient recovery for processing (Cores 130-807C-19R, -23R through -26R, -30R, -35R, -37R, -38R, and -40R through -44R) yield the inclination frequency graph shown in Figure 39B. In contrast to a bimodal distribution that would be expected if both normal and reversed direction were recorded in roughly equal proportion, the data define a skewed distribution with a maximum inclination at approximately 22°. Paleolatitudes for Site 807 extrapolated from the Pacific APWP range from about 13° at the beginning of the Eocene to about 8° at its end. The maximum is therefore in the expected range of inclinations for a normal polarity record, but overprinting as suggested in the other frequency graphs could also be present.

In summary, it appears that two factors limit interpretation of the available data. First, 15-mT demagnetization appears insufficient to remove overprinting in many intervals. Second, the expected inclinations of Site 807 on the Ontong Java Plateau are commonly too shallow to allow a clear distinction of normal and reversed polarity groups in the frequency analyses presented. It is suspected that samples from Site 289 (Hammond et al., 1975), which were AF-cleaned to only 10 mT, may suffer from these same limitations.

Paleocene and Cretaceous

Most Paleocene-Campanian sections recovered were composed of section pieces too small to be interpreted with our pass-through magnetometer measurements. The transition from these limestones to the brown and red clays recovered in Core 130-807C-71R, however, deserves special mention. In this core nearly complete recovery allowed an evaluation of the clay NRM (Fig. 40), which was observed to be several orders of magnitude greater than that of the adjacent limestone. The NRM has an extremely consistent shallow inclination that may record a viscous present-day overprint. If this can be confirmed in shore-based studies, it may provide a means of orienting any primary declination present in these rocks.

Basalts

Basalt NRMs are dominantly negative and steeper than 20°. If the NRM is dominated by a primary remanence, as suggested in accordance with the unaltered nature of the flows, the entire basalt sequence is of normal polarity. Several intervals that do not show these NRM inclinations display inclinations that are positive and fairly shallow. After stepwise AF demagnetization at 5, 10, and 15 mT steps, these intervals have negative inclinations similar to those of the rest of the basalts. As in the claystones, if this low-coercivity overprint can be shown to represent the present-day field direction at Site 807, it may be useful for orienting the primary declination.

The Aptian-Albian age of the sediments overlying the basalts recovered at Hole 807C give the volcanic sequence great potential for refining the Pacific APWP. Three factors make the study of Hole 807C basalts especially promising in shore-based studies: (1) the presence of two to three sediment interbeds, which suggests that the sequence may represent enough time to average a significant amount of secular variation; (2) the unaltered state of the rocks; and (3) the occurrence of massive flows interbedded with pillow flows that can provide control on possible tilting of individual pillows.

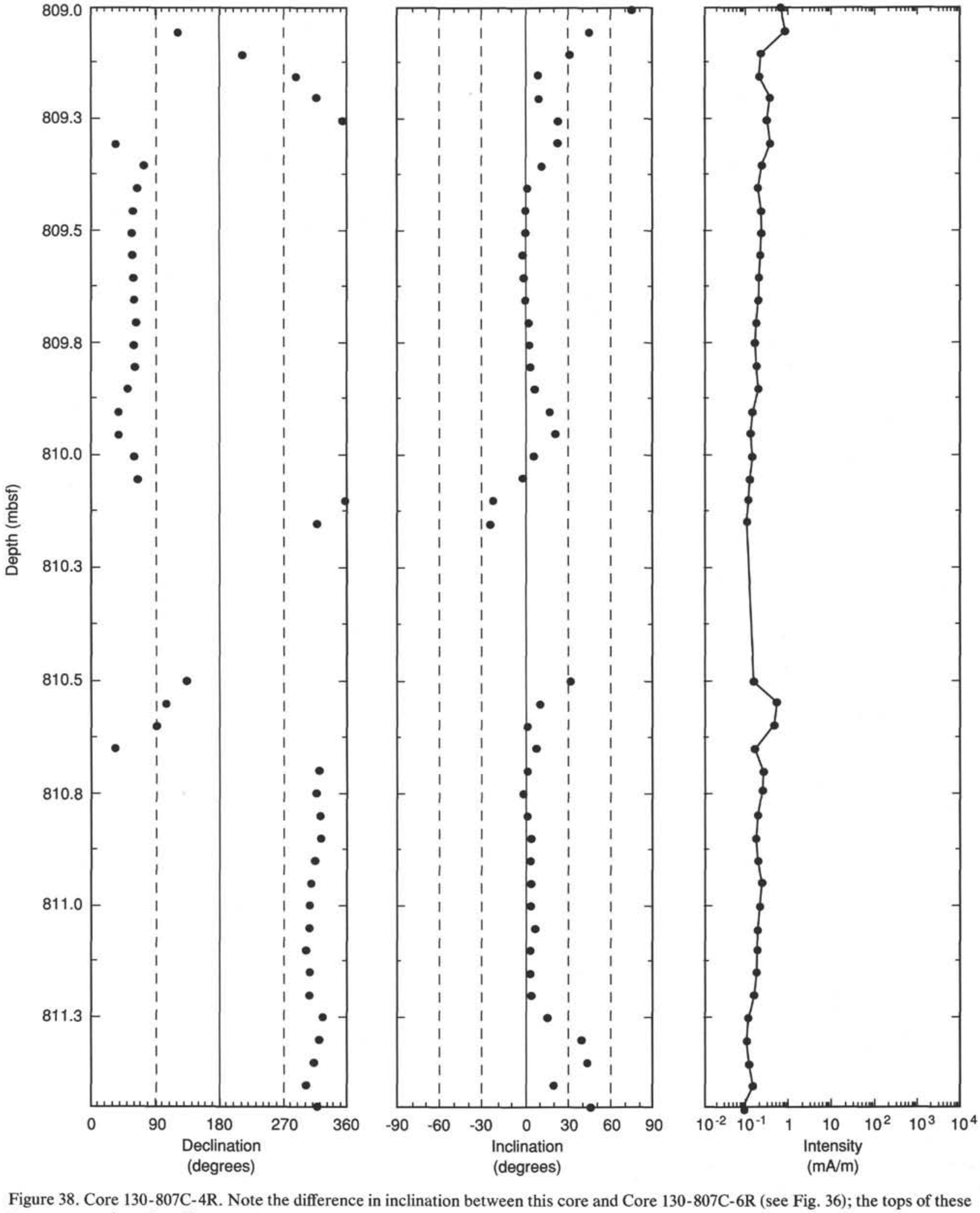

Figure 38. Core 130-807C-4R. Note the difference in inclination between this core and Core 130-807C-6R (see Fig. 36); the tops of these two cores are less than 20 m apart.

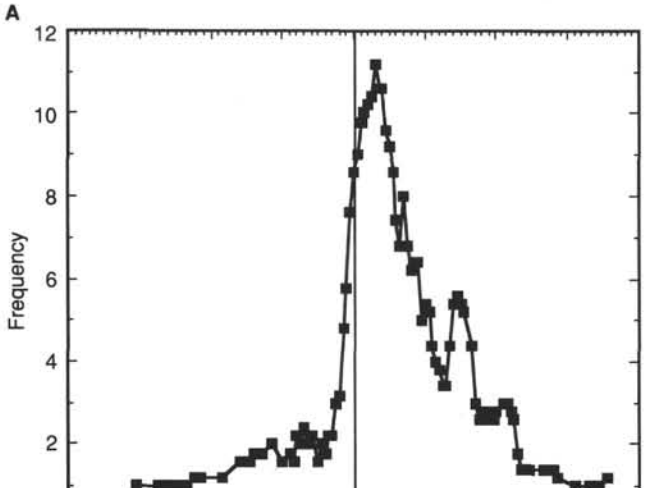

Figure 39. Frequency of 1° intervals of 15-mT-cleaned magnetization. **A.** Cores 130-807C-2R, -4R, -6R, -9R, -12R, -15R, and -17R, representing the early Oligocene. **B.** Cores 130-807C-19R, -23R through -26R, -30R, 35R, -37R, -38R, and -40R through -44R, representing the Eocene.

SEDIMENTATION RATES

Three holes were drilled at Site 807. Hole 807A was first cored with the APC and then deepened with the XCB to refusal at a depth of 822.9 mbsf and an age of 33.5 Ma. The average sedimentation rate in the interval from the lower Oligocene through the Holocene is 24.6 m/m.y. Hole 807B was cored with the APC to refusal at a depth of 278.6 mbsf and an age of 8.3 Ma, yielding an average sedimentation rate of about 33.6 m/m.y. in the interval from the lower Miocene through the Holocene. Hole 807C was washed to 780.0 mbsf and then cored with the RCB into basement. An average sedimentation rate of 17.7 m/m.y. was calculated for the biogenous sediments between the seafloor and the red clay contact at 1351.5 mbsf. This average rate is substantially lower than the Neogene rates. Increasing compaction with depth, condensed Paleogene sections, and the presence of several shorter Paleogene hiatuses all help to explain the apparent decrease in sedimentation rate with increasing age. Variable input rates of biogenic sediment components through time also have contributed to create the observed differences.

The biostratigraphic results from the three holes are presented in Table 8, and age-depth plots for Site 807 are shown in Figures 41–44. The age-depth plots from this hole have many features in common with Sites 805 and 806. First, a major change in slope of the age-depth indicators occurs close to 2 Ma, subsequently leading to peak rates of over 40 m/m.y. in the upper Miocene. Another general slope change occurs in the lower upper Miocene, indicating reduced sedimentation (on the order of 15–20 m/m.y.) through the middle and most of the lower Miocene. The basal Miocene through Oligocene interval is characterized by a doubling in sedimentation rates (30–40 m/m.y.), approaching those of the upper Miocene (Table 9). One 2-m.y.-long hiatus is indicated in the basal part of the late Oligocene, between 28.2 and 30.0 Ma (at 702.35 mbsf).

Age-depth plots from Hole 807C, representing the 50-m.y. interval from 30 to 80 Ma, are shown in Figure 42. This graph displays the general structure of the Paleogene and Upper Cretaceous rate history: rather high rates in the Oligocene through middle Eocene and Upper Cretaceous intervals, and comparatively low rates in the lower Eocene through Paleocene interval. The Oligocene through lower Eocene interval is shown in greater detail in Figure 43.

A hiatus that has its younger end precisely at the middle Eocene–upper Eocene boundary (40 Ma) is clearly indicated, although the position of its old end is less well constrained. Another hiatus, in combination with an extremely condensed section, occurs at about 1100 mbsf, between about 47 to 54 Ma. These hiatuses are associated with the termination and onset of the chert interval, respectively. The entire chert interval from about 970 through 1100 mbsf is characterized by anomalously low core recovery, which introduces large uncertainties in the depth positions of marker events and, consequently, sedimentation rate estimates.

Age-depth constraints in the lower Eocene through Upper Cretaceous interval are shown graphically in Figure 44. Sedimentation rates decrease progressively from about 17 m/m.y. in the lower Eocene to 2–3 m/m.y. in the basal Paleocene. This interval is preceded by Maestrichtian–upper Campanian rates that are on the order of 13–20 m/m.y. Sedimentation rates have not been established from the upper Albian–lower Cenomanian red clay interval (below 1351.5 mbsf), or the short interval of Albian-Aptian limestones that underlie the red clays and rest on the basement.

The sedimentation rates from all three holes at Site 807 are summarized in Figure 45. The difference in upper Miocene rates between Holes 807A and 807B stems from the use of different marker events (Hole 807B was terminated above the nannofossil Zone NN9/NN10 boundary at 8.7 Ma). The age control in the cross-over interval from Holes 807A to 807C is poorly constrained.

The Neogene sedimentation rate histories from all Leg 130 sites (Sites 803–807) are compared in Figure 46. The sites are listed as a function of increasing water depth, from Site 806 (shallowest) to Site 804 (deepest). This comparison clearly indicates a trend of decreasing rate with increasing water depth, at least back to almost 9 Ma. Assuming that the productivity input remained fairly similar at these sites at any given time; and, considering the fact that the sediments in these sections mainly consist of biogenous carbonate, it appears reasonable to conclude that the substantial decrease in sedimentation rate with depth reflects loss of carbonate by means of dissolution.

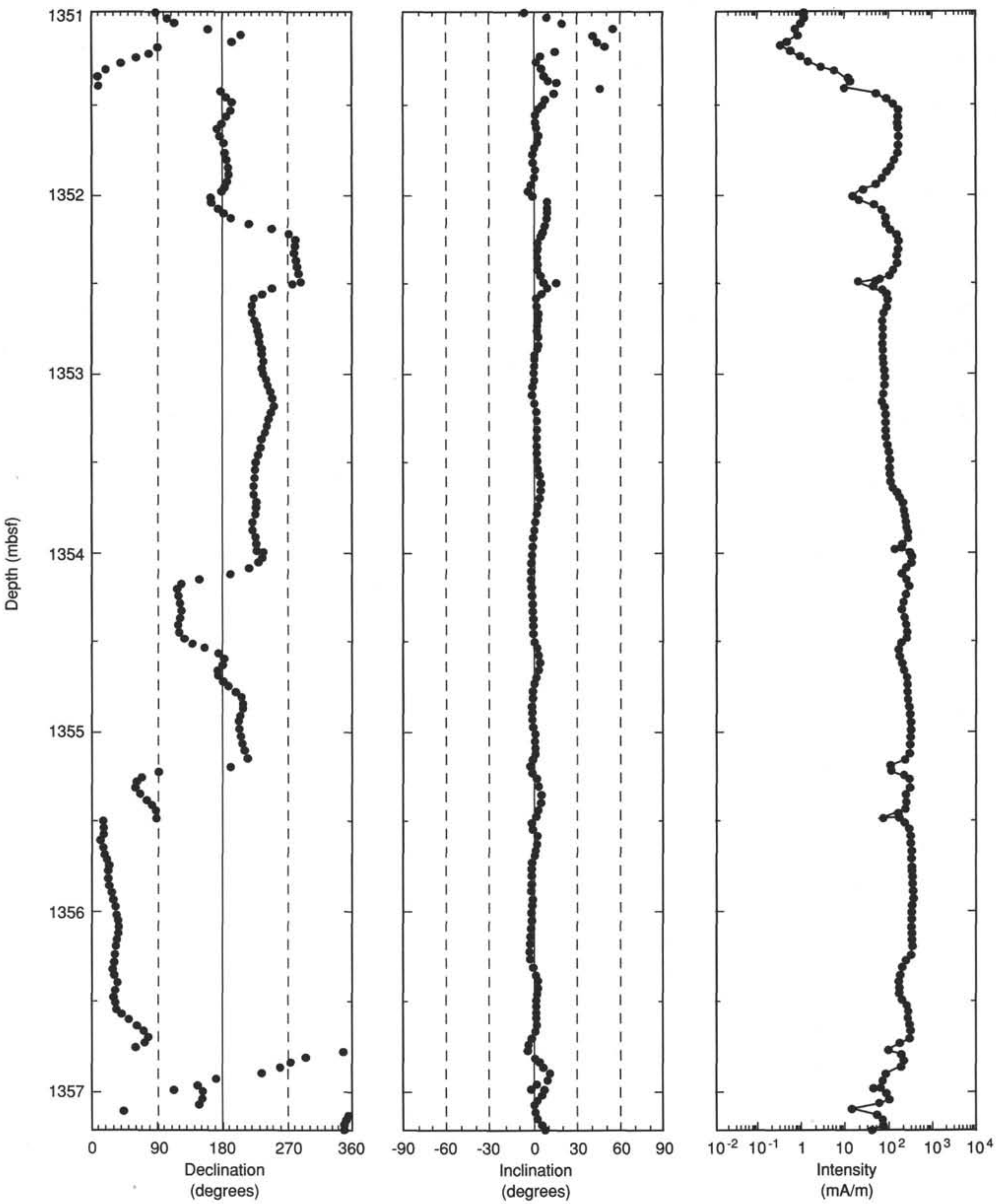

Figure 40. Pass-through cryogenic magnetometer record showing the natural remanent magnetization (NRM) of Core 130-807C-71R. The increase in intensity between 1351.0 and 1351.5 mbsf corresponds to the transition from limestone to claystone. Shifts in the declination record are caused by breaks between continuous pieces.

Table 8. Biostratigraphic events determined at Site 807.

Events	Upper depth (mbsf)	Lower depth (mbsf)	Age (Ma)
130-807A-			
LO *P. lacunosa* (N)	7.40	16.90	0.46
LO *G. tosaensis* (F)	7.40	16.90	0.60
LO *C. macintyrei* (N)	16.90	26.40	1.45
LO *G. fistulosus* (F)	26.40	35.90	1.60
LO *D. brouweri* (N)	26.40	35.90	1.89
FO *G. truncatulinoides* (F)	26.40	35.90	1.90
OA *D. triradiatus* (N)	26.40	35.90	2.07
LO *T. convexa* var. *aspinosa* (D)	16.90	26.40	2.10
LO *T. davisiana* (R)	35.90	45.40	2.43
LO *D. surculus* (N)	35.90	45.40	2.45
LO *S. peregrina* (R)	45.40	54.90	2.63
LO *D. tamalis* (N)	35.90	45.40	2.65
LO *G. altispira* (F)	54.90	64.40	2.90
FO *G. fistulosus* (F)	64.40	73.90	2.90
LO *Sphaeroidinellopsis* spp. (F)	35.90	45.40	3.00
FO *S. dehiscens* s.s. (F)	64.40	73.90	3.00
LO *P. fistula* (R)	64.40	73.90	3.27
LO *G. margaritae* (F)	64.40	73.90	3.40
LO *Sphenolithus* (N)	64.40	73.90	3.45
LO *P. doliolum* (R)	83.40	92.90	3.54
LO *R. pseudoumbilica* (N)	73.90	83.40	3.56
FO *A. ypsilon* (R)	73.90	83.40	3.78
LO *S. pentas* (R)	73.90	83.40	3.78
FO *S. tetras* (R)	83.40	92.90	3.84
LO *S. berminghami* (R)	92.90	102.40	3.86
FO *S. pentas* (R)	121.40	130.90	4.25
FO *N. jouseae* (D)	102.40	111.90	4.50
LO *C. acutus* (N)	83.40	92.90	4.60
LO *S. omnitubus* (R)	92.90	102.40	4.75
LO *D. quinqueramus* (N)	121.40	130.90	5.00
LO *S. delmontensis* (R)	168.90	178.40	5.00
LO *S. corona* (R)	178.40	187.90	5.05
FO *S. dehiscens* s.l. (F)	130.90	140.40	5.10
FO *G. tumida* (F)	121.40	130.90	5.20
LO *G. dehiscens* (F)	140.40	149.90	5.30
LO *A. tritubus* (R)	140.40	149.90	5.35
LO *N. miocenica* (D)	102.40	111.90	5.60
FO *P. primalis* (F)	159.40	168.90	5.80
FO *S. omnitubus* (R)	197.40	206.90	6.40
LO *C. caepa* (R)	187.90	197.40	6.40
LO *N. porteri* (D)	178.40	187.90	6.70
LO *D. hughesi* (R)	206.90	216.40	7.15
LO *N. porteri* (D)	178.40	187.90	7.20
FO *D. quinqueramus* (N)	235.40	244.90	7.50
LO *D. ontogenesis* (R)	206.90	216.40	7.45
LO *C. yabei* (D)	244.90	254.40	7.50
FO *A. tritubus* (R)	225.90	235.40	7.74
LO *C. nodulifer* var. *cyclopus* (D)	197.40	206.90	7.90
FO *S. berminghami* (R)	264.10	273.80	7.95
LO *A. ellipticus* var. *javanica* (D)	197.40	206.90	8.00
LO *D. petterssoni* (R}	264.10	273.80	8.15
LO *S. wolffii* (R)	254.40	264.10	8.15
LO *B. miralestensis* (R)	244.90	254.40	8.15
LO *D. laticonus* (R)	225.90	235.40	8.15
LO *C. yabei* (D)	244.90	254.40	8.60
LO *D. hamatus* (N)	283.50	292.70	8.70
FO *D. hughesi* (R)	283.50	292.70	8.75
LO *Catinaster* spp. (N)	283.50	292.70	8.80
LO *A. moronensis* (D)	312.00	321.20	8.90
FO *D. neohamatus* (N)	292.70	302.30	9.00
LO *C. japonica* (R)	302.30	312.00	10.15
FO *N. acostaensis* (F)	273.80	283.50	10.20
LO *G. siakensis* (F)	292.70	302.30	10.40
LO *L. thornburgi* (R)	292.70	302.30	10.45
FO *D. hamatus* (N)	302.30	312.00	10.50
LO *L. thornburgi* (R)	292.70	302.30	11.00
FO *C. coalitus* (N)	302.30	312.00	11.10
LO *A. moronensis* (D)	312.00	321.20	11.30
FO *G. nepenthes* (F)	312.00	321.20	11.30
LO *G. fohsi lobata* (F)	321.20	330.90	11.50
LO *C. cornuta* (R)	330.90	340.60	11.75
LO *S. jouseana* (D)	321.20	330.90	12.30
LO *A. ellipticus* var. *spiralis* (D)	321.20	330.90	12.30
LO *C. nitescens* (N)	340.60	350.20	12.80
LO *C. lewisianus* (D)	330.90	340.60	12.90

Table 8 (continued).

Events	Upper depth (mbsf)	Lower depth (mbsf)	Age (Ma)
FO *G. fohsi lobata* (F)	350.20	359.90	13.10
LO *C. floridanus* (N)	369.70	379.50	13.10
LO *C. lewisianus* (D)	330.90	340.60	13.50
LO *S. heteromorphus* (N)	369.70	379.50	13.60
LO *C. pulchellus* var. *maculatus* (D)	330.90	340.60	13.90
FO *G. praefohsi* (F)	389.20	396.90	13.90
FO *A. ellipticus* var. *spiralis* (D)	379.50	389.20	14.10
LO *G. peripheroronda* (F)	389.20	398.90	14.60
FO *G. peripheroacuta* (F)	398.90	408.60	14.90
FO *A. ingens* (D)	408.60	418.30	15.50
TA *D. deflandrei* (N)	427.80	437.50	16.10
FO *S. heteromorphus* (N)	456.80	466.40	18.60
LO *S. belemnos* (N)	456.80	466.40	18.80
FO *S. belemnos* (N)	476.10	485.80	20.00
LO *G. kugleri* (F)	505.10	514.80	21.80
FO *D. druggii* (N)	553.00	562.60	23.60
FO *G. kugleri* (F)	581.90	601.30	23.70
LO *S. ciperoensis* (N)	611.00	620.60	25.20
FO *G. pseudokugleri* (F)	639.90	649.60	26.30
LO *S. distentus* (N)	678.20	687.80	27.50
LO *G. opima* (F)	659.20	668.90	28.20
LO *G. opima* (F)	697.50	707.20	28.20
LO *Chiloguembelina* spp. (F)	697.50	707.20	30.00
FO *G. angulisuturalis* (F)	755.20	764.90	31.60
FO *G. opima* (F)	784.20	793.90	32.70
LO *G. ampliapertura* s.s. (F)	793.90	803.60	32.80
LO *C. excavatus* (D)	813.20	822.90	33.00
130-807B-			
LO *P. lacunosa* (N)	3.10	12.60	0.46
LO *G. tosaensis* (F)	3.10	12.60	0.60
LO *C. macintyrei* (N)	12.60	22.10	1.45
LO *G. fistulosus* (F)	22.10	31.60	1.60
LO *D. brouweri* (N)	22.10	31.60	1.89
FO *G. truncatulinoides* (F)	31.60	41.10	1.90
OA *D. triradiatus* (N)	31.60	41.10	2.07
LO *D. surculus* (N)	50.60	60.10	2.45
LO *G. altispira* (F)	50.60	60.10	2.90
FO *S. dehiscens* s.s. (F)	79.10	88.60	3.00
FO *G. tosaensis*	41.10	50.60	3.10
LO *Sphenolithus* (N)	60.10	69.60	3.45
LO *R. pseudoumbilica* (N)	69.60	79.10	3.56
LO *C. acutus* (N)	107.60	117.10	4.60
LO *D. quinqueramus* (N)	126.60	145.60	5.00
FO *G. tumida* (F)	126.60	131.60	5.20
LO *G. dehiscens* (F)	98.10	107.60	5.30
FO *P. primalis* (F)	155.10	164.60	5.80
FO *G. plesiotumida* (F)	221.60	231.10	7.10
FO *D. quinqueramus* (N)	231.10	250.10	7.50
FO *G. acostaensis* (F)	269.10	278.60	10.20
130-807C-			
LO *R. umbilica* (N)	857.40	867.10	33.80
LO *Pseudohastegerina* (F)	876.60	881.90	34.00
LO *E. formosa* (N)	881.90	888.90	34.90
LO *G. cerroazulensis* (F)	908.90	913.90	36.60
LO *Hantkenina* (F)	908.90	913.90	36.60
LO *D. saipanensis* (N)	908.90	913.90	36.70
LO *D. barbadiensis* (N)	908.90	913.90	37.00
LO *C. reticulatum* (N)	933.70	938.70	37.70
LO *C. protoannula* (N)	943.70	948.40	38.20
LO *C. grandis* (N)	987.10	996.80	40.00
LO *Acarinina* (F)	987.10	1006.50	40.60
LO *T. rohri* (F)	987.10	1006.50	40.60
LO *M. spinulosa* (F)	987.10	1006.50	41.10
LO *C. solitus* (N)	987.10	996.80	42.30
FO *D. hesslandii* (N)	1006.50	1016.10	42.90
LO *A. bullbrooki* (F)	987.10	1006.50	43.00
FO *R. umbilica* (N)	1054.00	1063.70	44.40
FO *G. pomeroli* (F)	1063.70	1082.40	44.70
LO *N. alata* (N)	1073.20	1082.40	45.40
LO *M. aragonensis* (F)	1063.70	1082.40	46.00
LO *C. gigas* (N)	1082.40	1092.00	47.00
FO *C. gigas* (N)	1092.00	1097.70	47.40
FO *N. alata* (N)	1092.00	1097.70	49.80
LO *D. sublodoensis* (N)	1092.00	1097.70	49.70

Table 8 (continued).

Events	Upper depth (mbsf)	Lower depth (mbsf)	Age (Ma)
LO *D. lodoensis* (N)	1097.70	1102.40	50.40
LO *T. orthostylus* (N)	1102.40	1106.40	54.00
LO *D. sublodoensis* (N)	1092.00	1097.70	49.70
LO *D. lodoensis* (N)	1097.70	1102.40	50.40
LO *T. orthostylus* (N)	1102.40	1106.40	54.00
FO *D. lodoensis* (N)	1126.75	1137.10	55.00
FO *T. orthostylus* (N)	1140.20	1145.20	56.10
FO *D. diastypus* (N)	1140.20	1145.20	56.60
LO *Fasciculithus* (N)	1150.20	1155.20	56.80
LO *E. robusta* (N)	1161.10	1162.60	57.70
FO *D. multiradiatus* (N)	1162.60	1169.80	58.90
LO *H. kleinpellii* (N)	1172.36	1173.01	60.10
FO *D. mohleri* (N)	1173.01	1173.12	60.20
FO *H. kleinpellii* (N)	1173.12	1173.60	60.90
FO *H. cantabriae* (N)	1173.55	1179.40	61.40
FO *Fasciculithus* spp. (N)	1182.20	1182.63	62.30
FO *Sphenolithus* spp. (N)	1182.20	1182.63	62.80
K/T (FO abund. *Thoracosphaera*)	1193.14	1193.33	66.40
LO *T. trifidium* (N)	1261.20	1270.80	71.90
FO *T. trifidium* (N)	1348.00	1348.37	76.00

Notes: The depth uncertainty predominantly represents sampling intervals used. References for the age estimates are presented in the "Explanatory Notes" chapter (this volume). N = nannofossil, F = foraminifer, D = diatom, R = radiolarian, FO = first occurrence, LO = last occurrence, OA = onset acme, and K/T = Cretaceous/Tertiary. Magnetostratigraphic reversal boundaries followed by designation (T) or (O) refer to "termination" or "onset," respectively.

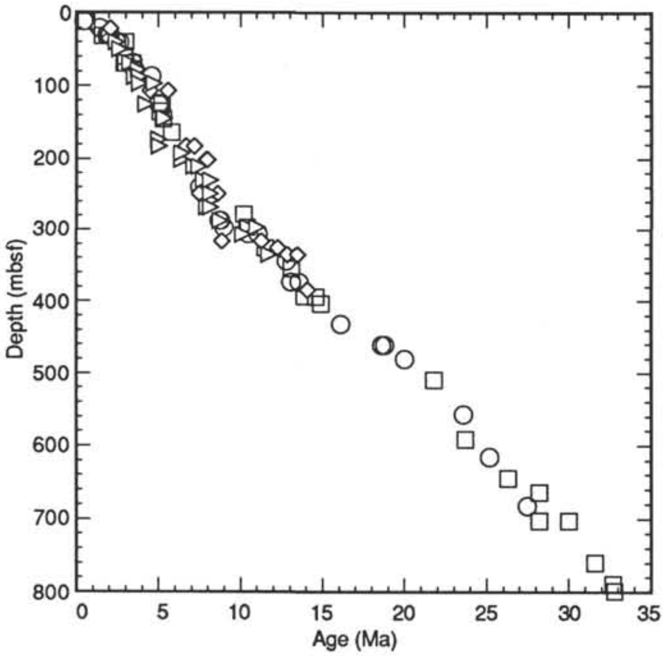

Figure 41. Age-depth relationships of biostratigraphic markers, Hole 807A. Circles = nannofossils, squares = foraminifers, diamonds = diatoms, and triangles = radiolarian.

The deepest site (804) exhibits one anomalous time interval, between approximately 4 and 5 Ma (lower Pliocene). This interval is characterized by enhanced dissolution and perhaps by minor hiatus formation.

The difference in rate histories between Site 806 and Sites 803, 805, and 807 between about 9 and 13 Ma presumably reflects the combined effect of increasing dissolution gradients with depth as well as the paleolocation of the individual sites relative to the equatorial zone of divergence, upwelling, and high productivity. Site 804 has a higher sedimentation rate in the 9–13-Ma interval than the next three shallower sites. This fact presumably reflects the effect of mass wasting.

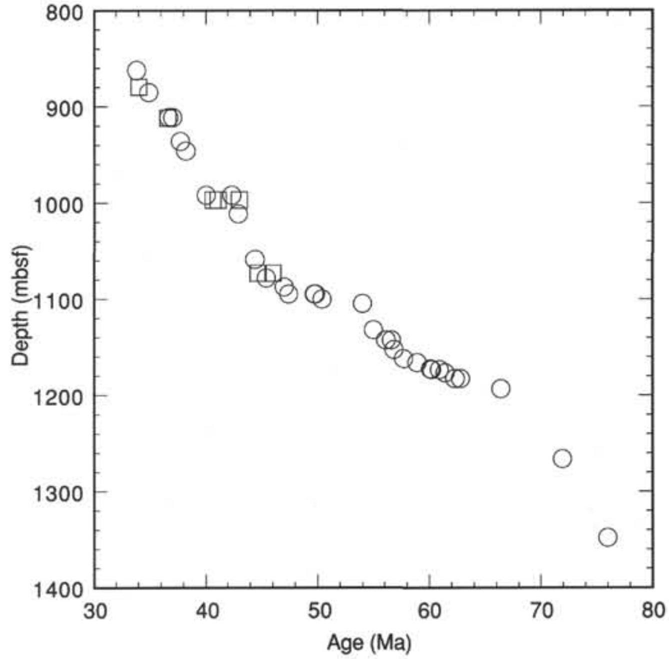

Figure 42. Age-depth relationships of biostratigraphic markers, Hole 807C. Symbols used are as in Figure 41.

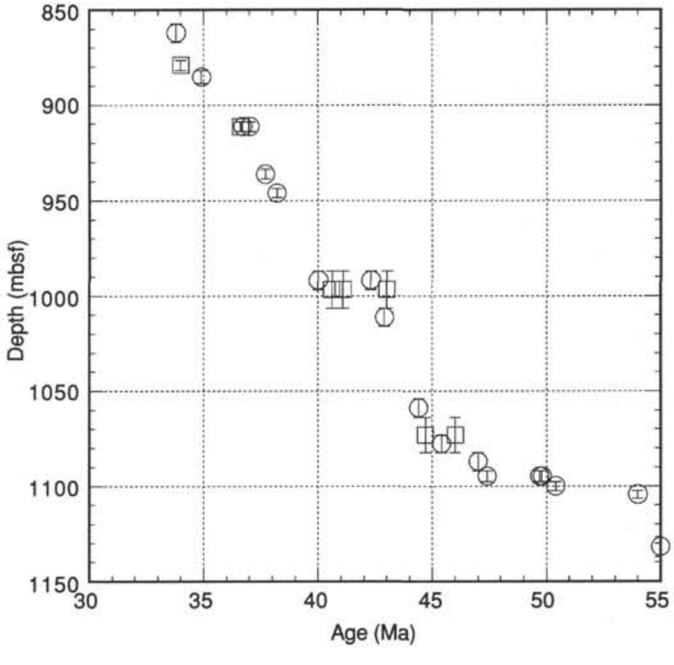

Figure 43. Age-depth relationships of biostratigraphic markers from the Oligocene through lower Eocene interval, Hole 807C. Error bars show sample interval uncertainties. Symbols used are as in Figure 41.

INORGANIC GEOCHEMISTRY

Thirty-six interstitial water samples were collected at Site 807, thirty-one from Hole 807A at depths ranging from 4.5 to 778.9 mbsf, and five from Hole 807C at depths ranging from

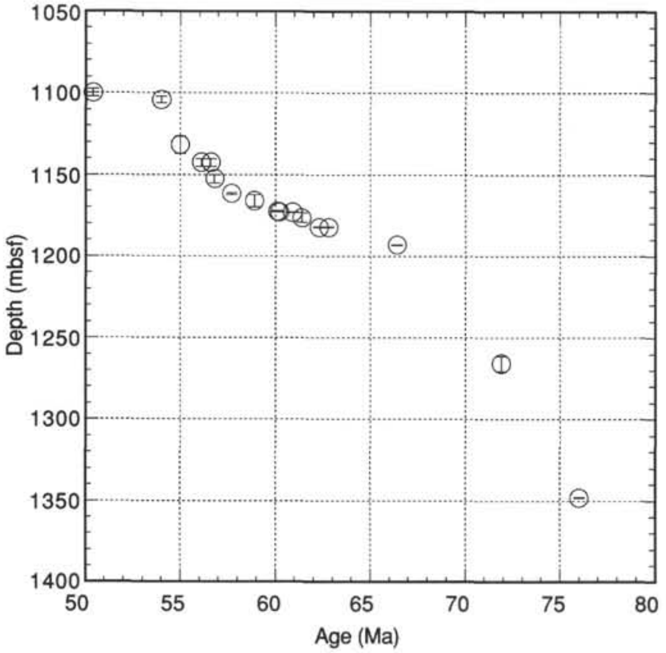

Figure 44. Age-depth relationships of biostratigraphic markers from the lower Eocene through upper Campanian interval, Hole 807C. Error bars show sample interval uncertainties. Symbols used are as in Figure 41.

810.4 to 1092.2 mbsf. For this report, these samples are considered as constituting a single depth profile. Interstitial water samples cover the depth range of the nannofossil ooze and chalk of Unit I, with the two deepest interstitial water samples from the limestones of Unit II (see "Lithostratigraphy" section, this chapter). Chemical gradients in the interstitial waters at this site (Table 10) are similar in character to those at the other sites drilled on this leg, being governed by the biogenic-rich, organic-carbon-poor character of the sediments and by the diffusive influence of basalt alteration reactions at depth. The interstitial water chemistry (dissolved silica concentrations) also reflects the extensive silicification in Unit II. The gradients at this site, the northernmost drilled and at the second shallowest water depth, are generally intermediate in magnitude relative to those at the other sites.

Chlorinity increases downhole by almost 2% to 563 mM at 22.9 mbsf (Core 130-807A-3H) and increases further to values greater than 580 mM by 681.1 mbsf (Core 130-807A-72X), for a total increase of almost 6% over the sampled interval (Fig. 47). Salinity, measured by refraction as total dissolved solids, increases with depth to values around 36.5–37.0 g/kg by 681.1 mbsf (Table 10). Sodium concentrations measured by flame emission spectrophotometry (Table 10) and those estimated by charge balance calculations generally agree to within 2%. Sodium concentrations increase from 476 mM at 4.5 mbsf to values around 510 mM at depths greater than 713.1 mbsf, a total increase of 7%. Sodium concentrations at depth in this site are lower than those at Site 806 and similar to those at Site 805. Alkalinity increases from 3.5 mM at 4.5 mbsf to >6 mM from 306.7 to 335.3 mbsf; it then decreases with depth to <4 mM by 681.1 mbsf (Fig. 47). The alkalinity maximum at this site occurs at a greater depth below the seafloor and is broader than the maxima at the sites drilled in deeper water. At depths <300 mbsf, alkalinity is lower at this site than at Site 806; at depths >300 mbsf, alkalinity is equal to or greater than at Site 806.

Sulfate concentrations decrease more than 20% to values <22 mM by 306.7 mbsf (Fig. 47). Sulfate depletion at this site continues to greater depths and is equal to or slightly larger than that at the sites in deeper water. Sulfate depletion here is less than at Site 806 by a factor of about 2, presumably because of the shallower water depth at Site 806 being favorable for a higher organic carbon supply to the sediments or because Site 806 is nearly on the equator and Site 807 is at 3.5°N.

Phosphate concentrations are below the detection limit of 1–2 μM in all but the shallowest sample (4.5 mbsf; Table 10). Ammonia concentrations increase to a quasi-constant level of >300 μM by 280 mbsf, persisting at these values throughout the depth range sampled (Fig. 47). In the upper 200 m, the ammonia profile is similar to that at Site 805 at a greater water depth; however, at greater sub-bottom depths, concentrations are higher at Site 807. Ammonia concentrations at Site 807 are a factor of 2 lower than those at Site 806, similar to sulfate depletion.

Dissolved silica concentrations increase with depth to over 1500 μM by 905.3 mbsf, with a depth profile similar to those at the other sites drilled (Fig. 47). From the sample at 940.1 mbsf near the base of lithologic Unit I continuing to the deepest sample at 1092.2 mbsf in Unit II, dissolved silica concentra-

Table 9. Estimated sedimentation rates, Site 807, and the control points determining those rates.

Control point	Depth (mbsf)	Age (Ma)	Sedimentation rate (m/m.y.)
130-807A-			
Top section	0	0	
OA *D. triradiatus* (N)	31.15	2.07	15.05
LO *D. quinqueramus* (N)	126.15	5.00	32.42
LO *D. hamatus* (N)	288.10	8.70	43.77
LO *S. heteromorphus* (N)	374.60	13.60	17.65
LO *G. kugleri* (F)	509.95	21.80	16.51
LO *G. opima* (F)	702.35	28.20	30.06
Hiatus younger side	702.35	28.20	—
Hiatus older side	702.35	30.20	—
LO *Chiloguembelina* spp. (F)	702.35	30.20	37.08
LO *G. ampliapertura* s.s. (F)	798.75	32.80	37.08
Terminal depth	822.90	33.45	
130-807B-			
Top section	0	0	
LO *D. brouweri* (N)	26.85	1.89	14.21
LO *R. pseudoumbilica* (N)	74.35	3.56	28.44
FO *G. tumida* (F)	129.10	5.20	33.38
FO *D. quinqueramus* (N)	240.60	7.50	48.48
Terminal depth	278.60	8.28	
130-807C-			
LO *R. umbilica* (N)	862.25	33.80	
LO *G. cerroazulensis* (F)	911.40	36.60	17.55
LO *C. grandis* (N)	991.95	40.00	23.69
Hiatus young side	991.95	40.00	—
Hiatus old side	991.95	42.30	—
LO *C. solitus* (N)	991.95	42.30	31.86
FO *R. umbilica* (N)	1058.85	44.40	31.86
FO *C. gigas* (N)	1094.85	47.40	12.00
Hiatus young side	1094.85	47.40	—
Hiatus old side	1094.85	49.80	—
FO *N. alata* (N)	1094.85	49.80	2.27
LO *T. orthostylus* (N)	1104.40	54.00	2.27
LO *Fasciculithus* (N)	1152.70	56.80	17.25
LO *E. robusta* (N)	1161.85	57.70	10.17
FO *Fasciculithus* spp. (N)	1182.42	62.30	4.47
K/T (FO abund. *Thoracosphaera*)	1193.24	66.40	2.64
LO *T. trifidium* (N)	1266.00	71.90	13.23
FO *T. trifidium* (N)	1348.19	76.00	20.05
Red clay contact	1351.50	76.17	

Notes: References for the age estimates are presented in the "Explanatory Notes" chapter (this volume), as well as the Leg 130 philosophy for determining the sedimentation rates. N = nannofossil, F = foraminifer, D = diatom, R = radiolarian, FO = first occurrence, LO = last occurrence, OA = onset acme, and K/T = Cretaceous/Tertiary.

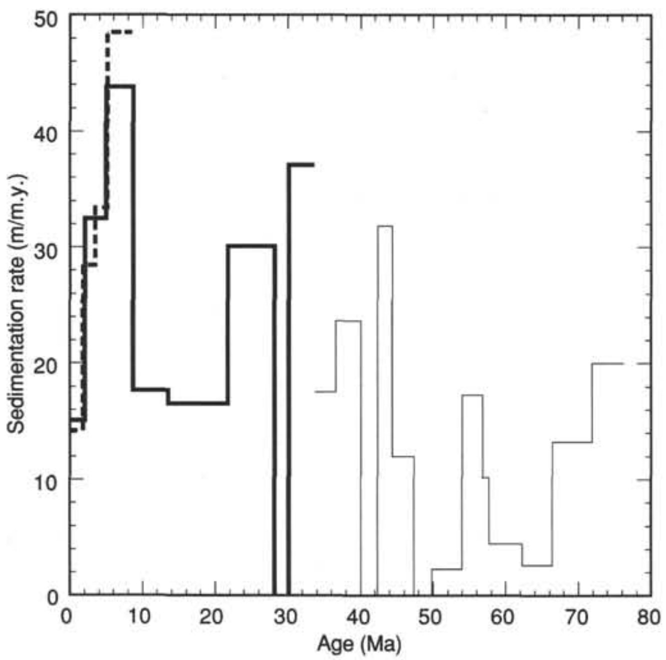

Figure 45. Sedimentation rate history, Site 807. Heavy solid line = Hole 807A, dashed line = Hole 807B, and thin solid line = Hole 807C.

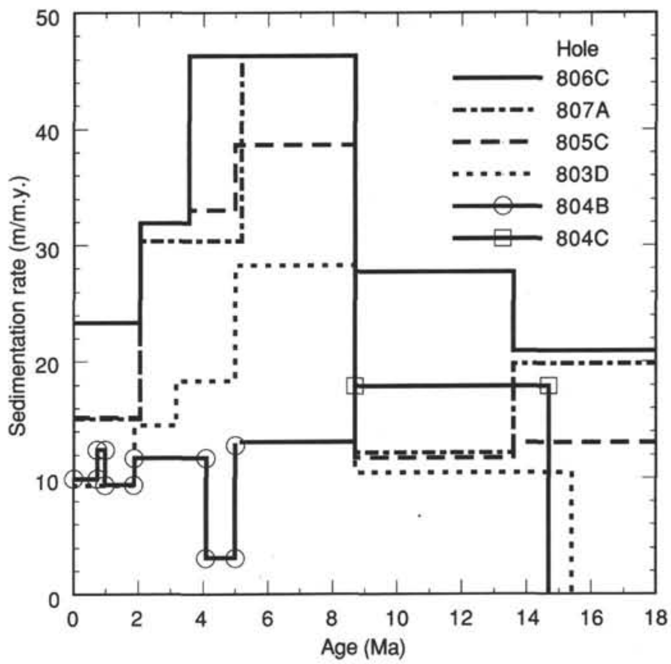

Figure 46. Comparison of Leg 130 sedimentation rate histories (0–18 Ma).

tions decrease rapidly by over a factor of 2, presumably as the result of the extensive limestone silicification and chert formation observed in Unit II (see "Lithostratigraphy" section, this chapter).

Dissolved manganese concentrations are below the detection limit of 2–3 μM in all but the shallowest two samples (Table 10). There is no increase in dissolved Mn with the dissolved Si increase, possibly reflecting the organic-carbon-poor nature of the sediments (Gieskes, 1981).

Calcium concentrations increase with depth by a factor of just over 2 to 22.1 mM at 1092.2 mbsf, with an average gradient of 1.1 mM/100 m (Fig. 47). This is the smallest depth gradient observed in the Leg 130 sites. There seems to be no simple pattern in the Ca gradients related to latitude or to sedimentation rate variation. Magnesium concentrations decrease with depth, with an overall gradient of -1.4 mM/100 m (Fig. 47), the smallest overall depth gradient observed. Calcium and Mg concentrations are linearly correlated overall (R^2 = 0.95) with a ΔCa/ΔMg ratio of −0.78, but there is some evidence of nonconservative Mg behavior throughout, indicating a sink for Mg in the sediments as well as in the underlying basalt (McDuff and Gieskes, 1976)

Strontium concentrations increase with depth to >900 μM by 165.4 mbsf, are generally consistent to 451.5 mbsf, and then slightly decrease with depth (Fig. 47). The Sr profile is similar throughout its depth range to that at Site 803, but it increases less with depth below the seafloor in the upper sediment column than do Sites 805 and 806.

Lithium concentrations decrease from 24.2 μM at 4.5 mbsf to minimum values of <13 μM from 137.1 to 279.7 mbsf; they then increase to close to 20 μM around 425.7–451.5 mbsf (Fig. 47). Minimum concentrations of lithium were the lowest observed in the Leg 130 sites. Lithium concentrations display a complex structure with depth below 451.5 mbsf.

Potassium concentrations decrease from ~11 mM at 4.5 mbsf to 8.4 mM at 1092.2 mbsf (Fig. 47); they linearly correlate with Ca (R^2 = 0.85). The potassium depth gradient is comparable with that at Site 806 over equivalent depth ranges; these are the smallest observed in these sites. Rubidium concentrations also decrease with depth from 1.7 μM at 4.5 mbsf to 1.0 μM by 1092.2 mbsf (Fig. 47); they linearly correlate with Ca (R^2 = 0.87). The rubidium depth gradient is steeper than that at Site 806 and smaller than at Sites 803, 804, and 805.

Although basalt alteration as indicated in the interstitial water signature apparently differs from site to site, there is no simple pattern relating the magnitudes of all the various gradients (Ca, Mg, K, and Rb) that reflects the degree of influence from basalt alteration from site to site.

CARBON GEOCHEMISTRY

Shipboard carbon geochemical analyses of sediments from Site 807 included determinations of inorganic carbon (503 samples), total carbon (61 samples), and volatile hydrocarbons (44 samples). The inorganic carbon and total carbon measurements were performed on dried ground samples collected for physical properties analyses. The methods used are outlined in the "Explanatory Notes" chapter (this volume), whereas background and detailed descriptions are given in Emeis and Kvenvolden (1986).

Volatile hydrocarbons in the sediments were routinely monitored as required by safety and pollution considerations. Samples were collected using the headspace-sampling technique and measured for methane, ethane, and propane. As in the previous Leg 130 sites, no significant amounts of these gases were detected. Inorganic carbon (IC) was determined using a Coulometrics carbon dioxide coulometer. Percent $CaCO_3$ is calculated according to the equation: $CaCO_3$ = IC · 8.334. The data are presented in Table 11 and plotted vs. depth in Figure 6.

The carbonate curve closely reflects the lithostratigraphic units described in the "Lithostratigraphy" section (this chapter). Unit I (0–968 mbsf, Holocene to upper Eocene) consists of nannofossil-rich oozes and chalks and is characterized by very high carbonate contents, ranging from 85% to 95%. Long-term variations with noticeably higher values (up to 95%

Table 10. Interstitial water geochemical data, Holes 807A and 807C.

Core, section, interval (cm)	Depth (mbsf)	pH	Alk. (mM)	Sal. (g/kg)	Cl^- (mM)	Na^+ (mM)	SO_4^{2-} (mM)	PO_4^{3-} (μM)	NH_4^+ (μM)	SiO_2 (μM)	Mn^{2+} (μM)	Ca^{2+} (mM)	Mg^{2+} (mM)	Sr^{2+} (μM)	Li (μM)	K^+ (mM)	Rb (μM)
130-807A-																	
1H-3, 145–150	4.45	7.5	3.51	35.0	553	476	27.4	3.0	6	401	13	10.6	52.3	130	24.2	10.8	1.67
2H-4, 145–150	13.35	7.5	3.64	36.0	558	484	27.4	LD	47	480	4	10.9	52.3	208	21.0	11.4	1.65
3H-4, 145–150	22.85	7.5	4.17	37.5	563	487	27.5	LD	55	503	LD	11.3	51.8	284	20.1	11.2	1.55
4H-4, 145–150	32.35	7.6	4.04	35.5	564	487	26.7	LD	88	543	LD	11.3	51.4	356	19.6	11.4	1.73
5H-4, 145–150	41.85	7.6	4.16	35.5	561	487	26.4	LD	96	570	LD	11.4	50.9	425	18.2	11.4	1.72
6H-4, 145–150	51.35	7.6	4.29	35.5	565	487	26.1	LD	111	592	LD	11.7	50.6	476	17.3	11.3	1.68
9H-4, 145–150	79.85	7.6	4.69	35.0	561	486	26.0	LD	161	673	LD	12.2	48.6	619	15.5	11.4	1.66
12H-4, 145–150	108.35	7.2	5.08	35.0	561	483	25.0	LD	193	723	LD	12.7	47.6	753	13.2	11.0	1.64
15H-5, 145–150	137.10	7.2	5.36	35.0	565	488	23.6	LD	224	773	LD	13.3	46.9	840	12.3	10.7	1.63
18H-4, 145–150	165.35	7.6	5.63	35.0	567	488	22.9	LD	236	800	LD	13.9	45.7	904	11.4	10.9	1.62
21H-4, 145–150	193.85	7.6	5.78	34.5	561	487	22.6	LD	268	852	LD	14.6	44.4	927	11.4	10.9	1.60
24H-4, 145–150	222.35	7.6	5.97	35.0	565	492	22.2	LD	290	915	LD	15.0	43.6	905	11.3	10.7	1.56
27H-4, 145–150	250.85	7.8	5.92	37.5	563	486	22.5	LD	286	948	LD	15.5	43.2	896	11.3	10.9	1.59
30X-4, 140–150	279.70	7.1	5.80	35.0	561	491	22.0	LD	302	919	LD	15.8	42.2	896	12.2	10.8	1.53
33X-3, 140–150	306.70	7.1	6.23	35.5	569	493	21.8	LD	300	950	LD	16.4	41.8	907	13.6	10.7	1.47
36X-3, 140–150	335.30	7.1	6.32	35.5	571	490	21.6	LD	305	969	LD	16.8	41.6	899	14.9	10.5	1.46
39X-2, 140–150	362.80	7.6	5.73	36.0	574	493	21.4	LD	320	994	LD	17.2	41.1	907	15.8	10.5	1.47
42X-4, 140–150	395.10	7.6	5.26	35.3	573	497	21.4	LD	319	1014	LD	17.6	40.3	896	18.3	10.4	1.47
45X-5, 140–150	425.70	7.1	5.24	35.5	570	502	21.9	LD	315	1025	LD	18.0	40.3	876	19.4	10.4	1.45
48X-3, 140–150	451.50	7.6	ND	35.5	578	503	21.5	LD	314	1091	LD	18.4	40.0	900	19.9	10.3	1.40
51X-3, 140–150	480.50	7.6	5.01	35.5	580	503	21.8	LD	331	1081	LD	19.0	39.4	896	17.6	10.3	1.43
54X-4, 0–10	509.60	7.5	5.05	35.5	579	497	21.4	LD	331	1104	LD	19.0	39.6	878	16.2	10.2	1.38
57X-4, 140–150	539.60	7.7	4.25	36.0	576	502	21.6	LD	329	1104	LD	19.3	40.0	860	15.3	10.1	1.39
60X-4, 140–150	568.50	7.1	5.30	36.0	577	502	21.8	LD	333	1143	LD	19.5	39.2	874	14.0	9.96	1.39
63X-4, 0–10	596.10	7.2	5.01	36.0	583	499	21.1	LD	322	1158	LD	19.7	39.0	836	15.3	9.95	1.33
66X-2, 140–150	623.50	7.6	4.85	36.0	575	498	21.4	LD	307	1158	LD	19.6	39.5	800	15.3	9.82	1.32
70X-4, 140–150	665.10	7.6	4.36	36.0	579	501	21.0	LD	326	1228	LD	19.9	39.3	817	13.5	9.70	1.30
72X-2, 140–150	681.10	7.6	3.94	36.5	582	507	21.0	LD	340	1266	LD	20.2	38.8	862	12.1	9.85	1.36
75X-4, 140–150	713.10	ND	ND	ND	585	515	21.2	LD	330	1262	LD	20.5	38.5	853	11.7	9.81	1.31
78X-2, 0–10	737.70	ND	ND	ND	585	516	21.2	ND	333	1289	ND	20.8	38.2	866	12.1	9.62	1.31
82X-3, 140–150	778.90	7.6	4.00	36.5	583	505	21.5	LD	342	1364	LD	21.2	38.9	865	11.7	9.35	1.26
130-807C-																	
4R-1, 140–150	810.40	7.6	3.94	36.5	581	503	21.5	ND	328	1442	LD	21.2	38.0	883	11.7	9.39	1.22
17R-1, 140–150	905.30	7.6	3.68	36.3	583	511	21.4	ND	343	1517	LD	21.8	37.5	901	11.3	9.25	1.16
23R-1, 140–150	940.10	ND	ND	35.5	586	505	21.4	ND	320	1317	ND	21.2	38.0	840	14.0	8.87	1.12
30R-1, 71–76	997.51	ND	ND	ND	585	510	22.1	ND	327	725	ND	21.7	37.9	844	14.4	8.87	1.09
40R-1, 23–31	1092.23	ND	ND	37.0	584	504	21.8	ND	309	688	LD	22.1	37.4	789	15.8	8.42	1.01

Note: LD = concentration lower than detection limit and ND = not determined.

$CaCO_3$) from 90 to 300 mbsf (late Pliocene to upper Miocene) and from 450 to 550 mbsf (middle to lower Miocene; Fig. 6 and Table 11) were observed. In Samples 130-807A-25H-1, 108–110 cm, -48X-2, 99–101 cm, and -72X-4, 67–69 cm (217.5, 449.5, and 683.4 mbsf, respectively), the carbonate content is significantly lower than in the surrounding samples (73%–78%). None of these samples represent the dominant lithology of their respective sections. The upper two samples were taken from interbedded silica-rich layers and the lower one from an ash-rich layer.

The chert-rich limestones in Subunit IIA and the upper part of Subunit IIB (968–1351.4 mbsf; middle and lower Eocene) have $CaCO_3$ values between 51% and 97% $CaCO_3$, whereas the chert-poor limestones of the lower part of Subunit IIB (1140–1350 mbsf; lower Eocene to upper Cenomanian) are characterized by high carbonate values from 95% to almost 99%.

The dark claystones in Subunit IIIA (1351.4–1369.7 mbsf; lower Cenomanian to upper Albian) have carbonate contents less than 0.3% (Fig. 6 and Table 11), which is similar to equivalent intervals recovered in Hole 803D.

Total organic carbon (TOC) was determined only for samples from Hole 807A and is defined as the difference between total carbon (NCS-analyzer) and inorganic carbon (Coulometer). TOC values range from 0.02% to 0.6% and are similar to TOC values observed in sediments of Site 806. It should be noted that the measurements are near the detection limit of the shipboard analytical methods used. They will be verified by shore-based analyses.

PHYSICAL PROPERTIES

The physical properties program at Site 807 included multisensor track (MST) measurements of whole-round cores, and index property, vane shear strength and *P*-wave velocity measurements of split cores. Methods for these measurements are described in the "Explanatory Notes" chapter (this volume). One vane shear strength measurement per section was taken in Holes 807A and 807B to the depth at which induration prevented vane insertion (around 280 mbsf). *P*-wave velocity measurements were made and index properties samples taken at a sampling interval of two per section in the upper 150 m of Hole 807A, and one per section in the rest of Hole 807A and in Holes 807B and 807C. In general, the recovery of APC cores at Holes 807A and 807B allowed us to obtain a complete suite of physical properties measurements. Recovery decreased in the XCB cores and deteriorated significantly in the RCB cores; this lack of recovery is reflected in gaps in the physical properties data sets.

Vane Shear Strength

The ODP motorized minivane was used to measure undrained shear strength in split core sections (see "Explanatory Notes" chapter, this volume). Measurements were performed in successive APC and XCB cores until the sediment became too lithified (near 280 mbsf). Residual shear strengths were obtained where cracking of the sediment around the vane did not dominate failure (see discussion of vane shear strength data in the

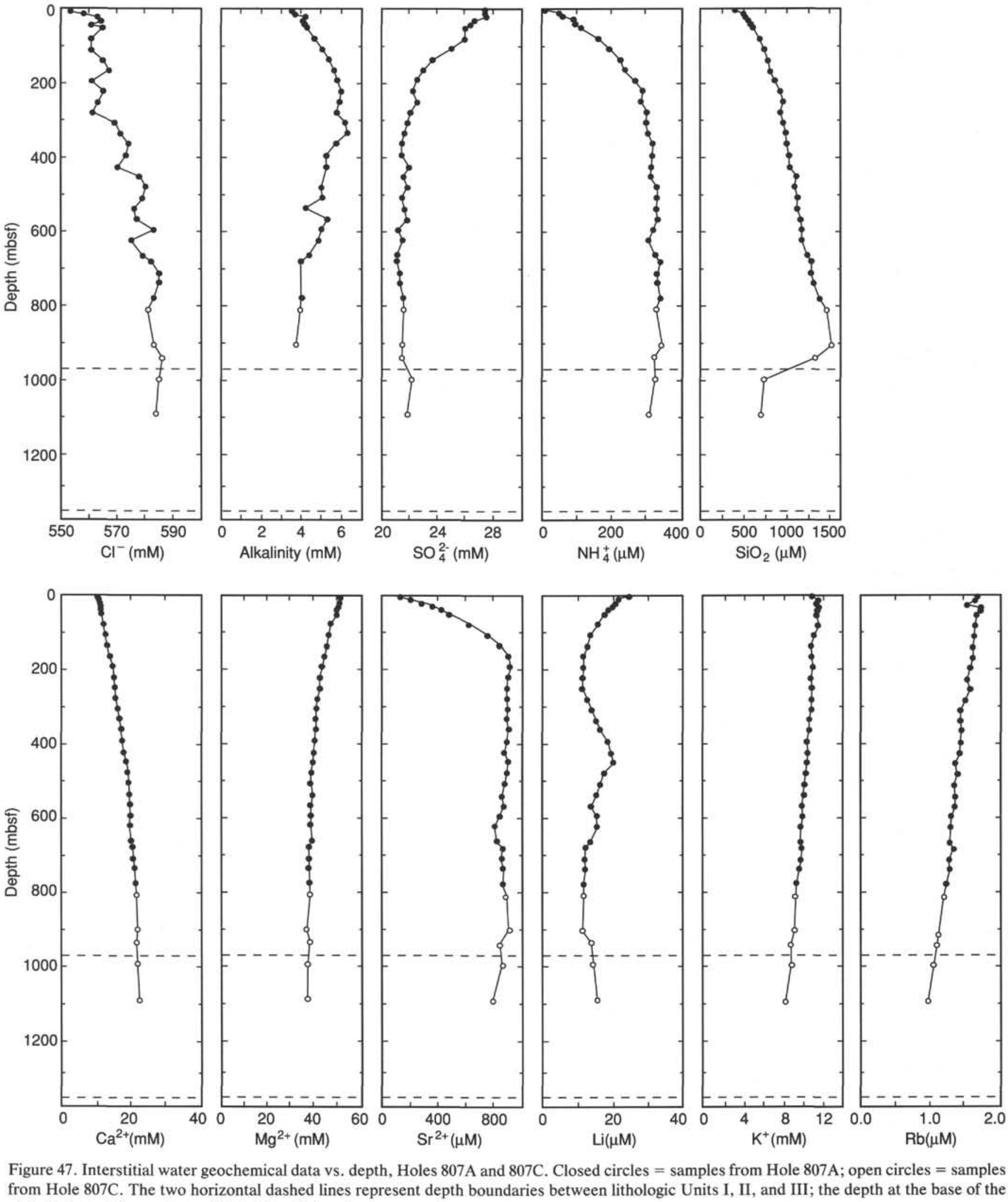

Figure 47. Interstitial water geochemical data vs. depth, Holes 807A and 807C. Closed circles = samples from Hole 807A; open circles = samples from Hole 807C. The two horizontal dashed lines represent depth boundaries between lithologic Units I, II, and III; the depth at the base of the plots is that of the contact of Unit III with basalt.

Table 11. Concentrations of total carbon and inorganic carbon, Holes 807A and 807B.

Core, section, interval (cm)	Depth (mbsf)	Inorganic carbon (%)	$CaCO_3$ (%)
130-807A-			
1H-1, 95–97	0.95	10.61	88.4
1H-2, 8–10	1.58	10.65	88.7
1H-3, 13–15	3.13	10.48	87.3
1H-4, 14–16	4.64	10.40	86.6
1H-5, 13–15	6.13	10.63	88.5
2H-1, 94–96	8.34	10.78	89.8
2H-2, 14–16	9.04	10.96	91.3
2H-3, 14–16	10.54	10.54	87.8
2H-4, 14–16	12.04	10.65	88.7
2H-5, 14–16	13.54	10.66	88.8
2H-6, 14–16	15.04	11.01	91.7
2H-7, 14–16	16.54	10.79	89.9
3H-1, 94–96	17.84	10.70	89.1
3H-2, 15–17	18.55	10.66	88.8
3H-3, 14–16	20.04	10.64	88.6
3H-4, 21–23	21.61	10.81	90.0
3H-5, 14–16	23.04	10.68	89.0
3H-6, 15–17	24.55	10.43	86.9
3H-7, 24–26	26.14	10.80	90.0
4H-1, 94–96	27.34	10.56	88.0
4H-2, 15–17	28.05	10.55	87.9
4H-3, 15–17	29.55	10.75	89.5
4H-4, 15–17	31.05	10.59	88.2
4H-5, 14–16	32.54	10.84	90.3
4H-6, 15–17	34.05	10.90	90.8
4H-7, 30–32	35.70	10.80	90.0
5H-1, 108–110	36.98	10.85	90.4
5H-2, 35–37	37.75	10.85	90.4
5H-3, 40–42	39.30	10.90	90.8
5H-4, 39–41	40.79	11.12	92.6
5H-5, 39–41	42.29	11.01	91.7
5H-6, 40–42	43.80	10.99	91.5
5H-7, 29–31	45.19	10.87	90.5
6H-2, 33–35	47.23	10.99	91.5
6H-3, 35–37	48.75	10.99	91.5
6H-4, 35–37	50.25	10.88	90.6
6H-5, 35–37	51.75	10.74	89.5
6H-6, 35–37	53.25	11.03	91.9
7H-1, 108–110	55.98	10.82	90.1
7H-2, 33–35	56.73	10.83	90.2
7H-3, 33–35	58.23	10.98	91.5
7H-4, 33–34	59.73	11.01	91.7
7H-5, 33–35	61.23	10.91	90.9
7H-6, 33–35	62.73	11.05	92.0
8H-1, 107–109	65.47	11.08	92.3
8H-2, 34–36	66.24	11.19	93.2
8H-3, 33–35	67.73	11.09	92.4
8H-4, 42–44	69.32	11.17	93.0
8H-5, 39–41	70.79	11.05	92.0
8H-6, 39–41	72.29	11.09	92.4
8H-7, 34–36	73.74	11.13	92.7
9H-1, 33–35	74.23	11.12	92.6
9H-2, 33–35	75.73	11.15	92.9
9H-3, 33–35	77.23	11.03	91.9
9H-4, 33–35	78.73	10.87	90.5
9H-5, 33–35	80.23	10.98	91.5
9H-6, 33–35	81.73	11.17	93.0
10H-1, 108–110	84.48	11.00	91.6
10H-2, 108–110	85.98	11.30	94.1
10H-3, 108–110	87.48	11.18	93.1
10H-4, 108–110	88.98	11.06	92.1
10H-5, 108–110	90.48	11.10	92.5
10H-6, 108–110	91.98	11.08	92.3
11H-1, 106–108	93.96	11.02	91.8
11H-2, 107–109	95.47	11.11	92.5
11H-3, 107–109	96.97	11.09	92.4
11H-4, 107–109	98.47	10.96	91.3
11H-5, 107–109	99.97	11.18	93.1
11H-6, 107–109	101.47	11.27	93.9
12H-1, 106–108	103.46	11.19	93.2
12H-2, 107–109	104.97	11.06	92.1
12H-3, 106–108	106.46	11.07	92.2
12H-5, 106–108	109.46	11.04	92.0

Table 11 (continued).

Core, section, interval (cm)	Depth (mbsf)	Inorganic carbon (%)	$CaCO_3$ (%)
12H-6, 106–108	110.96	10.98	91.5
13H-2, 106–108	114.46	11.07	92.2
13H-3, 106–108	115.96	11.00	91.6
13H-4, 106–108	117.46	11.27	93.9
13H-5, 108–110	118.98	11.13	92.7
13H-6, 108–110	120.48	11.05	92.0
14H-3, 31–33	124.71	11.20	93.3
14H-4, 30–32	126.20	10.97	91.4
14H-5, 31–33	127.71	10.68	89.0
14H-6, 30–32	129.20	11.11	92.5
15H-3, 108–110	133.73	11.17	93.0
15H-4, 109–111	135.24	10.94	91.1
15H-5, 107–109	136.72	10.99	91.5
15H-6, 107–109	138.22	10.98	91.5
15H-7, 107–109	139.72	11.14	92.8
16H-1, 107–109	141.47	11.16	93.0
16H-2, 107–109	142.97	11.06	92.1
16H-3, 107–109	144.47	11.19	93.2
16H-4, 107–109	145.97	11.23	93.5
16H-5, 107–109	147.47	11.17	93.0
16H-6, 118–120	149.08	11.25	93.7
17H-1, 73–75	150.63	11.28	94.0
17H-2, 89–91	152.29	11.14	92.8
17H-3, 75–77	153.65	11.18	93.1
17H-4, 89–91	155.29	11.25	93.7
17H-5, 74–76	156.64	11.15	92.9
17H-6, 75–77	158.15	11.20	93.3
18H-1, 74–76	160.14	11.16	93.0
18H-2, 75–77	161.65	11.16	93.0
18H-3, 72–74	163.12	11.11	92.5
18H-4, 74–76	164.64	11.17	93.0
18H-5, 74–76	166.14	11.22	93.5
18H-6, 75–77	167.65	11.20	93.3
19H-1, 73–75	169.63	11.33	94.4
19H-2, 72–74	171.12	11.22	93.5
19H-3, 71–73	172.61	11.19	93.2
19H-4, 85–87	174.25	11.34	94.5
19H-5, 72–74	175.62	11.07	92.2
19H-6, 74–76	177.14	11.22	93.5
20H-1, 75–77	179.15	11.27	93.9
20H-2, 74–76	180.64	11.16	93.0
20H-3, 72–74	182.12	11.30	94.1
20H-4, 74–76	183.64	11.23	93.5
20H-5, 72–74	185.12	11.24	93.6
20H-6, 74–76	186.64	11.30	94.1
21H-1, 115–117	189.05	11.22	93.5
21H-2, 107–109	190.47	11.32	94.3
21H-3, 110–112	192.00	11.15	92.9
21H-4, 90–92	193.30	11.13	92.7
21H-5, 107–109	194.97	11.17	93.0
21H-6, 109–111	196.49	11.26	93.8
22H-1, 109–111	198.49	11.27	93.9
22H-2, 99–101	199.89	11.33	94.4
22H-3, 110–112	201.50	11.23	93.5
22H-4, 109–111	202.99	11.22	93.5
22H-5, 110–112	204.50	11.35	94.5
22H-6, 112–114	206.02	11.30	94.1
23H-1, 105–107	207.95	11.25	93.7
23H-2, 109–111	209.49	11.23	93.5
23H-3, 107–109	210.97	11.33	94.4
23H-4, 110–112	212.50	11.22	93.5
23H-5, 108–110	213.98	11.08	92.3
23H-6, 109–111	215.49	11.15	92.9
26H-1, 109–111	236.49	10.91	90.9
26H-3, 108–110	239.48	11.08	92.3
26H-4, 109–111	240.99	10.96	91.3
26H-5, 109–111	242.49	11.00	91.6
26H-6, 109–111	243.99	11.15	92.9
27H-1, 109–111	245.99	11.21	93.4
27H-3, 109–111	248.99	10.99	91.5
27H-4, 109–111	250.49	10.97	91.4
28X-1, 94–96	255.34	10.86	90.5
28X-2, 30–32	256.20	10.86	90.5
28X-3, 52–54	257.92	10.80	90.0
28X-4, 30–32	259.20	11.12	92.6
28X-5, 100–102	261.40	10.87	90.5

Table 11 (continued).

Core, section, interval (cm)	Depth (mbsf)	Inorganic carbon (%)	$CaCO_3$ (%)
28X-6, 29–30	262.19	11.11	92.5
29X-1, 61–64	264.71	11.16	93.0
29X-2, 109–112	266.69	11.23	93.5
29X-3, 70–73	267.80	11.12	92.6
29X-4, 66–68	269.26	11.29	94.0
29X-5, 84–86	270.94	11.15	92.9
29X-6, 60–63	272.20	11.18	93.1
30X-2, 56–58	275.86	11.19	93.2
30X-3, 87–89	277.67	11.12	92.6
30X-4, 65–67	278.95	11.16	93.0
30X-5, 100–102	280.80	11.09	92.4
30X-6, 70–72	282.00	11.27	93.9
31X-1, 95–97	284.45	11.21	93.4
31X-2, 123–125	286.23	11.04	92.0
31X-3, 66–68	287.16	11.24	93.6
31X-4, 68–71	288.68	11.22	93.5
31X-5, 70–72	290.20	11.16	93.0
32X-1, 144–146	294.14	11.08	92.3
32X-2, 110–112	295.30	11.15	92.9
32X-3, 126–128	296.96	11.16	93.0
32X-4, 93–95	298.13	11.15	92.9
33X-1, 35–37	302.65	11.02	91.8
33X-2, 135–137	305.15	11.09	92.4
33X-3, 53–55	305.83	11.02	91.8
33X-4, 127–129	308.07	10.79	89.9
33X-5, 145–147	309.75	10.88	90.6
33X-6, 77–79	310.57	11.06	92.1
34X-1, 68–70	312.68	10.70	89.1
34X-2, 73–75	314.23	11.06	92.1
34X-3, 100–102	316.00	11.16	93.0
34X-4, 107–109	317.57	11.08	92.3
34X-5, 42–44	318.42	11.00	91.6
34X-6, 131–133	320.81	11.19	93.2
36X-1, 133–134	332.23	11.04	92.0
36X-2, 141–143	333.81	10.83	90.2
36X-3, 107–109	334.97	10.62	88.5
36X-4, 135–137	336.75	10.93	91.0
36X-5, 113–115	338.03	10.70	89.1
36X-6, 81–83	339.21	10.54	87.8
37X-2, 87–89	342.97	10.78	89.8
37X-3, 95–97	344.55	10.71	89.2
37X-4, 50–52	345.60	10.96	91.3
37X-5, 8–9	346.68	10.62	88.5
38X-1, 140–142	351.60	10.91	90.9
38X-2, 112–113	352.82	10.96	91.3
38X-3, 142–144	354.62	10.95	91.2
38X-4, 96–98	355.66	10.72	89.3
38X-5, 78–80	356.98	11.03	91.9
39X-1, 37–39	360.27	10.60	88.3
39X-2, 91–93	362.31	10.86	90.5
39X-3, 114–116	364.04	10.89	90.7
39X-4, 47–49	364.87	10.82	90.1
39X-5, 142–144	367.32	10.29	85.7
40X-1, 80–82	370.50	10.93	91.0
40X-2, 57–59	371.77	10.96	91.3
40X-3, 59–61	373.29	10.93	91.0
40X-4, 145–147	375.65	10.97	91.4
40X-5, 121–123	376.91	11.17	93.0
40X-6, 109–111	378.29	11.03	91.9
41X-1, 90–92	380.40	11.28	94.0
41X-2, 75–77	381.75	10.97	91.4
41X-3, 72–74	383.22	10.73	89.4
41X-4, 76–78	384.76	11.14	92.8
41X-5, 83–85	386.33	10.17	84.7
41X-6, 84–86	387.84	10.60	88.3
42X-1, 106–108	390.26	11.06	92.1
42X-2, 102–104	391.72	10.86	90.5
42X-3, 106–108	393.26	10.88	90.6
42X-4, 79–81	394.49	10.82	90.1
42X-5, 60–62	395.80	11.05	92.0
42X-6, 40–42	397.10	10.88	90.6
43X-1, 81–83	399.71	11.03	91.9
43X-2, 56–58	400.96	10.75	89.5
43X-3, 67–69	402.57	10.88	90.6
43X-4, 67–69	404.07	10.66	88.8
43X-5, 76–78	405.66	11.11	92.5

Table 11 (continued).

Core, section, interval (cm)	Depth (mbsf)	Inorganic carbon (%)	$CaCO_3$ (%)
44X-1, 75–77	409.35	10.34	86.1
44X-2, 141–143	411.51	10.64	88.6
44X-3, 110–112	412.70	11.11	92.5
44X-4, 102–104	414.12	10.96	91.3
44X-5, 124–126	415.84	10.99	91.5
45X-1, 98–100	419.28	10.89	90.7
45X-2, 97–99	420.77	11.04	92.0
45X-3, 90–92	422.20	11.09	92.4
45X-4, 95–97	423.75	11.21	93.4
45X-5, 57–59	424.87	11.30	94.1
45X-6, 65–67	426.45	11.18	93.1
46X-1, 116–118	428.96	11.45	95.4
46X-2, 112–114	430.42	10.98	91.5
46X-3, 107–109	431.87	10.30	85.8
46X-4, 108–110	433.38	11.51	95.9
46X-5, 81–83	434.61	11.00	91.6
46X-6, 78–80	436.08	11.18	93.1
47X-1, 111–113	438.61	11.20	93.3
47X-2, 122–124	440.22	11.10	92.5
47X-3, 111–112	441.61	11.38	94.8
47X-4, 113–115	443.13	11.25	93.7
47X-5, 103–105	444.53	11.10	92.5
47X-6, 51–53	445.51	11.03	91.9
48X-1, 100–102	448.10	10.88	90.6
48X-2, 99–101	449.59	9.35	77.9
48X-3, 101–103	451.11	10.96	91.3
48X-4, 93–95	452.53	11.14	92.8
48X-5, 84–86	453.94	11.20	93.3
48X-6, 100–102	455.60	11.40	95.0
49X-1, 53–55	457.33	11.55	96.2
49X-2, 92–94	459.22	11.63	96.9
49X-3, 65–67	460.45	11.52	96.0
49X-4, 74–76	462.04	11.36	94.6
49X-5, 72–74	463.52	11.13	92.7
50X-1, 89–91	467.29	11.39	94.9
50X-2, 93–95	468.83	11.54	96.1
50X-3, 89–91	470.29	11.79	98.2
50X-4, 100–102	471.90	11.42	95.1
50X-5, 97–99	473.37	11.39	94.9
50X-6, 98–100	474.88	11.50	95.8
51X-1, 34–36	476.44	11.25	93.7
51X-2, 40–42	478.00	11.40	95.0
51X-3, 43–44	479.53	11.51	95.9
51X-4, 38–40	480.98	11.43	95.2
51X-5, 33–35	482.43	11.48	95.6
51X-6, 16–18	483.76	11.40	95.0
52X-1, 108–110	486.88	11.33	94.4
52X-2, 14–16	487.44	11.51	95.9
52X-5, 61–63	492.41	11.51	95.9
53X-1, 105–107	496.45	11.39	94.9
53X-2, 93–95	497.83	11.49	95.7
53X-3, 97–99	499.37	11.45	95.4
53X-4, 90–92	500.80	11.53	96.0
53X-5, 91–93	502.31	11.09	92.4
54X-1, 84–86	505.94	11.29	94.0
54X-2, 97–99	507.57	11.49	95.7
54X-3, 114–116	509.24	11.63	96.9
54X-4, 113–115	510.73	11.41	95.0
54X-5, 80–82	511.90	11.60	96.6
54X-6, 27–29	512.87	11.33	94.4
55X-3, 61–63	518.41	11.44	95.3
55X-4, 65–67	519.95	11.45	95.4
55X-5, 103–105	521.83	11.44	95.3
55X-6, 43–45	522.73	11.48	95.6
56X-1, 146–148	525.46	11.42	95.1
56X-2, 110–112	526.60	11.51	95.9
56X-3, 53–55	527.53	11.57	96.4
56X-4, 131–133	529.81	11.47	95.5
56X-6, 49–50	531.99	11.54	96.1
57X-1, 85–87	534.55	11.23	93.5
57X-2, 86–88	536.06	11.51	95.9
57X-3, 95–97	537.65	11.41	95.0
57X-4, 65–67	538.85	11.25	93.7
57X-5, 56–58	540.26	11.20	93.3
58X-1, 105–107	544.45	11.53	96.0
58X-2, 104–106	545.94	11.60	96.6

Table 11 (continued).

Core, section, interval (cm)	Depth (mbsf)	Inorganic carbon (%)	$CaCO_3$ (%)
58X-3, 143–145	547.83	11.47	95.5
58X-4, 138–140	549.28	11.50	95.8
59X-2, 124–126	555.74	11.38	94.8
59X-3, 107–109	557.07	11.48	95.6
59X-4, 135–137	558.85	11.50	95.8
60X-1, 11–13	562.71	11.45	95.4
60X-3, 38–40	565.98	11.46	95.5
60X-4, 72–74	567.82	11.48	95.6
61X-1, 97–99	573.27	11.16	93.0
61X-2, 111–113	574.91	11.21	93.4
61X-3, 121–123	576.51	11.36	94.6
61X-4, 145–147	578.25	11.24	93.6
61X-5, 143–145	579.73	11.00	91.6
61X-6, 92–94	580.72	11.12	92.6
62X-2, 113–115	584.53	10.80	90.0
62X-3, 100–102	585.90	11.37	94.7
62X-4, 96–98	587.36	11.01	91.7
62X-5, 88–90	588.78	11.24	93.6
63X-1, 110–112	592.70	11.28	94.0
63X-2, 32–34	593.42	11.25	93.7
63X-3, 32–34	594.92	11.11	92.5
63X-4, 59–61	596.69	11.08	92.3
63X-5, 46–48	598.06	11.22	93.5
64X-1, 9–11	601.39	11.22	93.5
64X-2, 109–111	603.89	10.76	89.6
64X-3, 124–126	605.54	10.99	91.5
64X-4, 81–83	606.61	10.94	91.1
64X-5, 59–61	607.89	10.99	91.5
65X-1, 67–69	611.67	10.94	91.1
65X-2, 62–64	613.12	10.89	90.7
65X-3, 73–75	614.73	11.12	92.6
65X-4, 65–67	616.15	11.02	91.8
65X-5, 52–54	617.52	10.80	90.0
66X-1, 85–87	621.45	11.34	94.5
66X-3, 79–81	624.39	10.94	91.1
66X-4, 85–87	625.95	11.08	92.3
67X-3, 92–94	634.22	11.02	91.8
68X-1, 105–107	640.95	11.20	93.3
68X-2, 111–113	642.51	11.56	96.3
68X-3, 105–107	643.95	10.96	91.3
68X-4, 89–91	645.29	11.09	92.4
70X-3, 60–62	662.80	11.13	92.7
70X-5, 70–72	665.90	11.14	92.8
71X-1, 126–128	670.16	11.12	92.6
71X-2, 123–125	671.63	11.19	93.2
71X-3, 109–111	672.99	11.19	93.2
71X-4, 112–114	674.52	11.28	94.0
71X-5, 108–110	675.98	11.34	94.5
72X-1, 74–76	678.94	10.84	90.3
72X-2, 66–68	680.36	11.22	93.5
72X-3, 78–80	681.98	10.93	91.0
72X-4, 67–69	683.37	8.87	73.9
73X-2, 90–92	690.20	11.32	94.3
73X-3, 86–88	691.66	11.22	93.5
73X-4, 80–82	693.10	10.93	91.0
73X-5, 75–77	694.55	11.28	94.0
73X-6, 35–37	695.65	10.48	87.3
74X-1, 62–64	698.12	11.01	91.7
74X-2, 59–61	699.59	11.33	94.4
74X-3, 63–65	701.13	11.29	94.0
75X-1, 73–75	707.93	11.33	94.4
75X-2, 86–88	709.56	11.46	95.5
75X-3, 72–74	710.92	11.39	94.9
75X-4, 83–85	712.53	11.18	93.1
76X-1, 94–96	717.84	11.09	92.4
76X-2, 120–122	719.60	11.09	92.4
76X-3, 114–116	721.04	11.08	92.3
76X-4, 95–97	722.35	11.19	93.2
76X-5, 82–84	723.72	11.26	93.8
77X-1, 83–85	727.33	11.24	93.6
77X-2, 105–107	729.05	11.10	92.5
77X-3, 78–80	730.28	11.06	92.1
77X-4, 75–77	731.75	11.14	92.8
77X-5, 73–75	733.23	11.22	93.5
78X-1, 110–112	737.30	11.18	93.1
78X-2, 88–90	738.58	11.00	91.6

Table 11 (continued).

Core, section, interval (cm)	Depth (mbsf)	Inorganic carbon (%)	$CaCO_3$ (%)
78X-3, 27–29	739.47	11.21	93.4
78X-4, 110–112	741.80	11.18	93.1
78X-5, 65–67	742.85	11.11	92.5
79X-1, 35–37	745.85	11.29	94.0
80X-1, 43–45	755.63	11.28	94.0
80X-2, 93–95	757.63	10.97	91.4
80X-3, 79–81	758.99	10.93	91.0
82X-2, 69–71	776.69	11.41	95.0
82X-3, 109–111	778.59	11.41	95.0
82X-4, 73–75	779.73	11.34	94.5
83X-2, 4–6	785.74	11.21	93.4
83X-3, 3–5	787.23	11.38	94.8
83X-4, 23–25	788.93	11.26	93.8
84X-1, 48–52	794.38	11.31	94.2
130-807C-			
2R-1, 35	790.05	11.40	95.0
2R-2, 26	791.46	11.53	96.1
4R-1, 51	809.51	11.40	95.0
4R-2, 66	811.16	10.86	90.5
6R-1, 91	829.21	11.39	94.9
6R-2, 92	830.72	11.34	94.5
6R-3, 91	832.21	11.12	92.7
6R-4, 91	833.71	11.34	94.5
6R-5, 80	835.10	11.16	93.0
9R-1, 21	857.61	11.00	91.7
12R-1, 26	876.86	11.40	95.0
15R-1, 17	894.07	11.30	94.2
16R-1, 58	899.48	11.00	91.7
17R-1, 31	904.21	11.04	92.0
17R-2, 48	905.88	11.11	92.6
18R-CC, 8	908.98	10.50	87.5
19R-1, 34	914.24	11.04	92.0
21R-1, 4	923.94	11.03	91.9
23R-1, 49	939.19	10.94	91.2
23R-2, 42	940.62	10.20	85.0
23R-3, 43	942.13	11.02	91.8
23R-4, 37	943.57	10.98	91.5
24R-1, 70	944.40	11.02	91.8
24R-2, 70	945.90	10.92	91.0
25R-1, 35	948.75	10.50	87.5
26R-1, 56	958.66	11.38	94.8
49R-1, 75	1150.95	11.77	98.1
50R-1, 71	1155.91	11.87	98.9
51R-1, 70	1160.90	11.83	98.6
51R-2, 67	1162.37	11.81	98.4
51R-3, 70	1163.90	11.82	98.5
52R-1, 82	1170.62	11.62	96.8
52R-2, 119	1172.49	11.64	97.0
52R-3, 31	1173.11	11.32	94.3
53R-1, 68	1180.08	11.51	95.9
53R-2, 74	1181.64	11.77	98.1
53R-3, 62	1183.02	11.69	97.4
53R-4, 122	1185.09	11.41	95.1
56R-1, 134	1207.94	11.58	96.5
56R-2, 140	1209.50	11.68	97.3
56R-3, 50	1210.10	11.46	95.5
57R-1, 115	1217.45	11.64	97.0
57R-2, 98	1218.78	11.65	97.1
58R-1, 10	1222.60	11.69	97.4
59R-1, 54	1232.74	11.70	97.5
59R-2, 68	1234.38	11.66	97.2
61R-1, 57	1252.07	11.66	97.2
61R-2, 89	1253.89	11.66	97.2
62R-1, 83	1262.03	11.64	97.0
62R-2, 63	1263.33	11.52	96.0
62R-3, 94	1265.14	11.48	95.7
63R-1, 28	1271.08	11.54	96.2
63R-2, 57	1272.87	11.62	96.8
63R-3, 90	1274.70	11.35	94.6
64R-1, 95	1281.45	11.57	96.4
64R-2, 70	1282.70	11.60	96.7
65R-1, 51	1290.61	11.59	96.6
65R-2, 41	1292.01	11.63	96.9
66R-1, 125	1301.05	11.59	96.6
66R-2, 73	1302.03	11.46	95.5

Table 11 (continued).

Core, section, interval (cm)	Depth (mbsf)	Inorganic carbon (%)	$CaCO_3$ (%)
66R-3, 85	1303.65	11.46	95.5
67R-1, 74	1310.24	11.52	96.0
67R-2, 111	1312.05	11.50	95.8
67R-3, 73	1313.17	11.50	95.8
67R-4, 66	1314.60	11.56	96.3
67R-5, 36	1315.80	11.47	95.6
68R-1, 67	1319.77	11.52	96.0
68R-2, 28	1320.88	11.46	95.5
68R-3, 58	1322.68	11.35	94.6
69R-2, 106	1331.36	11.58	96.5
69R-3, 3	1331.83	11.56	96.3
69R-4, 86	1334.16	11.52	96.0
69R-5, 15	1334.95	11.44	95.3
70R-1, 69	1339.09	11.56	96.3
70R-2, 108	1340.98	11.32	94.3
70R-3, 97	1342.37	11.56	96.3
70R-4, 52	1343.42	11.62	96.8
71R-1, 45	1348.45	11.16	93.0
71R-2, 130	1350.80	7.54	62.8
71R-3, 106	1352.06	0.036	0.3
71R-4, 59	1353.09	0.024	0.2
71R-5, 47	1354.47	0.036	0.3
71R-6, 27	1355.77	0.024	0.2
72R-2, 47	1359.67	0.024	0.2
73R-1, 67	1368.07	0.024	0.2
73R-2, 55	1369.45	0.024	0.2

Note: A description of the method for determining $CaCO_3$ can be found in the "Explanatory Notes" chapter (this volume).

"Physical Properties" section, "Site 803" chapter, this volume). Peak vane shear strength data are plotted vs. depth in Figure 48 for Holes 807A and 807B and are listed in Table 12.

As has been noted in the previous reports of vane shear strength data for Leg 130, the strength profiles are strongly influenced by the overprint of core-length cycles of disturbance. This problem is discussed in greater detail in the "Physical Properties" section of the "Site 803" chapter (this volume).

The peak vane shear strengths at Site 807 generally range from 5 to 20 kPa. The sediments at this site are predominantly silt-sized (see "Lithostratigraphy" section, this chapter), and shear strength is expected to be highly dependent on changes in grain size. However, shipboard grain size data were not routinely obtained near the vane test intervals, so the relationship between the two parameters is difficult to examine at present. Peak vane strengths increase below 240 mbsf in response to the onset of cementation.

Index Properties

Index properties samples were taken from split cores at those locations where the velocity measurements were made. Wet and dry weights and dry volumes of these samples were measured and used to calculate wet-bulk density, grain density, water content (based on dry weight), porosity, and dry-bulk density. The procedures and calculations used are outlined in the "Explanatory Notes" chapter (this volume). Table 13 presents the index properties data for the three holes at Site 807.

Figure 49 presents calcium carbonate content and grain density for Holes 807A and 807C. Carbonate content, measured on the dried index properties samples, is generally greater than 85%, as it was for other Leg 130 sites. Grain densities reflect this high carbonate content, with values near 2.7 g/cm^3 for most of the recovered sediments. Grain density minima are generally correlated with minima in carbonate content. The association of low-carbonate content with low-grain density reflects the higher silica content of these samples (grain density of biogenic silica is 2.2 g/cm^3). For example, the zone between 1000 and 1130 mbsf (chert-rich interval) shows a peak-to-peak correlation between carbonate content and grain density measurements performed over this interval. Between 1350 and 1370 mbsf, carbonate content decreases suddenly, corresponding to the presence of claystones in this interval. Grain density also decreases in this interval, reflecting an increase in radiolarian concentration.

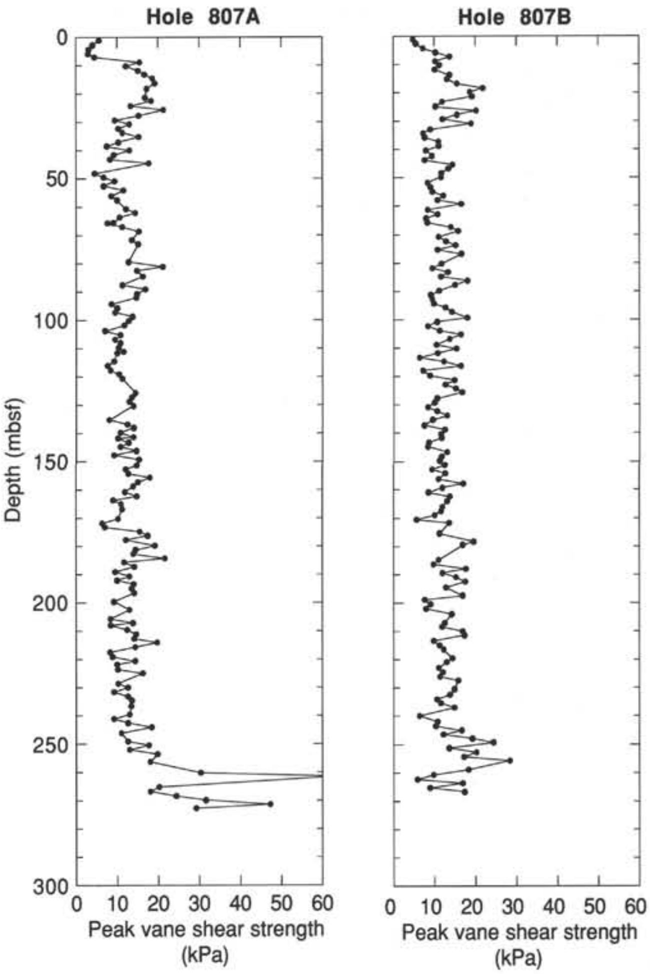

Figure 48. Shear strength vs. depth, Holes 807A and 807B.

Figure 50 presents wet-bulk density, porosity, and water content (calculated as a percentage of dry weight) vs. depth for Holes 807A and 807C. The ooze-chalk transition is located at approximately 290 mbsf, with interbedded ooze and chalk from about 250 to 290 mbsf (see "Lithostratigraphy" section, this chapter). In general, bulk density increases with depth (corresponding to decreases in porosity and water content) through the ooze and chalk sequences. From approximately 950 to 1150 mbsf, the interval of transition from ooze to limestone, the index properties change sharply. Large fluctuations in the index properties were observed and are probably a result of variations in the relative amounts of silica. From approximately 1180 to 1350 mbsf, in the interval containing limestones, bulk density decreases downhole (with corresponding increases of porosity and water content). The reason for this is not understood, at present. The downhole trend in the resistivity logging profile also reverses in this interval (see "Logging" section, this chapter). Finally, the abrupt change in the index properties below 1350 mbsf is caused by the

Table 12. Shear strength data, Holes 807A and 807B.

Core, section, interval (cm)	Depth (mbsf)	Peak shear strength (kPa)	Residual shear strength (kPa)
130-807A-			
1H-1, 120	1.20	5.6	1.12
1H-2, 135	2.85	4.0	1.12
1H-3, 135	4.35	3.1	0.67
1H-4, 135	5.85	2.9	0.45
1H-5, 110	7.10	4.5	0.90
2H-1, 136	8.76	15.5	6.96
2H-2, 135	10.25	12.1	4.72
2H-3, 135	11.75	15.1	5.17
2H-4, 135	13.25	16.7	7.41
2H-5, 110	14.50	18.6	
2H-6, 136	16.26	19.1	7.64
3H-1, 135	18.25	17.2	7.64
3H-3, 136	21.26	16.8	
3H-4, 114	22.54	18.3	8.31
3H-5, 135	24.25	13.3	
3H-6, 132	25.72	21.3	12.80
4H-1, 135	27.75	15.3	6.07
4H-2, 135	29.25	9.4	3.82
4H-3, 135	30.75	13.0	
4H-4, 135	32.25	10.3	
4H-5, 135	33.75	11.3	4.72
4H-6, 136	35.26	15.3	
5H-1, 120	37.10	10.3	
5H-2, 116	38.56	7.4	2.81
5H-3, 117	40.07	13.0	4.27
5H-4, 119	41.59	9.1	2.02
5H-5, 119	43.09	8.2	1.17
5H-6, 119	44.59	17.7	
6H-2, 118	48.08	4.5	0.34
6H-3, 120	49.60	6.7	
6H-4, 100	50.90	9.3	2.92
6H-5, 120	52.60	6.7	1.35
6H-6, 120	54.10	11.5	3.82
7H-1, 120	56.10	8.5	2.92
7H-2, 120	57.60	9.9	2.47
7H-4, 120	60.60	12.1	4.04
7H-5, 120	62.10	14.4	6.29
7H-6, 120	63.60	10.6	4.27
8H-1, 119	65.59	9.0	2.02
8H-1, 122	65.62	7.6	3.15
8H-2, 120	67.10	11.2	
8H-3, 122	68.62	15.3	6.51
8H-5, 122	71.62	13.5	3.59
8H-6, 117	73.07	15.1	3.59
9H-4, 100	79.40	12.8	4.27
9H-5, 120	81.10	21.1	6.74
9H-6, 120	82.60	14.8	4.72
10H-1, 120	84.60	16.2	
10H-3, 120	87.60	11.2	3.15
10H-4, 120	89.10	16.8	6.07
10H-5, 120	90.60	14.8	5.62
10H-6, 120	92.10	14.6	
11H-1, 135	94.25	8.5	1.80
11H-2, 135	95.75	9.9	2.25
11H-3, 135	97.25	9.4	1.80
11H-4, 135	98.75	13.7	3.15
11H-5, 130	100.20	12.8	
11H-6, 137	101.77	11.7	3.48
12H-1, 135	103.75	7.0	
12H-2, 135	105.25	10.8	2.92
12H-3, 135	106.75	9.4	2.47
12H-4, 115	108.05	10.8	2.92
12H-5, 131	109.71	10.3	3.59
12H-6, 121	111.11	11.5	
12H-7, 21	111.61	9.9	3.37
13H-2, 113	114.53	9.2	2.70
13H-3, 120	116.10	7.6	2.47
13H-4, 135	117.75	8.3	2.02
13H-5, 113	119.03	10.4	3.59
13H-6, 121	120.61	11.2	3.37
14H-3, 135	125.75	14.4	5.17
14H-4, 135	127.25	13.5	4.27
14H-5, 141	128.81	12.9	3.15

Table 12 (continued).

Core, section, interval (cm)	Depth (mbsf)	Peak shear strength (kPa)	Residual shear strength (kPa)
14H-6, 140	130.30	13.9	4.27
15H-3, 136	135.26	8.0	1.80
15H-4, 136	136.76	12.4	2.92
15H-5, 115	138.05	14.0	6.51
15H-6, 136	139.76	10.8	2.47
15H-7, 140	141.30	13.9	3.82
16H-1, 135	141.75	10.1	1.12
16H-2, 139	143.29	12.8	2.70
16H-3, 140	144.80	10.8	2.47
16H-4, 136	146.26	14.6	3.15
16H-5, 136	147.76	9.2	2.70
16H-6, 136	149.26	15.3	4.72
17H-1, 136	151.26	14.8	6.74
17H-2, 135	152.75	12.1	
17H-3, 136	154.26	12.8	6.29
17H-4, 136	155.76	18.0	8.09
17H-5, 134	157.24	15.1	4.72
17H-6, 135	158.75	13.9	
18H-1, 135	160.75	11.9	
18H-2, 135	162.25	14.8	3.82
18H-3, 135	163.75	9.0	
18H-4, 116	165.06	11.0	4.04
18H-5, 135	166.75	11.2	2.47
19H-1, 135	170.25	10.2	2.70
19H-2, 135	171.75	6.3	
19H-3, 135	173.25	7.0	1.57
19H-4, 136	174.76	15.5	3.59
19H-5, 135	176.25	17.5	
19H-6, 135	177.75	12.1	5.17
20H-1, 136	179.76	19.1	
20H-2, 135	181.25	14.5	
20H-3, 135	182.75	13.9	
20H-4, 135	184.25	21.6	10.11
20H-5, 135	185.75	11.7	3.37
20H-6, 135	187.25	14.2	6.29
21H-1, 122	189.12	9.5	2.47
21H-2, 123	190.63	13.0	3.82
21H-3, 122	192.12	9.9	3.15
21H-4, 110	193.50	14.0	
21H-5, 115	195.05	13.5	
21H-6, 121	196.61	14.2	
22H-1, 124	199.64	9.2	
22H-3, 121	202.61	13.0	
22H-5, 120	205.60	8.3	
22H-6, 125	207.15	13.8	
23H-1, 112	208.02	8.4	
23H-2, 123	209.63	12.4	
23H-3, 125	211.15	14.6	
23H-4, 130	212.70	14.2	
23H-5, 125	214.15	19.7	
23H-6, 122	215.62	14.4	
24H-1, 120	217.60	8.2	
24H-2, 120	219.10	8.8	
24H-3, 120	220.60	14.4	
24H-4, 100	221.90	9.9	
24H-5, 120	223.60	10.1	
24H-6, 120	225.10	16.2	
25H-2, 120	228.60	10.2	
25H-3, 120	230.10	12.6	
25H-4, 120	231.60	9.2	
25H-5, 120	233.10	12.6	
25H-6, 120	234.60	13.5	
26H-1, 120	236.60	13.4	
26H-3, 120	239.60	13.0	
26H-4, 120	241.10	9.2	
26H-5, 120	242.60	12.6	
26H-6, 120	244.10	18.4	
27H-1, 120	246.10	11.0	
27H-3, 120	249.10	12.6	
27H-4, 100	250.40	17.7	
27H-5, 120	252.10	13.0	
27H-6, 120	253.60	19.8	
28X-2, 39	256.29	18.0	
28X-4, 135	260.25	30.3	
28X-5, 119	261.59	64.0	

Table 12 (continued).

Core, section, interval (cm)	Depth (mbsf)	Peak shear strength (kPa)	Residual shear strength (kPa)
29X-1, 120	265.30	20.2	
29X-2, 126	266.86	18.0	
29X-3, 125	268.35	24.3	
29X-4, 133	269.93	31.5	
29X-5, 116	271.26	47.2	
29X-6, 123	272.83	29.2	
130-807B-			
1H-1, 120	1.20	4.7	
1H-2, 120	2.70	5.4	
2H-1, 120	4.30	7.2	
2H-2, 120	5.80	10.3	
2H-3, 120	7.30	13.7	
2H-4, 120	8.80	10.2	
2H-5, 120	10.30	11.2	
2H-6, 120	11.80	10.1	
3H-1, 120	13.80	13.7	
3H-2, 120	15.30	13.1	
3H-3, 120	16.80	15.5	
3H-4, 120	18.30	21.8	
3H-5, 120	19.80	18.6	
3H-6, 120	21.30	19.1	
4H-1, 120	23.30	11.9	
4H-2, 130	24.90	10.3	
4H-3, 130	26.40	20.2	
4H-4, 120	27.80	15.5	
4H-5, 120	29.30	12.0	
4H-6, 120	30.80	18.9	
5H-1, 120	32.80	9.0	
5H-2, 120	34.30	7.2	
5H-3, 120	35.80	7.6	
5H-4, 120	37.30	11.0	
5H-5, 120	38.80	11.1	
5H-6, 120	40.30	7.9	
6H-1, 120	42.30	9.4	
6H-2, 120	43.80	7.6	
6H-3, 120	45.30	14.4	
6H-4, 120	46.80	13.4	
6H-5, 120	48.30	11.7	
6H-6, 120	49.80	11.6	
7H-1, 120	51.80	8.3	
7H-2, 120	53.30	9.0	
7H-3, 120	54.80	9.5	
7H-4, 120	56.30	12.1	
7H-5, 120	57.80	10.8	
7H-6, 120	59.30	16.5	
8H-1, 120	61.30	8.3	
8H-2, 120	62.80	10.7	
8H-3, 120	64.30	7.9	
8H-4, 120	65.80	8.2	
8H-5, 120	67.30	13.9	
8H-6, 120	68.80	15.7	
9H-1, 120	70.80	11.0	
9H-2, 120	72.30	12.8	
9H-3, 120	73.80	15.1	
9H-4, 120	75.30	10.8	
9H-5, 120	76.80	16.5	
10H-1, 120	80.30	11.7	
10H-2, 120	81.80	9.4	
10H-3, 120	83.30	13.2	
10H-4, 120	84.80	11.5	
10H-5, 120	86.30	18.0	
10H-6, 120	87.80	14.9	
11H-1, 120	89.80	11.1	
11H-2, 120	91.30	9.0	
11H-3, 120	92.80	9.4	
11H-4, 120	94.30	9.8	
11H-5, 120	95.80	12.6	
11H-6, 120	97.30	14.2	
12H-1, 120	99.30	17.9	
12H-2, 120	100.80	10.6	
12H-3, 120	102.30	8.3	
12H-4, 120	103.80	11.2	
12H-5, 120	105.30	16.4	
12H-6, 120	106.80	13.6	

Table 12 (continued).

Core, section, interval (cm)	Depth (mbsf)	Peak shear strength (kPa)	Residual shear strength (kPa)
13H-1, 122	108.82	10.4	
13H-2, 116	110.26	15.3	
13H-3, 120	111.80	10.7	
13H-4, 125	113.35	6.3	
13H-5, 128	114.88	12.2	
13H-6, 120	116.30	16.4	
13H-7, 125	117.85	7.1	
14H-2, 118	119.78	8.8	
14H-3, 118	121.28	14.8	
14H-4, 128	122.88	12.6	
14H-5, 113	124.23	15.1	
14H-6, 116	125.76	16.7	
15H-1, 120	127.80	10.6	
15H-2, 120	129.30	9.9	
15H-3, 120	130.80	8.3	
15H-4, 120	132.30	10.6	
15H-5, 120	133.80	13.0	
15H-6, 120	135.30	9.5	
16H-1, 120	137.30	7.4	
16H-2, 120	138.80	12.4	
16H-3, 120	140.30	11.5	
16H-4, 120	141.80	11.7	
16H-5, 120	143.30	8.5	
16H-6, 120	144.80	8.3	
17H-1, 120	146.80	13.0	
17H-2, 120	148.30	11.7	
17H-3, 120	149.80	11.2	
17H-4, 120	151.30	12.4	
17H-5, 120	152.80	9.4	
17H-6, 120	154.30	12.6	
18H-1, 121	156.31	11.0	
18H-2, 124	157.84	17.0	
18H-3, 123	159.33	11.9	
18H-4, 135	160.95	8.5	
18H-5, 135	162.45	13.7	
18H-6, 134	163.94	13.1	
19H-1, 135	165.95	11.9	
19H-2, 135	167.45	11.6	
19H-3, 135	168.95	10.0	
19H-4, 135	170.45	5.6	
19H-5, 108	171.68	13.5	
20H-1, 135	175.45	11.2	
20H-3, 123	178.33	19.5	
20H-4, 89	179.49	16.8	
21H-1, 135	184.95	11.0	
21H-2, 135	186.45	9.7	
21H-3, 135	187.95	17.6	
21H-4, 135	189.45	11.9	
21H-5, 135	190.95	15.2	
21H-6, 135	192.45	17.5	
22H-1, 135	194.45	12.8	
22H-3, 135	197.45	16.8	
22H-4, 135	198.95	7.6	
22H-5, 135	200.45	9.0	
22H-6, 135	201.95	7.9	
23H-1, 137	203.97	14.2	
23H-3, 135	206.95	12.4	
23H-4, 135	208.45	11.8	
23H-5, 135	209.95	16.8	
23H-6, 135	211.45	17.3	
24H-1, 135	213.45	9.8	
24H-2, 135	214.95	11.2	
24H-3, 135	216.45	12.2	
24H-5, 135	219.45	14.3	
24H-6, 135	220.95	12.9	
25H-1, 135	222.95	11.0	
25H-2, 135	224.45	12.0	
25H-3, 142	226.02	11.3	
25H-4, 140	227.50	15.7	
25H-6, 140	230.50	14.8	
26H-1, 140	232.50	13.7	
26H-2, 140	234.00	10.6	
26H-3, 130	235.40	11.5	
26H-4, 140	237.00	14.8	
26H-6, 138	239.98	6.3	

Table 12 (continued).

Core, section, interval (cm)	Depth (mbsf)	Peak shear strength (kPa)	Residual shear strength (kPa)
27H-1, 140	242.00	10.8	
27H-2, 140	243.50	10.3	
27H-3, 140	245.00	16.6	
27H-4, 140	246.50	12.1	
27H-5, 137	247.97	19.1	
27H-6, 128	249.38	24.3	
28H-1, 128	251.38	13.5	
28H-2, 124	252.84	20.2	
28H-3, 124	254.34	17.1	
28H-4, 115	255.75	28.3	
28H-6, 136	258.96	18.2	
29H-1, 120	260.80	9.7	
29H-2, 120	262.30	5.8	
29H-3, 120	263.80	16.8	
29H-4, 120	265.30	8.8	
29H-5, 120	266.80	17.3	

occurrence of claystones with radiolarites. No index property measurements were obtained on the basalt.

Figure 51 presents wet-bulk density data vs. depth for the upper 350 m in Holes 807A and 807B. In general, these profiles are similar to those observed at the other sites of Leg 130 within carbonate ooze. They are characterized by a general increase with depth. Bulk density increases sharply in the upper 20 m of the sediment column. A slight decrease in bulk density over the next 30 m corresponds to a sharp decrease in mean grain size over this interval (see "Lithostratigraphy" section, this chapter). Below this anomalous section, bulk density increases with depth, to values near 1.65 g/cm^3 at approximately 200 mbsf. From 200 to approximately 260 mbsf, bulk density decreases. This decrease corresponds to a notable decrease in carbonate content over this interval. Similar decreases were observed at other Leg 130 sites, although at slightly different depths in the sediment column.

P-wave Velocity

Horizontal (parallel to bedding) and vertical (perpendicular to bedding) *P*-wave velocities were measured at Site 807. Velocity measurements were performed with the digital sound velocimeter (DSV) and the Hamilton Frame, depending on the degree of lithification. In Hole 807A, the DSV apparatus was replaced by the Hamilton Frame at approximately 275 mbsf, slightly above the ooze-chalk transition at 290 mbsf (see "Lithostratigraphy" section, this chapter). The DSV apparatus was used in all cores from Hole 807B that contained ooze, and the Hamilton Frame was used on all cores from Hole 807C. Results of the velocity analyses are given in Table 14. Figure 52 shows the changes of velocity with depth at Site 807 (merged data sets from Hole 807A and 807C). Figure 53 shows changes of velocity in Holes 807A and 807B in the uppermost 350 mbsf. Table 14 is on microfiche (back pocket).

Velocity measured at Site 807 ranges from 1530 m/s (calcareous ooze) to 5500 m/s (basalt). Velocity values generally increase with depth, although there are major changes in the velocity-depth gradient. There are also intervals of anomalously low (or high) values that reflect major lithologic changes.

In the ooze, horizontal velocity values are usually higher than vertical velocity values (Fig. 53). This may result from anisotropy in the sediment fabric, or from the opening of fine cracks parallel to bedding that result from the release of overburden pressure during core recovery. These fine cracks would tend to reduce *P*-wave propagation in a vertical direction. In the indurated sediment section at Site 807, beginning at the ooze-chalk transition (around 290 mbsf), anisotropy is reversed, with vertical velocities usually higher than horizontal velocities (Figs. 52 and 53). The reason for this anisotropy in lithified sediment is, as yet, unknown.

In the uppermost 100 mbsf, velocities do not change much, with values averaging 1560 m/s. The low velocities measured between 103 and 117 mbsf in Hole 807A (Fig. 53) are probably a result of improper DSV calibration and will be corrected on shore.

Between 100 and approximately 300 mbsf, velocity increases slowly but continuously with depth (Fig. 53), with values ranging from about 1580 m/s at 100 mbsf to 1650 m/s at 300 mbsf. This increase in velocity presumably reflects the increase of sediment consolidation and the onset of cementation in this interval. The first visible effect of cementation on lithology is the occurrence, below 250 mbsf, of chalk "biscuits" interspersed in the soft ooze. The ooze-chalk transition occurs at about 290 mbsf (see "Lithostratigraphy" section, this chapter). Anomalously low velocity values recorded between 275 and 286 mbsf correspond to the first measurements made with the Hamilton Frame. The sediment in this interval is weakly cemented and fractures easily when inserted between the Hamilton Frame transducers, thus affecting *P*-wave propagation.

Between 300 and approximately 1000 mbsf, velocity increases at a greater rate than in the previous interval. The general trend is linear, with extreme velocity values ranging from 1650 m/s at 300 mbsf to about 2000 m/s at 1000 mbsf. Two zones of generally higher velocity values are superimposed on this depth trend; one between 400 and 500 mbsf, and the other between approximately 620 and 780 mbsf. The interval between 300 and 1000 mbsf roughly corresponds to Subunit IB (chalk interval) (see "Lithostratigraphy" section, this chapter). The velocity increase over this interval is probably caused by the progressive induration of chalk. The two zones of higher velocity values presumably reflect local increases of this induration.

Because of poor recovery in the interval between 970 and 1100 mbsf (see "Lithostratigraphy" section, this chapter), velocity data are sparse. *P*-wave velocities generally increase between 1000 and 1100 mbsf (Fig. 52). Below 1100 mbsf, velocities are highly variable (Fig. 52). The interval between 1100 and 1350 mbsf is divided into two zones of different velocities, even though there is no major lithologic difference in this interval (limestone Subunit IIB; see "Lithostratigraphy" section, this chapter). Velocities average 4100 m/s, but are highly variable, between 1100 and 1240 mbsf. Velocities decrease rapidly at 1240 mbsf, and between 1250 and 1350 mbsf they average 3500 m/s, also with large fluctuations.

The claystone interval between 1350 and 1370 mbsf is marked by an interval of low velocity (around 2000 m/s). Basalt drilled at the bottom of Hole 807C leads to a drastic increase in the velocity profile, with values reaching 5200 m/s at 1400 mbsf.

IGNEOUS PETROLOGY

Introduction

Igneous basement was reached at 1379.7 mbsf in Hole 807C (Section 130-807C-74R-1). Basement coring continued for 149.7 m until drilling ceased at 1528.4 mbsf (Section 130-807C-93R-3); average recovery was 60.2%. The basement rocks are predominantly tholeiitic basalts (Albian-Aptian? in age), consisting of both pillow and massive lavas, the latter mostly <3 m thick but including one 28-m-thick flow. In addition, two thin sedimentary horizons were cored and partially recovered: (1) an Aptian(?) limestone and tuff and (2) a soft, yellow-brown, smectite-rich limestone (Intervals 130-807C-80R-1, 70–120 cm, and -82R-3, 72–79 cm, respectively). Well-logging information indicates that there is a third sedimentary bed between these two that was not recovered (see "Logging" section, this chapter).

We have divided the basalts into five main stratigraphic subunits based on (1) the two recovered inter-lava sedimentary layers, themselves designated as basement Subunits B and D, and (2) the pronounced change in flow character between the thick, massive lava (Subunit F) and the flow packets above and below it, which are dominated by thin massive flows and pillows (Fig. 54). All the basalts are very fine grained to fine grained, nonvesicular, hypocrystalline, and aphyric to sparsely phyric. Subunit A rocks are characterized by rare phenocrysts of plagioclase as much as 3 mm in length, superficially similar to the lavas at Site 803; whereas basalts of the lower subunits (C, E, F, and G) have small (<1 mm wide), euhedral to subhedral, olivine microphenocrysts that are generally replaced with green or black clays.

Remarkably, in view of their age, most of the rocks are altered only slightly, and alteration rarely exceeds a moderate level. For the most part, alteration is restricted to the vicinity of veins, most of which are small (<5 mm thick) and filled with clays or calcite. Several thicker veins (up to 7 cm thick) of dark blue, blue-green, or brown clays and iron oxides or hydroxides are present, particularly in Sections 130-807C-88R-3 and -88R-4; similar, but much thinner, veins occur elsewhere. These veins appear to record the passage of hydrothermal fluids derived from greater depths. Two fragments of what appear to be chertified basalt were found in association with these veins. Small (1 mm long) blebs of metallic copper were identified in Section 130-807C-82R-2 at 40 and 58 cm. Several 2- to 5-cm-thick green or yellow-brown veins (containing celadonite, smectite, chert, and/or calcite) also were encountered; these may represent thin, baked, inter-lava sediment layers when they occur between glassy pillow rims or breccias (Intervals 130-807C-88R-3, 7–12 cm; -89R-1, 143–150 cm, and -88R-4, 95–103 cm) or sediment injected into fractures in the basalts (Interval 130-807C-83R-6, 78–86 cm).

A summary of the main features of the igneous stratigraphic subunits is given below. Sedimentary Subunits B and D are described in the "Lithostratigraphy" section (this chapter). Based on the presence of chilled glassy rinds, each of the basaltic subunits - except for Subunit F - is composed of multiple cooling "units" comparable with the fine-scale basement subdivisions at Site 803. Some of these cooling "units" probably represent individual eruptions, particularly the thicker massive flows; others undoubtedly are merely local sheets and pillows comprising parts of larger eruptions. Detailed visual core descriptions are appended at the end of this volume.

Summary of Igneous Subunits

Subunit A: 46 m thick (Sections 130-807C-74R-1, 25 cm, to -80R-1, 70 cm); contains at least 35 glass-bounded pillows and thin massive cooling "units" or subdivisions (<2 m thick); all aphyric, very fine-grained basalt with rare euhedral plagioclase phenocrysts up to 3 mm long; superficially similar to Site 803 basalts.

Subunit C: 16 m thick (Sections 130-807C-80R-1, 120 cm, to -82R-3, 70 cm); pillow lavas and thin massive flows (<3 m thick) forming at least 9 cooling "units"; aphyric, very fine-grained to fine-grained basalt with sparse euhedral to subhedral olivine microphenocrysts (0.2–1 mm across) that are largely replaced by green and black clays.

Subunit E: 5 m thick (Sections 130-807C-82R-3, 79 cm, to -82R-6, 120 cm); mineralogically and morphologically like Subunit C; contains at least 6 glass-rimmed cooling "units" or subdivisions.

Subunit F: 28 m thick (Sections 130-807C-82R-6, 120 cm, to -85R-7, 125 cm); a single massive flow, very fine-grained at its glassy top and bottom, and fine-grained in the interior; similar to Subunits C and E mineralogically.

Subunit G: 53 m thick (Sections 130-807C-85R-7, 125 cm, to -93R-3, 55 cm); like Subunits C and E morphologically and mineralogically; contains at least 34 cooling "units" or subdivisions, which tend to be slightly thicker (up to 3 m thick) with increasing depth; well-log gamma-ray results suggest that a second thick flow may lie beneath this subunit only slightly below the bottom of the hole (see "Logging" section, this chapter).

Petrography

Shipboard thin-section studies of representative samples from each subunit emphasized the comparatively mild degree of alteration in these basalts, and the general paucity of phenocrysts (detailed visual core descriptions are attached at the end of this volume). Textures are intersertal to intergranular, with minor subophitic patches. Groundmasses are fairly fresh, though glass largely has been replaced with dark cryptocrystalline material, probably mainly smectite. In addition to the altered olivine microphenocrysts already mentioned, Subunits C, E, F, and G contain rare, fresh plagioclase and clinopyroxene microphenocrysts. Unlike Subunit A, however, larger phenocrysts are essentially absent in the 103 m of the lower basement sequence.

Shore-based Chemical Analyses of Shipboard Samples

Because the shipboard X-ray fluorescence (XRF) spectrometer was inoperable by the time the ship reached Site 807, chemical analyses were done onshore at the University of Keele, following standard methods (e.g., Floyd, 1986). What follows is a very preliminary report of the data. Nineteen samples representing all subunits but "E" were analyzed for major and trace elements by XRF; water loss on ignition (LOI) was determined gravimetrically. The results are listed in Table 15.

The fresher condition of the Site 807 lavas as compared with those at Site 803 is reflected in their lower LOI values (<0.67 vs. 1.19–3.17 wt%). Like the Site 803 basalts, the Site 807 basalts are somewhat evolved tholeiites, but they have slightly higher average Mg contents (7.3 vs. 6.0 wt%). Four are mildly quartz-normative; three of these are from Subunit A and the lower subunits. The former is characterized by somewhat lower MgO and SiO_2 concentrations; higher Na_{2O}, TiO_2, and Y values; and markedly higher Sr and Zr concentrations than the lower subunits (see Table 15 and Fig. 55). Likewise, ratios of Ti/Zr (96–99) and Zr/Y (3.2–3.4) for Subunit A are, respectively, slightly greater than for the lower subunits (102–107 and 2.6–3.0), although all values are within the range exhibited by normal MORB.

K_2O and Rb concentrations are higher in Subunit A, but the largest K_2O value (0.63 wt%) was observed in Subunit C. Several of the samples from Subunits F and G have very low K_2O contents (0.03–0.06 wt%), values that are at the very low end of the spectrum for normal MORB. Similar basalts were found on the Manihiki Plateau (Jackson et al., 1976), in the Nauru Basin to the east of Site 807 (e.g., Floyd, 1986), and on the island of Malaita and Santa Isabel at the western edge of the Ontong Java Plateau (J. Mahoney, unpubl. data, 1989).

Chemical variations within individual subunits generally appear to be smaller than in the single stratigraphic subunit

Table 13. Index properties data, Site 807.

Core, section, interval (cm)	Depth (mbsf)	Wet-bulk density (g/cm^3)	Grain density (g/ cm^3)	Water content (% dry wt)	Porosity (%)	Dry-bulk density (g/cm^3)
130-807A-						
1H-1, 95	0.95	1.52	2.65	87.3	69.1	0.81
1H-2, 8	1.58	1.51	2.67	89.4	69.7	0.80
1H-2, 94	2.44	1.47	2.67	100.3	72.1	0.74
1H-3, 13	3.13	1.51	2.67	90.9	70.1	0.79
1H-3, 93	3.93	1.48	2.66	97.8	71.5	0.75
1H-4, 14	4.64	1.54	2.70	83.9	68.6	0.84
1H-4, 94	5.44	1.56	2.71	79.8	67.6	0.87
1H-5, 13	6.13	1.52	2.69	90.0	70.1	0.80
1H-5, 95	6.95	1.48	2.68	100.0	72.1	0.74
2H-1, 94	8.34	1.54	2.67	81.8	67.8	0.85
2H-2, 14	9.04	1.53	2.65	84.2	68.3	0.83
2H-2, 94	9.84	1.52	2.70	88.0	69.6	0.81
2H-3, 14	10.54	1.53	2.69	85.9	69.1	0.82
2H-4, 14	12.04	1.54	2.72	84.2	68.9	0.84
2H-4, 94	12.84	1.55	2.65	80.4	67.3	0.86
2H-5, 14	13.54	1.53	2.69	86.3	69.2	0.82
2H-5, 94	14.34	1.53	2.65	83.8	68.3	0.83
2H-6, 14	15.04	1.55	2.68	82.0	68.0	0.85
2H-6, 94	15.84	1.53	2.62	83.9	68.0	0.83
2H-7, 14	16.54	1.52	2.70	88.6	69.8	0.81
3H-1, 94	17.84	1.55	2.71	81.6	68.1	0.85
3H-2, 15	18.55	1.56	2.73	81.9	68.4	0.86
3H-2, 95	19.35	1.50	2.67	92.7	70.5	0.78
3H-3, 14	20.04	1.52	2.67	87.3	69.3	0.81
3H-3, 95	20.85	1.56	2.68	78.3	67.0	0.88
3H-4, 21	21.61	1.58	2.68	74.8	66.0	0.90
3H-4, 84	22.24	1.55	2.73	83.1	68.7	0.85
3H-5, 14	23.04	1.55	2.68	80.8	67.7	0.86
3H-5, 96	23.86	1.58	2.70	75.1	66.3	0.90
3H-6, 15	24.55	1.55	2.67	80.9	67.6	0.86
3H-6, 95	25.35	1.54	2.68	83.8	68.4	0.84
3H-7, 24	26.14	1.54	2.71	85.8	69.2	0.83
4H-1, 94	27.34	1.53	2.69	86.7	69.2	0.82
4H-2, 15	28.05	1.57	2.68	77.0	66.6	0.89
4H-2, 94	28.84	1.56	2.70	78.9	67.3	0.87
4H-3, 95	30.35	1.52	2.67	89.0	69.7	0.80
4H-3, 95	30.35	1.50	2.70	94.1	71.0	0.77
4H-4, 15	31.05	1.51	2.68	91.9	70.4	0.78
4H-4, 95	31.85	1.51	2.68	91.7	70.4	0.79
4H-5, 14	32.54	1.54	2.71	85.7	69.2	0.83
4H-5, 95	33.35	1.54	2.68	84.0	68.5	0.84
4H-6, 15	34.05	1.55	2.72	82.1	68.3	0.85
4H-6, 95	34.85	1.53	2.68	84.6	68.7	0.83
4H-7, 30	35.70	1.56	2.71	80.9	68.0	0.86
5H-1, 108	36.98	1.52	2.68	87.4	69.3	0.81
5H-2, 35	37.75	1.52	2.67	89.1	69.7	0.80
5H-2, 109	38.49	1.55	2.66	81.2	67.6	0.85
5H-3, 40	39.30	1.55	2.68	82.3	68.1	0.85
5H-3, 108	39.98	1.57	2.68	78.0	66.9	0.88
5H-4, 39	40.79	1.56	2.69	78.4	67.1	0.88
5H-4, 108	41.48	1.55	2.68	80.6	67.6	0.86
5H-5, 39	42.29	1.53	2.70	87.5	69.6	0.81
5H-5, 108	42.98	1.53	2.65	84.3	68.3	0.83
5H-6, 40	43.80	1.53	2.67	85.6	68.9	0.82
5H-6, 108	44.48	1.51	2.66	90.5	69.9	0.79
5H-7, 29	45.19	1.52	2.66	87.9	69.3	0.81
6H-2, 33	47.23	1.53	2.69	86.3	69.2	0.82
6H-3, 35	48.75	1.54	2.71	84.2	68.8	0.84
6H-3, 110	49.50	1.56	2.66	77.7	66.6	0.88
6H-4, 35	50.25	1.54	2.73	86.7	69.6	0.82
6H-4, 109	50.99	1.53	2.65	85.0	68.5	0.83
6H-5, 35	51.75	1.55	2.69	81.4	67.9	0.85
6H-5, 110	52.50	1.53	2.66	84.0	68.4	0.83
6H-6, 35	53.25	1.55	2.68	80.9	67.7	0.86
6H-6, 109	53.99	1.54	2.72	85.7	69.2	0.83
7H-1, 108	55.98	1.55	2.68	80.1	67.5	0.86
7H-2, 33	56.73	1.52	2.68	88.5	69.6	0.81
7H-2, 108	57.48	1.53	2.68	84.9	68.7	0.83
7H-3, 33	58.23	1.52	2.66	86.5	69.0	0.82
7H-3, 108	58.98	1.52	2.65	86.4	68.9	0.82
7H-4, 33	59.73	1.53	2.67	86.1	69.0	0.82
7H-4, 110	60.50	1.55	2.68	81.3	67.8	0.85
7H-5, 33	61.23	1.55	2.66	81.0	67.6	0.86
7H-5, 110	62.00	1.54	2.67	83.8	68.4	0.84

Table 13 (continued).

Core, section, interval (cm)	Depth (mbsf)	Wet-bulk density (g/cm^3)	Grain density (g/ cm^3)	Water content (% dry wt)	Porosity (%)	Dry-bulk density (g/cm^3)
7H-6, 33	62.73	1.53	2.67	86.1	69.0	0.82
7H-6, 108	63.48	1.54	2.71	84.5	68.9	0.83
8H-1, 107	65.47	1.54	2.65	82.1	67.8	0.85
8H-2, 34	66.24	1.55	2.64	79.2	66.9	0.87
8H-2, 110	67.00	1.53	2.66	85.2	68.6	0.83
8H-3, 33	67.73	1.54	2.70	83.2	68.4	0.84
8H-3, 110	68.50	1.54	2.66	82.7	68.0	0.84
8H-4, 42	69.32	1.53	2.67	84.7	68.6	0.83
8H-4, 110	70.00	1.54	2.68	84.3	68.6	0.83
8H-5, 39	70.79	1.54	2.67	82.5	68.1	0.85
8H-5, 110	71.50	1.56	2.71	80.7	67.9	0.86
8H-6, 39	72.29	1.56	2.68	79.2	67.3	0.87
8H-6, 100	72.90	1.52	2.66	88.4	69.4	0.80
8H-7, 34	73.74	1.54	2.68	84.0	68.5	0.84
9H-1, 33	74.23	1.56	2.69	79.2	67.3	0.87
9H-1, 108	74.98	1.58	2.70	75.0	66.2	0.90
9H-2, 33	75.73	1.58	2.68	75.0	66.0	0.90
9H-2, 108	76.48	1.58	2.69	74.7	66.0	0.91
9H-3, 33	77.23	1.54	2.68	82.6	68.1	0.85
9H-3, 108	77.98	1.60	2.68	71.3	64.9	0.93
9H-4, 33	78.73	1.52	2.62	86.4	68.6	0.81
9H-4, 108	79.48	1.54	2.66	82.3	67.9	0.85
9H-5, 33	80.23	1.55	2.67	81.0	67.6	0.86
9H-5, 108	80.98	1.59	2.69	73.3	65.6	0.92
9H-6, 33	81.73	1.56	2.68	78.9	67.1	0.87
9H-6, 108	82.48	1.55	2.67	81.7	67.8	0.85
10H-1, 108	84.48	1.58	2.70	76.5	66.6	0.89
10H-2, 108	85.98	1.54	2.70	84.3	68.8	0.84
10H-3, 108	87.48	1.56	2.67	78.5	67.0	0.87
10H-5, 108	90.48	1.60	2.69	70.9	64.9	0.94
10H-6, 108	91.98	1.57	2.69	78.1	67.0	0.88
11H-1, 106	93.96	1.56	2.66	77.7	66.7	0.88
11H-2, 107	95.47	1.57	2.64	74.4	65.5	0.90
11H-3, 107	96.97	1.54	2.69	82.8	68.3	0.84
11H-4, 107	98.47	1.58	2.66	74.6	65.7	0.90
11H-5, 107	99.97	1.55	2.66	79.3	67.1	0.87
11H-6, 107	101.47	1.58	2.67	73.5	65.5	0.91
12H-1, 106	103.46	1.60	2.70	70.8	64.9	0.94
12H-2, 107	104.97	1.59	2.68	71.9	65.1	0.93
12H-3, 106	106.46	1.61	2.69	69.5	64.4	0.95
12H-5, 106	109.46	1.58	2.69	74.8	66.1	0.90
12H-6, 106	110.96	1.58	2.67	73.7	65.5	0.91
13H-2, 106	114.46	1.59	2.69	72.7	65.4	0.92
13H-3, 106	115.96	1.59	2.70	72.9	65.5	0.92
13H-4, 106	117.46	1.61	2.69	69.6	64.5	0.95
13H-5, 106	118.96	1.60	2.70	72.1	65.3	0.93
13H-6, 106	120.46	1.59	2.71	73.7	65.9	0.92
14H-3, 31	124.71	1.62	2.71	68.5	64.3	0.96
14H-3, 108	125.48	1.59	2.71	73.1	65.7	0.92
14H-4, 30	126.20	1.61	2.72	69.5	64.6	0.95
14H-4, 108	126.98	1.62	2.73	70.0	64.9	0.95
14H-5, 31	127.71	1.59	2.72	74.4	66.2	0.91
14H-5, 108	128.48	1.60	2.69	71.2	64.9	0.93
14H-6, 30	129.20	1.62	2.71	68.7	64.3	0.96
14H-6, 108	129.98	1.61	2.69	69.9	64.6	0.95
15H-3, 108	134.98	1.59	2.73	75.5	66.6	0.90
15H-4, 109	136.49	1.57	2.69	78.2	67.0	0.88
15H-5, 107	137.97	1.63	2.69	65.8	63.2	0.98
15H-6, 107	139.47	1.62	2.70	67.2	63.7	0.97
15H-7, 107	140.97	1.63	2.71	67.4	63.9	0.97
16H-1, 107	141.47	1.60	2.68	71.1	64.9	0.93
16H-2, 107	142.97	1.63	2.69	66.6	63.4	0.98
16H-3, 107	144.47	1.63	2.67	64.6	62.5	0.99
16H-4, 107	145.97	1.64	2.70	65.1	63.0	0.99
16H-5, 107	147.47	1.63	2.69	65.0	62.8	0.99
16H-6, 118	149.08	1.67	2.70	59.4	60.8	1.05
17H-1, 73	150.63	1.64	2.72	65.9	63.4	0.99
17H-2, 89	152.29	1.61	2.68	69.2	64.2	0.95
17H-3, 75	153.65	1.61	2.68	68.4	63.9	0.96
17H-4, 89	155.29	1.65	2.70	63.4	62.4	1.01
17H-5, 74	156.64	1.66	2.71	62.4	62.1	1.02
17H-6, 75	158.15	1.66	2.73	62.3	62.2	1.02
18H-1, 74	160.14	1.62	2.69	67.6	63.8	0.97
18H-2, 75	161.65	1.63	2.71	66.0	63.4	0.98
18H-3, 72	163.12	1.61	2.73	70.9	65.2	0.94
18H-4, 74	164.64	1.63	2.67	65.3	62.8	0.98

Table 13 (continued).

Core, section, interval (cm)	Depth (mbsf)	Wet-bulk density (g/cm^3)	Grain density (g/ cm^3)	Water content (% dry wt)	Porosity (%)	Dry-bulk density (g/cm^3)
18H-5, 74	166.14	1.63	2.71	67.2	63.9	0.97
18H-6, 75	167.65	1.63	2.71	66.6	63.6	0.98
19H-1, 73	169.63	1.63	2.69	64.9	62.8	0.99
19H-2, 72	171.12	1.65	2.72	63.8	62.7	1.01
19H-3, 71	172.61	1.65	2.72	63.9	62.8	1.01
19H-4, 85	174.25	1.64	2.71	65.1	63.1	0.99
19H-5, 72	175.62	1.64	2.73	66.2	63.6	0.98
19H-6, 74	177.14	1.67	2.70	60.4	61.3	1.04
20H-1, 75	179.15	1.64	2.73	66.0	63.5	0.99
20H-2, 74	180.64	1.64	2.69	64.5	62.7	1.00
20H-3, 72	182.12	1.67	2.71	60.7	61.4	1.04
20H-4, 74	183.64	1.64	2.72	65.2	63.2	0.99
20H-5, 72	185.12	1.68	2.70	58.6	60.5	1.06
20H-6, 74	186.64	1.67	2.73	61.1	61.8	1.04
21H-1, 115	189.05	1.65	2.72	63.4	62.6	1.01
21H-2, 107	190.47	1.64	2.69	63.6	62.3	1.00
21H-3, 110	192.00	1.65	2.71	64.1	62.7	1.00
21H-4, 90	193.30	1.64	2.71	64.6	62.9	1.00
21H-5, 107	194.97	1.64	2.70	64.9	63.0	0.99
21H-6, 109	196.49	1.69	2.72	58.1	60.5	1.07
22H-1, 109	199.49	1.68	2.71	59.3	60.9	1.05
22H-2, 99	200.89	1.66	2.72	62.3	62.1	1.02
22H-3, 110	202.50	1.68	2.71	58.7	60.7	1.06
22H-4, 109	203.99	1.67	2.72	60.7	61.6	1.04
22H-5, 110	205.50	1.68	2.71	59.3	60.9	1.05
22H-6, 112	207.02	1.68	2.70	58.0	60.3	1.07
23H-1, 105	207.95	1.67	2.72	61.2	61.7	1.03
23H-2, 109	209.49	1.64	2.70	64.0	62.6	1.00
23H-3, 107	210.97	1.68	2.68	58.4	60.3	1.06
23H-4, 110	212.50	1.66	2.73	62.1	62.2	1.03
23H-5, 108	213.98	1.72	2.71	53.6	58.5	1.12
23H-6, 109	215.49	1.65	2.69	63.2	62.2	1.01
26H-1, 109	236.49	1.65	2.72	63.3	62.5	1.01
26H-3, 108	239.48	1.64	2.69	64.7	62.8	1.00
26H-4, 109	240.99	1.64	2.66	63.5	62.1	1.00
26H-5, 109	242.49	1.62	2.68	68.0	63.8	0.96
26H-6, 109	243.99	1.65	2.69	62.6	62.0	1.02
27H-1, 109	245.99	1.66	2.69	60.5	61.3	1.04
27H-3, 109	248.99	1.65	2.69	62.2	61.9	1.02
27H-4, 109	250.49	1.61	2.68	68.5	64.0	0.96
27H-5, 109	251.99	1.64	2.70	64.4	62.8	1.00
27H-6, 109	253.49	1.62	2.69	66.7	63.4	0.97
28X-1, 94	255.34	1.64	2.69	63.8	62.4	1.00
28X-2, 30	256.20	1.61	2.67	68.2	63.8	0.96
28X-3, 52	257.92	1.61	2.65	68.0	63.6	0.96
28X-4, 30	259.20	1.62	2.66	65.9	63.0	0.98
28X-5, 100	261.40	1.60	2.62	68.5	63.5	0.95
28X-6, 27	262.17	1.61	2.65	67.2	63.3	0.97
29X-1, 61	264.71	1.65	2.67	61.2	61.3	1.03
29X-2, 109	266.69	1.68	2.68	57.4	59.8	1.07
29X-3, 70	267.80	1.64	2.68	63.3	62.2	1.01
29X-4, 66	269.26	1.67	2.72	60.5	61.5	1.04
29X-5, 84	270.94	1.66	2.66	59.6	60.6	1.04
29X-6, 60	262.50	1.69	2.68	56.8	59.6	1.08
30X-2, 56	275.86	1.64	2.69	63.8	62.5	1.00
30X-3, 87	277.67	1.68	2.68	57.8	60.1	1.07
30X-4, 65	278.95	1.67	2.69	59.6	60.9	1.05
30X-5, 100	280.80	1.61	2.67	67.9	63.7	0.96
30X-6, 70	282.00	1.64	2.65	63.4	62.0	1.00
31X-1, 95	284.45	1.65	2.66	61.0	61.2	1.03
31X-3, 66	287.16	1.67	2.69	60.0	61.0	1.04
31X-4, 68	288.68	1.63	2.67	65.1	62.7	0.99
31X-5, 70	290.20	1.62	2.66	65.6	62.8	0.98
32X-1, 144	294.14	1.63	2.64	63.2	61.7	1.00
32X-2, 110	295.30	1.68	2.68	57.8	60.0	1.06
32X-3, 126	296.96	1.68	2.71	58.0	60.3	1.07
32X-4, 93	298.13	1.70	2.72	56.2	59.7	1.09
33X-1, 35	302.65	1.65	2.67	62.2	61.7	1.02
33X-2, 53	304.33	1.69	2.67	56.2	59.3	1.08
33X-3, 135	306.65	1.67	2.68	59.5	60.7	1.05
33X-4, 127	308.07	1.72	2.71	52.9	58.2	1.13
33X-5, 145	309.75	1.70	2.70	55.2	59.1	1.10
33X-6, 77	310.57	1.60	2.66	69.5	64.1	0.95
34X-1, 68	312.68	1.72	2.68	51.9	57.5	1.13
34X-2, 73	314.23	1.69	2.67	56.7	59.5	1.08
34X-3, 100	316.00	1.68	2.66	57.5	59.7	1.06

Table 13 (continued).

Core, section, interval (cm)	Depth (mbsf)	Wet-bulk density (g/cm^3)	Grain density (g/ cm^3)	Water content (% dry wt)	Porosity (%)	Dry-bulk density (g/cm^3)
34X-4, 107	317.57	1.72	2.68	52.7	57.8	1.12
34X-5, 42	318.42	1.75	2.67	47.8	55.3	1.18
34X-6, 131	320.81	1.67	2.71	59.6	61.0	1.05
35X-1, 133	322.53	1.72	2.70	53.5	58.4	1.12
35X-2, 140	324.10	—	—	58.3	—	—
35X-3, 111	325.31	1.69	2.69	56.5	59.5	1.08
35X-4, 144	327.14	1.68	2.70	57.9	60.3	1.07
35X-5, 104	328.24	1.68	2.69	58.5	60.4	1.06
36X-1, 133	332.23	1.69	2.69	56.3	59.5	1.08
36X-2, 141	333.81	1.67	2.69	59.4	60.8	1.05
36X-3, 107	334.97	1.70	2.71	55.4	59.2	1.10
36X-4, 135	336.75	1.68	2.75	60.2	61.6	1.05
36X-5, 113	338.03	1.72	2.68	52.9	57.9	1.12
36X-6, 82	339.22	1.67	2.69	59.6	60.9	1.05
37X-2, 87	342.97	1.70	2.72	55.7	59.5	1.09
37X-3, 95	344.55	1.69	2.69	56.6	59.6	1.08
37X-4, 50	345.60	1.70	2.74	56.8	60.1	1.09
37X-5, 8	346.68	1.71	2.71	53.9	58.6	1.11
38X-1, 140	351.60	1.68	2.73	60.1	61.4	1.05
38X-2, 112	352.82	1.68	2.73	59.9	61.3	1.05
38X-3, 142	354.62	1.67	2.72	60.2	61.3	1.04
38X-4, 96	355.66	1.60	2.74	72.1	65.6	0.93
38X-5, 78	356.98	1.66	2.70	61.0	61.5	1.03
39X-1, 37	360.27	1.63	2.63	64.0	62.0	0.99
39X-2, 91	362.31	1.67	2.72	60.3	61.4	1.04
39X-3, 114	364.04	1.60	2.64	69.2	63.9	0.95
39X-4, 47	364.87	1.69	2.77	59.0	61.3	1.06
39X-5, 142	367.32	1.67	2.68	59.4	60.7	1.05
39X-6, 141	368.81	1.67	2.69	59.7	60.9	1.05
40X-1, 80	370.50	1.69	2.70	56.9	59.8	1.08
40X-2, 57	371.77	1.71	2.69	54.0	58.5	1.11
40X-3, 59	373.29	1.69	2.68	55.7	59.2	1.09
40X-4, 145	375.65	1.68	2.67	57.7	59.9	1.06
40X-5, 121	376.91	1.71	2.68	53.2	58.0	1.12
40X-6, 109	378.29	1.73	2.68	50.7	56.9	1.15
41X-1, 90	380.40	1.75	2.70	49.7	56.6	1.17
41X-2, 75	381.75	1.76	2.72	48.2	56.0	1.19
41X-3, 72	383.22	1.68	2.67	57.0	59.6	1.07
41X-4, 76	384.76	1.76	2.70	48.3	55.8	1.18
41X-5, 83	386.33	1.73	2.70	51.4	57.4	1.14
41X-6, 84	387.84	1.79	2.76	46.7	55.5	1.22
42X-1, 106	390.26	1.77	2.71	47.0	55.3	1.21
42X-2, 102	391.72	1.78	2.72	46.5	55.1	1.21
42X-3, 106	393.26	1.83	2.88	46.0	56.3	1.25
42X-4, 79	394.49	1.79	2.71	44.8	54.1	1.24
42X-5, 60	395.80	1.78	2.74	46.6	55.3	1.22
42X-6, 40	397.10	1.77	2.74	48.8	56.5	1.19
43X-1, 81	399.71	1.75	2.68	48.6	55.9	1.18
43X-2, 57	400.97	1.74	2.70	50.0	56.7	1.16
43X-3, 67	402.57	1.78	2.71	45.9	54.7	1.22
43X-4, 67	404.07	1.81	2.70	42.6	52.8	1.27
43X-5, 76	405.66	1.78	2.74	47.3	55.7	1.21
44X-1, 75	409.35	1.76	2.68	46.8	54.9	1.20
44X-2, 141	411.51	1.85	2.71	39.3	50.9	1.33
44X-3, 110	412.70	1.75	2.69	48.3	55.8	1.18
44X-4, 102	414.12	1.74	2.73	50.8	57.4	1.16
44X-5, 124	415.84	1.84	2.70	39.9	51.1	1.31
45X-1, 98	419.28	1.82	2.69	41.5	52.1	1.28
45X-2, 97	420.77	1.78	2.70	45.7	54.5	1.22
45X-3, 90	422.20	1.81	2.68	41.7	52.1	1.28
45X-4, 95	423.75	1.84	2.73	40.4	51.7	1.31
45X-5, 57	424.87	1.76	2.70	47.7	55.6	1.19
45X-6, 65	426.45	1.77	2.70	47.1	55.2	1.20
46X-1, 116	428.96	1.78	2.74	46.7	55.4	1.22
46X-2, 112	430.42	1.78	2.70	45.3	54.3	1.23
46X-3, 107	431.87	1.82	2.66	40.0	50.9	1.30
46X-4, 108	433.38	1.75	2.71	48.9	56.3	1.18
46X-5, 81	434.61	1.85	2.70	39.2	50.7	1.33
46X-6, 78	436.08	1.79	2.68	43.6	53.2	1.25
47X-1, 111	438.61	1.75	2.70	49.5	56.5	1.17
47X-2, 122	440.22	1.78	2.69	45.6	54.4	1.22
47X-3, 110	441.60	1.80	2.69	43.5	53.2	1.25
47X-4, 113	443.13	1.81	2.67	41.5	51.9	1.28
47X-5, 103	444.53	1.79	2.69	44.5	53.8	1.24
47X-6, 51	445.51	1.79	2.71	45.1	54.3	1.23
48X-1, 100	448.10	1.80	2.68	43.5	53.1	1.25

Table 13 (continued).

Core, section, interval (cm)	Depth (mbsf)	Wet-bulk density (g/cm^3)	Grain density (g/cm^3)	Water content (% dry wt)	Porosity (%)	Dry-bulk density (g/cm^3)
48X-2, 99	449.59	1.79	2.65	43.0	52.6	1.25
48X-3, 101	451.11	1.82	2.71	41.5	52.2	1.29
48X-4, 93	452.53	1.81	2.69	42.1	52.4	1.28
48X-5, 84	453.94	1.83	2.72	41.7	52.4	1.29
48X-6, 100	455.60	1.80	2.70	43.5	53.3	1.26
49X-1, 53	457.33	1.74	2.70	49.9	56.6	1.16
49X-2, 92	459.22	1.78	2.70	45.2	54.2	1.23
49X-3, 65	460.45	1.81	2.70	42.4	52.7	1.27
49X-4, 74	462.04	1.82	2.69	40.7	51.5	1.30
49X-5, 72	463.52	1.88	2.70	36.2	48.8	1.38
50X-1, 89	467.29	1.84	2.71	39.6	51.1	1.32
50X-2, 93	468.83	1.82	2.72	41.9	52.5	1.28
50X-3, 90	470.30	1.78	2.71	45.9	54.6	1.22
50X-4, 100	471.90	1.84	2.71	40.3	51.5	1.31
50X-5, 99	473.39	1.81	2.71	42.6	52.8	1.27
50X-6, 98	474.88	1.87	2.73	37.6	49.9	1.36
51X-1, 33	476.43	1.84	2.70	39.9	51.2	1.31
51X-2, 41	478.01	1.83	2.72	40.9	51.9	1.30
51X-3, 42	479.52	1.83	2.68	40.4	51.3	1.30
51X-4, 38	480.98	1.86	2.68	36.9	49.0	1.36
51X-5, 33	482.43	1.81	2.71	42.7	52.9	1.27
51X-6, 18	483.78	1.84	2.71	40.4	51.6	1.31
52X-1, 108	486.88	1.79	2.69	44.3	53.7	1.24
52X-3, 14	488.94	1.84	2.71	39.7	51.1	1.32
52X-5, 61	492.41	1.77	2.69	46.7	55.0	1.21
53X-1, 105	496.45	1.84	2.70	39.3	50.8	1.32
53X-2, 93	497.83	1.79	2.69	44.0	53.4	1.24
53X-3, 97	499.37	1.80	2.72	44.3	54.0	1.25
53X-4, 90	500.80	1.79	2.71	44.9	54.2	1.24
53X-5, 91	502.31	1.90	2.70	34.3	47.4	1.42
54X-1, 96	506.06	1.79	2.73	45.1	54.4	1.24
54X-2, 97	507.57	1.78	2.71	46.3	54.9	1.22
54X-3, 114	509.24	1.80	2.73	44.2	53.9	1.25
54X-4, 113	510.73	1.77	2.73	47.8	55.8	1.20
54X-5, 80	511.90	1.74	2.72	50.8	57.3	1.15
54X-6, 27	512.87	1.72	2.67	51.5	57.2	1.14
55X-2, 116	517.46	1.77	2.70	46.9	55.1	1.20
55X-3, 61	518.41	1.77	2.71	47.2	55.4	1.20
55X-4, 65	519.95	1.83	2.72	41.3	52.2	1.29
55X-5, 103	521.83	1.75	2.70	49.5	56.5	1.17
55X-6, 43	522.73	1.76	2.69	47.7	55.5	1.19
56X-1, 146	525.46	1.79	2.70	44.3	53.8	1.24
56X-2, 110	526.60	1.78	2.70	45.8	54.6	1.22
56X-3, 53	527.53	1.81	2.71	42.9	53.0	1.27
56X-4, 131	529.81	1.85	2.74	39.9	51.5	1.32
56X-6, 49	531.99	1.83	2.69	40.1	51.2	1.31
57X-1, 85	534.55	1.79	2.71	44.6	54.0	1.24
57X-2, 86	536.06	1.79	2.71	44.7	54.1	1.24
57X-4, 65	538.85	1.79	2.72	45.2	54.4	1.23
57X-5, 56	540.26	1.76	2.68	47.3	55.1	1.20
58X-1, 105	544.45	1.79	2.70	44.3	53.8	1.24
58X-2, 104	545.94	1.79	2.75	46.1	55.2	1.23
58X-3, 143	547.83	1.79	2.74	46.2	55.1	1.22
58X-4, 136	549.26	1.80	2.74	45.0	54.5	1.24
59X-2, 124	555.74	1.83	2.72	41.5	52.3	1.29
59X-3, 107	557.07	1.66	2.79	63.7	63.2	1.02
59X-4, 135	558.85	1.83	2.73	41.8	52.6	1.29
60X-1, 11	562.71	1.81	2.70	42.2	52.5	1.28
60X-3, 38	565.98	1.81	2.72	43.8	53.6	1.26
60X-4, 72	567.82	1.84	2.74	40.3	51.7	1.31
61X-1, 97	573.27	1.79	2.72	45.6	54.6	1.23
61X-2, 111	574.91	1.77	2.70	46.9	55.2	1.21
61X-3, 121	576.51	—	—	48.7	—	—
61X-4, 145	578.25	1.81	2.70	42.9	52.9	1.26
61X-5, 143	579.73	1.80	2.72	44.3	53.9	1.25
61X-6, 92	580.72	1.77	2.67	45.5	54.1	1.22
62X-3, 100	585.90	1.79	2.69	44.0	53.5	1.25
62X-4, 96	587.36	1.80	2.71	43.8	53.5	1.25
62X-5, 88	588.78	1.83	2.71	41.5	52.2	1.29
63X-1, 110	592.70	1.83	2.71	41.0	51.9	1.30
63X-2, 50	593.60	1.85	2.72	39.4	51.0	1.33
63X-3, 32	594.92	1.84	2.72	40.2	51.5	1.31
63X-4, 59	596.69	1.89	2.72	36.1	48.8	1.39
63X-5, 46	598.06	1.86	2.71	37.6	49.7	1.36
64X-1, 9	601.39	1.84	2.70	39.7	51.0	1.32
64X-2, 109	603.89	1.91	2.70	33.3	46.6	1.43

Table 13 (continued).

Core, section, interval (cm)	Depth (mbsf)	Wet-bulk density (g/cm^3)	Grain density (g/ cm^3)	Water content (% dry wt)	Porosity (%)	Dry-bulk density (g/cm^3)
64X-3, 124	605.54	1.87	2.70	37.0	49.2	1.36
64X-4, 81	606.61	1.82	2.69	41.2	51.8	1.29
64X-5, 59	607.89	1.84	2.72	40.7	51.9	1.30
65X-1, 67	611.67	1.82	2.68	41.2	51.8	1.29
65X-2, 62	613.12	1.86	2.70	38.1	50.0	1.35
65X-3, 73	614.73	1.78	2.67	44.6	53.6	1.23
65X-4, 65	616.15	1.84	2.68	38.6	50.1	1.33
65X-5, 52	617.52	1.81	2.69	42.6	52.7	1.27
66X-1, 85	621.45	1.83	2.72	40.9	52.0	1.30
66X-3, 79	624.39	1.86	2.71	38.2	50.2	1.34
66X-4, 85	625.95	1.82	2.69	40.8	51.6	1.30
67X-3, 92	634.22	1.78	2.67	45.1	53.9	1.23
68X-1, 105	640.95	1.84	2.72	40.0	51.4	1.31
68X-2, 111	642.51	1.88	2.71	36.6	49.1	1.37
68X-3, 105	643.95	1.84	2.71	39.7	51.1	1.32
68X-4, 89	645.29	1.84	2.69	39.6	50.8	1.32
70X-3, 60	662.80	1.86	2.68	37.4	49.3	1.35
70X-4, 17	663.87	1.86	2.68	36.9	49.0	1.36
70X-5, 70	665.90	1.91	2.70	33.4	46.7	1.43
71X-1, 126	670.16	1.86	2.69	37.4	49.4	1.35
71X-2, 123	671.63	1.87	2.70	36.6	49.0	1.37
71X-3, 109	672.99	1.87	2.71	37.5	49.6	1.36
71X-4, 112	674.52	1.85	2.73	39.5	51.1	1.33
71X-5, 108	675.98	1.85	2.71	38.9	50.6	1.33
72X-1, 74	678.94	1.86	2.70	37.6	49.6	1.35
72X-2, 66	680.36	1.84	2.70	39.1	50.7	1.33
72X-3, 78	681.98	1.88	2.72	36.4	49.1	1.38
72X-4, 67	683.37	1.83	2.62	37.8	49.1	1.33
73X-2, 90	690.20	1.81	2.72	42.6	52.9	1.27
73X-3, 85	691.65	1.84	2.69	39.1	50.6	1.32
73X-4, 78	693.08	1.86	2.69	37.8	49.7	1.35
73X-5, 75	694.55	1.85	2.70	38.5	50.2	1.34
73X-6, 35	695.65	1.87	2.67	36.2	48.4	1.37
74X-1, 62	698.12	1.88	2.68	35.2	47.8	1.39
74X-2, 59	699.59	1.85	2.72	38.8	50.6	1.34
74X-3, 63	701.13	1.84	2.66	38.3	49.8	1.33
75X-1, 73	707.93	1.85	2.71	39.4	51.0	1.32
75X-2, 86	709.56	1.85	2.72	39.2	50.9	1.33
75X-3, 73	710.93	1.89	2.70	35.3	48.1	1.40
75X-4, 83	712.53	1.87	2.69	36.4	48.7	1.37
76X-1, 94	717.84	1.86	2.70	37.5	49.6	1.36
76X-2, 120	719.60	1.91	2.70	33.5	46.8	1.43
76X-3, 114	721.04	1.86	2.71	38.0	50.0	1.35
76X-4, 95	722.35	1.90	2.71	34.7	47.7	1.41
76X-5, 82	723.72	1.87	2.71	36.9	49.3	1.37
77X-1, 83	727.33	1.88	2.69	35.8	48.4	1.38
77X-2, 105	729.05	1.85	2.70	38.6	50.3	1.33
77X-3, 78	730.28	1.85	2.67	37.9	49.6	1.34
77X-4, 75	731.75	1.84	2.68	39.5	50.7	1.32
77X-5, 73	733.23	1.87	2.72	37.7	49.9	1.36
78X-1, 110	737.30	1.86	2.71	37.9	49.9	1.35
78X-2, 88	738.58	1.86	2.69	37.6	49.6	1.35
78X-3, 27	739.47	1.82	2.68	41.0	51.7	1.29
78X-4, 110	741.80	1.83	2.70	40.2	51.3	1.31
78X-5, 65	742.85	1.82	2.69	41.0	51.7	1.29
79X-1, 35	745.85	1.83	2.70	40.5	51.5	1.30
79X-3, 31	748.81	1.90	2.71	35.1	48.1	1.40
80X-1, 43	755.63	1.81	2.70	42.8	52.9	1.27
80X-2, 93	757.63	1.82	2.69	41.4	52.0	1.29
80X-3, 79	758.99	1.81	2.67	41.1	51.6	1.29
82X-2, 69	776.69	1.85	2.71	39.0	50.6	1.33
82X-3, 109	778.59	1.78	2.70	45.6	54.5	1.22
82X-4, 73	779.73	1.79	2.72	45.7	54.7	1.23
83X-2, 4	785.54	1.82	2.69	41.4	52.0	1.29
83X-3, 3	787.03	1.85	2.70	38.5	50.3	1.34
83X-4, 23	788.73	1.81	2.70	42.3	52.6	1.27
130-807B-						
1H-1, 109	1.09	1.52	2.69	87.8	69.5	0.81
1H-2, 104	2.54	1.51	2.69	91.2	70.3	0.79
2H-1, 109	4.19	1.52	2.70	90.4	70.2	0.80
2H-2, 96	5.56	1.45	2.70	109.9	74.0	0.69
2H-3, 111	7.21	1.54	2.76	87.7	70.0	0.82
2H-4, 107	8.67	1.57	2.72	79.3	67.6	0.87
2H-5, 110	10.20	1.54	2.70	84.5	68.8	0.83
2H-6, 110	11.70	1.53	2.73	86.8	69.6	0.82

Table 13 (continued).

Core, section, interval (cm)	Depth (mbsf)	Wet-bulk density (g/cm^3)	Grain density (g/ cm^3)	Water content (% dry wt)	Porosity (%)	Dry-bulk density (g/cm^3)
3H-1, 109	13.69	1.50	2.70	94.1	71.0	0.77
3H-2, 109	15.19	1.56	2.72	81.3	68.1	0.86
3H-3, 109	16.69	1.54	2.71	85.5	69.1	0.83
3H-4, 109	18.19	1.52	2.70	89.7	70.0	0.80
3H-5, 112	19.72	1.56	2.71	79.6	67.6	0.87
3H-6, 110	21.20	1.55	2.69	82.0	68.1	0.85
4H-1, 126	23.36	1.58	2.72	76.6	66.8	0.89
4H-2, 109	24.69	1.52	2.69	87.8	69.5	0.81
4H-3, 137	26.47	1.60	2.70	71.9	65.3	0.93
4H-4, 105	27.65	1.54	2.72	84.6	69.0	0.84
4H-5, 110	29.20	1.51	2.68	90.2	70.0	0.79
4H-6, 110	30.70	1.53	2.74	88.7	70.1	0.81
5H-1, 111	32.71	1.56	2.70	78.8	67.3	0.87
5H-2, 107	34.17	1.58	2.70	75.9	66.5	0.90
5H-3, 110	35.70	1.57	2.70	77.5	66.9	0.88
5H-4, 109	37.19	1.56	2.73	80.0	67.9	0.87
5H-5, 126	38.86	1.58	2.75	76.7	67.1	0.90
5H-6, 128	40.38	1.57	2.71	77.9	67.1	0.88
6H-1, 115	42.25	1.55	2.70	81.9	68.1	0.85
6H-2, 110	43.70	1.51	2.67	90.0	69.9	0.79
6H-3, 114	45.24	1.60	2.72	73.4	65.9	0.92
6H-4, 112	46.72	1.56	2.69	78.7	67.2	0.87
6H-5, 110	48.20	1.55	2.72	81.7	68.2	0.86
6H-6, 110	49.70	1.57	2.69	77.1	66.8	0.89
7H-1, 106	51.66	1.55	2.70	81.4	68.0	0.86
7H-2, 107	53.17	1.56	2.70	79.6	67.5	0.87
7H-3, 107	54.67	1.54	2.71	83.6	68.7	0.84
7H-4, 109	56.19	1.54	2.69	85.1	68.9	0.83
7H-5, 109	57.69	1.56	2.69	80.3	67.6	0.86
7H-6, 109	59.19	1.56	2.72	79.7	67.7	0.87
8H-1, 109	61.19	1.57	2.71	79.1	67.5	0.87
8H-2, 109	62.69	1.57	2.71	79.0	67.4	0.87
8H-3, 107	64.17	1.54	2.71	83.8	68.7	0.84
8H-4, 110	65.70	1.58	2.72	77.0	67.0	0.89
8H-5, 110	67.20	1.56	2.70	78.8	67.3	0.87
8H-6, 108	68.68	1.58	2.70	76.2	66.5	0.89
9H-1, 108	70.68	1.55	2.69	80.4	67.6	0.86
9H-2, 109	72.19	1.59	2.69	73.1	65.5	0.92
9H-3, 109	73.69	1.63	2.73	67.3	64.0	0.97
9H-4, 110	75.20	1.59	2.70	74.4	66.0	0.91
9H-5, 109	76.69	1.56	2.72	79.7	67.7	0.87
9H-6, 109	78.19	1.58	2.67	73.3	65.4	0.91
10H-1, 108	80.18	1.59	2.72	74.8	66.3	0.91
10H-2, 108	81.68	1.59	2.71	74.9	66.3	0.91
10H-3, 108	83.18	1.58	2.66	74.8	65.9	0.90
10H-4, 108	84.68	1.58	2.73	77.4	67.1	0.89
10H-5, 108	86.18	1.60	2.70	72.4	65.4	0.93
10H-6, 108	87.68	1.59	2.70	73.5	65.7	0.92
11H-1, 108	89.68	1.59	2.69	72.6	65.4	0.92
11H-2, 108	91.18	1.59	2.69	73.8	65.8	0.91
11H-3, 108	92.68	1.56	2.73	80.9	68.2	0.86
11H-4, 108	94.18	1.59	2.67	73.2	65.4	0.92
11H-5, 108	95.68	1.60	2.68	70.6	64.7	0.94
11H-6, 108	97.18	1.63	2.72	66.8	63.8	0.98
12H-1, 108	99.18	1.60	2.69	70.8	64.8	0.94
12H-2, 108	100.68	1.60	2.68	71.1	64.8	0.93
12H-3, 108	102.18	1.61	2.70	70.2	64.7	0.95
12H-4, 108	103.68	1.60	2.70	72.6	65.5	0.92
12H-5, 108	105.18	1.61	2.72	69.6	64.7	0.95
12H-6, 108	106.68	1.61	2.70	70.1	64.7	0.95
13H-1, 109	108.69	1.62	2.73	68.7	64.5	0.96
13H-2, 109	110.19	1.59	2.69	72.8	65.5	0.92
13H-3, 113	111.73	1.59	2.71	73.4	65.8	0.92
13H-4, 110	113.20	1.59	2.70	73.2	65.6	0.92
13H-5, 139	114.99	1.58	2.73	76.8	67.0	0.89
13H-6, 111	116.21	1.60	2.68	71.1	64.9	0.93
14H-1, 108	118.18	1.58	2.67	74.3	65.8	0.91
14H-2, 110	119.70	1.61	2.75	71.1	65.5	0.94
14H-3, 104	121.14	1.58	2.65	73.0	65.2	0.92
14H-4, 109	122.69	1.59	2.68	72.8	65.4	0.92
14H-5, 106	124.16	1.60	2.71	71.4	65.2	0.94
14H-6, 106	125.66	1.58	2.69	74.7	66.0	0.91
15H-1, 109	127.69	1.62	2.71	69.2	64.5	0.96
15H-2, 108	129.18	1.61	2.69	69.6	64.4	0.95
15H-3, 109	130.69	1.59	2.70	73.2	65.7	0.92
15H-4, 109	132.19	1.61	2.70	70.3	64.7	0.94

Table 13 (continued).

Core, section, interval (cm)	Depth (mbsf)	Wet-bulk density (g/cm^3)	Grain density (g/cm^3)	Water content (% dry wt)	Porosity (%)	Dry-bulk density (g/cm^3)
15H-5, 109	133.69	1.60	2.68	71.1	64.8	0.93
15H-6, 109	135.19	1.58	2.69	74.9	66.1	0.90
16H-1, 108	137.18	1.61	2.69	68.7	64.2	0.96
16H-2, 109	138.69	1.63	2.70	66.1	63.3	0.98
16H-3, 109	140.19	1.66	2.71	62.4	62.1	1.02
16H-4, 109	141.69	1.64	2.72	65.5	63.3	0.99
16H-5, 109	143.19	1.64	2.72	65.4	63.2	0.99
16H-6, 109	144.69	1.64	2.70	65.0	63.0	0.99
17H-1, 109	146.69	1.64	2.77	67.4	64.3	0.98
17H-2, 109	148.19	1.64	2.69	64.4	62.7	1.00
17H-3, 109	149.69	1.63	2.71	66.3	63.5	0.98
17H-4, 109	151.19	1.61	2.70	69.4	64.5	0.95
17H-5, 109	152.69	1.64	2.72	64.5	62.9	1.00
17H-6, 109	154.19	1.63	2.71	66.5	63.5	0.98
18H-1, 111	156.21	1.63	2.72	66.8	63.8	0.98
18H-2, 108	157.68	1.61	2.69	69.8	64.5	0.95
18H-3, 109	159.19	1.59	2.68	71.8	65.1	0.93
18H-4, 108	160.68	1.62	2.71	67.8	64.0	0.97
18H-5, 108	162.18	1.61	2.69	70.0	64.6	0.95
18H-6, 108	163.68	1.61	2.72	70.4	65.0	0.94
19H-1, 107	165.67	1.63	2.73	67.5	64.1	0.97
19H-2, 107	167.17	1.68	2.77	60.5	61.9	1.05
19H-3, 108	168.68	1.66	2.74	63.2	62.6	1.02
19H-4, 108	170.18	1.60	2.69	70.9	64.8	0.94
19H-5, 83	171.43	1.65	2.72	64.2	62.9	1.00
20H-1, 107	175.17	1.65	2.72	62.8	62.3	1.02
20H-2, 107	176.67	1.68	2.71	58.9	60.7	1.06
20H-3, 107	178.17	1.65	2.70	62.7	62.1	1.02
20H-4, 50	179.10	1.68	2.72	58.9	60.8	1.06
21H-1, 106	184.66	1.68	2.74	60.4	61.6	1.04
21H-2, 106	186.16	1.65	2.68	62.2	61.7	1.02
21H-3, 106	187.66	1.64	2.71	64.4	62.8	1.00
21H-4, 106	189.16	1.65	2.71	62.6	62.1	1.02
21H-5, 106	190.66	1.64	2.69	64.1	62.5	1.00
21H-6, 106	192.16	1.62	2.68	66.9	63.5	0.97
22H-1, 106	194.16	1.68	2.73	59.1	61.0	1.06
22H-2, 106	195.66	1.70	2.69	55.3	59.1	1.09
22H-3, 106	197.16	1.67	2.72	60.0	61.3	1.05
22H-4, 106	198.66	1.65	2.72	64.3	62.8	1.00
22H-5, 106	200.16	1.67	2.70	60.4	61.3	1.04
22H-6, 106	201.66	1.68	2.74	59.5	61.2	1.05
23H-1, 106	203.66	1.69	2.70	57.4	60.0	1.07
23H-2, 106	205.16	1.67	2.73	60.9	61.7	1.04
23H-3, 106	206.66	1.68	2.71	58.1	60.4	1.06
23H-4, 106	208.16	1.66	2.70	61.0	61.5	1.03
23H-5, 122	209.82	1.65	2.72	64.6	63.0	1.00
23H-6, 122	211.32	1.68	2.70	57.7	60.2	1.07
24H-1, 122	213.32	1.63	2.70	66.9	63.7	0.97
24H-2, 106	214.66	1.65	2.71	62.4	62.1	1.02
24H-3, 118	216.28	1.62	2.71	68.4	64.2	0.96
24H-4, 118	217.78	1.62	2.68	66.5	63.3	0.98
24H-5, 106	219.16	1.68	2.68	57.4	59.9	1.07
24H-6, 106	220.66	1.63	2.70	66.6	63.5	0.98
25H-1, 105	222.65	1.66	2.70	60.6	61.3	1.04
25H-3, 105	225.65	1.64	2.71	64.7	63.0	1.00
25H-4, 106	227.16	1.60	2.68	70.0	64.5	0.94
25H-5, 107	228.67	1.61	2.69	68.4	64.0	0.96
25H-6, 123	230.33	1.61	2.68	70.0	64.5	0.94
26H-1, 106	232.16	1.63	2.70	65.4	63.1	0.99
26H-2, 124	233.84	1.63	2.67	65.5	62.9	0.98
26H-3, 108	235.18	1.64	2.71	65.4	63.2	0.99
26H-4, 107	236.67	1.63	2.68	65.6	63.0	0.98
26H-6, 115	239.75	1.66	2.68	60.7	61.2	1.03
27H-1, 106	241.66	1.66	2.69	61.6	61.7	1.03
27H-2, 106	243.16	1.64	2.70	63.9	62.6	1.00
27H-3, 85	244.45	1.66	2.71	62.4	62.1	1.02
27H-4, 106	246.16	1.65	2.69	62.1	61.8	1.02
27H-5, 86	247.46	1.62	2.66	66.1	63.0	0.98
27H-6, 101	249.11	1.60	2.68	70.7	64.7	0.94
28H-1, 119	251.29	1.61	2.66	67.7	63.5	0.96
28H-2, 103	252.63	1.63	2.68	66.1	63.2	0.98
28H-3, 103	254.13	1.67	2.67	59.3	60.6	1.05
28H-4, 103	255.63	1.63	2.73	66.8	63.9	0.98
28H-5, 104	257.14	1.65	2.68	61.8	61.6	1.02
28H-6, 61	258.21	1.60	2.69	70.7	64.8	0.94
29H-1, 109	260.69	1.68	2.71	58.4	60.5	1.06

Table 13 (continued).

Core, section, interval (cm)	Depth (mbsf)	Wet-bulk density (g/cm^3)	Grain density (g/cm^3)	Water content (% dry wt)	Porosity (%)	Dry-bulk density (g/cm^3)
29H-2, 109	262.19	1.65	2.68	62.2	61.7	1.02
29H-3, 106	263.66	1.67	2.69	58.9	60.5	1.05
29H-4, 109	265.19	—	—	62.5	—	—
29H-5, 109	266.69	1.64	2.69	64.0	62.5	1.00
29H-6, 109	268.19	—	—	58.5	—	—
30H-1, 109	270.19	1.71	2.69	53.5	58.2	1.12
30H-2, 109	271.69	1.65	2.72	63.6	62.6	1.01
30H-3, 109	273.19	1.66	2.69	61.4	61.5	1.03
30H-4, 109	274.69	1.69	2.72	57.6	60.3	1.07
30H-5, 109	276.19	—	—	60.0	—	—
30H-6, 104	277.64	—	—	60.4	—	—
130-807C-						
2R-1, 35	790.05	1.82	2.68	40.8	51.6	1.29
2R-2, 26	791.46	1.85	2.72	39.3	51.0	1.33
4R-1, 55	809.55	1.82	2.70	41.3	52.0	1.29
4R-2, 66	811.16	1.87	2.68	36.1	48.5	1.38
6R-1, 91	829.21	1.77	2.70	46.5	55.0	1.21
6R-2, 92	830.72	1.79	2.71	45.0	54.2	1.23
6R-3, 91	832.21	1.80	2.69	43.5	53.2	1.25
6R-4, 91	833.71	1.78	2.71	46.5	55.0	1.21
6R-5, 80	835.10	1.80	2.71	43.7	53.5	1.25
9R-1, 21	857.61	1.80	2.70	43.5	53.2	1.25
12R-1, 26	876.86	1.83	2.73	41.8	52.5	1.29
15R-1, 17	894.07	1.86	2.70	37.3	49.5	1.36
16R-1, 58	899.48	1.92	2.71	33.2	46.6	1.44
17R-1, 31	904.21	1.83	2.68	40.5	51.4	1.30
17R-2, 48	905.88	1.83	2.67	39.2	50.5	1.32
18R-CC, 8	—	1.84	2.65	38.1	49.5	1.33
19R-1, 33	914.23	1.83	2.71	40.7	51.7	1.30
21R-1, 4	923.94	1.91	2.71	33.7	47.0	1.43
23R-1, 49	939.19	1.84	2.68	38.8	50.2	1.33
23R-2, 42	940.62	1.92	2.65	31.2	44.6	1.46
23R-3, 43	942.13	1.89	2.70	35.4	48.1	1.39
23R-4, 37	943.57	1.88	2.69	35.9	48.4	1.38
24R-1, 70	944.40	1.88	2.68	35.4	48.0	1.39
24R-2, 70	945.90	1.82	2.67	40.2	51.0	1.30
25R-1, 35	948.75	1.90	2.69	34.0	47.1	1.42
26R-1, 56	958.66	2.10	2.70	21.0	35.6	1.74
30R-1, 34	997.14	1.98	2.72	29.0	43.4	1.54
30R-2, 49	998.79	1.96	2.70	29.5	43.7	1.52
31R-1, 26	1006.76	2.22	2.55	11.1	21.7	1.99
35R-1, 20	1044.50	1.94	2.71	31.7	45.5	1.47
37R-1, 3	1063.73	2.11	2.55	16.5	29.1	1.81
38R-1, 38	1073.58	2.02	2.74	26.5	41.4	1.60
40R-1, 89	1092.89	2.18	2.62	15.1	27.8	1.89
41R-1, 32	1098.02	2.25	2.62	11.8	23.2	2.01
42R-1, 41	1102.81	2.21	2.63	13.7	26.0	1.95
43R-1, 18	1106.58	2.28	2.53	8.1	16.7	2.11
44R-1, 44	1116.44	2.20	2.72	16.4	30.2	1.89
45R-1, 62	1126.22	2.29	2.69	11.7	23.4	2.05
45R-2, 49	1127.59	2.38	2.66	7.9	16.9	2.21
47R-2, 65	1142.35	2.44	2.73	7.5	16.5	2.27
48R-2, 98	1147.68	2.46	2.72	6.6	14.8	2.31
49R-1, 77	1150.97	2.51	2.73	5.6	13.0	2.37
50R-1, 71	1155.91	2.56	2.79	5.4	12.7	2.43
51R-1, 70	1160.90	2.45	2.72	6.9	15.5	2.30
51R-2, 67	1162.37	2.47	2.71	6.1	14.0	2.33
51R-3, 71	1163.91	2.56	2.71	3.8	9.2	2.46
52R-1, 82	1170.62	2.46	2.71	6.6	14.8	2.31
52R-2, 119	1172.49	2.56	2.75	4.5	10.8	2.45
52R-3, 31	1173.11	2.54	2.71	4.4	10.3	2.43
53R-1, 68	1180.08	2.61	2.75	3.3	8.2	2.52
53R-2, 74	1181.64	2.65	2.73	1.9	4.8	2.60
53R-3, 62	1183.02	2.30	2.69	11.3	22.8	2.07
53R-4, 122	1185.12	2.52	2.71	4.8	11.2	2.41
56R-1, 134	1207.94	2.50	2.72	5.7	13.1	2.36
56R-2, 140	1209.50	2.54	2.78	5.9	13.9	2.39
56R-3, 50	1210.10	2.48	2.74	6.5	14.8	2.33
57R-1, 115	1217.45	2.45	2.73	7.4	16.5	2.28
57R-2, 98	1218.78	2.47	2.74	6.9	15.5	2.31
58R-1, 10	1222.60	2.48	2.71	6.0	13.7	2.34
59R-1, 55	1232.75	2.40	2.71	8.6	18.5	2.21
59R-2, 68	1234.38	2.40	2.74	9.2	19.6	2.20
61R-1, 56	1252.06	2.43	2.78	9.1	19.8	2.23
61R-2, 88	1253.88	2.43	2.76	8.7	18.9	2.23

Table 13 (continued).

Core, section, interval (cm)	Depth (mbsf)	Wet-bulk density (g/cm^3)	Grain density (g/cm^3)	Water content (% dry wt)	Porosity (%)	Dry-bulk density (g/cm^3)
62R-1, 83	1262.03	2.34	2.74	11.0	22.7	2.11
62R-2, 63	1263.33	2.38	2.74	9.7	20.5	2.17
62R-3, 93	1265.13	2.38	2.75	10.0	21.2	2.17
63R-1, 28	1271.08	2.40	2.74	9.2	19.8	2.19
63R-2, 57	1272.87	2.40	2.73	8.9	19.2	2.21
63R-3, 88	1274.68	2.38	2.77	10.4	21.9	2.16
64R-1, 95	1281.45	2.39	2.72	9.1	19.5	2.19
64R-2, 72	1282.72	2.40	2.75	9.5	20.4	2.19
65R-1, 53	1290.63	2.36	2.75	10.8	22.5	2.13
65R-2, 41	1292.01	2.34	2.74	11.3	23.2	2.11
66R-1, 127	1301.07	2.32	2.74	11.9	24.2	2.07
66R-2, 74	1302.04	2.30	2.72	12.1	24.3	2.05
66R-3, 84	1303.64	2.31	2.73	12.0	24.2	2.06
67R-1, 75	1310.25	2.35	2.72	10.4	21.7	2.13
67R-2, 109	1312.09	2.38	2.72	9.5	20.1	2.17
67R-3, 73	1313.23	2.35	2.71	10.1	21.1	2.14
67R-4, 82	1314.82	2.34	2.71	10.5	21.8	2.12
67R-5, 37	1315.87	2.33	2.73	11.4	23.3	2.09
68R-1, 67	1319.77	2.32	2.72	11.5	23.4	2.08
68R-2, 28	1320.88	2.31	2.70	11.4	23.1	2.08
68R-3, 58	1322.68	2.37	2.71	9.6	20.2	2.16
69R-2, 106	1331.36	2.38	2.73	9.7	20.5	2.17
69R-3, 3	1331.83	2.38	2.72	9.3	19.8	2.18
69R-4, 86	1334.16	2.38	2.74	10.0	21.1	2.16
69R-5, 15	1334.95	2.38	2.74	9.8	20.8	2.17
70R-1, 69	1339.09	2.36	2.71	10.1	21.0	2.14
70R-2, 108	1340.98	2.42	2.74	8.6	18.7	2.22
70R-3, 97	1342.37	2.35	2.73	10.8	22.4	2.12
70R-4, 52	1343.42	2.26	2.58	10.4	20.8	2.04
71R-1, 45	1348.45	2.33	2.71	11.0	22.5	2.10
71R-2, 130	1350.80	2.32	2.73	11.6	23.6	2.08
71R-3, 106	1352.06	2.10	2.81	23.9	39.5	1.69
71R-4, 59	1353.09	2.02	2.70	25.7	40.3	1.61
71R-5, 47	1354.47	2.03	2.71	25.4	40.1	1.62
71R-6, 27	1355.77	2.04	2.63	22.3	36.4	1.67
72R-2, 42	1359.62	1.75	2.44	39.9	48.6	1.25
73R-1, 67	1368.07	1.84	2.45	31.3	42.7	1.40
73R-2, 55	1369.45	2.07	2.67	21.7	36.1	1.70

sampled at Site 803 (i.e., the entire basement section cored at Site 803). Variations between Subunits C, E, F, and G are limited as well and are illustrated in the Zr vs. TiO_2 plot in Figure 56. Site 803 results lie in an intermediate position between the data for the upper and lower Site 807 subunits; the same is true for the Sr data. More detailed comparisons are premature at present, in view of the different levels of alteration at the two sites, the lack of Nb data for Site 807, and the absence of intercalibration between the shipboard and Keele XRF machines.

Preliminary Conclusions

In contrast to Site 803, basement Subunit F in Hole 807C provides clear evidence for the existence of thick basalt flows on the Ontong Java Plateau comparable with those typical of major continental flood basalt provinces. The general lack of large phenocrysts also is reminiscent of some continental flood basalts, such as those of the Grande Ronde Formation in the Columbia River province of the western United States (e.g., Hooper, 1988). Moreover, even the thinner massive, olivine-bearing flows at Site 807 tend to be markedly thicker than those at Site 803 (up to 3 m vs. <1 m), which lies on the edge of the Ontong Java Plateau. Because of the absence of large phenocrysts in the lower subunits, the samples recovered can generally be treated as representative of erupted liquid compositions. Their little-altered nature and the lack of substantial sedimentary interbeds in the lower portion of the basement section suggest that they were erupted over a short time interval and were effectively sealed off from significant interaction with seawater by overlying flows and sediments. The plagioclase-bearing lavas of Subunit A are fairly enriched in Sr, Ti, and Zr and are chemically distinct from those of the lower subunits, which are depleted in these elements. The passage of a somewhat greater interval of time between Subunits C and A than between the eruption of the lower subunits may be indicated by the mineralogical and chemical differences and the presence of a >0.6-m-thick limestone layer between them. Both the upper and lower subunits appear distinct from the basalts at Site 803.

LOGGING

Logging Operations

Hole 807A

Logging operations at Hole 807A are summarized in Table 16. As at all sites on Leg 130, a wiper trip was made to clear the hole before logging. In addition, the hole was first flushed with bentonite, after which seawater was circulated to clean the hole. The first logging run was made with the geophysical logging string, consisting of the natural gamma-ray tool (NGT), the long-spaced sonic digital tool (LSS), the resistivity tool (DIT), and the temperature tool (TLT).

The tool string was run to the end of pipe, and a down log was recorded from 85.6 (just before leaving pipe) to 802.6 mbsf. The down log was stopped short of the bottom of the hole to prepare for the main logging run up the hole. The tool

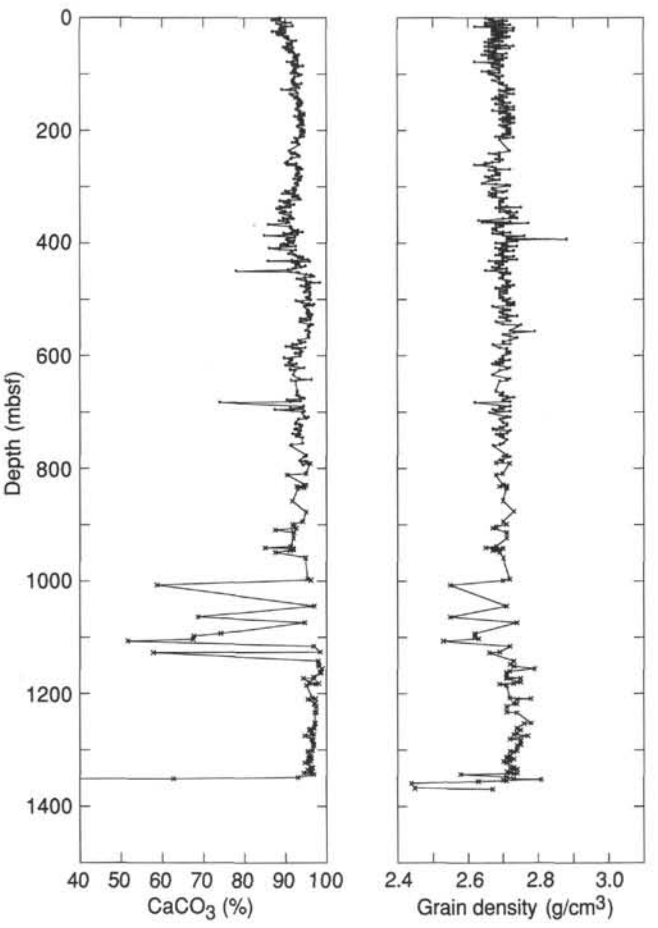

Figure 49. Carbonate content and grain density vs. depth, Site 807 (merged data sets from Holes 807A [dots] and 807C [crosses]).

string set down at the base of the hole at 820.5 mbsf, or <2.5 m short of the total drilled section. The heave compensator was turned on and the uplog begun, with all tools operating normally. The entire section from 820 mbsf to the base of pipe at 89.6 mbsf was logged successfully. No repeat log was run as Hole 807C also was to be logged.

The second logging run was conducted with an abbreviated geochemical tool string consisting of the NGT, the aluminum clay tool (ACT), and the density tool (HLDT). The geochemical spectral tool (GST) was left out of the string because it failed deck tests. During the rig-up, the bullnose, an assembly at the end of the tool string that allows the string to pass in and out of the XCB bit, sheared a bolt and was lost overboard. A substitute assembly was built, and the hole was reentered after a 1.5-hr delay.

The geochemical logging run was relatively trouble-free. However, there was some debris at the bottom of the hole that kept the HLDT caliper from fully opening until 785 mbsf. As a result, the density data are unreasonably low below this depth. The only other problem during this run occurred when power was accidentally cut to the heave compensator while the tool string was at 323.4 mbsf. The tool string was lowered slightly, the heave compensator was restarted, and the logging run continued. Some spikes in the NGT logs appear at this level.

Hole 807C

Upon completion of coring at Hole 807C, the drill string was pulled out of the hole, the rotary core bit was mechanically released, and the drill pipe was run back into the hole to a depth of 170 mbsf. The tool strings used in Hole 807C and a summary of the operations are presented in Table 16; acronyms used are listed in Table 17.

The first two logging runs (the geophysical string [NGT/LSS/DIT/TLT] and the geochemical string [NGT/ACT/HLDT]) were completed successfully from the base of the hole at 1528 mbsf to the casing at 350 mbsf. In the first run, the quality of the sonic log suffered because the hard and perhaps irregular nature of the borehole wall in the lower part of the hole induced many dropouts and cycle skips in the recorded data. Density data only are recorded from 1508 mbsf upward because debris at the bottom of the hole prevented the HLDT caliper from opening.

On the third run, the FMS (an imaging resistivity tool) was used to obtain detailed information about the structure of the basalts, *in-situ* stress (by means of breakouts), and the thickness of the chert layers in the sediments. The GPIT, an orientation recording tool, was attached to the string and was used to ascertain the hole inclination and deviation and to record the absolute orientation of the FMS resistivity pads. The base of the hole was logged twice with the tool string, once from 1509 to 947 mbsf, and again from 1508 to 1096 mbsf. The FMS images are presented on microfiche in the back pocket of this volume.

Both logging passes were stopped by a bridge that blocked the lower part of the hole. The upper boundary of the logged intervals was determined by the diameter of the borehole. The HLDT caliper data from the previous logging run indicated that the hole above 950 mbsf was washed out to at least 18 in. The FMS can only extend its pads to 15 in.; thus, it could not be used in the upper section of the borehole. The second run was stopped at 1096 mbsf because roughly half of the section above was wider than the FMS calipers. Sections in the logs affected by washouts can be recognized by intervals in which the FMS tool string twisted rapidly in the hole.

Log Stratigraphic Units at Hole 807A

Results of gamma-ray, electrical resistivity, sonic velocity, and bulk density logging in Hole 807A are shown in Figure 57. Each of the logs show some degree of downhole variability, but there are no common events in the profiles that clearly define individual log stratigraphic units. The lack of distinctive character in the logs reflects the uniform composition of these carbonate-rich sediments. The upper 950+ m of sediments were placed in a single lithostratigraphic unit (see "Lithostratigraphy" section, this chapter), with a subdivision at 293 mbsf identified as the ooze-chalk transition.

The log stratigraphic units shown in Figure 57 are based on natural subdivisions of logging data, which can be seen in a cross-plot of velocity and electrical resistivity (Fig. 58). Electrical resistivity is an analog of porosity in sediments and sedimentary rocks (Archie, 1942), although the correlation between the two properties is not constant or well understood in sediments that are undergoing compaction and lithification. The velocity vs. resistivity data show different, subparallel trends that relate to compaction and diagenesis. These data have been used as the basis for division of the Hole 807A data into the two major units with six subdivisions that are shown by different symbols in Figure 58 and are characterized in Table 18.

Logging Unit A represents the part of the sediment column that is undergoing the most significant change in physical properties. The rate of change is reflected in the values of the depth gradients for each of the properties listed in Table 18. Velocity, resistivity, and density all increase within Logging Unit A (top of logged interval to 474 mbsf). In Logging Unit B,

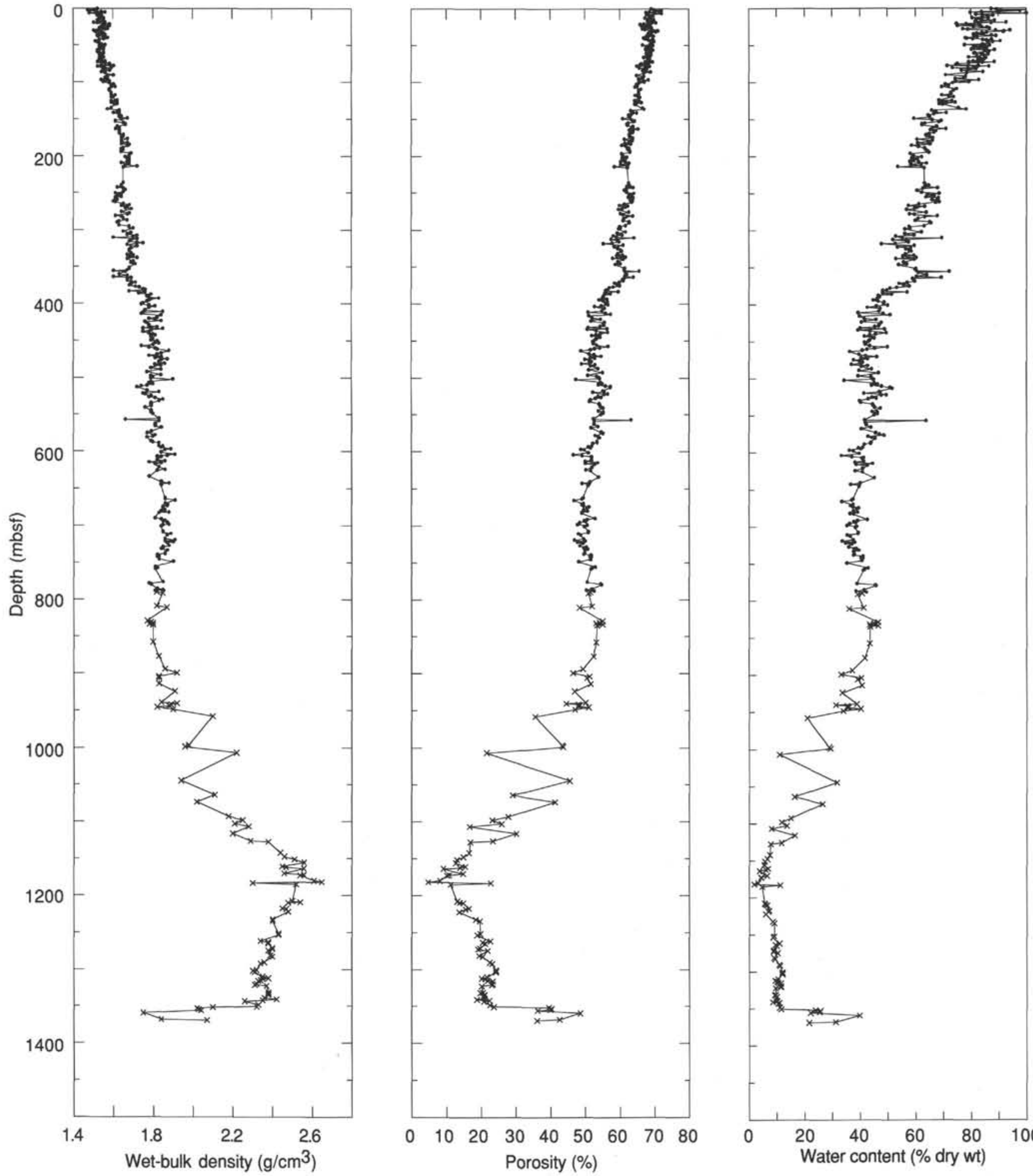

Figure 50. Wet-bulk density, porosity, and water content vs. depth, Site 807 (merged data sets from Holes 807A [dots] and 807C [crosses]).

the changes from 474 mbsf to the bottom of the logged interval (approximately 810 mbsf, depending on the position of the tool in the string and the logging run) are very small or negative. Only within Logging Subunit B2 are depth gradients of the logged properties near those of the subunits of Logging Unit A.

Comparison with Laboratory Data

Logging and laboratory data for compressional wave velocity and bulk density are plotted vs. depth in Figure 59. There is good agreement between the two determinations of density and an increase in the difference between laboratory

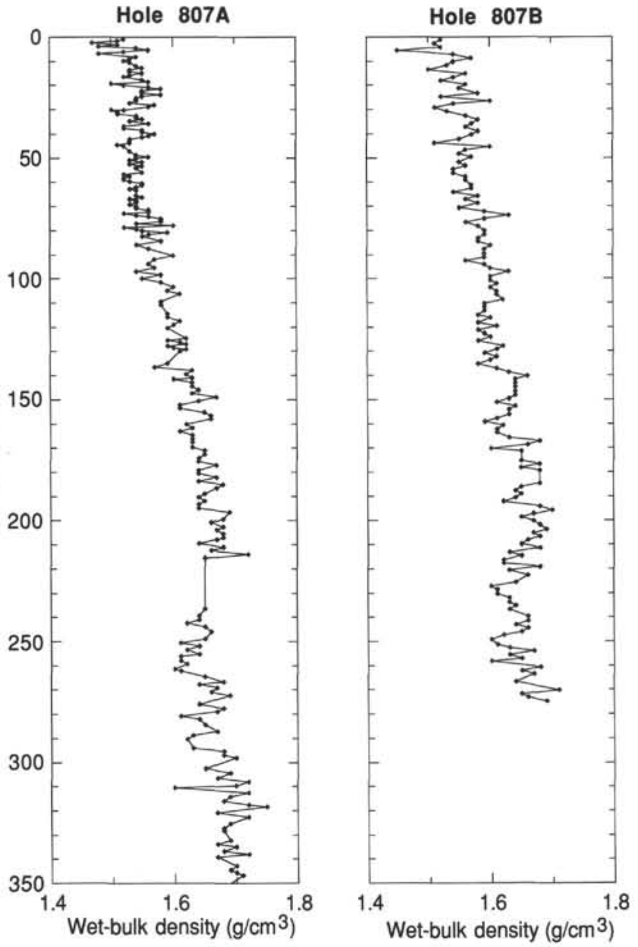

Figure 51. Wet-bulk density vs. depth for the uppermost 350 mbsf, Holes 807A and 807B.

and logging velocity with depth. Laboratory bulk densities are lower than log values by about 0.05 g/cm^3 throughout the entire column. Most changes in density are seen in both laboratory and well-log data, lending credence to both of the results. The minimum in log density centered on 240 mbsf is not entirely supported by laboratory measurements and may be lower than *in-situ* values. However, there is definitely a density decrease between 220 and 240 mbsf, as seen in both logging and laboratory data.

Agreement between velocity data are less systematic. A velocity minimum seen in the log at 140 mbsf is not reflected in the laboratory measurements and is probably not real. Lower in the section (e.g., 410–450 and 480–520 mbsf), there are variations in laboratory velocities that are either not seen in the log or are not as extreme in the log as in the laboratory samples. These differences in the two data sets may result from the state of preservation of the cored material or because the most competent, and therefore probably the acoustically "fastest," samples generally are removed from the core for velocity determination. Fracturing of rock samples has a significant effect on measurements of velocity out of proportion to the change in porosity the fractures might induce (Toksöz et al., 1976). Thus, the differences in fractured and unfractured samples on the surface will tend to amplify more subtle differences in logging data caused by microstructural changes in the sediments *in situ*.

Gamma-ray activity, aluminum counts (from the ACT), and determinations of carbonate content of laboratory samples (see "Inorganic Geochemistry" section, this chapter) are roughly correlated, as shown in Figure 60. Broad maxima and minima in gamma-ray activity are matched by peaks in aluminum counts, suggesting clay or volcanic glass (aluminosilicates) as the source of the radioactivity. The maxima in aluminum and gamma-ray activity are mirrored by minima in carbonate content, although the abrupt nature of the shift in gamma-ray and aluminum values in the logs at 450 mbsf is not seen in the calcium carbonate content record.

Comparison with Lithostratigraphy

The approximate location of the boundary between lithologic Subunits IA and IB is indicated in Figures 57 and 58. The position of the boundary in the cross plot is approximate because the depth of the Subunit IA/IB boundary does not cleanly separate the data in the case of the cross-plots. The level assigned to the ooze/chalk boundary is somewhat arbitrary (see "Lithostratigraphy" section, this chapter) and is actually within a zone of transition. The transitional nature of the zone can be seen particularly well in Figure 58, where the lithologic Subunit IA/IB boundary lies in the middle of the logging Unit A2 field. Most of the points within lithologic Subunit IA have lower velocities and resistivities than those in Subunit IB, but all of the data from the interval of logging Unit A2 fall on a single velocity/resistivity trend and are indicative of a single process or state of microstructure of the sediment.

Results of Logging at Hole 807C

Sediment logs from the lower section of Hole 807C (750–1400 mbsf) and logs from the basement (1350–1530 mbsf) are presented in Figures 61 and 62. The upper part of the log has been omitted because of the excellent agreement of the Hole 807C logs with those recorded in Hole 807A (see below for discussion). The well logs from Hole 807C provide substantial evidence that the cores recovered in the lower parts of the hole are representative of the lithology in general. Lithostratigraphic boundaries have been superimposed on the logging data in Figure 61 (see "Lithostratigraphy" section, this chapter). The boundary between lithologic Units I and II was picked at a depth of 968 mbsf in the recovered core. This depth is approximately 13 m below the depth where velocity and resistivity logs abruptly increase and define a unit boundary. The lithologic Unit I/II boundary is based on the transition from chalk to cherty chalk. Velocity, density, and resistivity all increase across this boundary because of the lower porosity of the chert and the effect of increased cementation by silica of the calcareous sediments.

The boundary between lithologic Subunits IIA and IIB is located at 1098 mbsf in both the core descriptions and in the logging data (Fig. 61). The transformation across the boundary of chalk and silicified chalks to limestone is clearly seen in the logging data as an increase in velocity, density, and electrical resistivity. There are local maxima in all three of these properties between 1150 and 1200 mbsf that do not correspond to anything mentioned in the lithostratigraphic discussion, although the appearance of limestone clasts in the core does appear to correlate with stable logging values between 1230 mbsf and the base of lithologic Unit II at 1351 mbsf.

The claystone, siltstone, and limestone of lithologic Unit III appear in the logs as an interval of reduced velocity, resistivity, and density. Local maxima in the profiles are interpreted as limestone stringers within a predominantly silt- and claystone unit. The boundary of the sediments with basaltic basement is well defined at 1380 mbsf.

Basement logs are presented in Figure 62. Velocity data are not presented because of excessive noise in the unprocessed logs. Smoothed gamma-ray data are shown because of the

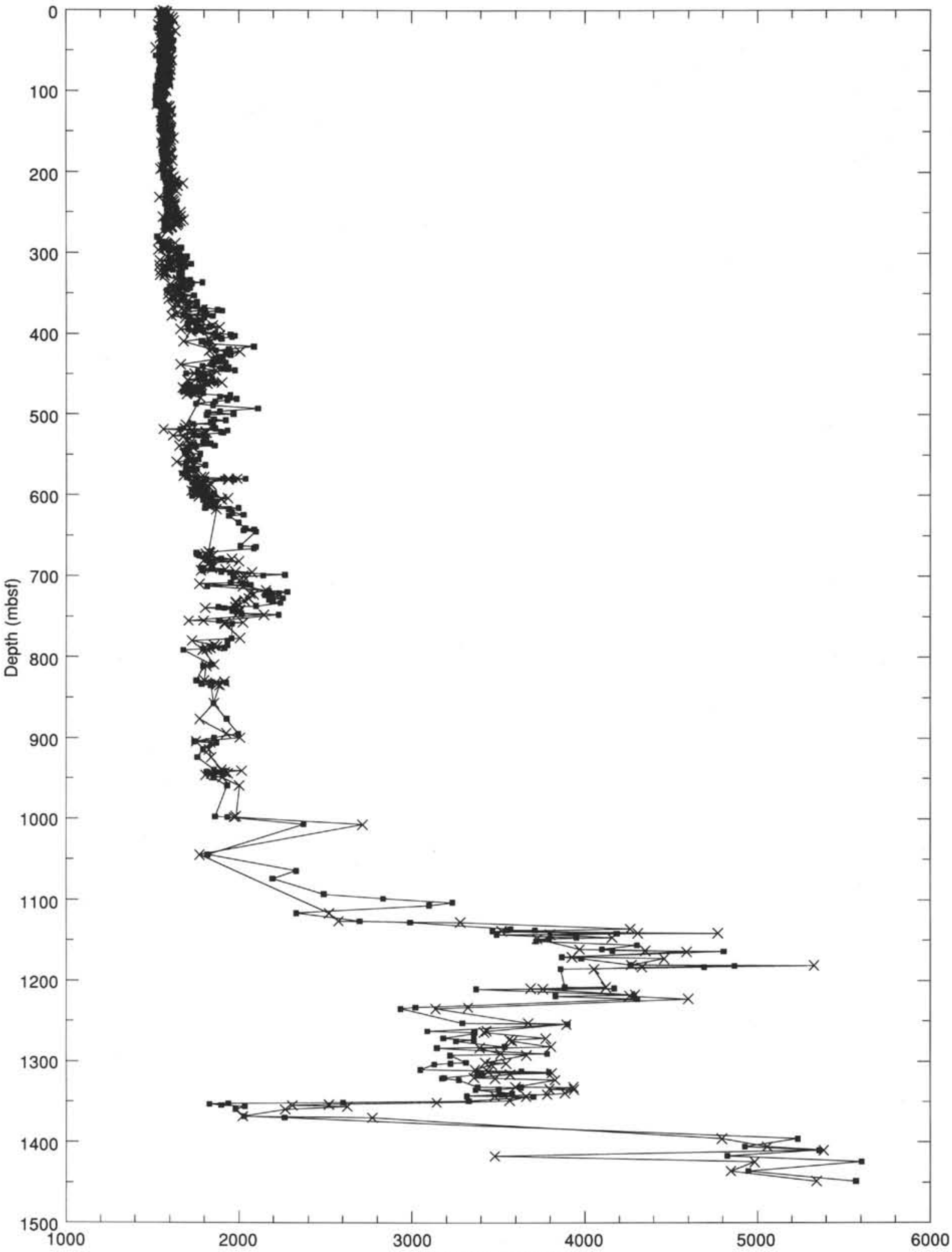

Figure 52. Laboratory compressional wave velocity vs. depth, Site 807 (merged data sets from Holes 807A and 807C). Lines with squares represent vertical (longitudinal) measurements (perpendicular to bedding), and lines with crosses represent horizontal (transverse) measurements (parallel to bedding).

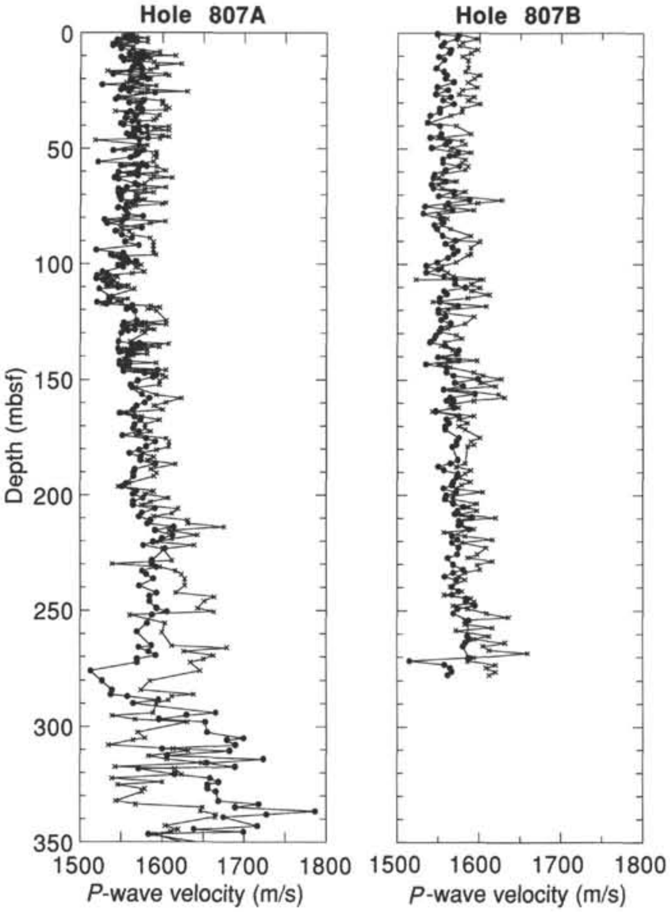

Figure 53. Laboratory compressional wave velocity vs. depth in the uppermost 350 mbsf, Holes 807A and 807B. Symbols used are as in Figure 52.

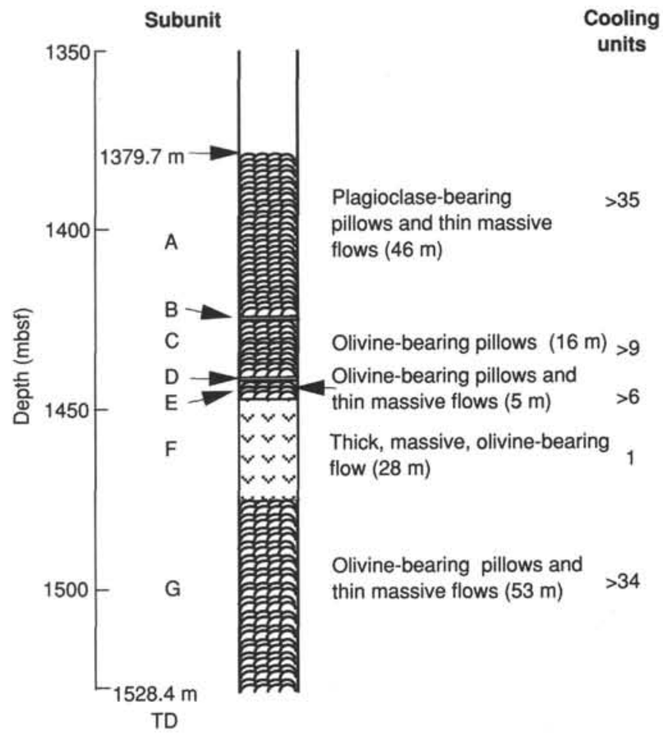

Figure 54. Lithologic column of basement, Hole 807C, showing distribution of pillows and thin, massive flows (Subunits A, C, E, and G) and thick, massive flow (Subunit F) as well as two thin sedimentary interbeds (Subunits B and D). Cooling "units" estimated from glassy chilled rinds are given on the right for each subunit.

generally greater level of gamma-ray activity in the altered sections of the basaltic basement and the spikes produced by thin pockets or layers of sediment. The basement is clearly defined by an increase in density and resistivity at 1380 mbsf. A distinctive feature in the logs is the definition of the massive basalt flow that is characterized by a minimum in gamma-ray activity between 1447 and 1471 mbsf. Sediment layers or pockets are seen in the logs as maxima in gamma-ray activity and minima in density and electrical resistivity. Two of the intervals (1425 and 1439 mbsf) correspond to sediments recovered in the core. A third interval at 1435 mbsf is seen in the logs but was not recovered. Finally, the increase in resistivity at the bottom of Hole 807C (1562 mbsf) may represent the top of another massive basalt unit, although this interpretation cannot be supported as other measurements did not reach this depth.

Comparison of Logs from Holes 807A and 807C

Logs in Hole 807C overlapped the logs from Hole 807A in the interval from 350 to 803 mbsf. Coincident sections from 550 to 650 mbsf have been presented side-by-side in Figure 63. Correlation of data between the two holes is remarkable. Electrical resistivity data show an almost perfect match, with a difference of approximately 1 m between matching peaks at the top of the section and almost 2 m at the bottom, for a 1% difference in section thickness. Density and velocity logs show almost as much correspondence although the data vary at a shorter wavelength. There are two factors that may cause some degradation in the fit between the velocity and density logs from the two holes: (1) data from Hole 807C were decimated by 50% for the plot (i.e., there are twice as many data points in the Hole 807A data set as there are in the Hole 807C data) to save computer space; and (2) the state of the sea at the time of logging. Hole 807C was logged in seas that were almost flat, whereas there was a larger swell during logging operations at Hole 807A. In parts of the density and velocity sections, the Hole 807A data look like a smoothed version of the Hole 807C data. This could be a natural "smoothing" caused by small (around 0.5 m) oscillations of the logging tool downhole during the Hole 807A logging. The resistivity tool investigates a larger volume of the formation surrounding the hole, and thus may be somewhat less sensitive to ship's heave than the velocity or density tools. Regardless of the minor details, the overall agreement of the logs from two adjacent holes lends validity to even the minor peaks seen in the well logging data.

SEISMIC STRATIGRAPHY

Site 807, the northernmost of the Leg 130 drill sites, is characterized by a thick sequence of parallel, closely spaced reflectors that are typical of the top of the Ontong Java Plateau. Located over a small basement basin, the selected site has one of the thickest (1.13 s) sections in the area. Most of the thickening is in the deepest part of the section where material from surrounding highs appears to have moved into the basement low (Fig. 64). The asymmetry of the basement structure is partly preserved through the sediment column, resulting in a pronounced surficial topographic feature directly over the basement high.

At several levels within the section, the loss of lateral coherency of the reflectors provides evidence of minor sedi-

Table 15. Major element, trace element, and CIPW-normative compositions of basalts from Hole 807C.

Core, section	74R-1	75R-2	76R-1	77R-1	78R-2	79R-5	80R-1	81R-2	82R-2	83R-2	84R-2	85R-5	86R-1	87R-2	88R-1	89R-1	90R-3	92R-2	93R-1
Interval (cm)	124–127	61–64	69–71	48–51	69–72	28–30	49–51	74–77	42–45	30–33	111–115	112–115	100–103	37–40	70–75	38–42	72–76	100–103	25–28
Subunit	A	A	A	A	A	A	A	C	C	F	F	F	G	G	G	G	G	G	G
Major elements (wt%):																			
SiO_2	48.65	48.17	49.06	48.88	48.76	49.46	48.44	50.21	50.57	50.07	50.48	50.01	49.19	50.45	50.22	49.44	49.37	50.35	50.17
TiO_2	1.66	1.59	1.61	1.61	1.59	1.65	1.66	1.20	1.21	1.14	1.14	1.10	1.14	1.20	1.15	1.17	1.15	1.16	1.15
Al_2O_3	14.73	14.07	14.35	14.33	14.05	14.62	14.79	15.08	14.91	13.91	13.95	13.85	14.25	15.20	14.08	14.10	14.09	14.46	14.24
$^{a}Fe_2O_3$	12.54	13.51	13.33	13.27	13.49	12.75	12.77	10.53	10.96	12.88	12.64	12.99	12.92	10.25	13.24	13.05	12.64	12.28	12.72
MnO	0.18	0.20	0.18	0.19	0.27	0.18	0.40	0.22	0.23	0.19	0.19	0.18	0.22	0.19	0.21	0.22	0.21	0.20	0.21
MgO	6.05	7.26	6.42	6.70	7.18	6.45	7.02	8.01	7.61	7.41	7.55	7.89	7.20	7.93	7.22	7.73	7.71	7.40	7.45
CaO	12.43	11.77	11.94	11.99	11.75	12.30	12.27	11.42	11.84	11.85	11.77	11.89	11.94	12.51	12.14	12.28	12.30	12.02	12.15
Na_2O	2.45	2.32	2.43	2.49	2.34	2.49	2.41	2.28	2.29	2.08	2.05	2.01	2.15	2.40	2.17	2.08	2.16	2.17	2.13
K_2O	0.41	0.35	0.12	0.13	0.31	0.11	0.07	0.63	0.41	0.06	0.06	0.06	0.35	0.06	0.19	0.03	0.06	0.05	0.15
P_2O_5	0.14	0.14	0.13	0.14	0.14	0.14	0.14	0.11	0.10	0.09	0.10	0.09	0.11	0.10	0.10	0.10	0.09	0.09	0.10
Total	99.91	99.99	99.78	99.99	100.30	100.57	100.07	100.34	100.51	99.63	100.07	100.12	99.49	100.36	100.53	100.18	99.65	100.13	100.18
LOI	0.66	0.62	0.20	0.27	0.40	0.41	0.10	0.67	0.38	0.05	0.15	0.03	0.02	0.07	−0.19	−0.02	−0.13	−0.07	−0.29
^{b}CIPW norms:																			
Quartz										0.71	1.09	0.17						0.47	
Orthoclase	2.42	2.07	0.71	0.77	1.83	0.65	0.41	3.72	2.42	0.35	0.35	0.35	2.07	0.35	1.12	0.18	0.35	0.30	0.89
Albite	20.73	19.63	20.56	21.07	19.80	21.07	20.39	19.29	19.38	17.60	17.35	17.01	18.19	20.31	18.36	17.60	18.28	18.36	18.02
Anorthite	27.99	26.95	27.90	27.55	26.92	28.40	29.34	29.06	29.20	28.45	28.69	28.60	28.21	30.53	28.12	29.06	28.58	29.57	28.86
Diopside	27.08	25.16	25.21	25.62	25.11	26.17	25.22	21.92	23.63	24.50	23.91	24.50	24.99	25.16	25.95	25.68	26.18	24.22	25.32
Hypersthene	8.65	10.27	15.76	12.76	12.91	14.38	10.66	16.24	18.55	22.35	23.08	23.77	16.25	16.03	20.37	19.17	17.21	21.65	21.13
Olivine	5.63	8.45	2.60	5.14	6.45	2.71	7.16	4.19	1.58				3.99	2.73	0.94	2.67	3.50		0.53
Magnetite	2.16	2.33	2.30	2.29	2.33	2.20	2.20	1.89	1.89	2.22	2.23	2.24	2.23	1.77	2.29	2.25	2.18	2.12	2.20
Ilmenite	3.15	3.02	3.06	3.06	3.02	3.13	3.15	2.28	2.30	2.17	2.17	2.09	2.17	2.28	2.18	2.22	2.18	2.20	2.18
Apatite	0.32	0.32	0.30	0.32	0.32	0.32	0.32	0.25	0.23	0.21	0.23	0.21	0.25	0.23	0.23	0.23	0.21	0.21	0.23
Trace elements (ppm):																			
Zr	102	99	99	99	97	102	101	67	68	68	67	62	65	69	65	67	64	68	67
V	331	327	325	316	305	332	327	347	346	331	321	323	343	347	339	346	331	337	348
Sr	218	198	173	172	166	175	176	121	123	113	110	107	109	115	107	110	107	110	108
Rb	10	8	3	2	6	2	1	9	7	2	2		1	7	1	5	1	1	03
Zn	100	99	93	96	91	98	98	93	105	88	90	82	97	103	92	98	93	93	93
Cu	146	139	137	139	137	138	144	42	98	150	141	143	131	147	141	144	143	143	139
Ni	96	115	100	99	95	97	97	103	99	86	86	90	92	118	87	94	103	90	96
Cr	170	154	156	153	143	150	146	167	140	120	126	152	157	169	154	144	155	156	157
Y	30	29	30	29	30	31	30	24	23	26	25	22	25	27	24	23	24	26	24
Ga	19	21	17	20	20	21	18	19	19	17	15	18	18	19	15	18	17	17	17

Notes: Analyses were conducted at the University of Keele. CIPW-normative after Johanssen, 1931, for example. LOI = loss on ignition.
[a] All Fe expressed as Fe_2O_3.
[b] Fe_2O_3/FeO set at 0.15 and Mg number = (atomic) 100 Mg/Mg + Fe^{2+}.

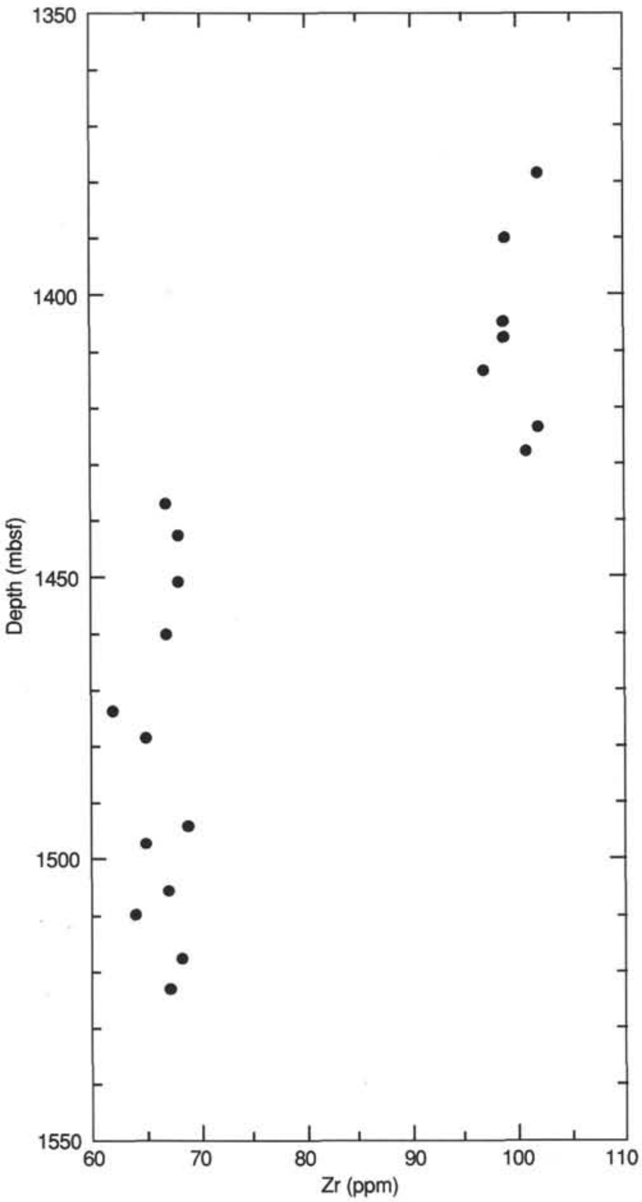

Figure 55. Zr vs. depth for Site 807 basalts. Note the abrupt break between high and low Zr lavas, which corresponds to Subunit A and Subunits C, E, F, and G, respectively.

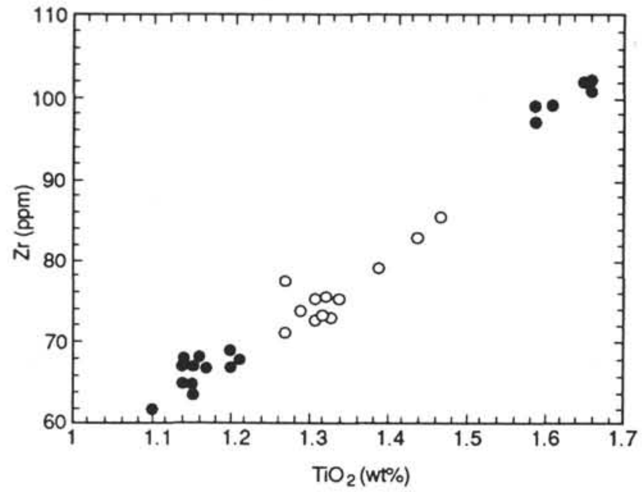

Figure 56. Zr vs. TiO_2 for Site 803 (open circles) and 807 (closed circles) basalts.

ment disruption. These occur between 0.14 and 0.24 sbsf and between 0.28 and 0.41 sbsf. In each of these intervals, the sedimentologists noted an abundance of microfaults (see "Lithostratigraphy" section, this chapter). A third interval (0.44–0.53 sbsf) also shows seismic evidence of minor disruption and thickening, but a sedimentological expression of this disturbance was not observed.

Site 807 was not surveyed by the *Thomas Washington* during its Leg 130 site survey cruise (see Mayer et al., this volume); thus, a brief survey of the site was conducted by the *JOIDES Resolution* before beacon deployment. Details of this survey and of the seismic system used are presented in the "Underway Geophysics" chapter (this volume).

As at the previous sites, we have used the results of both laboratory and logging measurements to convert seismic traveltime to depth-in-section, and we employ seismic modeling to check on the accuracy of this traveltime-to-depth conversion. For Site 807, laboratory measurements of velocity and density were made approximately every 75 or 150 cm (see "Physical Properties" section, this chapter), and velocity and density logs (15-cm sample interval, 60-cm sensor spacing) were run for the section between 90 and 1530 mbsf (see "Logging" section, this chapter). Two separate logging runs were made at Site 807, the first on the section from 90 to 800 mbsf and the second from approximately 350 to 1530 mbsf. In this section, we will only use the results of the first logging run and physical properties data from Hole 807A. The results from Hole 807C will be incorporated into shore-based studies.

Laboratory measurements of density and velocity were converted to *in-situ* values using the methods described in Mayer et al. (1985) and merged with the logging data. A comparison of the *in-situ* corrected laboratory data with the log data reveals several inconsistencies that must be addressed before the data can be properly merged (Figs. 65 and 66).

If we assume that the log-derived densities and velocities represent *in-situ* values, then laboratory measurements, properly corrected to *in situ*, should be the same as the logging values. At the previous sites, the corrected laboratory values have, for the most part, been in good agreement with the logging data, implying that the procedure used to correct laboratory data to *in-situ* values is reasonable. Discrepancies between the laboratory and logging values (e.g., at Site 805 between 140 and 160 mbsf; see "Logging" section, "Site 805" chapter, this volume) have, at previous sites, been attributed to poor hole conditions that have degraded the logs in certain intervals. Comparing the Site 807 logs with the laboratory data reveals that between 90 and 200 mbsf the corrected density values are in reasonable agreement with the logging data; however, between 200 and 260 mbsf the logging values are significantly lower than the lab measurements (Fig. 65). Between 220 and 250 mbsf, the logged densities are so low that they are unquestionably in error.

A comparison of the log and laboratory velocity measurements (Fig. 66) reveals that between 90 and 140 mbsf the logging data are in agreement with the corrected laboratory

Table 16. Logging operations, Holes 807A and 807C.

Local day	Local time	Cumulative hours	[a]Depth (mbsf)	
130-807A-				
3/2/90	5:40			Last core on deck
3/2/90	12:21			Start rig up
3/2/90	13:44	0		RIH with geophysical tool string (NGT/LSS/DIT/TLT)
3/2/90	14:45	1.0		At mud line
3/2/90	14:55	1.2	85.6	Start downlog
3/2/90	16:08	2.4	802.8	Stop downlog
3/2/90	16:10	2.4	820.5	At bottom of hole; 2.4 m of fill
3/2/90	16:10	2.4	820.5	Start uplog; NGT/LSS/DIT/TLT; up at 900 ft/hr; heave compensator on
3/2/90	18:51	5.1	89.6	Tool in pipe at 9530 fbrf; POOH
3/2/90	20:02	6.3		Tool string on deck
3/2/90	20:38	6.9		Dropped bullnose down mousehole when bolt sheared
3/2/90	21:55	8.2		Substitute bullnose built; tool string being built up
3/2/90	22:05	8.4		RIH with NGT/ACT/HLDT
3/2/90	23:13	9.5	0	Passing mud line going down
3/2/90	23:45	10.0	821.1	On bottom with NGT/ACT/HLDT; start uplog, heave compensator on; 600 ft/hr
3/3/90	2:30	12.8	323.4	Power pulled to winch shack from engine room; heave compensator down
3/3/90	2:40	12.9	354.8	Drop to 354.8 mbsf to turn heave compensator back on continue log
3/3/90	3:57	14.2	109.4	Heave compensator turned off
3/3/90	4:09	14.4	75.6	Tool string in pipe; POOH
3/3/90	5:23	15.7		NGT/ACT/HLDT at wellhead; sources removed
3/3/90	6:30	16.8		Rigged down from logging runs on Hole 807A
130-807C-				
3/21/90	19:30	0		Start rig up
3/21/90	20:54	1.4		RIH with geophysical tool string (NGT/LSS/DIT/TLT)
3/21/90	21:59	2.5		At mud line
3/21/90	22:13	2.7	330.4	Start downlog; heave compensator on
3/21/90	23:36	4.1	1492.9	Stop downlog
3/21/90	23:39	4.1	1528.3	At bottom of hole; 0.6 m of fill
3/21/90	23:39	4.1	1528.3	Start uplog; NGT/LSS/DIT/TLT; up at 900 ft/hr
3/22/90	3:58	8.5	348.7	Tool in casing; POOH
3/22/90	5:25	9.9		Tool string on deck
3/22/90	6:19	10.8		RIH with NGT/ACT/HLDT
3/22/90	7:53	12.4	1525.8	On bottom with NGT/ACT/HLDT; start uplog, heave compensator on; 600 ft/hr
3/22/90	8:11	12.7	1467.9	Caliper jammed by debris in lower section, stop log
3/22/90	8:16	12.8	1527.0	On bottom again; start main uplog; 600 ft/hr
3/22/90	14:25	18.9	348.7	Tool string in casing; POOH
3/22/90	16:44	21.2		RIH with NGT/FMS/GPIT/TLT
3/22/90	18:06	22.6	0	Passing mud line, pause for TLT tie point
3/22/90	19:14	23.7	1509.1	Set down on bridge; start main uplog, heave compensator on, 900 ft/hr
3/22/90	21:23	25.9	947.3	Stop main uplog; hole above too wide for FMS caliper go down for repeat
3/22/90	21:50	26.3	1507.8	Start repeat uplog from same bridge; 900 ft/hr
3/22/90	23:11	27.7	1095.5	Stop repeat uplog; POOH
3/23/90	1:20	29.8		NGT/FMS/GPIT/TLT at wellhead
3/23/90	2:09	30.7		Rigged down from logging runs on Hole 807C

[a]Depth in Hole 807A based on mud-line depth below rigfloor of 2815.1 m, and depth in Hole 807C based on mud-line depth below rigfloor of 2817.0 m.

measurements and below 140 mbsf the two data sets diverge. Deeper than about 140 mbsf, the corrected laboratory velocities are consistently lower than the logged velocities. A detailed look at several indicators of borehole conditions reveals that there are changes in borehole behavior between 220 and 250 mbsf (see "Logging" section, this chapter). A full understanding of the effect of these borehole changes will have to await further study. It is clear, however, that the *in-situ* correction used throughout Leg 130 does not work at Sites 806 and 807 as well as it worked at previous sites (and in the central equatorial Pacific where it was derived). We speculate that this is a result of the fundamental difference in the consolidation behavior between the sediments that accumulate on the top of the plateau and those that accumulate in deeper water. These differences may be a result of variations in grain size (foraminifer abundance), early cementation, or clay content in these two environments.

To obtain the best possible data base for the seismic model, we eliminated the logging density values that were clearly inaccurate and used laboratory density data from the seafloor to 260 mbsf (and downhole density data deeper than that). The logging velocity data do not appear to be corrupted by borehole problems; thus, we used corrected laboratory velocity data only from the seafloor to 90 mbsf where no logging data was available. The compromise that we make in doing this is the loss of the detailed density sampling provided by

Table 17. Acronyms used in well logging.

Acronym	Definition or meaning
ACT	Aluminum clay tool
API	American Petroleum Institute standard units of gamma activity calibrated to test pit in Houston, TX
BHC	Borehole compensated sonic tool
DIT	Phasor dual induction tool
fbrf	Feet below rig floor
FMS	Formation microscanner
GPIT	Three-axis magnetometer-inclinometer logging tool
GST	Geochemical spectral tool
HLDT	High-temperature lithodensity tool
LSS	Long-spaced sonic logging tool
mbrf	Meters below rig floor
mbsf	Meters below seafloor
NGT	Natural gamma tool
POOH	Pull out of hole
RIH	Run into hole
SDT	Long-spaced sonic digital tool
TLT	LDGO temperature logging tool

logging, particularly in the interval from 200 to 260 mbsf where the laboratory sampling interval was reduced (Figs. 65 and 66).

The merged, corrected laboratory and logging data (velocity and density) were used to calculate acoustic impedance (Fig. 67), which was then convolved with a seismic source signature to generate a synthetic seismogram (see "Seismic Stratigraphy" section, "Site 803" chapter, this volume or Mayer et al., 1985, for details). The synthetic seismogram was compared to the field seismic profile to evaluate the accuracy of the traveltime-to-depth conversion. The field records used for this study are those collected by the *JOIDES Resolution* during the pre-drilling survey (see "Underway Geophysics" chapter, this volume). Because no source signature was available for the *JOIDES Resolution*'s seismic system, we used the source signature of the *Thomas Washington* seismic system. The *Thomas Washington* system appears to have a somewhat greater bandwidth than does the *JOIDES Resolution*, and thus the synthetic seismogram generated has a higher resolution than the field profile (Fig. 68).

As has been done at the previous sites, we looked in detail at several representative reflectors within the section. By examining the age and possible origin of these reflectors, we hoped to place the seismic record in a stratigraphic framework. The criteria for the selection of these reflectors were simply that they have large amplitudes and be laterally coherent *within the immediate area of Site 807*. No effort was made to select reflectors that were regionally correlatable (e.g., see Mayer et al., this volume), although the regional distribution of the named reflector patterns is evident (see "Summary and Conclusions" section, this chapter). As at Sites 805 and 806, we referred to the six named reflector series and intervals (Panama, Tethys, Antarctic, Drake, Texas, and Ontong Java; see "Seismic Stratigraphy" and "Summary and Conclusions" sections, "Site 805" chapter, this volume) to place the selected reflectors within a regional stratigraphic framework.

The comparison of the synthetic seismogram to the field profile at Site 807 (Fig. 68) produced a reasonable match, implying that the traveltime-to-depth conversion was acceptable. We have selected 11 reflectors in the 800 m of logged section; they are labeled on the plot of reflection coefficient vs. traveltime (Fig. 69); their traveltimes, depths, and ages are listed in Table 19.

Because of the longer outgoing pulse of the *JOIDES Resolution* seismic system, the youngest reflector that we could pick at Site 807 is associated with the "Panama" Series (7-1) at 3.6–3.8 Ma. This reflector has most of the characteristics of the "winnowing" physical property association (high velocity because of the large grain size and low density and carbonate content because of the removal of nannofossils, leaving an enrichment of silica), except that it has a high density rather than a low one (Figs. 67 and 70). This may mean that the grain size increase at this time is not a response to increased currents but, rather, is a function of a primary increase in foraminifer abundance or is associated with the increase in terrigenous components noted by the sedimentologists (see "Lithostratigraphy" section, this chapter).

In contrast, the next deeper reflector (7-2; 4.6–4.8 Ma) shows the complete "winnowing" physical property association but with extremely small changes in carbonate and density, which lead us to question whether winnowing is indeed the reflector-forming mechanism here. In an analysis of grain-size distribution parameters, the sedimentologists found no evidence for winnowing at Site 807 (see "Lithostratigraphy" section, this chapter). The mechanisms responsible for these physical property changes will be the subject of future study.

Reflector 7-3 (6.7 Ma) has all the indications of a diagenetically enhanced reflector (high velocity, high density, fine grain size, and a small increase in carbonate content), but it occurs at a depth at which the sedimentologists have not yet indicated the occurrence of chalk (Figs. 67 and 70). This may be the result of the greater sensitivity of the physical properties measurements to the onset of cementation, or a misinterpretation of the physical properties interrelationships. Again, shore-based studies of the physical properties interrelationships should resolve this issue. The final reflector of the "Tethys" series (7-4; 7.4–7.5 Ma) is once again associated with a grain size and velocity peak but no change in carbonate (there is little density data in this interval). A peak in foraminifer abundance was noted at this depth that may indicate a change in productivity or winnowing.

All of the deeper reflectors (7-5 through 7-11), with the exception of 7-9 (24.1–24.3 Ma), have the same physical properties associations, with density and velocity increasing or decreasing synchronously. As at Site 806, we interpret this to represent the diagenetic enhancement of an original oceanographic signal. Unlike Site 806, however, the carbonate content does not seem to vary in unison with the density and velocity, suggesting that the original oceanographic signal here may be somewhat different from that at Site 806. Reflector 7-9 is in the middle of an interval (570–630 mbsf) in which the velocity and density signals go out of phase. The reason for this is not yet understood but will be the subject of future study.

SUMMARY AND CONCLUSIONS

Site 807, located on the northern margin of the Ontong Java Plateau (latitude 3°36.4′N, longitude 156°37.5′E, 2805 m water depth) was drilled to answer questions regarding the origin and tectonic development of oceanic plateaus in general and the geologic history and paleoceanography of the Ontong Java Plateau in particular. Drilling objectives were (1) to provide Paleogene and Cretaceous sediments for studies of pre-Neogene paleoceanography; (2) to obtain basement rock for studies of the origin of the Ontong Java Plateau; and (3) to provide a second shallow-water site, off the equator, for comparison with Sites 803 and 806 on the Neogene equatorial depth transect. Criteria used to select Site 807 included (1) a position on the northern rim of the high plateau as far from Site 289 as feasible; (2) a location in fairly shallow water to obtain a well-preserved carbonate section; (3) the presence of

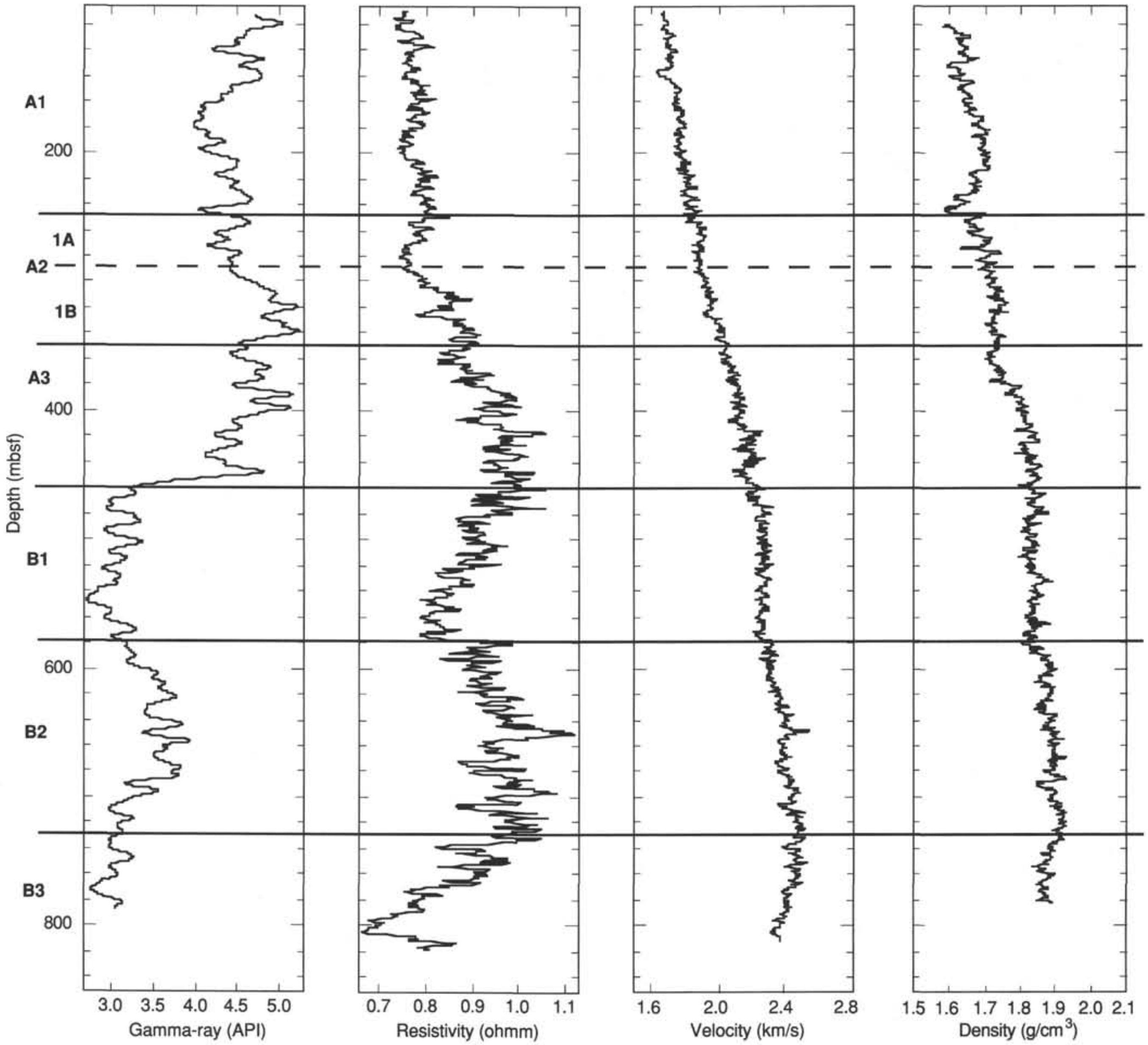

Figure 57. Well logging data, Hole 807A. Solid lines identify log stratigraphic units, dashed line defines lithostratigraphic unit division.

a thick section showing thinning in the upper layers and thickening in the lower layers in the seismic reflection profiles; and (4) the presence of an undeformed sedimentary and basement section in a location protected from potential bottom-current activity.

The site was positioned by means of a single-channel seismic (SCS) line acquired by the *Thomas Washington* during the EURYDICE Cruise 9 survey at 0255 UTC on 11 April 1975; it was resurveyed during Leg 130 (see "Underway Geophysics" chapter, this volume). Site 807 is located on the northern rim of a high plateau, roughly 475 km northwest of Sites 289/586, within a shallow basement graben about 0.5 km from the footwall of the northern side of the graben. The sedimentary section is thick, about 1.18 s of two-way traveltime in the SCS profile (see "Underway Geophysics" chapter, this volume) and shows well-behaved layering, disturbed by only minor thickening along the graben walls in the lower portion of the section, and a sheltered location from the ubiquitous bottom currents of the plateau. Thus, this site appeared to offer the best opportunity for recovering one of the most complete depositional sequences present on the plateau as well as representative basement samples.

Coring Results

Overview

Site 807 was occupied for 24.3 days. We cored 1701.6 m of Neogene, Paleogene, and Upper Cretaceous sediments, 533.0 m by APC (averaging 102% recovery), 568.5 m by XCB (80% recovery), and 599.7 m by RCB (27.4% recovery). We also cored 148.7 m of basement (dated as Lower Cretaceous), representing the deepest basement penetration yet achieved on a Pacific oceanic plateau (Fig. 71), and recovered 87.6 m of basalt and 0.6 m of interbedded sediment. Three holes were

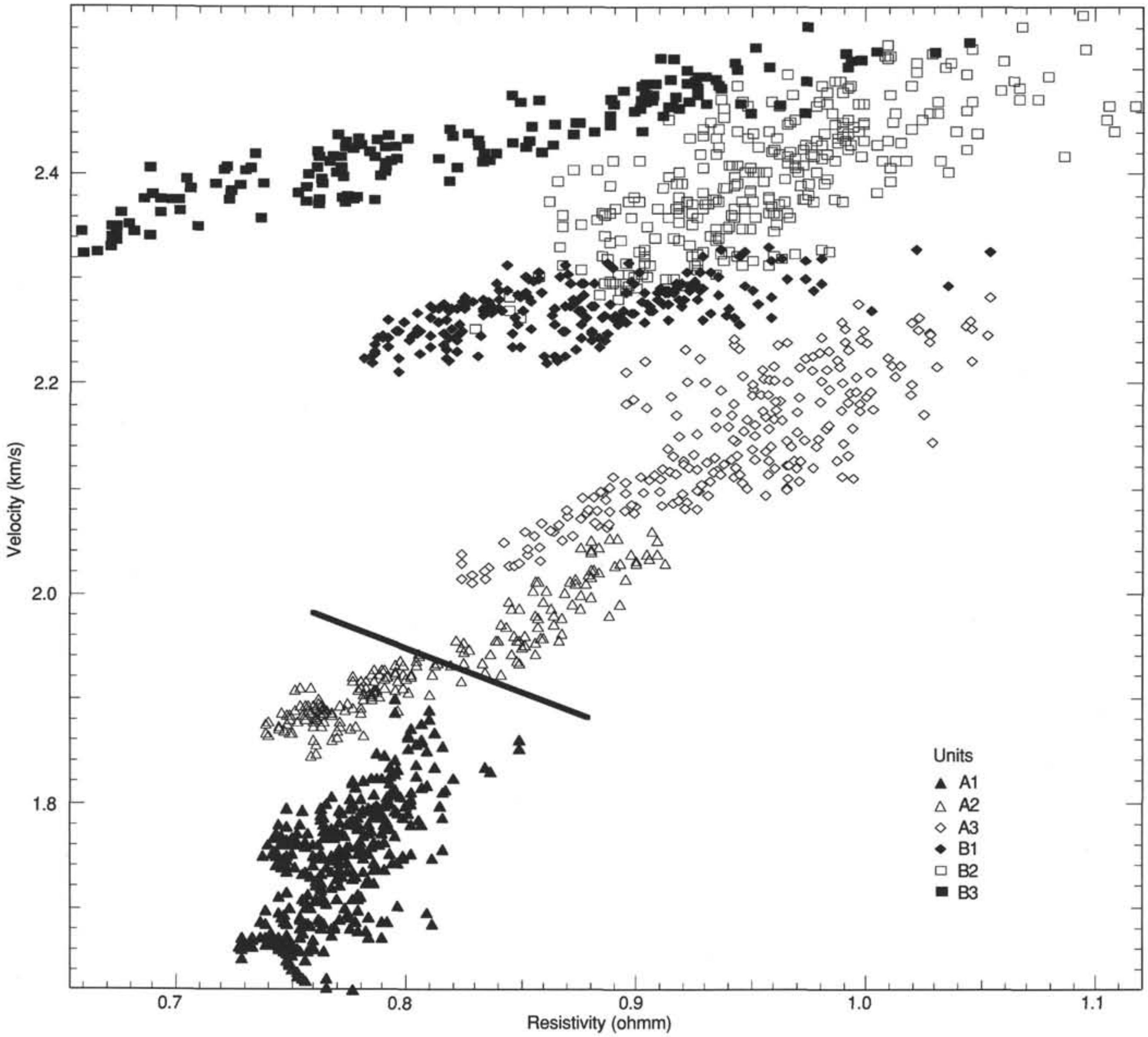

Figure 58. Electrical resistivity logging data plotted vs. compressional wave velocity logging data, Hole 807A. Solid bar represents the approximate location of the ooze-chalk transition identified in the recovered core.

drilled as follows: Hole 807A was cored with the APC to 254.4 mbsf and with the XCB to 822.9 mbsf; Hole 807B was cored with the APC to 278.6 mbsf; and Hole 807C was cored with the RCB from 780.0 to 1528.4 mbsf. Holes 807A and 807C were also successfully logged to total depth drilled, and a complete set of geophysical measurements were obtained (including FMS data in Hole 807C).

The sediments recovered range in age from Pleistocene to Early Cretaceous; they were divided into three lithologic units. Unit I (0–968.0 mbsf) is composed mainly of Pleistocene to upper/middle Eocene nannofossil ooze and chalk with foraminifers, with lesser amounts of foraminifer nannofossil ooze and chalk as well as nannofossil ooze and chalk. Unit II (968.0–1351.4 mbsf) is composed of upper/middle Eocene to upper Campanian limestone, chert, nannofossil chalk, and nannofossil chalk with foraminifers. Unit III (1351.4–1379.7 mbsf) is composed of lower Cenomanian to upper Albian–Aptian claystone, siltstone with varying amounts of radiolarians, and limestone. Igneous basement at Site 807 is represented by one lithologic unit, Unit IV (1379.7–1528.4 mbsf), which is predominantly composed of Albian-Aptian basalt.

The record is continuous from the Pleistocene to the upper Oligocene, at which time a stratigraphic break occurs at 702.4 mbsf (ca. 28–30 Ma), the first of three major stratigraphic breaks encountered above the Cretaceous/Tertiary boundary. Other breaks occur in the middle Eocene at 996.8, 1073.0, and 1094.8 mbsf (ca. 40–42 and 47–50 Ma). Much of the Paleocene-to-middle Eocene section is condensed, with the exception of part of the upper Paleocene. The K/T boundary was crossed at 1193.1 mbsf, and an apparently complete boundary sequence was recovered. The section below the K/T boundary also probably includes one or more stratigraphic breaks, in particular between the upper Campanian limestone

Table 18. Log stratigraphic units, Hole 807A.

Unit	Depth range (mbsf)	Gradient (km^{-1})	Characteristics
A1	?–253.5	0.5	Resistivity: gradual increase from 0.72 to 0.80 ohmm
		1.3	Velocity: gradient of 1.65–1.85 km/s
		0.7	Density: increasing from 1.60 to 1.70 g/cm^3, suspect minimum at lower boundary
A2	253.5–352	1.2	Resistivity: relative minimum of about 0.75 ohmm at 280 mbsf, increase to 0.87 ohmm
		2.0	Velocity: increase from 1.85 to 1.90 km/s at upper boundary, then generally constant, varying about 1.90 km/s, with an increase to 2.05 km/s at the lower boundary
		0.7	Density: increasing from 1.65 to 1.72 g/cm^3
A3	352–474	0.7	Resistivity: increasing from 0.87 to 0.95 ohmm at 400 mbsf, then constant with a scatter of 0.1 ohmm
		1.2	Velocity: increasing from 2.05 to 2.25 km/s at 415 mbsf, then varying about 2.20 km/s
		0.9	Density: constant to 380 mbsf, where there is a step from 1.72 to 1.80 g/cm^3, then increasing to 1.83 g/cm^3
B1	474–580	−1.2	Resistivity: decreasing from 0.95 to 0.80 ohmm about scatter of 0.1 ohmm
		0.0	Velocity: constant about 2.25 km/s
		0.2	Density: step increase from 1.83 to 1.85 g/cm^3 at 530 mbsf
B2	580–730.5	1.0	Resistivity: sharp increase from 0.85 to 0.95 ohmm at upper boundary, then gradual increase to 1.00 ohmm
		1.3	Velocity: increase at upper boundary to 2.25 to 2.30 km/s, then gradual increase to 2.50 km/s
		0.7	Density: increasing to 1.85 g/cm^3 within 10 m of upper boundary, then gradually increasing to 1.95 g/cm^3
B3	730.5–?	−1.7	Resistivity: decreasing from 0.95 to 0.70 ohmm, with less scatter at lower resistivities
		−1.7	Velocity: decreasing from 2.50 to 2.35 km/s
		−1.4	Density: decreasing from 1.92 to 1.85 g/cm^3 at 780 mbsf, bad data below this depth

and the lower Cenomanian claystone-siltstone sequences at 1351.4 mbsf and near the Aptian-Albian limestone-basalt contact encountered at 1379.7 mbsf in Core 130-807C-74R.

Stratigraphy of the Sediments

Unit I was divided into Subunits IA and IB, based on the depth of the ooze-chalk transition at 293 mbsf (ca. 10.4 Ma). The boundary is transitional, as the lower 30 m of Subunit IA contains a significant percentage of chalk in isolated nodules and layers and the upper 20 m of Subunit IB contains numerous thin intervals of ooze.

Subunit IA (0–293 mbsf) consists of Pleistocene to upper/middle Miocene foraminifer nannofossil ooze, nannofossil ooze with foraminifers, and minor amounts of nannofossil ooze, mostly ranging from sandy silt to silt and, only rarely, to silty clay. Foraminifer abundances vary from 4% to 40% and average about 23%. Significant maxima in mean grain size and foraminifer abundance were noted in Holes 807A and 807B at 25 mbsf (ca. 2 Ma), from 60 to 90 mbsf (ca. 4 Ma), at 160 mbsf (ca. 6 Ma), and between 220 and 250 mbsf (ca. 7–8 Ma). Significant minima were observed at 50 mbsf (2.5–3 Ma), at 135 mbsf (ca. 5 Ma), and between 190 and 210 mbsf (ca. 6.5 Ma). Carbonate content increases downhole from 88% in the Pleistocene section to an average of 92% in the Miocene section. Radiolarians and diatoms are present in trace amounts. Colors range from white (in the top 3 m) through pale brown to light gray. Horizontal color bands are pervasive, occurring in various shades of green or purple. Up to 2 cm thick and commonly in green and purple pairs, the bands first appear at 9 mbsf and increase in frequency downhole to a maximum in the upper Miocene, between 90 and 200 mbsf, below which they decrease in frequency. Bioturbation is extensive, as indicated by burrow structures, authigenic pyrite pellets, and trace fossils. The odor of H_2S also was detected upon splitting some of the cores. Burrows are commonly surrounded by discrete purple halos that crosscut and overprint color bands, suggesting the presence of redox gradients emanating from the burrows. Minor microfaulting is present.

Subunit IB (293–968.0 mbsf) consists of upper/middle Miocene to upper Eocene nannofossil chalk with foraminifers, foraminifer nannofossil chalk, and nannofossil chalk. Foraminifer abundances are high, about 20%, from 350 to 500 mbsf (ca. 13–21 Ma) and from 680 to 740 mbsf (ca. 27–31 Ma). Foraminifer abundances are low at the top of the subunit from 300 to 350 mbsf (ca. 11–13 Ma) and from 525 to 675 mbsf (ca. 22–27 Ma). Mean carbonate content for the subunit is about 93%. Carbonate maxima occur from 450 to 575 mbsf; minima occur from 325 to 425 mbsf and below 575 mbsf. Nine separate ash layers are present between 639 and 759 mbsf (ca. 26–32 Ma). The ash layers are dark gray and show the effects of bioturbation well. Radiolarians and diatoms are present in trace quantities. The chalk is predominantly white. Faint to distinct green color bands are common at the top of the subunit but are rare below 300 mbsf. The purple bands fluctuate in abundance throughout the subunit but are more frequent between 700 and 760 mbsf. The bands thin with depth to a thickness of <1 mm. Swarms of thin bands exhibiting wavy, braided, flaserlike patterns are common. Bioturbation is common as indicated by burrow mottles, trace fossils, and pyritized burrow linings that become flattened with depth.

Unit II was divided into Subunits IIA and IIB, based on the transition from chalk to limestone. The boundary between the two subunits is placed at 1098.0 mbsf, where a limestone lithology is indicated by the presence of over 50% nonbiogenic carbonate in the smear slides. The transition is also reflected in a substantial increase in average core recovery, from about 7% in Subunit IIA to about 44% in Subunit IIB.

Subunit IIA (968.0–1098.0 mbsf) consists of middle Eocene nannofossil chalk, nannofossil chalk with foraminifers, lime-

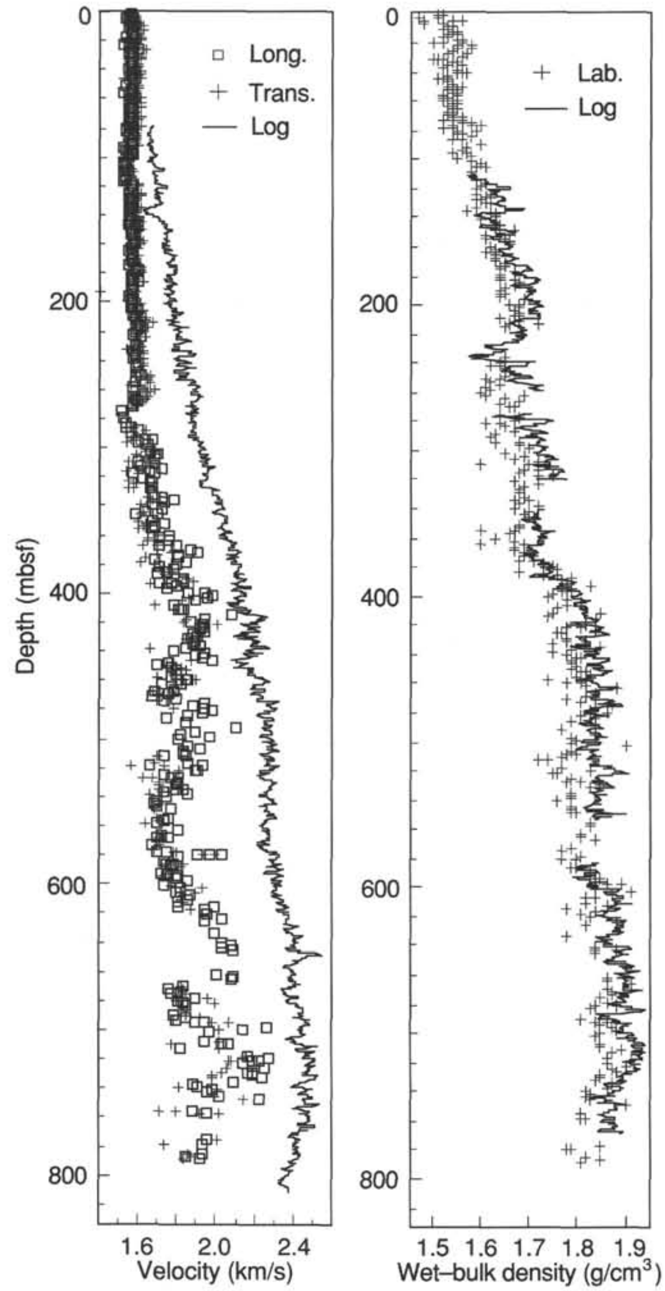

Figure 59. Comparison of laboratory sample measurements of compressional wave velocity and bulk density with logging data, Hole 807A. Laboratory data are plotted vs. depth but are not corrected for *in-situ* conditions. Long = longitudinal, trans = transverse, and lab = laboratory.

stone, silicified limestone, and chert. The chalk is white and moderately bioturbated. Burrows are commonly flattened and predominantly horizontal. Isolated occurrences of gray, anastomosing color bands or flaser structures were observed. Both the limestone and the silicified limestone are white. The chert is gray, apparently nodular, and commonly occurs with chalk coatings and millimeter- to centimeter-size chalk inclusions.

Subunit IIB (1098.0–1351.4 mbsf) consists of middle Eocene to upper Campanian limestone and chert. The limestone is predominantly white and moderately to highly bioturbated, as evidenced by weak mottling, finely disseminated pyrite, and flattened horizontal burrows. Stylolites occur throughout the subunit. Gray and red chert nodules and minor chert layers are present in all cores. At least 15 ash layers were found between 1140 and 1200 mbsf (ca. 56–67 Ma). The thickest is a 3-cm layer encountered at 1156.6 mbsf (ca. 57 Ma), whereas the remaining layers are about 1 cm thick. At least 10 dark gray to brown clay layers were found between 1300 and 1351 mbsf (ca. 74–76 Ma); these may represent altered volcanic ash (the upper 2 layers contain volcanic glass). Evidence for redeposition is ubiquitous below 1116 mbsf. Clasts of white limestone, about 5 mm in diameter, are dispersed throughout a slightly darker matrix from 1116 to 1197 mbsf, indicating a steady input of debris from the flanks of the graben. Nannofossils from a clast at 1127 mbsf are of Late Cretaceous age, whereas nannofossils in the matrix are of mixed Paleocene and Cretaceous age. Evidence for mass transport is pervasive below 1197 mbsf. Laminae or beds of well-sorted carbonate grains, 5 mm to 5 cm thick, were observed between 1197 and 1232 mbsf. Low-angle truncation surfaces and the well-sorted nature of the grains suggest that some of the parallel laminae are primarily formed by redeposition of winnowing. Clast-bearing intervals alternating with clast-free intervals over thicknesses of 1–5 m are common below 1232 mbsf. Most of the clasts, ranging from 1 to 5 cm in diameter, are white limestone, but gray clasts become more abundant below 1271 mbsf, and green clasts are present below 1290 mbsf. The green clasts may be altered basaltic glass. Dark brown claystone clasts are common below 1321 mbsf. The clast-bearing intervals probably represent debris-flow deposits. A fold at 1264 mbsf, underlying a 1-m-thick, graded, clast-bearing interval, supports the debris flow interpretation.

Unit III was divided into Subunits IIIA and IIIB, based on the relative abundances of claystone and limestone.

Subunit IIIA (1351.4–1369.7 mbsf) consists of lower Cenomanian to upper Albian claystone interbedded with siltstone with radiolarians, radiolarian siltstone, and radiolarian sandy siltstone. The claystone is very dark grayish brown. Bioturbated intervals are indicated by the presence of mottling and burrows, about 1 cm long. The siltstone interbeds, which are generally gray, are rare at the top of the subunit, but they become more abundant and increase in radiolarian content downhole. The contacts between the claystone and the siltstone interbeds are predominantly gradational, but sharp contacts and graded bedding are also present. Although few scour marks or load structures were observed, the overall interbedded pattern emphasizes the importance of episodic deposition at Site 807.

Subunit IIIB (1369.7–1379.7 mbsf) consists of upper Albian–Aptian limestone and chert. Although the limestone was recovered from 1369.7 to 1375.6 mbsf, as measured from the cores, a distinct decrease in the drilling rate at 1379.7 mbsf suggests that this depth is the contact between the limestone and the underlying basalt. The recovered limestone is generally gray and bioturbated. The upper part contains very fine, vertical, anastomosing fractures. The lower part contains wavy, lenticular beds, about 0.5–3 cm thick, as well as microfaults and abundant healed tensional cracks. The chert, found in both intervals, is black to dark gray and nodular in origin.

Basement Stratigraphy

Unit IV (1379.7–1528.4 mbsf), comprising basement at Site 807, is composed of Albian-Aptian tholeiitic basalt and interbedded limestone, and is divided into seven subunits, IVA through IVG, five of which are igneous (IVA, IVC, IVE, IVF, and IVG), and two of which are sedimentary (IVB and IVD).

Subunit IVA (1379.7–1424.6 mbsf): aphyric pillow lavas and thin (<2 m thick) massive flows with rare plagioclase phenocrysts up to 3 mm long, superficially similar to lavas at Site 803.

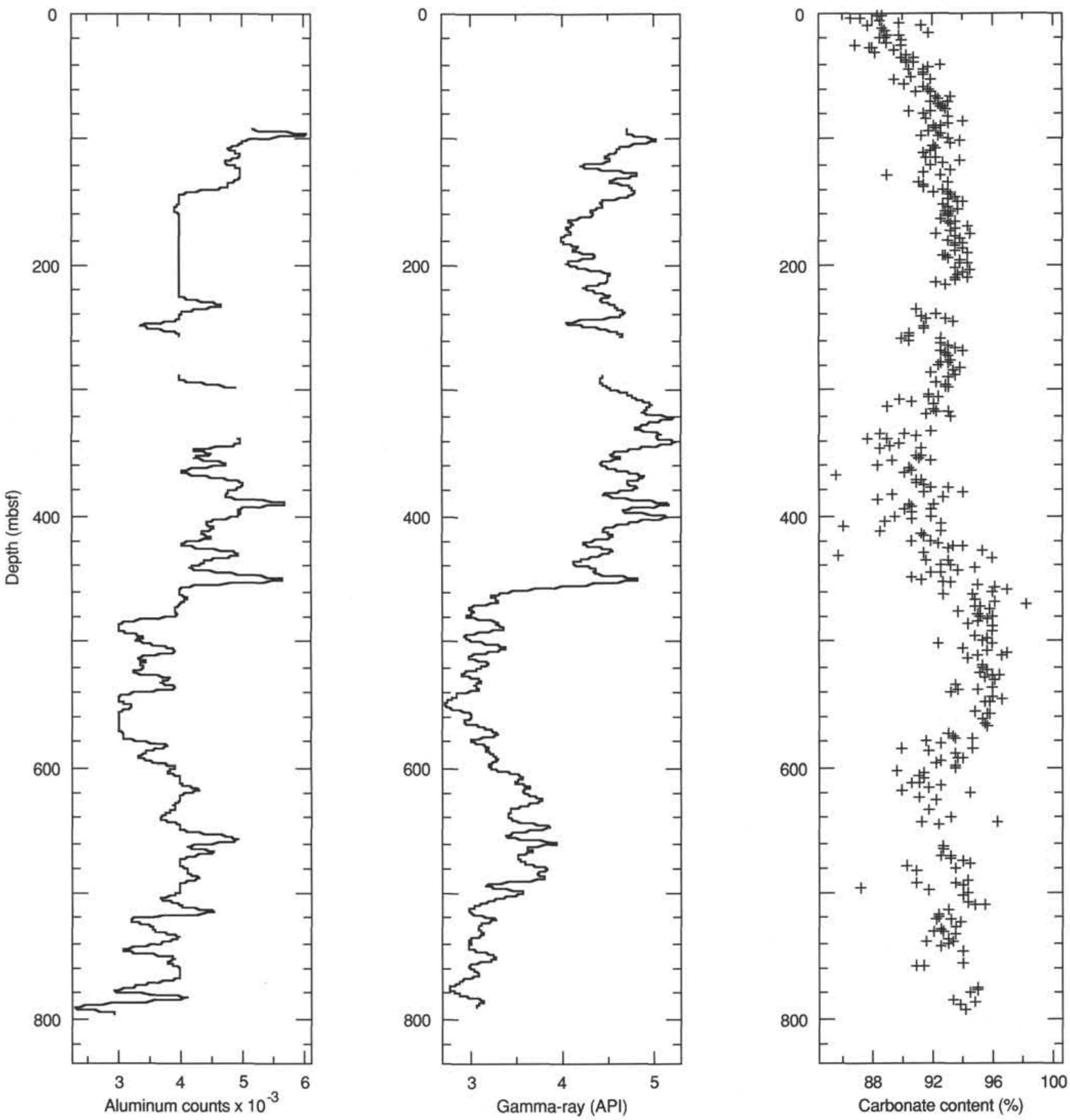

Figure 60. Aluminum and gamma-ray logging data, Hole 807A. Also included are the laboratory determinations of calcium carbonate content from the physical properties samples.

Subunit IVB (1424.6–1425.1 mbsf): Albian-Aptian limestone interbedded with vitric tuff. The limestone is white and contains numerous healed fractures. The tuff is dark reddish brown to reddish brown.

Subunit IVC (1425.1–1441.9 mbsf): aphyric pillow lavas and thin (<3 m thick) massive flows with sparse, euhedral to subhedral, olivine microphenocrysts (<1 mm long), largely replaced by green and black clays.

Subunit IVD (1441.9–1442.0 mbsf): Albian-Aptian limestone, which is olive brown and contains quartz and illite/glauconite.

Subunit IVE (1442.0–1447.0 mbsf): aphyric pillow lavas and thin (<3 m thick) massive flows with sparse, euhedral to subhedral, olivine microphenocrysts (<1 mm long), largely replaced by green and black clays.

Subunit IVF (1447.0–1475.0 mbsf): aphyric massive flow with sparse, euhedral to subhedral, olivine microphenocrysts (<1 mm long), largely replaced by green and black clays.

Subunit IVG (1475.0–1528.4 mbsf): aphyric pillow lavas and thin (<3 m thick) massive flows with sparse, euhedral to subhedral, olivine microphenocrysts (<1 mm long), largely replaced by green and black clays.

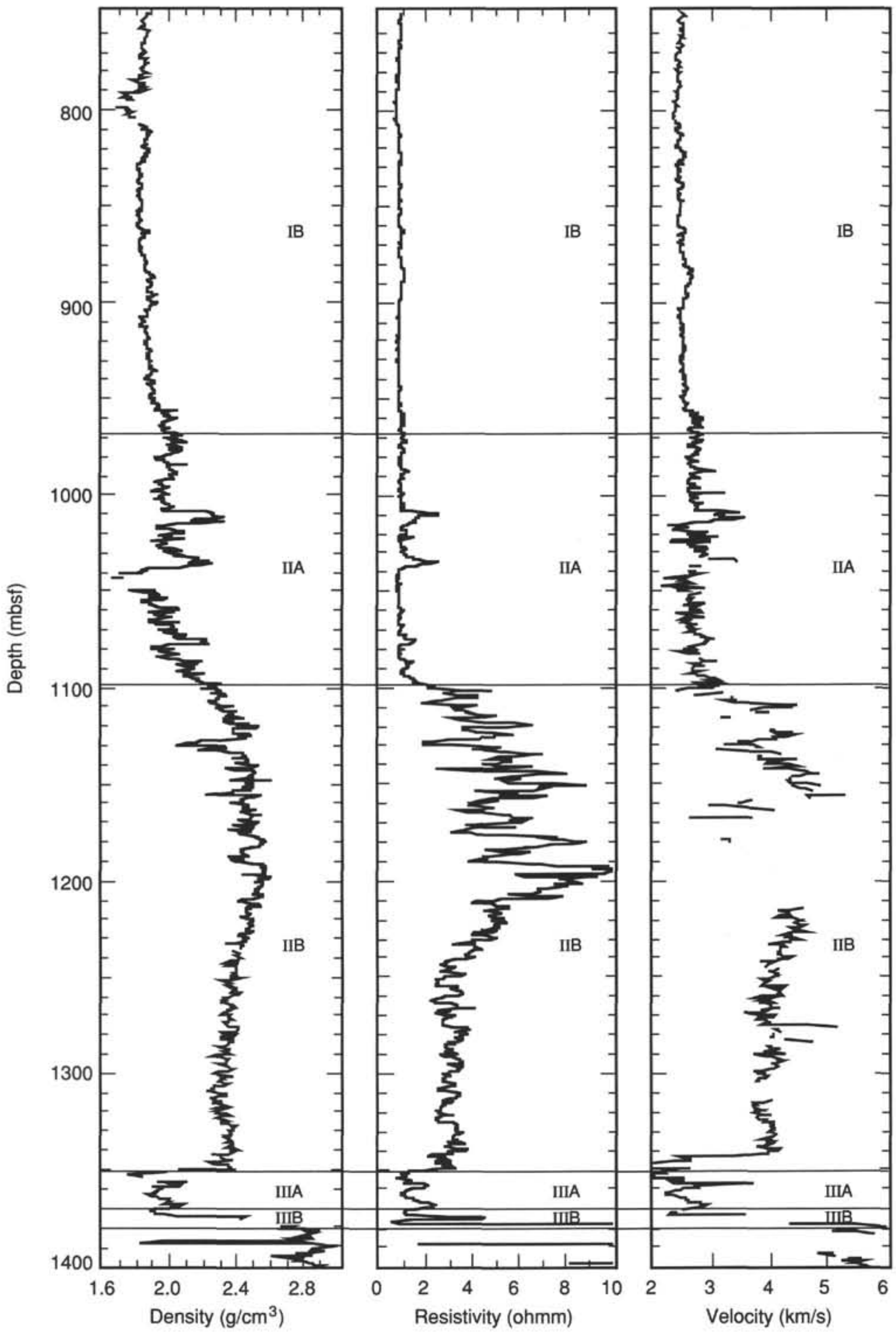

Figure 61. Compressional wave velocity, electrical resistivity, and bulk density logging data from the lower sedimentary section, Hole 807C. Basement depth is 1380 mbsf. Lithostratigraphic unit boundaries are superimposed on the plot.

Flecks of native copper were observed in several of the basalt cores below the sedimentary interbeds of Subunit IVB, particularly in vein material in Section 130-807C-82R-2 at 40 and 58 cm. Disseminated pyrite also was observed in glassy pillow rims and fractures. Another sedimentary interbed, unsampled in the coring but detected during logging, occurs within Subunit IVC at 1434 mbsf. All of the igneous subunits of Unit IV are composed of tholeiitic basalt, generally only slightly altered. Subunits IVA, IVC, IVE, and IVG are successions of pillow and thin (<3 m thick) massive flows. Subunit IVF, however, consists of a single massive flow, approximately 28 m thick. This flow documents the presence of thick flood basalt lavas on the Ontong Java Plateau. The general paucity of phenocrysts is reminiscent of some continental flood basalts, notably the Grande Ronde formation of the Columbia River Basalt Group.

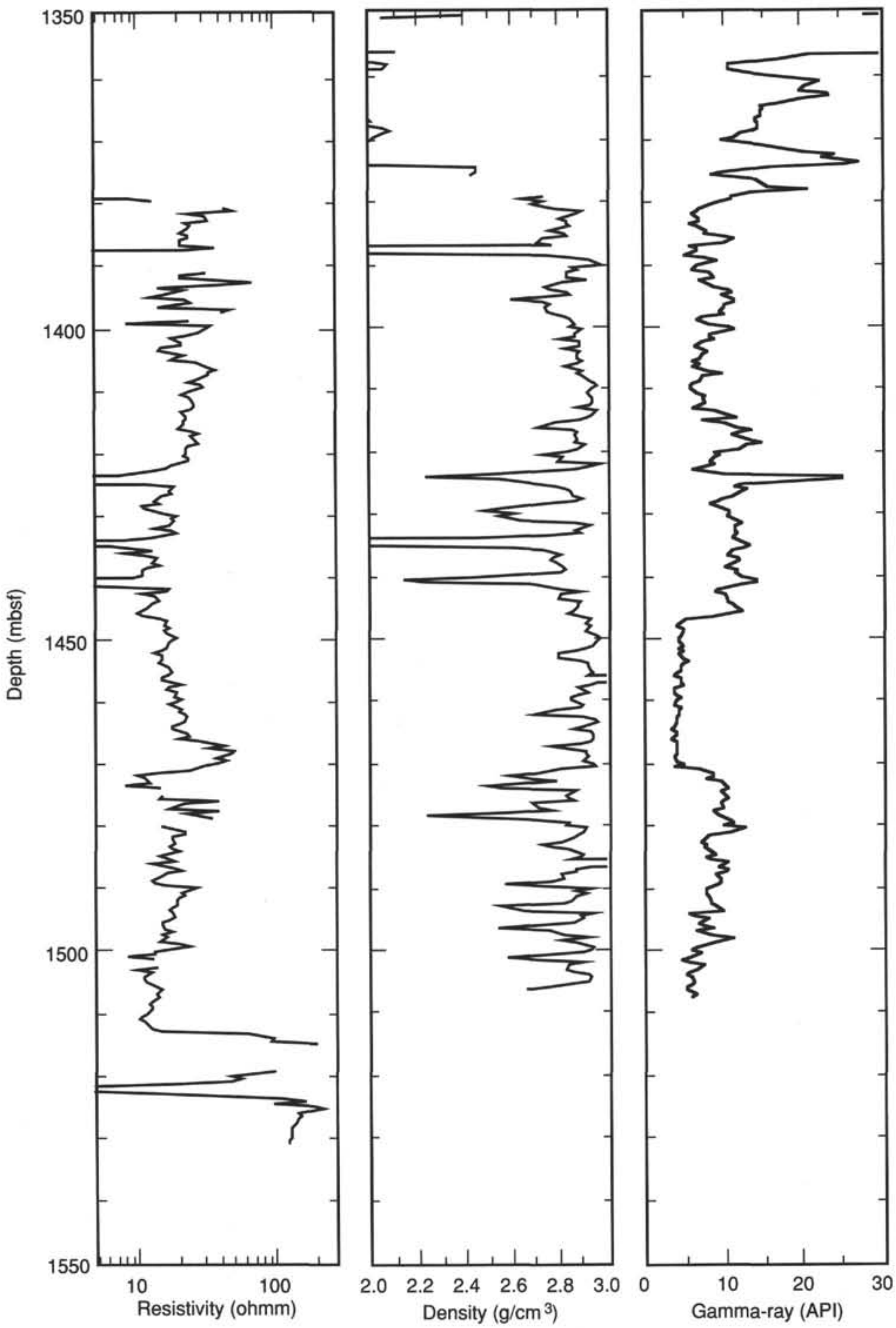

Figure 62. Basement logs of gamma-ray, resistivity, and bulk density, Hole 807C.

Special Studies

Paleomagnetic measurements were made on all APC and XCB cores from Hole 807A, on Cores 130-807B-1H through -10H from Hole 807B, and on all RCB cores from Hole 807C. The Pleistocene sediments of Holes 807A and 807B contain a well-defined record of the Brunhes/Matuyama boundary as well as the Jaramillo and Olduvai subchrons. These polarity boundaries enable a precise determination of Pleistocene sedimentation rates. Parts of the Miocene section, as well as parts of the Oligocene, Eocene, and Paleocene, also look promising for paleolatitude determinations. At the base of the sedimentary section in Hole 807C, the brown claystone/siltstone sequence has NRMs dominated by a viscous present-day overprint that may permit determination of a Cenomanian-Campanian paleodeclination. The Aptian-Albian age of the sediments overlying the basalt suggests that we have recovered a volcanic sequence that is especially promising for refining the Pacific Plate APWP. The NRMs of the basalts are dominantly steeper than 20° in inclination. If the NRMs are

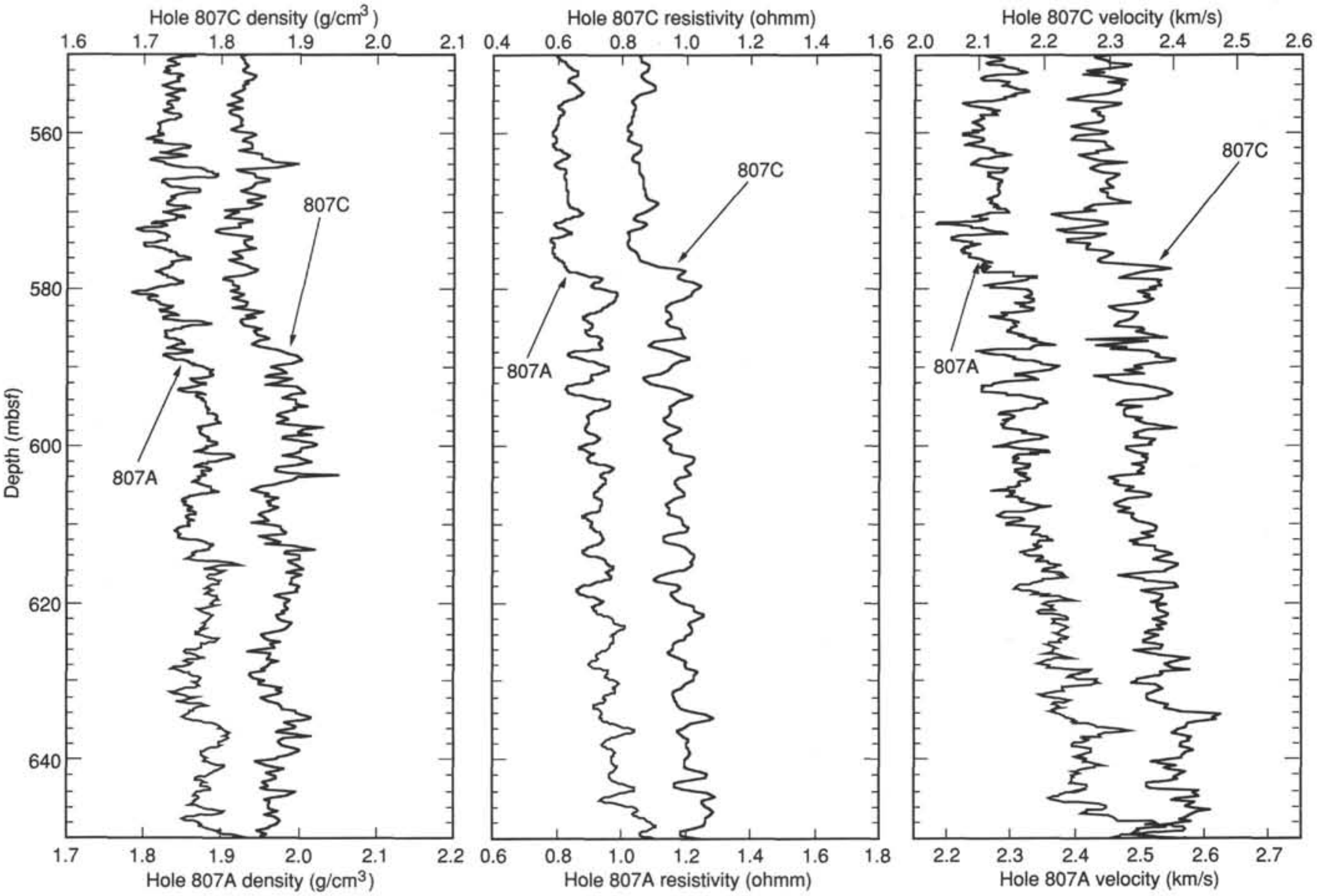

Figure 63. Comparison of logging data from Holes 807A and 807C over the interval from 550 to 650 mbsf from each log. Note that the Hole 807A data have been offset as follows in each instance to facilitate comparison: density by 0.1 g/cm^3, resistivity by 0.2 ohmm, and velocity by 0.15 km/s.

dominated by a primary remanence, as suggested in accordance with the freshness of the rocks, then the entire basalt sequence is of normal polarity.

Magnetic susceptibility measurements yielded good results well into Pliocene sediments. These data will be useful for fine-scale correlation and for studies of Milankovitch-type cycles.

Results from interstitial water geochemistry at Site 807 are similar to those obtained at Sites 803 and 804. The conservative gradients (Ca and Mg) compare favorably with those of Sites 288 and 289, suggesting similar rates for basalt alteration and diffusion. These and other gradients reflect the dominance of biogenic sediments and the paucity of organic carbon. Ca- and Mg-depth gradients are the least pronounced at Site 807, as compared with the other sites, and the Mg profile at Site 807 is anomalous in the lower part of the section where Mg concentrations remain constant with increasing depth. Dissolved silica concentrations generally increase with depth down to 900 mbsf (ca. 36 Ma), then decrease and level off at 1000 mbsf (ca. 42 Ma) in the silicified sediments of Unit II.

The combined carbonate content curve for Holes 807A and 807C (Fig. 72) closely reflects the lithostratigraphic units described at Site 807. The nannofossil oozes and chalks of Unit I are characterized by very high carbonate contents ranging from 85% to 95%. The chert-rich limestones in Subunit IIA and the upper part of Subunit IIB vary widely in carbonate content, ranging from 51% to 97%, whereas the chert-poor limestones of Subunit IIB are characterized by consistently high values ranging from 95% to almost 99%. In contrast, the claystones/siltstones of Subunit IIIA have carbonate contents <0.3% and are similar to equivalent intervals recovered above basement at Site 803.

Excellent well-log data were obtained from Holes 807A and 807C. The logs from both holes correlate well over scales of decimeters, instilling confidence in the measurements and also in the interpretation of cyclicity for Milankovitch time scales. The logging data from Hole 807A, in conjunction with a detailed suite of physical properties measurements obtained from the split cores, confirm the depth of the ooze-chalk transition based upon sediment descriptions. The logging data from Hole 807C likewise confirm the depth of the chalk-limestone transition and reveal the presence of local maxima and minima in velocity that correlate with chert/silicified chalk horizons and the claystone/siltstone beds deep in the section. Velocity, density, and resistivity all increase across the Unit I/II boundary because of the lower porosity of the chert and the effect of increased cementation of the calcareous sediment by silica. The Subunit IIA/IIB boundary is clearly seen in the logging data as an increase in velocity, density, and electrical resistivity and reflects the transformation of chalk and silicified chalk to limestone.

The logs allow an estimate of the amount of chert present in the section, which is seen to vary between 20% and 70% (Fig. 73), the higher values signifying the presence of massive cherts or beds of highly silicified limestone. The claystone,

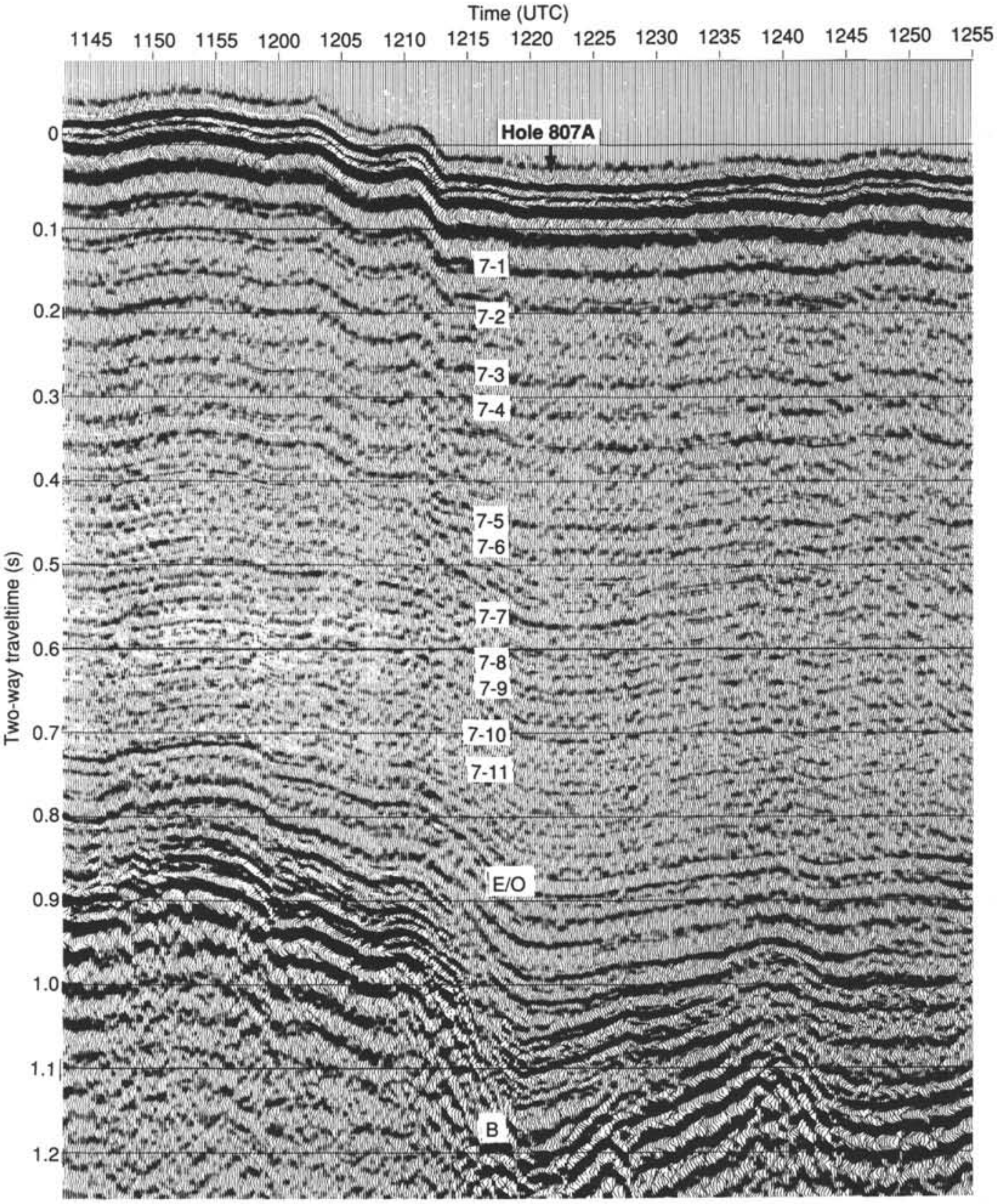

Figure 64. Seismic record collected by *JOIDES Resolution* over Site 807, using the 80- and 200-in.^{3} water guns, 70–250 Hz band-pass filter. For details of reflector picks, see Table 19. E/O = Eocene/Oligocene boundary and B = basement.

siltstone, and limestone of lithologic Unit III appear in the logs as an interval of reduced velocity, resistivity, and density. Basement is clearly defined as an increase in density, resistivity, and velocity. Gamma-ray, density, and resistivity logs together with the FMS data confirm the presence of a single massive flow in Subunit IVF and help identify the presence of sedimentary interbeds in the overlying pillowed flow subunits, including the one unsampled by the coring operation. Resistivity logs, moreover, suggest that another massive flow might be present at the bottom of the hole. For the sedimentary section, the logs provide important constraints on the generation of synthetic seismograms. Duplication of logging runs in the paired Holes 807B and 807C allows assessment of the precision of the logging data.

A reasonably complete seismic stratigraphy is present at Site 807. Comparison of the synthetic seismogram to the field profile (Fig. 68) produces a good match, implying that the traveltime-to-depth conversion is acceptable. Evidence for small-scale mass movement was observed at 0.14–0.24 and 0.28–0.41 sbsf (4.7–6.7 and 7.5–12.5 Ma, respectively). Thickened wedges of sediment occur between 0.44 and 0.53 sbsf (14.5–20.5 Ma) and around 1.00–1.02 sbsf (about 50.4 Ma). Basement occurs at approximately 1.18 sbsf (1379.7 mbsf, based on the drilling).

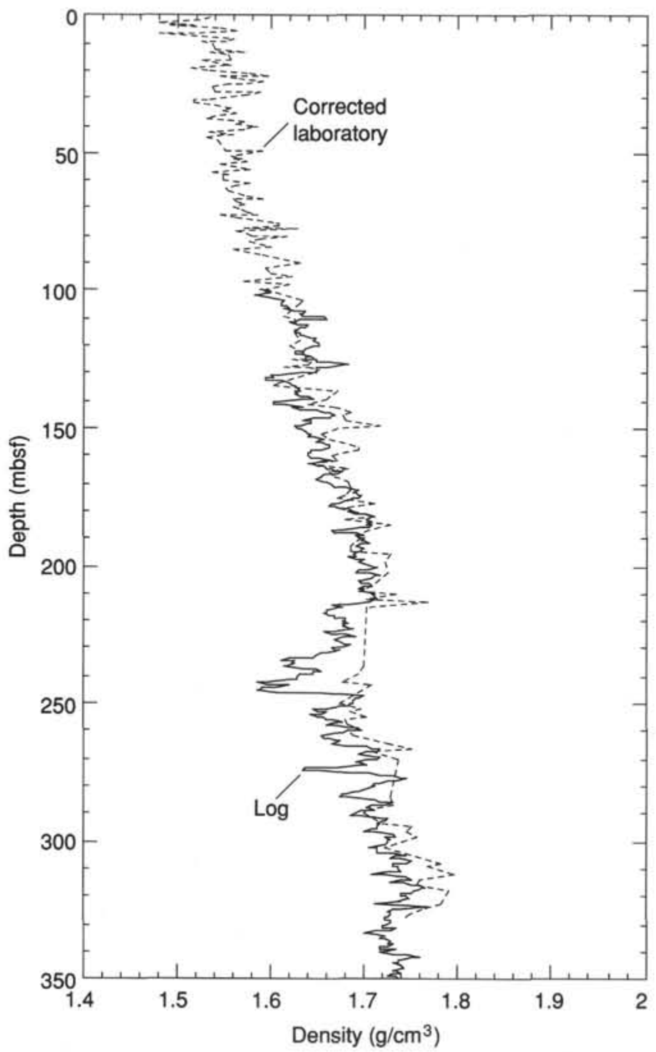

Figure 65. Merged laboratory and log density profile, Hole 807A. Laboratory values, corrected to *in situ,* are used from 0 to 260 mbsf, and log values are used from 260 to 783 mbsf.

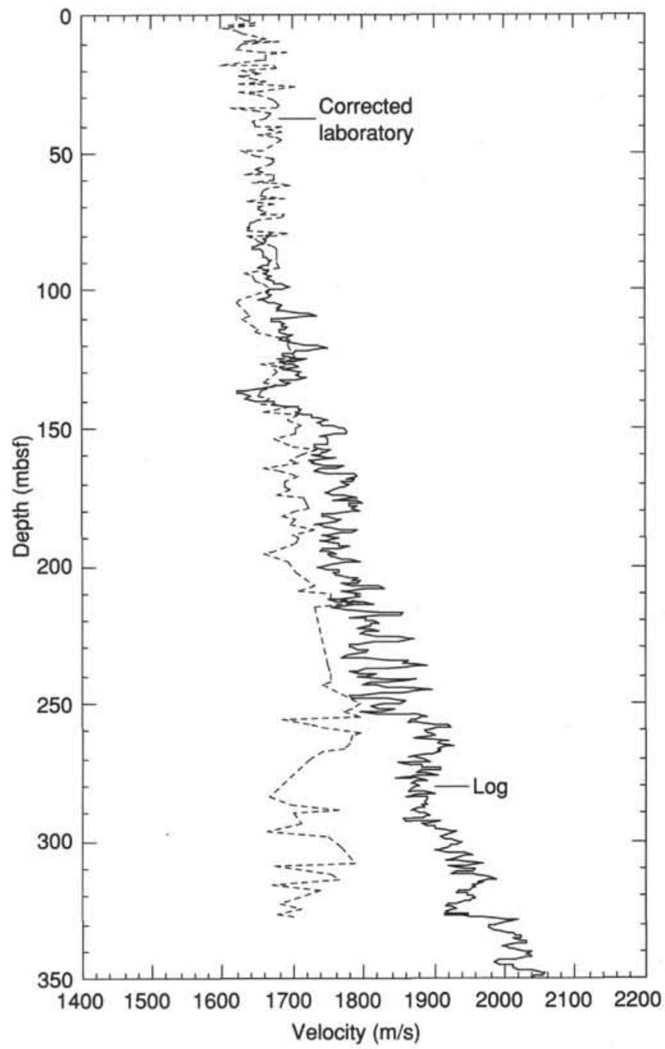

Figure 66. Merged laboratory and log velocity profile, Hole 807A. Laboratory values, corrected to *in situ,* are used from 0 to 90 mbsf, and log values are used from 180 to 783 mbsf.

Sequence of Events

The sequence of events as deduced from the drilling at Site 807 portrays the final stage of development of the world's largest submarine flood basalt plateau. The Ontong Java Plateau evidently formed, for the most part, by widespread effusion of massive flood basalts into deep water during Aptian time. The sequence of eruptive events that occurred toward the end of the formation of the plateau, as recorded at Sites 803 and 807, are as follows.

The final phase of flood basalt effusion was characterized by the eruption of a massive flow, which was closely followed by the eruption of a series of thin pillowed flows. This sequence was followed, in turn, by the eruption of another massive flow, again closely followed by the eruption of another series of thin pillowed flows. After an interval of time (of uncertain duration), represented by the deposition of a limestone-claystone facies at Site 807, the eruption of a late-stage sequence of pillowed flows occurred. Based on phenocryst assemblages, these probably are of a more evolved composition and represent the waning phase of volcanism at the site.

The first sediments to accumulate at the thermally elevated site were limestones and vitric tuffs, deposited above (but probably close to) the Early Cretaceous CCD (i.e., above 3000 mbsl). As the plateau cooled and contracted, the seafloor subsided, and a radiolarian ooze-clay facies began to accumulate as the site rapidly sank below the CCD. The graben that probably developed around the site during plateau subsidence apparently provided a sediment trap and sheltered accumulating sediment at the site from bottom-current activity, thus preserving the early depositional history of the Ontong Java Plateau.

Following deposition of the upper Albian–lower Cenomanian claystone-siltstone facies, there appears to be a major hiatus, possibly caused by deposition below the CCD. Subsequently, the upper Campanian–Maestrichtian limestones were laid down, presumably in response to a rapidly falling CCD. Sedimentation rates decreased from 10–20 m/m.y. in the late Maestrichtian to <5 m/m.y. in the early Paleocene. Mid-ocean volcanism apparently began on or near the Ontong Java Plateau in latest Maestrichtian time, as evidenced by the ash layer deposited just below the K/T boundary at Site 807. The volcanism, increasing in intensity (or proximity to the site),

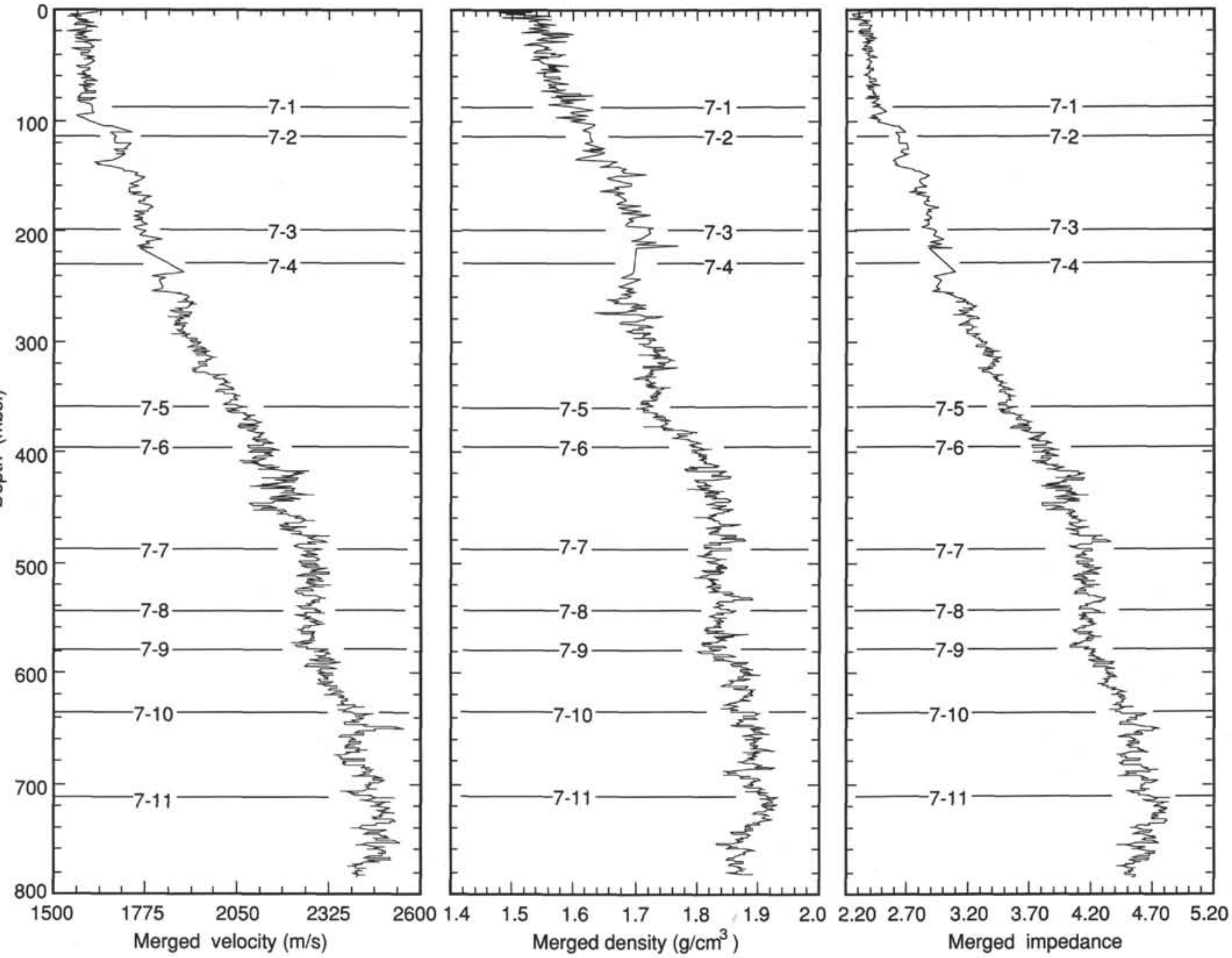

Figure 67. Velocity, wet-bulk density, and acoustic impedance data used to generate Site 807 synthetic seismogram. See text for discussion of reflector picks.

peaked in the late Paleocene (ca. 57 Ma) and then receded, disappearing entirely by middle Eocene time (ca. 54 Ma). After an initial low of near 1 m/m.y. in the early/middle Eocene (ca. 54–51 Ma), sedimentation rates increased in the Paleogene, peaking near 30 m/m.y. in the late middle Eocene (ca. 45–43 Ma). Hiatuses, however, also apparently occurred in the middle Eocene (ca. 50–47 and 43–40 Ma).

Volcanism began again in early-late Oligocene time (ca. 32–26 Ma), as the Ontong Java Plateau docked against the Melanesian Arc (Kroenke, 1984). A jump in sedimentation rate between 20 and 35 m/m.y. occurred in the early Oligocene (ca. 32–30 Ma), followed by another hiatus (ca. 28–30 Ma). Deposition thereafter was uninterrupted. Sedimentation rates ranged from 30 m/m.y. across the Oligocene/Miocene boundary (ca. 28–22 Ma), through 16–18 m/m.y. in the early to early late Miocene (ca. 22–4 Ma), to 44 m/m.y. in the late Miocene (ca. 8–5 Ma), before dropping to the Quaternary rate of about 15 m/m.y.

Comparison with Other Sites

Site 807 was the last site to be drilled on Leg 130, providing an opportunity for comparison with the results obtained previously. Only Neogene sedimentation patterns will be considered here; for additional topics, see Berger et al. (this volume).

The Neogene carbonate stratigraphy of Site 807 (Fig. 72; above 600 mbsf) shows the same general pattern as the profiles of Sites 805 and 806 (see "Summary and Conclusions" section, "Site 806" chapter, this volume). The major features are the broad carbonate maxima centered on the upper Miocene and the lowermost Miocene, and a minima in the middle Miocene and the Quaternary. The upper lower Miocene minimum seen in Site 805, and represented by hiatus formation in Sites 803 and 804, is not well expressed in Site 807. Additional measurements are necessary to check whether this discrepancy was caused by spotty sampling or by differences in carbonate patterns at different water depths, during the time when cold deep-water formation began.

The rather small depth difference between Sites 807 and 806 (300 m), at depths well above the present lysocline (3.3 km; Berger et al., 1982), results in very small absolute differences in carbonate percentages. The same is true for the comparison of carbonate values between Sites 807 and 805 (depth difference near 400 m). Averages for the last 15 m.y. are as follows (sequence is in the order of water depth):

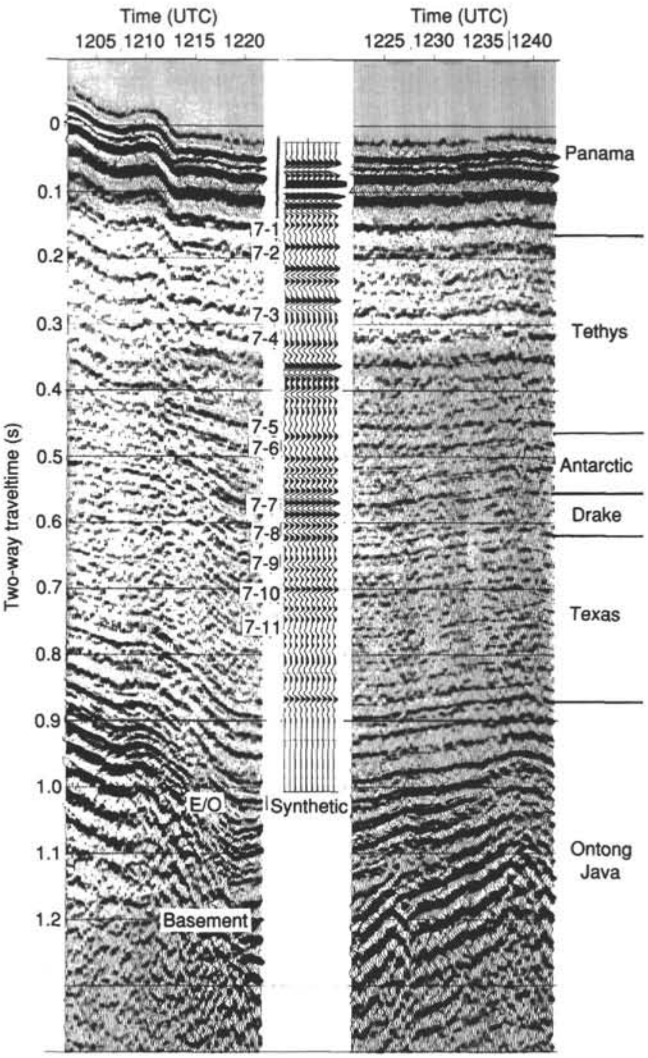

Figure 68. Comparison of synthetic seismogram and field record, Site 807.

Age	Site 806	Site 807	Site 805
0–5 Ma	90.65 ± 2.22	91.02 ± 1.768	9.52 ± 2.34
5–10 Ma	93.40 ± 1.26	92.80 ± 1.10	92.38 ± 2.04
10–15 Ma	92.95 ± 1.68	90.56 ± 1.85	91.40 ± 2.10

It can be seen that the carbonate percentages change very little over the interval, and that they overlap with each other's standard deviations. For the last 5 m.y., Site 807 has the highest carbonate values, presumably because of having less dilutant material than the shallower, equatorial Site 806 (volcanic input, silica). Between 5 and 10 Ma, the sequence is as expected from the depth differences. However, between 10 and 15 Ma, Site 807 has the lowest carbonate values of the three sites, presumably because at that period it is the closest to the equator, receiving an increased proportion of diatoms and radiolarians.

A comparison of sediment thicknesses of Site 807 with the other sites, for the major biostratigraphic subdivisions, is shown in Figure 74. The sedimentation rate trends are much clearer than the ones in the carbonate percentages. For the Neogene, Site 807 has 80% of the sediment accumulation of Site 806 and exceeds that of Site 805 by 11%. The proportional difference to Site 806 is greatest in the Pleistocene (70%) and is least in the late Pliocene and late Miocene (88% and 85%, respectively). The late Miocene "agreement" is presumably caused by the positions of Sites 807 and 806 relative to the equator. The close agreement in the late Pliocene is surprising, especially as it is followed by the strong difference in sedimentation rates in the Pleistocene. Apparently, the belt of high productivity was much wider in the late Pliocene than in the Pleistocene.

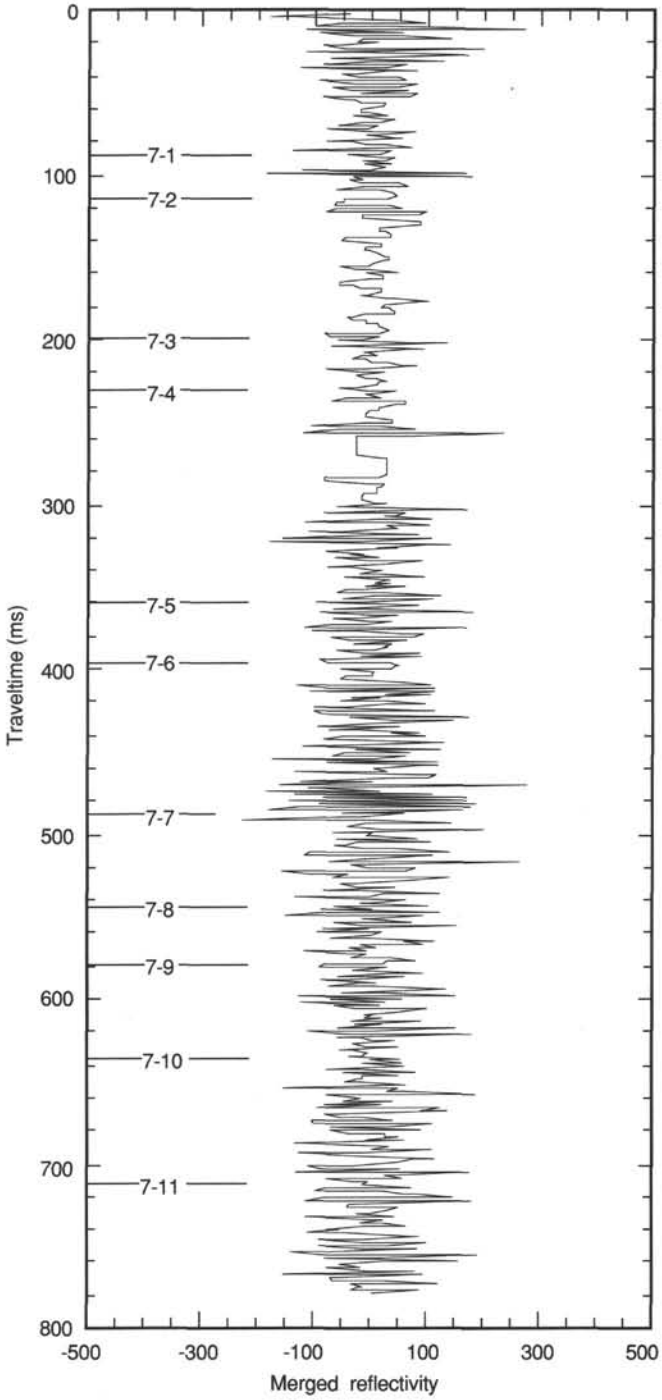

Figure 69. Reflection coefficient vs. traveltime, Hole 807A. See text for discussion of reflector picks.

A crude index of the Neogene dissolution gradient may be found by considering the ratios of the sediment thicknesses at

Table 19. Summary of traveltimes, depths, and ages for Site 807 reflectors.

Reflector	Traveltime Seismic (s)	Traveltime Synthetic (s)	Depth Seismic (m)	Depth Synthetic (m)	Age (Ma)	Series interval
7-1	0.100	0.110	80	87	3.6–3.8	Panama
7-2	0.150	0.140	120	114	4.6–4.8	Tethys
7-3	0.240	0.240	199	199	6.7	Tethys
7-4	0.278	0.275	235	230	7.4–7.5	Tethys
7-5	0.405	0.410	355	360	12.5–12.8	Antarctic
7-6	0.440	0.445	391	396	14.6–14.9	Antarctic
7-7	0.523	0.528	482	487	20.1–20.4	Drake
7-8	0.580	0.578	547	544	22.9–23.0	Drake
7-9	0.613	0.608	585	579	24.1–24.3	Texas
7-10	0.665	0.658	646	637	26.0–26.3	Texas
7-11	0.725	0.720	719	713	30.5–30.6	Texas

Notes: Depth and traveltimes to seismic events are picked on both the synthetic seismogram (synthetic) and the field record (seismic). Ages are from sedimentaiton rate curves (see "Sedimentation Rates" section, this chapter).

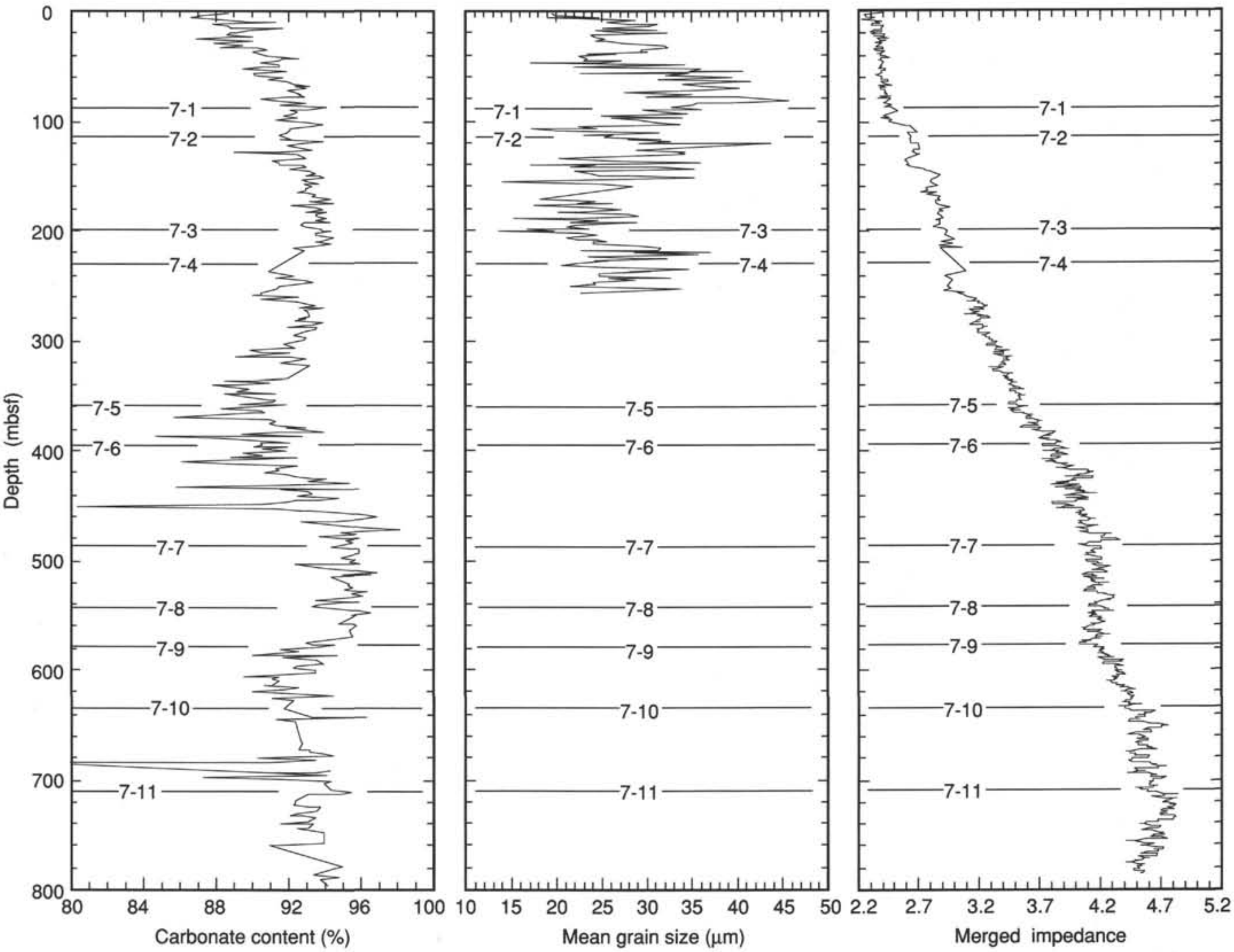

Figure 70. Carbonate content, grain size, and acoustic impedance vs. depth, Hole 807A. See text for discussion of reflector picks.

Site 806, 807, and 805. The gradient is supposed to increase over the last 25 m.y. (van Andel et al., 1975). No clear trend emerges from our data, however. The gradient appears to be greatest in the late early Miocene and early middle Miocene at the time of hiatus formation in the deeper sites. This time corresponds to NH2 in the hiatus scheme of Keller and Barron (1983) and to the onset of major Antarctic cooling (Savin et al., 1985).

The question why the pre-Neogene section is so much more riddled with hiatuses than the Neogene one must remain open. Of course, age itself is correlated with probability of removal (Moore and Heath, 1977). However, the history of the plateau, and especially its tectonic history as reflected in earthquakes, will have to be considered when discussing the distribution of major hiatuses. Regional mapping of seismic reflectors should help in this endeavor.

REFERENCES

Archie, G. E., 1942. The electrical resistivity log as an aid in determining some reservoir characteristics. *J. Petrol. Tech.*, 5:1–8.

Barron, J. A., 1985a. Late Eocene to Holocene diatom biostratigraphy of the equatorial Pacific Ocean, Deep Sea Drilling Project Leg 85. In Mayer, L., Theyer, F., Thomas, E., et al., *Init. Repts. DSDP*, 85: Washington (U.S. Govt. Printing Office), 413–456.

_______, 1985b. Late Eocene to Holocene diatom biostratigraphy of the equatorial Pacific Ocean, Deep Sea Drilling Project Leg 85. *In* Mayer, L., Theyer, F., Thomas, E., et al., *Init. Repts. DSDP*, 85: Washington (U.S. Govt. Printing Office), 413–456.

Berger, W. H., 1989. Global maps of ocean productivity. *In* Berger, W. H., Smetacek, V. S., and Wefer, G. (Eds.), *Productivity of the Oceans: Present and Past:* New York (Wiley and Sons), 429–455.

Berger, W. H., Bonneau, M.-C., and Parker, F. L., 1982. Foraminifera on the deep-sea floor: lysocline and dissolution rate. *Oceanol. Acta*, 5:249–258.

Berger, W. H., Johnson, T. C., and Hamilton, E. L., 1977. Sedimentation on Ontong-Java Plateau: observations on a classic "carbonate monitor." *In* Anderson, N. R., and Malahoff, A. (Eds.), *The Fate of Fossil Fuel CO2* in the Oceans: New York (Plenum Press), 543–567.

Berggren, W. A., Kent, D. V., and Van Couvering, J. A., 1985. The Neogene: Part 2. Neogene geochronology and chronostratigraphy. *In* Snelling, N. J. (Ed.), *The Chronology of the Geological Record.* Mem. Geol. Soc. (London), 10:211–260.

Emeis, K.-C., and Kvenvolden, K. A., 1986. Shipboard organic geochemistry on *JOIDES Resolution. ODP Tech. Note*, No. 7.

Fenner, J., 1984. Eocene-Oligocene planktic diatom stratigraphy in the low latitudes and the high southern latitudes. *Micropaleontology*, 30:319–342.

_______, 1985. Late Cretaceous to Oligocene planktic diatoms. *In* Bolli, H. M., Saunders, J. B., and Perch-Nielsen, K. (Eds.), *Plankton Stratigraphy:* Cambridge (Cambridge Univ. Press), 713–762.

Floyd, P. A., 1986. Petrology and geochemistry of oceanic intraplate sheet-flow basalts, Nauru Basin, Deep Sea Drilling Project Leg 89. *In* Moberly, R., Schlanger, S. O., et al., *Init. Repts. DSDP*, 89: Washington (U.S. Govt. Printing Office), 471–497.

Gieskes, J. M., 1981. Deep-sea drilling interstitial water studies: implications for chemical alteration of the oceanic crust, Layers I and II. *In* Warme, J. E., Douglas, R. G., and Winterer, E. L. (Eds.), *The Deep Sea Drilling Project: A Decade of Progress.* Spec. Publ., Soc. Econ. Paleontol. Mineral., 32:149–167.

Gordon, R. G., 1983. Late Cretaceous apparent polar wander of the Pacific Plate: evidence for a rapid shift of the Pacific hotspots with respect to the spin axis. *Geophys. Res. Lett.*, 10:709–712.

_______, in press. Test for bias in paleomagnetically determined paleolatitudes from Pacific Plate DSDP sediments. *J. Geophys. Res.*

Hammond, S. R., Kroenke, L. W., and Theyer, F., 1975. Northward motion of the Ontong-Java Plateau between 110 and 30 m.y.: a paleomagnetic investigation of DSDP Site 289. *In* Andrews, J. E., Packham, G., et al., *Init. Repts. DSDP*, 30: Washington (U.S. Govt. Printing Office) 415–418.

Hooper, P. R., 1988. The Columbia River basalt. *In* Macdougall, J. D. (Ed.), *Continental Flood Basalts:* Dordrecht, The Netherlands (Kluwer Academic Publ.), 1–34.

Hussong, D. M., Wipperman, L. K., and Kroenke, L. W., 1979. The crustal structure of the Ontong Java and Manihiki oceanic plateaus. *J. Geophys. Res.*, 84:6003–6010.

Jackson, E. D., Bargar, K. E., Fabbi, B. P., and Heropoulos, C., 1976. Petrology of the basaltic rocks drilled on Leg 33 of the Deep Sea Drilling Project. *In* Schlanger, S. O., Jackson, E. D., et al., *Init. Repts. DSDP*, 33: Washington (U.S. Govt. Printing Office), 571–630.

Johanssen, A., 1931. *A Descriptive Petrography of the Igneous Rocks* (Vol. 1): Chicago (Univ. of Chicago Press).

Karlin, R., and Levi, S., 1985. Geochemical and sedimentological control of the magnetic properties of hemipelagic sediments. *J. Geophys. Res.*, 90:10,373–10,392.

Keller, G., and Barron, J. A., 1983. Paleoceanographic implications of Miocene deep-sea hiatuses. *Geol. Soc. Am. Bull.*, 94:590–613.

Kroenke, L. W., 1972. Geology of the Ontong-Java Plateau. *Hawaii Inst. Geophys. Rep.*, HIG 72-5.

_______, 1984. Cenozoic tectonic development of the Southwest Pacific. *U. N. ESCAP, CCOP/SOPAC, Tech. Bull.*, No. 6.

Kroenke, L. W., Jouannic, C., and Woodward, P. (Comps.), 1983. Bathymetry of the Southwest Pacific: Chart 1 of the Geophysical Atlas of the Southwest Pacific, CCOP/SOPAC.

Mahoney, J. J., 1987. An isotopic survey of Pacific oceanic plateaus: implications for their nature and origin. *In* Keating, B. H., Fryer, P., Batiza, R., and Boehlert, G. W. (Eds.), *Seamounts, Islands, and Atolls.* Am. Geophys. Union Monogr., 43:207–220.

Mammerickx, J., and Smith, S. M., 1985. *Bathymetry of the North Central Pacific:* Boulder, CO (Geological Society of America), Map and Chart Ser., No. MC-52.

Manivit, H., and Feinberg, H., 1984. Correlation of magnetostratigraphy and nannofossil biostratigraphy in Upper Cretaceous and lower Paleocene sediments of the Walvis Ridge area. *In* Moore, T. C., Jr., Rabinowitz, P. D., et al., *Init. Repts. DSDP*, 74: Washington (U.S. Govt. Printing Office), 469–474.

Mayer, L. A., Shipley, T. H., Theyer, F., Wilkens, R. W., and Winterer, E. L., 1985. Seismic modeling and paleoceanography at Deep Sea Drilling Project Site 574. *In* Mayer, L. A., Theyer, F., Thomas, E., et al., *Init. Repts. DSDP*, 85: Washington, (U.S. Govt. Printing Office), 947–970.

McDuff, R. E., and Gieskes, J. M., 1976. Calcium and magnesium in DSDP interstitial waters: diffusion or reaction? *Earth Planet. Sci. Lett.*, 33:1–10.

Monechi, S., 1985. Campanian to Pleistocene calcareous nannofossil stratigraphy from the northwest Pacific Ocean, Deep Sea Drilling Project Leg 86. *In* Heath, G. R., Burckle, L. H., et al., *Init. Repts. DSDP*, 86: Washington (U.S. Govt. Printing Office), 301–336.

Moore, T., 1971. Radiolaria. *In* Tracey, J. I., Jr., Sutton, G. H., et al., *Init. Repts. DSDP*, 8: Washington (U.S. Govt. Printing Office), 727–775.

Moore, T. C., and Heath, G. R., 1977. Survival of deep-sea sedimentary sections. *Earth Planet. Sci. Lett.*, 37:71–80.

Ogushwitz, P. R., 1985. Applicability of the Biot theory. III. Wave speeds versus depth in marine sediments. *J. Acoust. Soc. Am.*, 77:453–463.

Okada, H., 1990. Quaternary and Paleogene calcareous nannofossils, Leg 115. *In* Duncan, R. A., Backman, J., Peterson, L. C., et al., *Proc. ODP, Sci. Results*, 115: College Station, TX (Ocean Drilling Program), 129–174.

Pessagno, E. A., Jr., 1977. *Lower Cretaceous Radiolarian Biostratigraphy of the Great Valley Sequence and Franciscan Complex, California Coast Ranges.* Spec. Publ., Cushman Found. Foraminiferal Res., No. 15.

Petronotis, K. E., and Gordon, R. G., 1989. Age dependence of skewness of magnetic anomalies above seafloor formed at the Pacific-Kula spreading center. *Geophys. Res. Lett.*, 16:315–318.

Romein, A.J.T., 1979. Lineages in early Paleogene calcareous nannoplankton. *Utrecht Micropaleontol. Bull.*, 22:1–231.

Sager, W. W., 1987. Late Eocene and Maestrichtian paleomagnetic poles for the Pacific plate: implications for the validity of seamount paleomagnetic data. *Tectonophysics*, 144:301–314.

Sanfilippo, A., and Riedel, W. R., 1985. Cretaceous Radiolaria. *In* Bolli, H. M., Saunders, J. B., and Perch-Nielsen, K. (Eds.), *Plankton Stratigraphy:* Cambridge (Cambridge Univ. Press), 573–630.

Sanfilippo, A., Westberg-Smith, M. J., and Riedel, W. R., 1985. Cenozoic Radiolaria. *In* Bolli, H. M., Saunders, J. B., and Perch-Nielsen, K. (Eds.), *Plankton Stratigraphy:* Cambridge (Cambridge Univ. Press), 631–712.

Saunders, J. B., Bernoulli, D., Müller-Merz, E., Oberhänsli, H., Perch-Nielsen, K., Riedel, W. R., Sanfilippo, A., and Torrini, R., Jr., 1984. Stratigraphy of late middle Eocene to early Oligocene in the Bath Cliff section Barbados, West Indies. *Micropaleontology*, 30:390–425.

Savin, S. M., Abel, L., Barrera, E., Hodell, D., Kennett, J. P., Murphy, M., Keller, G., Killingley, J., and Vincent, E., 1985. The evolution of Miocene surface and near-surface marine temperatures: oxygen isotopic evidence. *In* Kennett, J. P. (Ed.), *The Miocene Ocean: Paleoceanography and Biogeography*. Mem. Geol. Soc. Am., 163:49–82.

Schlanger, S. O., and Douglas, R. G., 1974. The pelagic ooze-chalk-limestone transition and its implication for marine stratigraphy. *In* Hsü, K. J., and Jenkyns, H. C. (Eds.), *Pelagic Sediments: On Land and Under the Sea*. Spec. Publ., Int. Assoc. Sedimentol., 1:117–148.

Shafik, S., 1975. Nannofossil biostratigraphy of the southwest Pacific, Deep Sea Drilling Project Leg 30. *In* Andrews, J. E., Packham, G., et al., *Init. Repts. DSDP*, 30: Washington (U.S. Govt. Printing Office), 549–598.

Shipboard Scientific Party, 1971. Site 64. *In* Winterer, E. L., Riedel, W. R., et al., 1971. *Init. Repts. DSDP*, 7: Washington (U.S. Govt. Printing Office), 473–606.

———, 1975a. Site 288. *In* Andrews, J. E., Packham, G., et al., *Init. Repts. DSDP*, 30: Washington (U.S. Govt. Printing Office), 175–229.

———, 1975b. Site 289. *In* Andrews, J. E., Packham, G., et al., *Init. Repts. DSDP*, 30: Washington (U.S. Govt. Printing Office), 231–281.

———, 1986a. Site 586. *In* Moberly, R., Schlanger, S. O., et al., *Init. Repts. DSDP*, 89: Washington (U.S. Govt. Printing Office), 213–281.

———, 1986b. Site 586: western equatorial Pacific. *In* Kennett, J. P., von der Borch, C. C., et al., *Init. Repts. DSDP*, 90: Washington (U.S. Govt. Printing Office), 19–114.

———, 1989. Explanatory notes. *In* Prell, W. L., Niitsuma, N., et al., *Proc. ODP, Init. Repts.*, 117: College Station, TX (Ocean Drilling Program), 11–33.

Tarduno, J. A., in press. Brief reversed polarity interval during the Cretaceous Normal Polarity Superchron. *Geology*.

Tarduno, J., Sliter, W. V., Bralower, T. J., McWilliams, M., Premoli Silva, I., and Ogg, J. G., 1989. M-sequence reversals recorded in DSDP sediment cores from the western Mid-Pacific Mountains and Magellan Rise. *Geol. Soc. Am. Bull.*, 101:1306–1316.

Thierstein, H. R., 1979. Paleoceanographic implications of organic carbon and carbonate distribution in Mesozoic deep sea sediments. *In* Talwani, M., Hay, W., and Ryan, W.B.F. (Eds.), *Deep Drilling Results in the Atlantic Ocean:* Am. Geophys. Union, Maurice Ewing Ser., 3:249–274.

———, 1981. Late Cretaceous nannoplankton and the change at the Cretaceous/Tertiary boundary. *In* Warme, J. E., et al. (Eds.), *The Deep Sea Drilling Project: A Decade of Progress*. Spec. Publ., Soc. Econ. Paleontol. Mineral., 32:355–394.

Thierstein, H. R., and Okada, H., 1979. The Cretaceous/Tertiary boundary event in the North Atlantic. *In* Tucholke, B. E., Vogt, P. R., et al., *Init. Repts. DSDP*, 43: Washington (U.S. Govt. Printing Office), 601–616.

Thurow, J., 1988. Cretaceous radiolarians of the North Atlantic Ocean: ODP Leg 103 (Sites 638, 640, and 641) and DSDP Legs 93 (Site 603) and 47B (Site 398). *In* Boillot, G., Winterer, E. L., et al., *Proc. ODP, Sci. Results*, 103: College Station, TX (Ocean Drilling Program), 379–418.

Toksöz, M. N., Cheng, C. H., and Timur, A., 1976. Velocities of seismic waves in porous rocks. *Geophysics*, 41:621–645.

Tucholke, B. E., and Vogt, P. R., 1979. Western North Atlantic: sedimentation evolution and aspects of tectonic history. *In* Tucholke, B. E., Vogt, P. R., et al., *Init. Repts. DSDP*, 43: Washington (U.S. Govt. Printing Office), 791–825.

van Andel, T. H., Heath, G. R., and Moore, T. C., Jr., 1975. Cenozoic history and paleoceanography of the central equatorial Pacific. *Mem. Geol. Soc. Am.*, 143:1–134.

Wood, A. B., 1930. *A Textbook of Sound:* London (G. Bell and Sons).

Wyllie, M.R.J., Gregory, A. R., and Gardner, G.H.F., 1958. An experimental investigation of factors affecting elastic wave velocities in porous media. *Geophysics*, 23:459–493.

Ms 130A-109

NOTE: All core description forms ("barrel sheets") and core photographs have been printed on coated paper and bound as Section 5, near the back of the book, beginning on page 559.

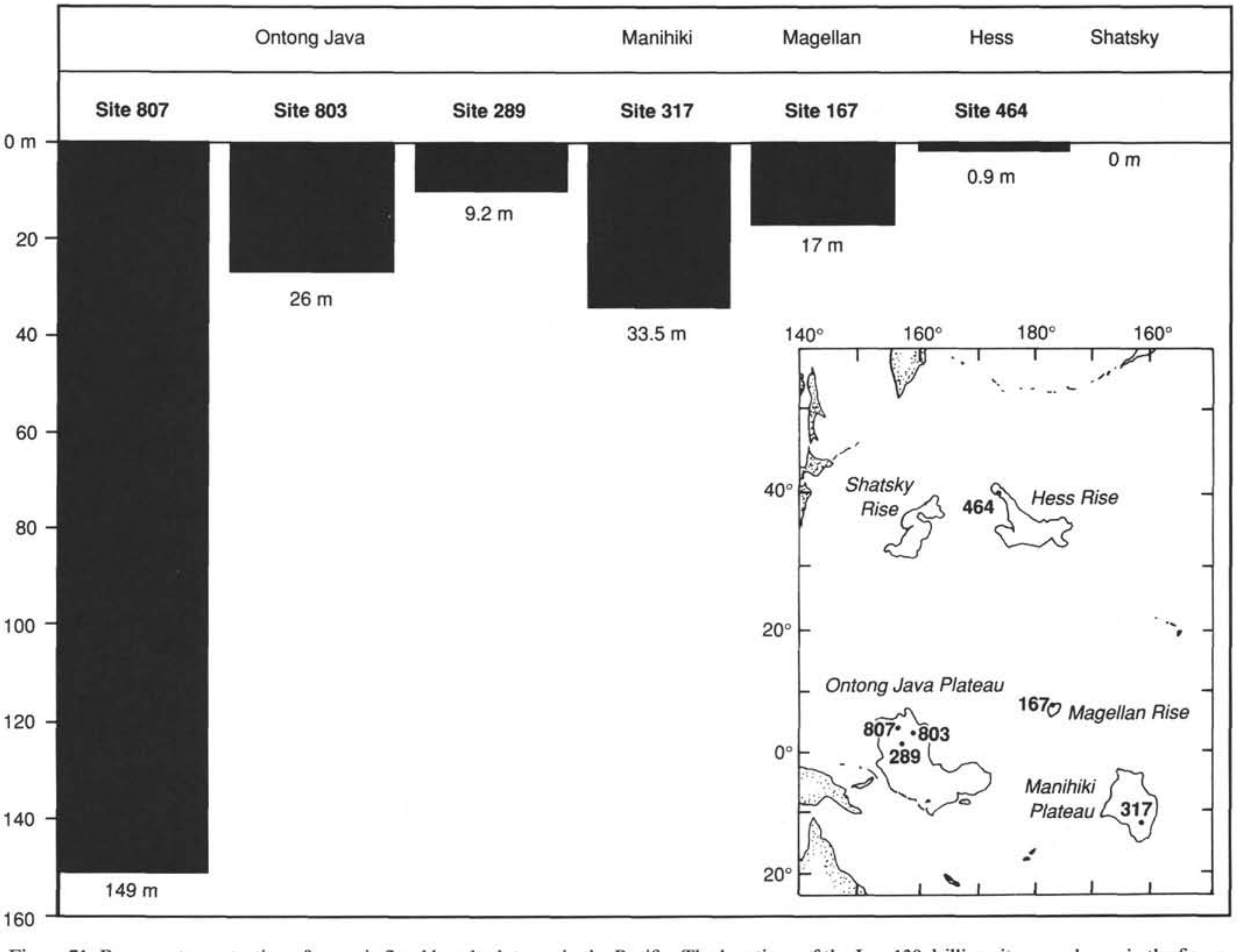

Figure 71. Basement penetration of oceanic flood basalt plateaus in the Pacific. The locations of the Leg 130 drilling sites are shown in the figure inset. The Icelandic Plateau in the Atlantic is slightly smaller than the Magellan Plateau, the smallest of the Pacific plateaus.

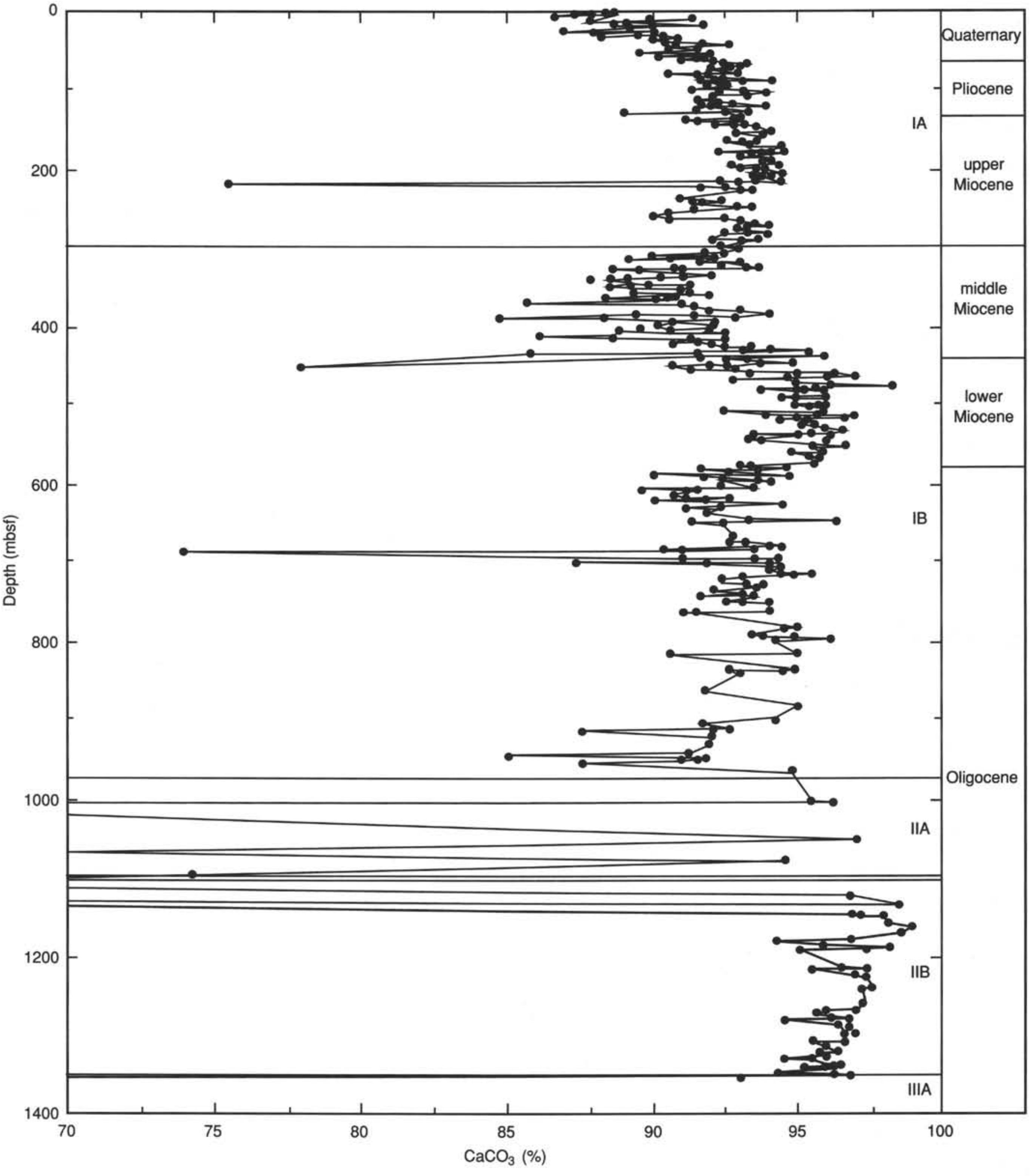

Figure 72. Carbonate content, Site 807 (from Holes 807A and 807C). Lithologic units and ages are shown on the right side of the figure.

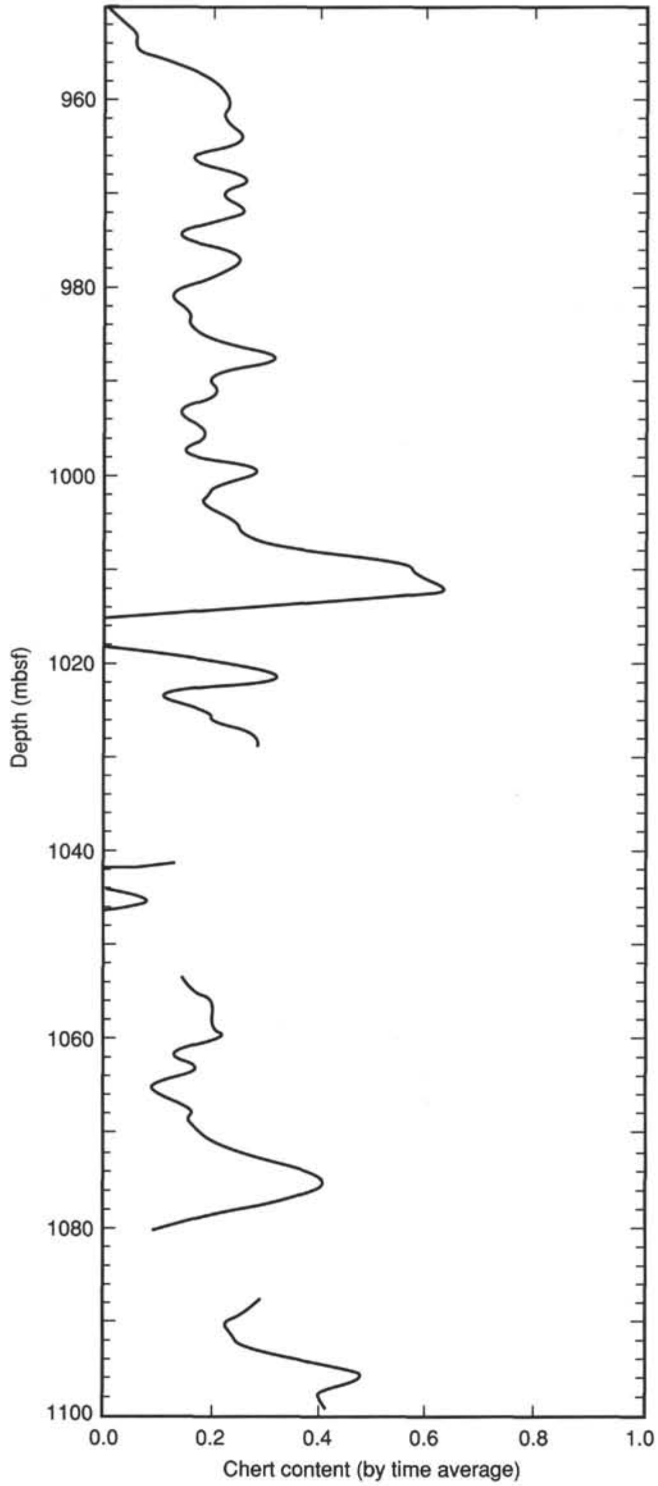

Figure 73. Chert content, Hole 807C, based on a time average of the velocity logging data (chert = 4.0 km/s, limestone = 2.5 km/s).

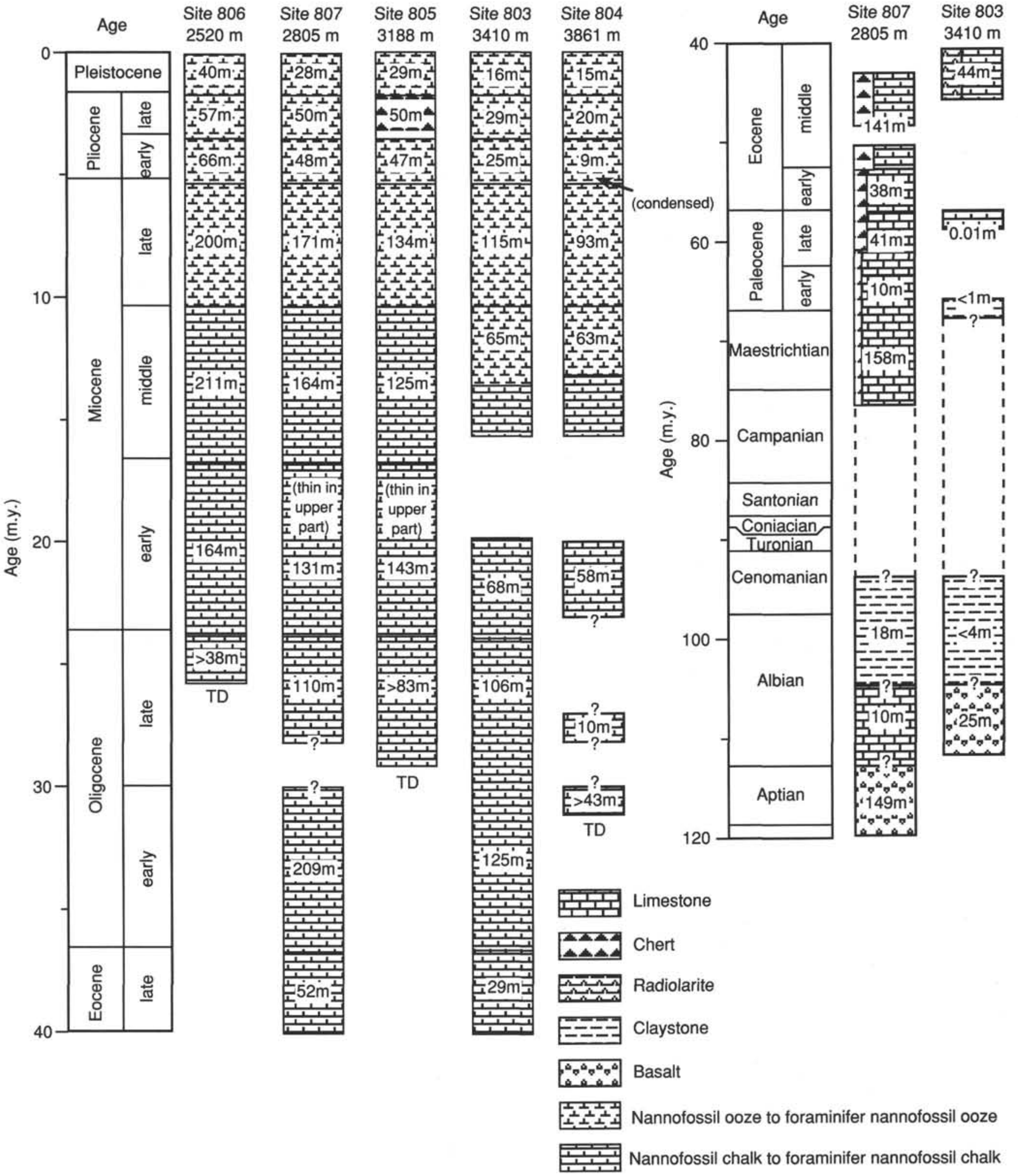

Figure 74. Leg 130 sites drilled on the Ontong Java Plateau, western equatorial Pacific, arranged according to depth. Recovered sediment is shown as a function of age rather than as depth below seafloor to highlight hiatuses within the drilled section. Sediment thicknesses given in the columns are approximate values based on shipboard biostratigraphy. Note, for example, that the upper Miocene at Site 806 is approximately 200 m thick and thins downslope to approximately 93 m at Site 804. Age control through much of the Cretaceous is poor as a result of the dissolution of calcareous microfossils.

Hole 807A: Resistivity-Sonic-Gamma Ray Log Summary

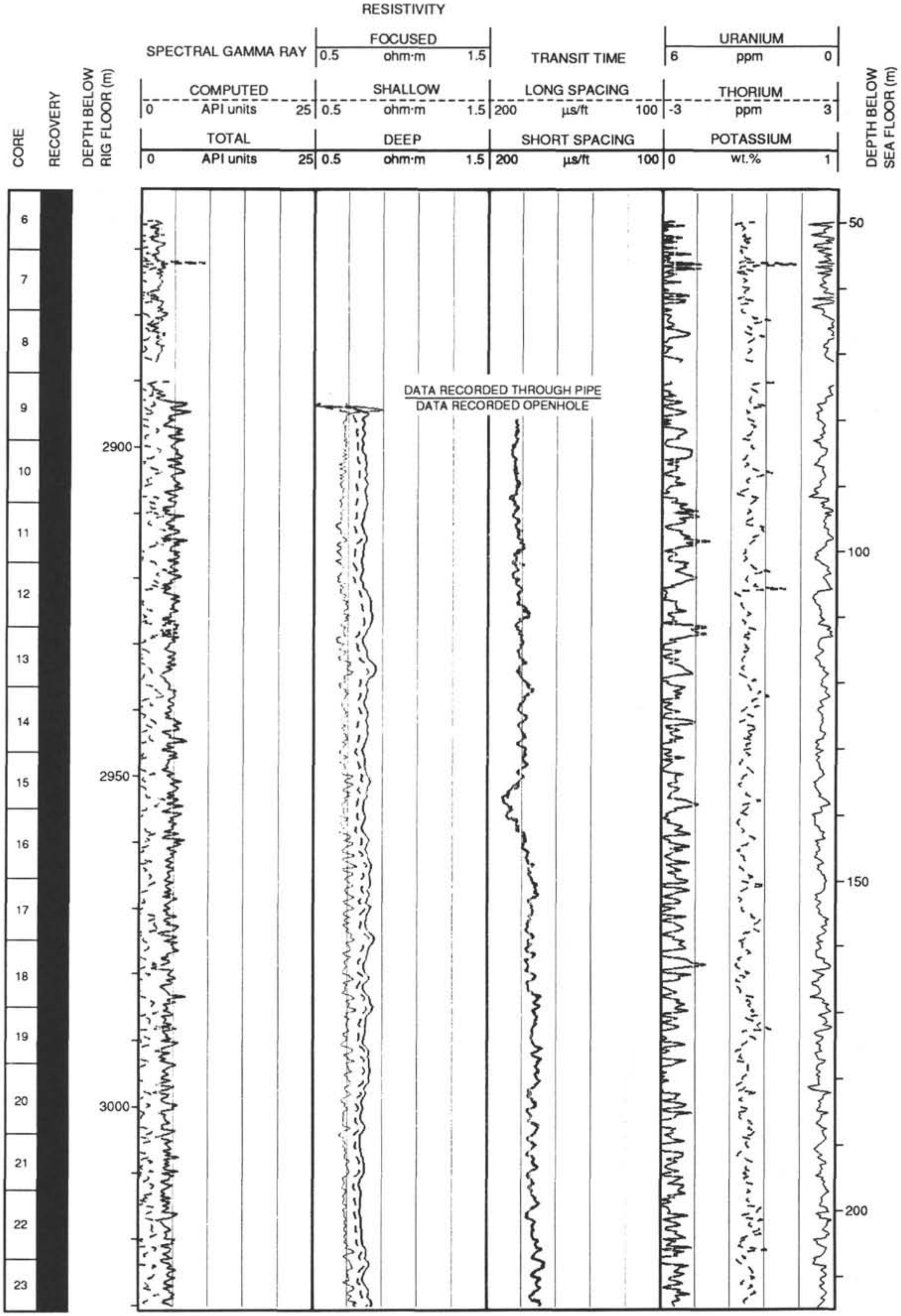

Hole 807A: Resistivity-Sonic-Gamma Ray Log Summary (continued)

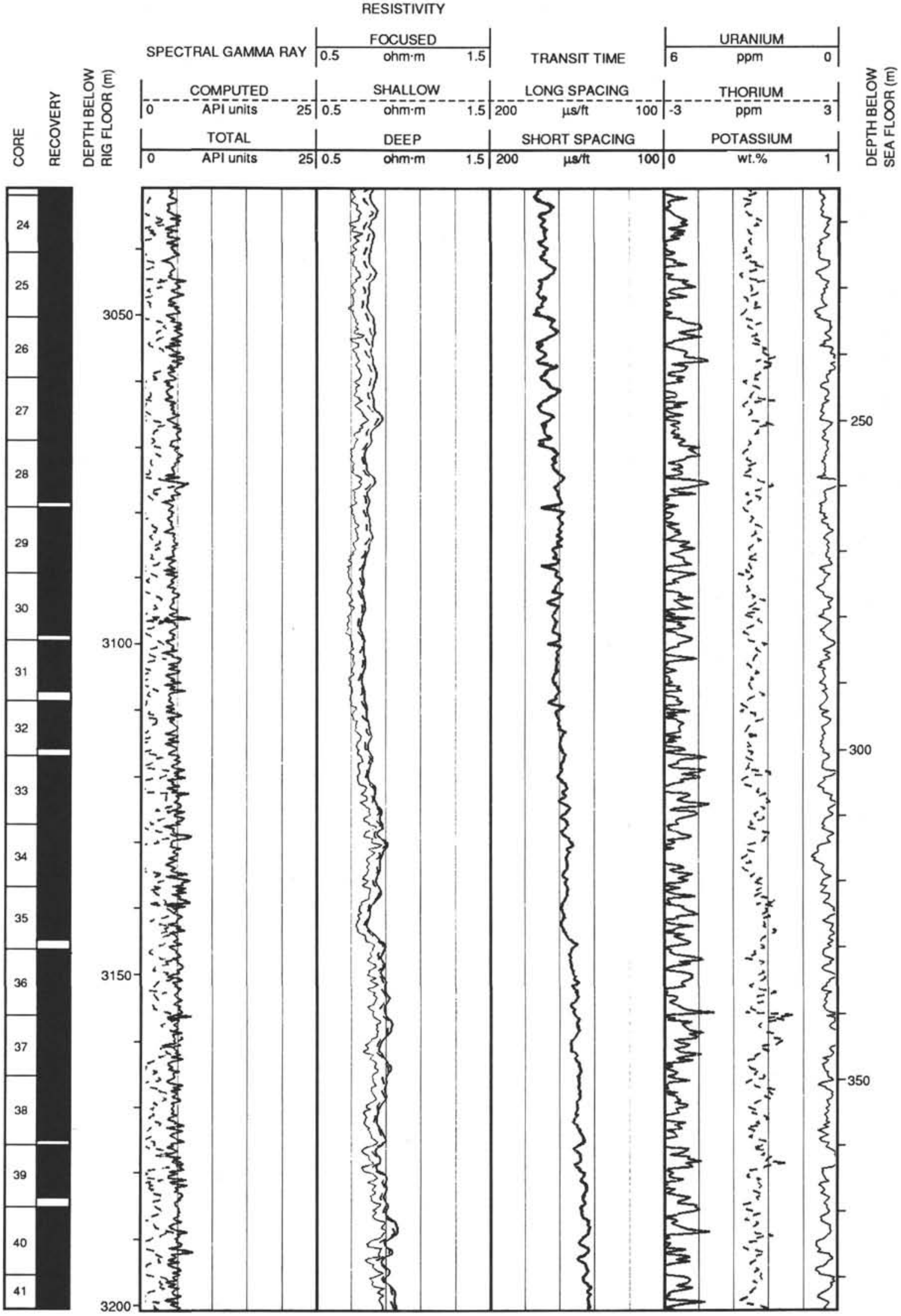

Hole 807A: Resistivity-Sonic-Gamma Ray Log Summary (continued)

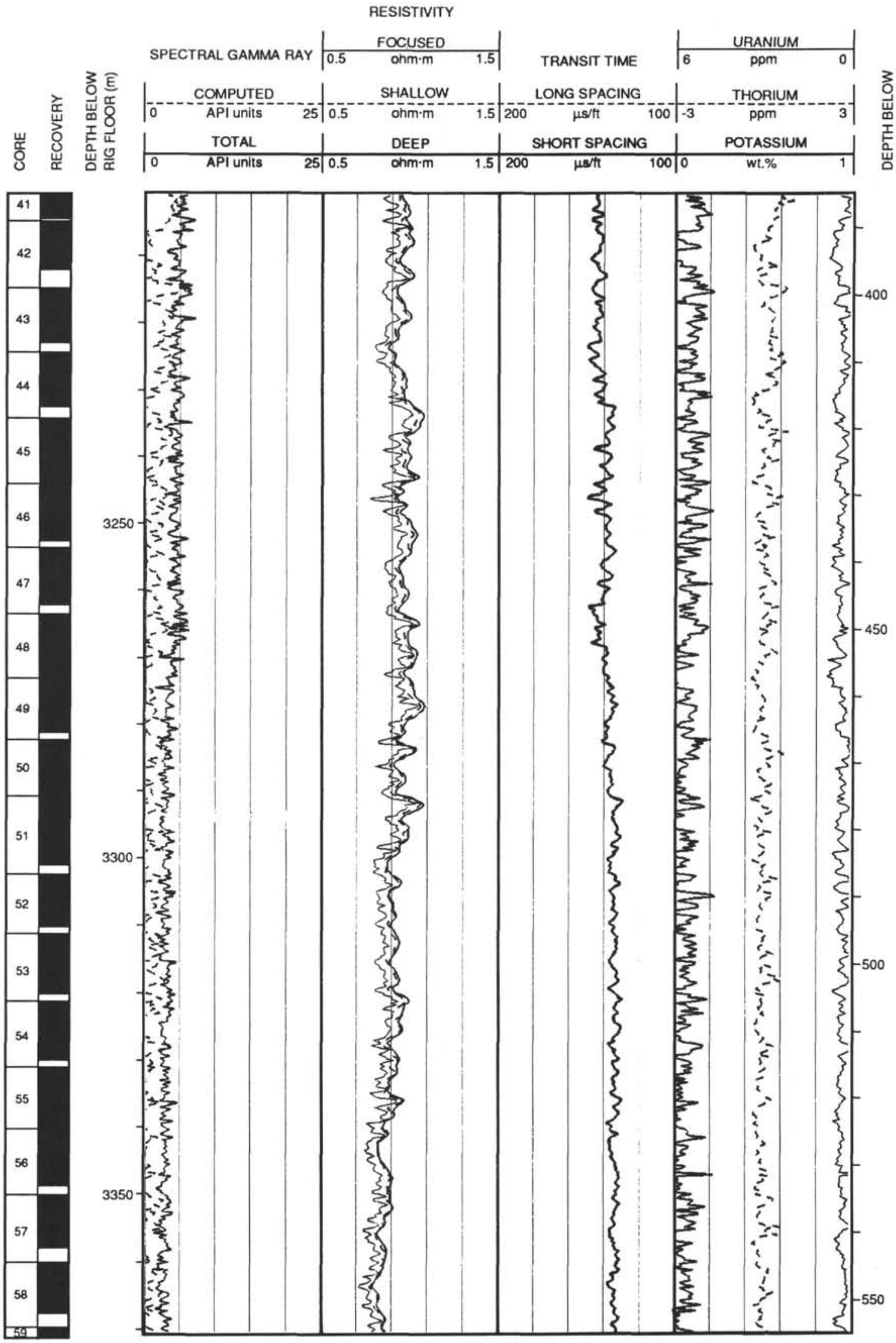

Hole 807A: Resistivity-Sonic-Gamma Ray Log Summary (continued)

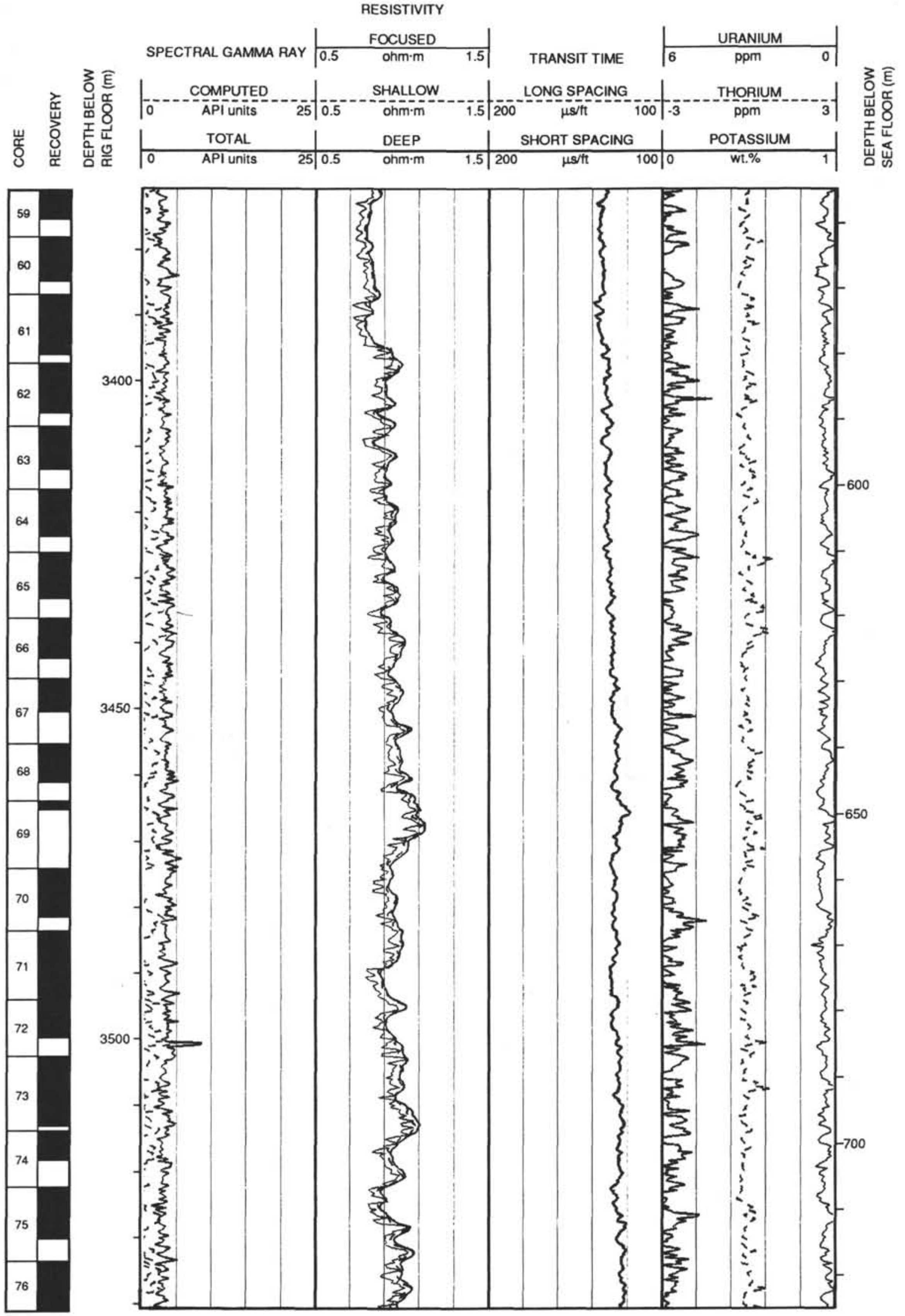

Hole 807A: Resistivity-Sonic-Gamma Ray Log Summary (continued)

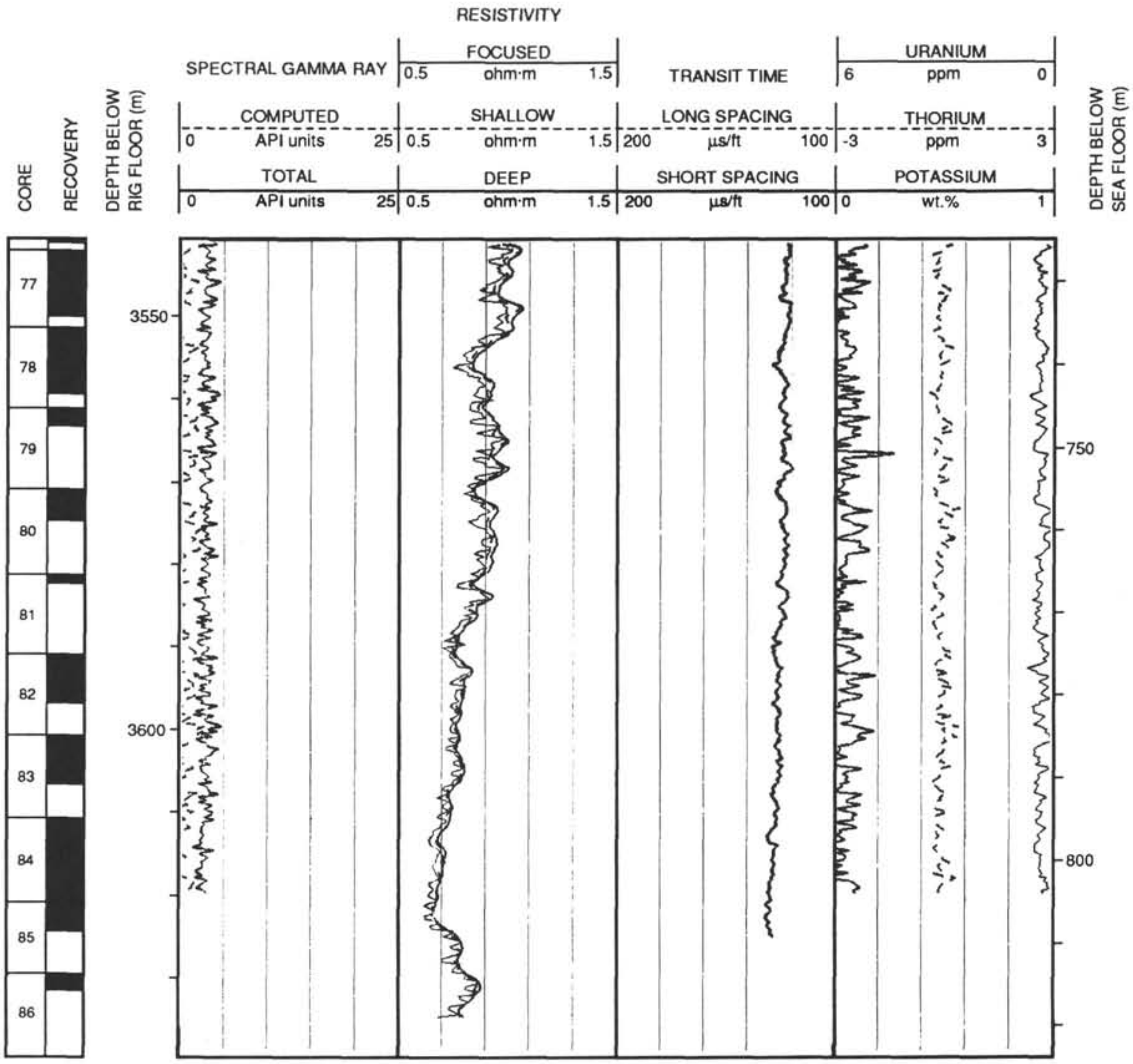

Hole 807A: Density-Gamma Ray-Aluminum Log Summary

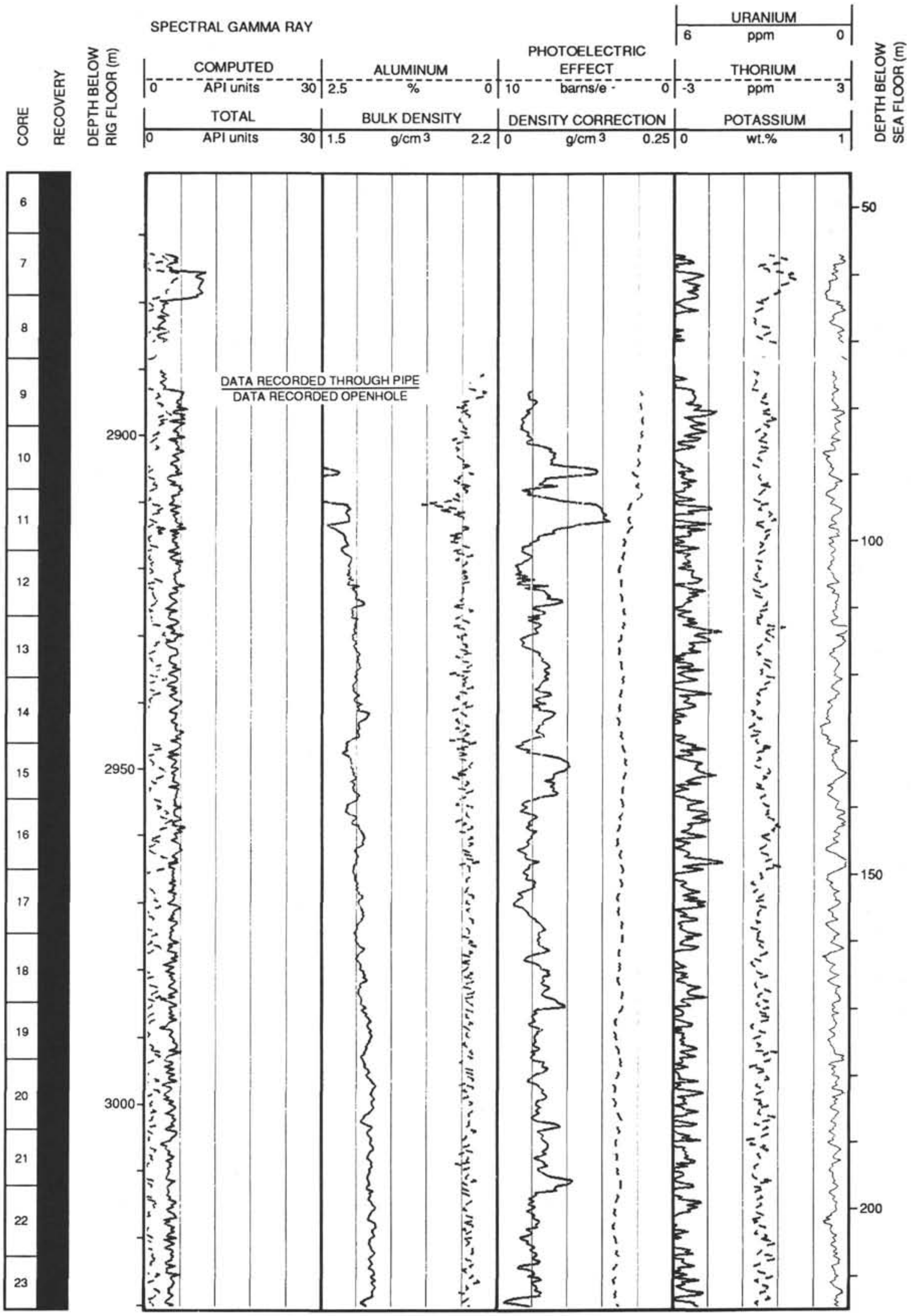

Hole 807A: Density-Gamma Ray-Aluminum Log Summary (continued)

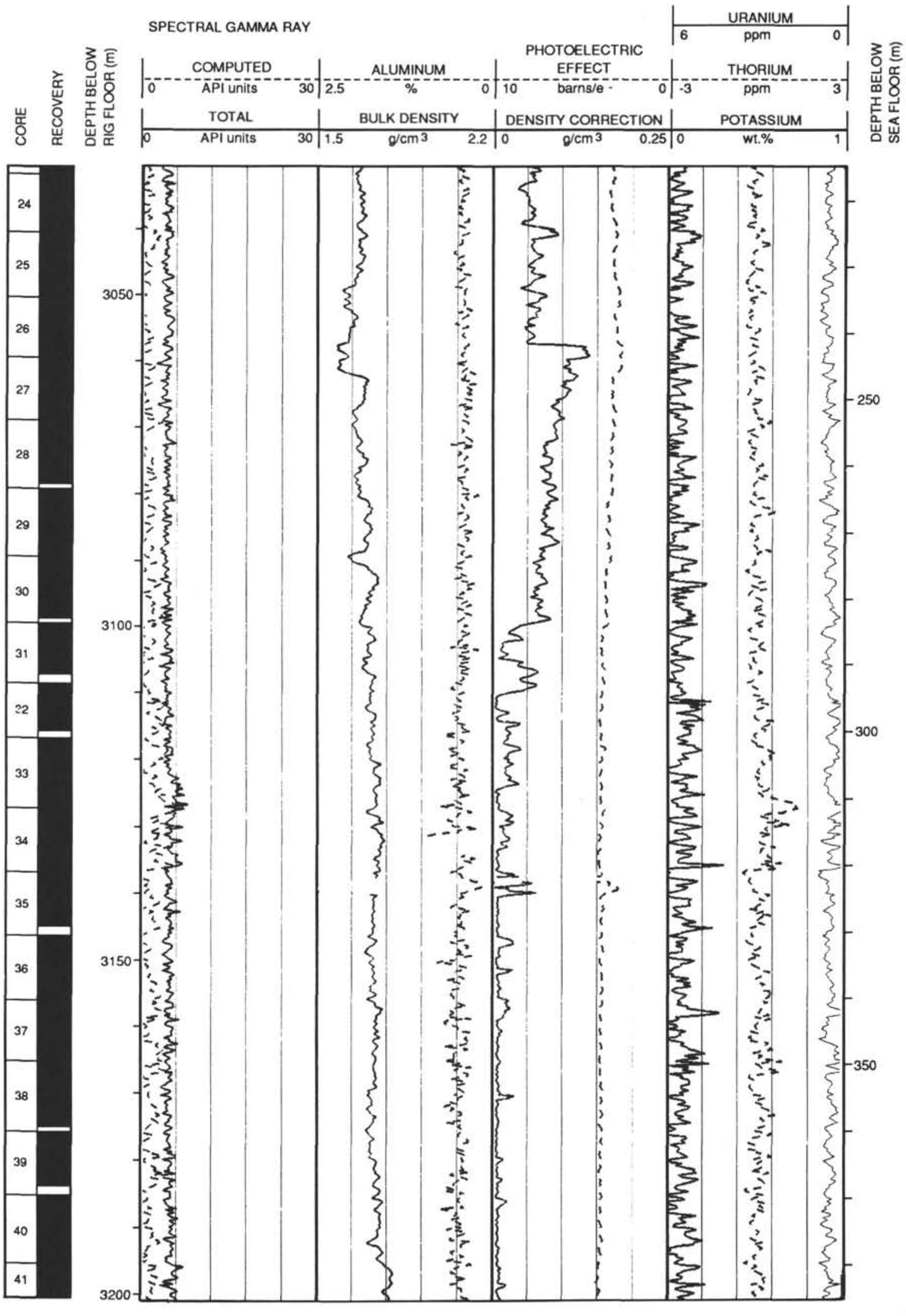

Hole 807A: Density-Gamma Ray-Aluminum Log Summary (continued)

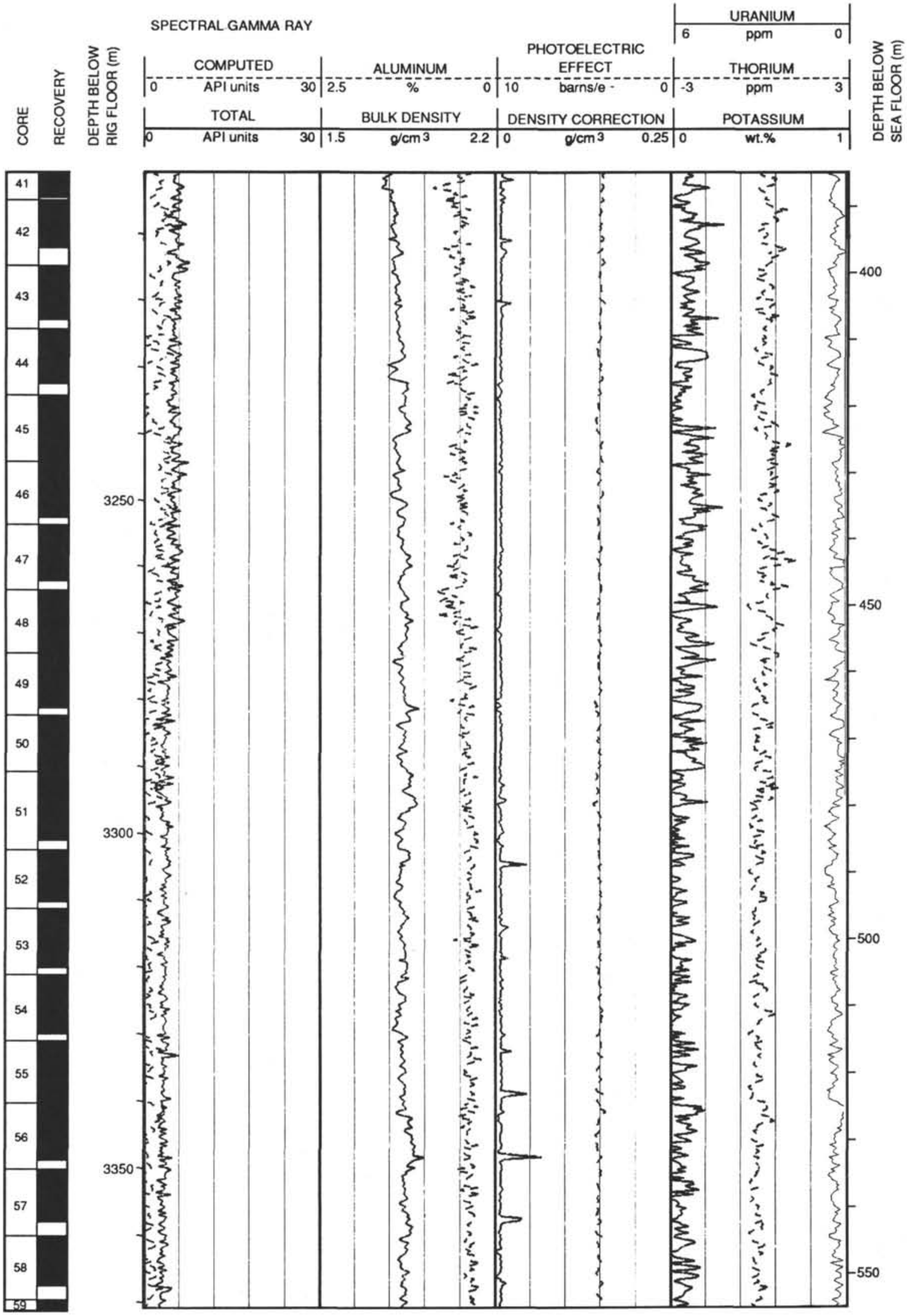

Hole 807A: Density-Gamma Ray-Aluminum Log Summary (continued)

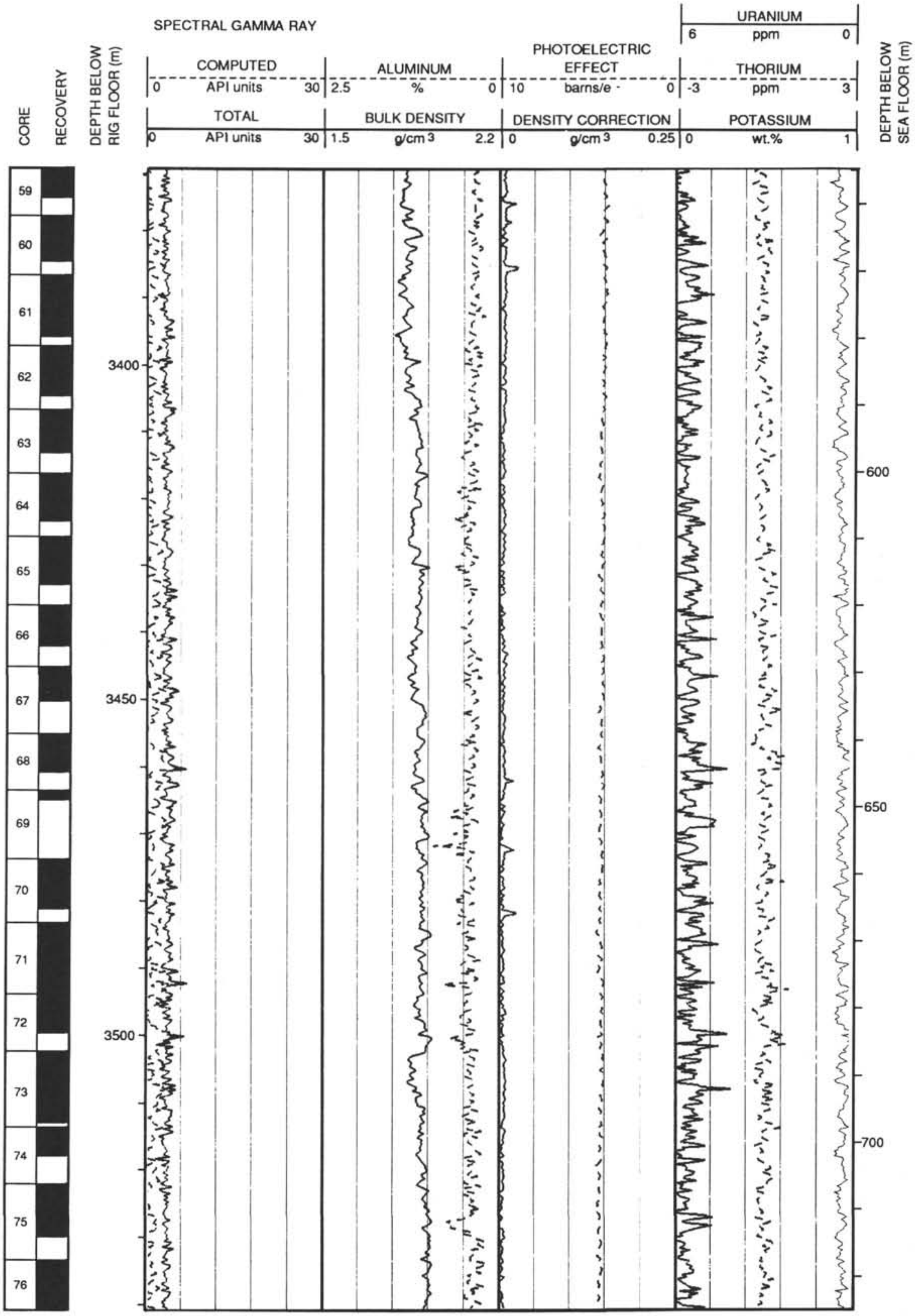

Hole 807A: Density-Gamma Ray-Aluminum Log Summary (continued)

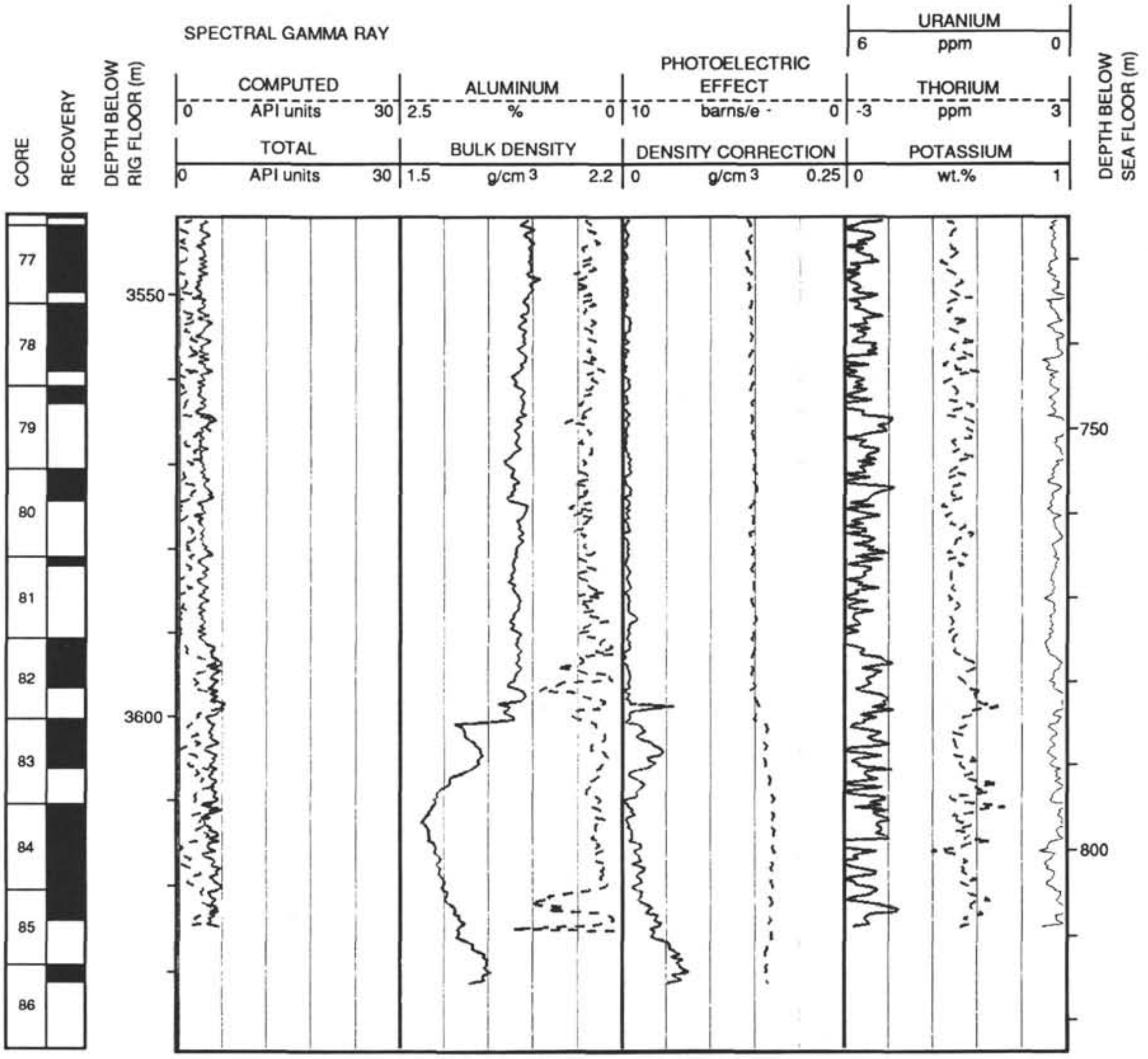

Hole 807C: Resistivity-Sonic-Gamma Ray Log Summary

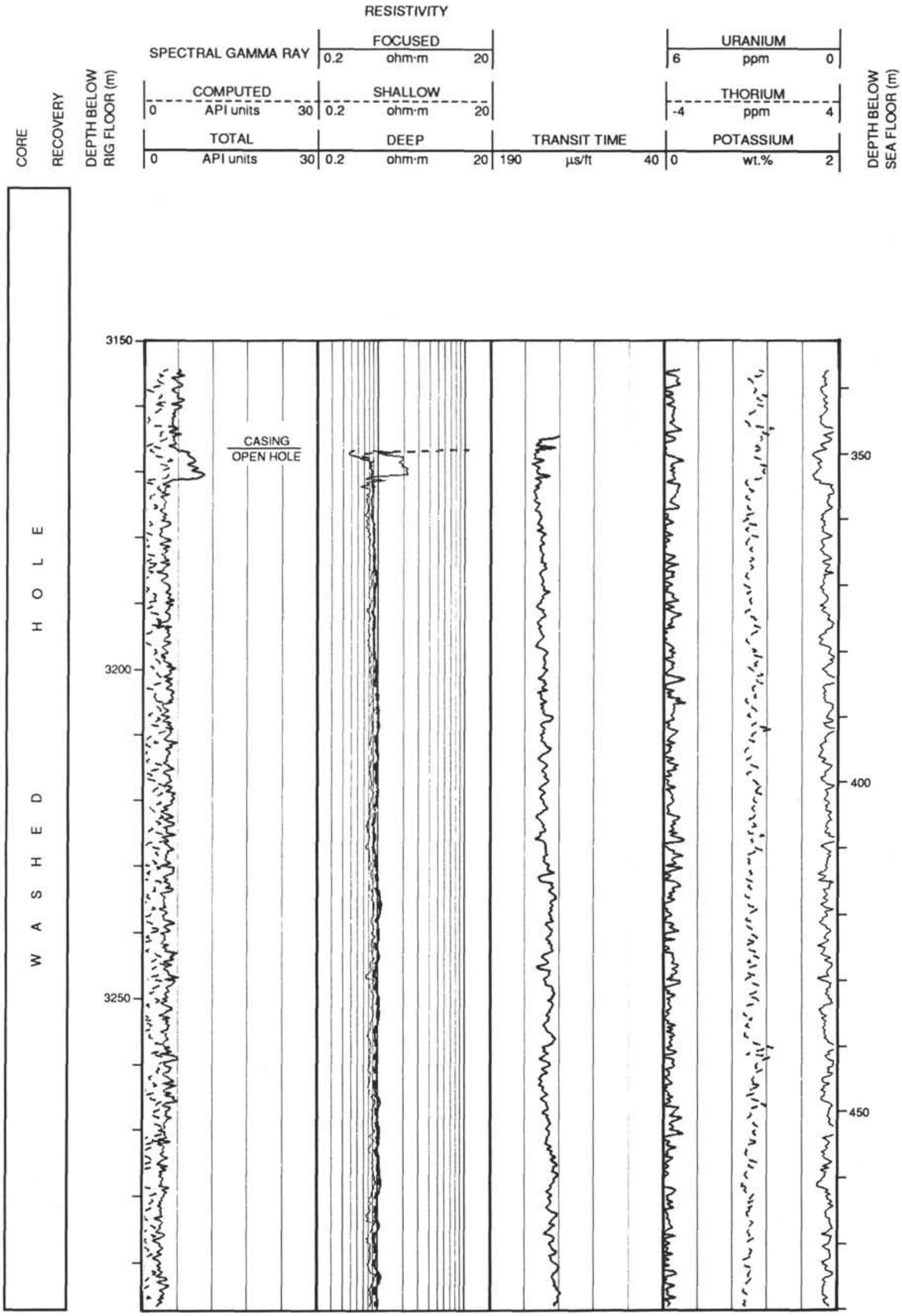

Hole 807C: Resistivity-Sonic-Gamma Ray Log Summary (continued)

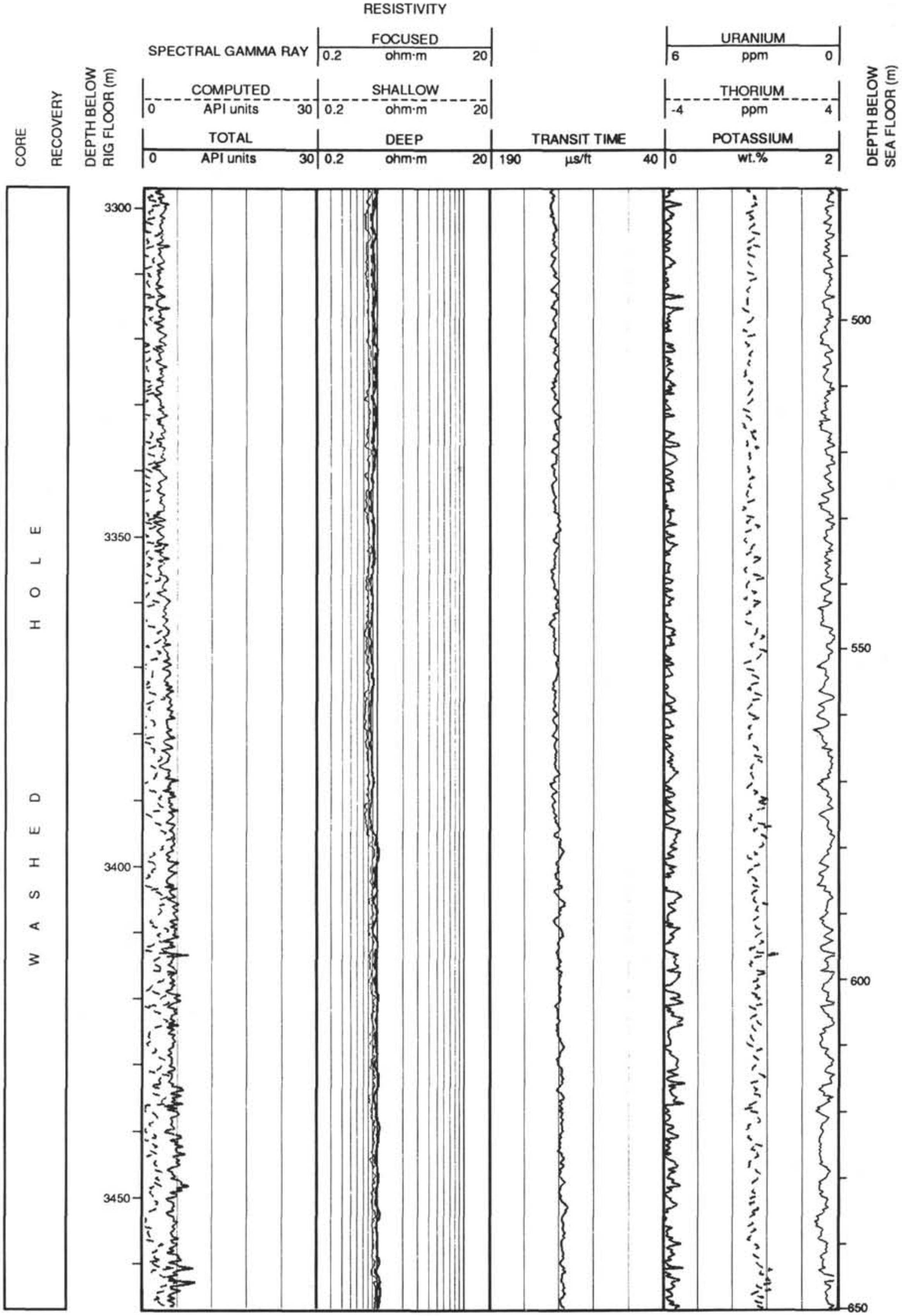

Hole 807C: Resistivity-Sonic-Gamma Ray Log Summary (continued)

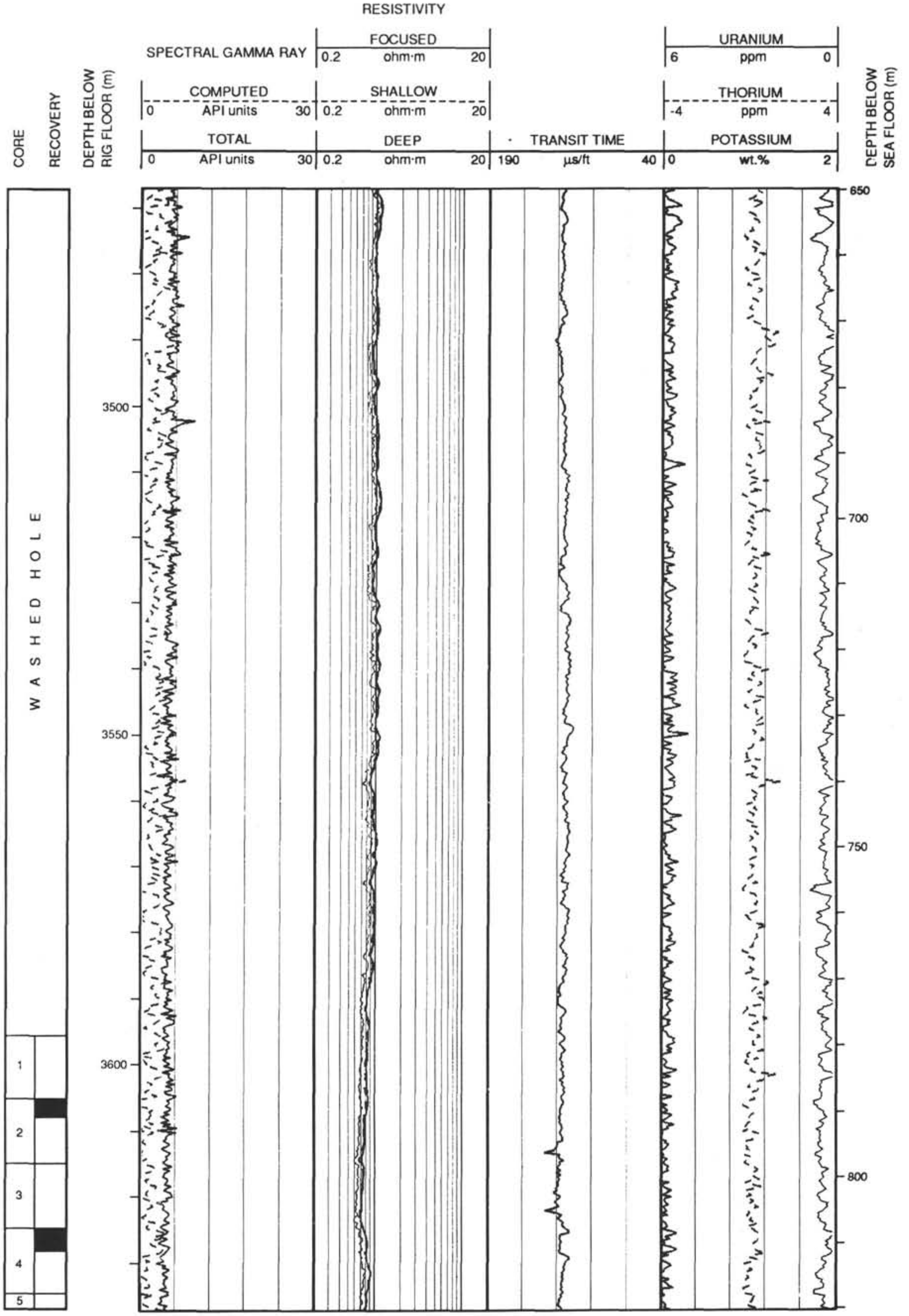

Hole 807C: Resistivity-Sonic-Gamma Ray Log Summary (continued)

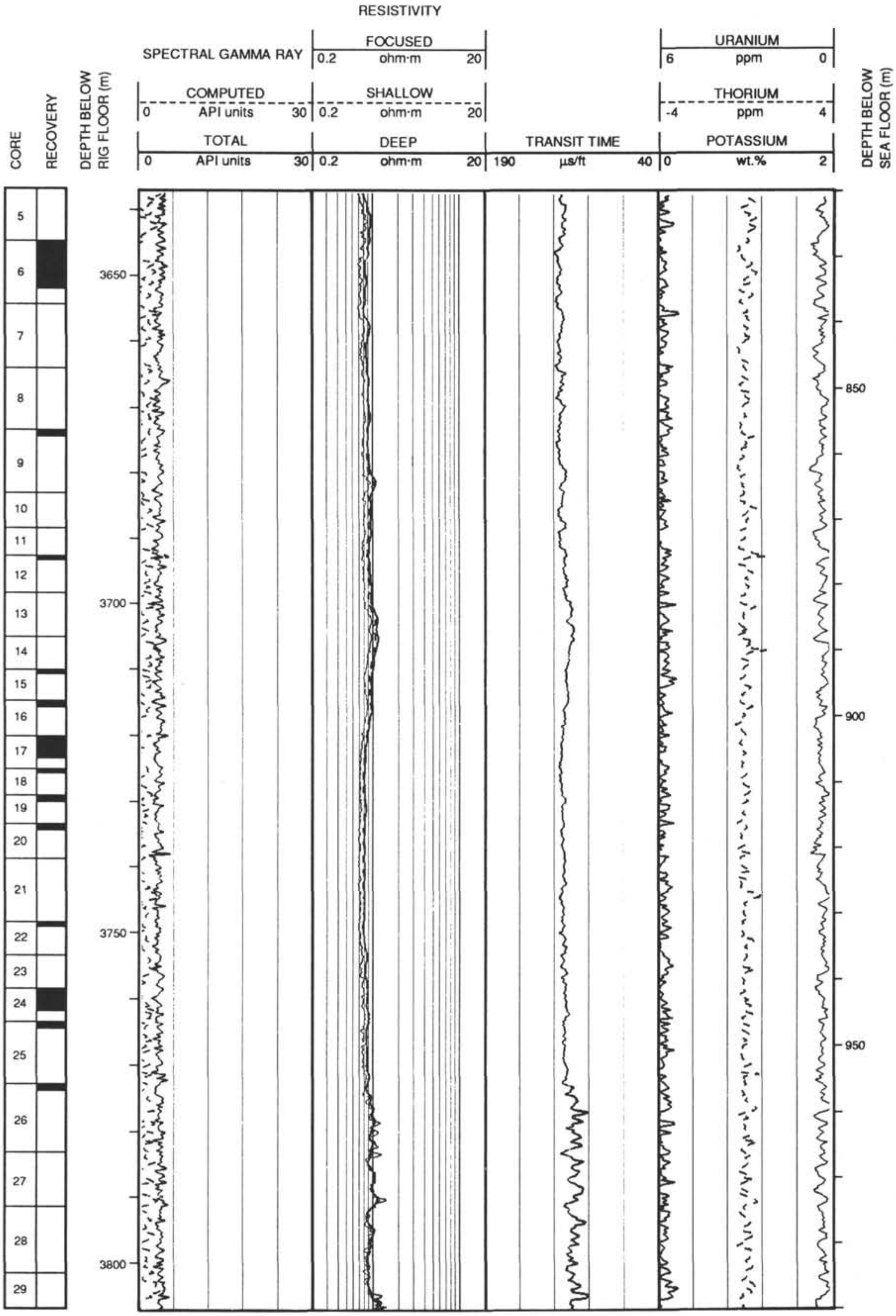

Hole 807C: Resistivity-Sonic-Gamma Ray Log Summary (continued)

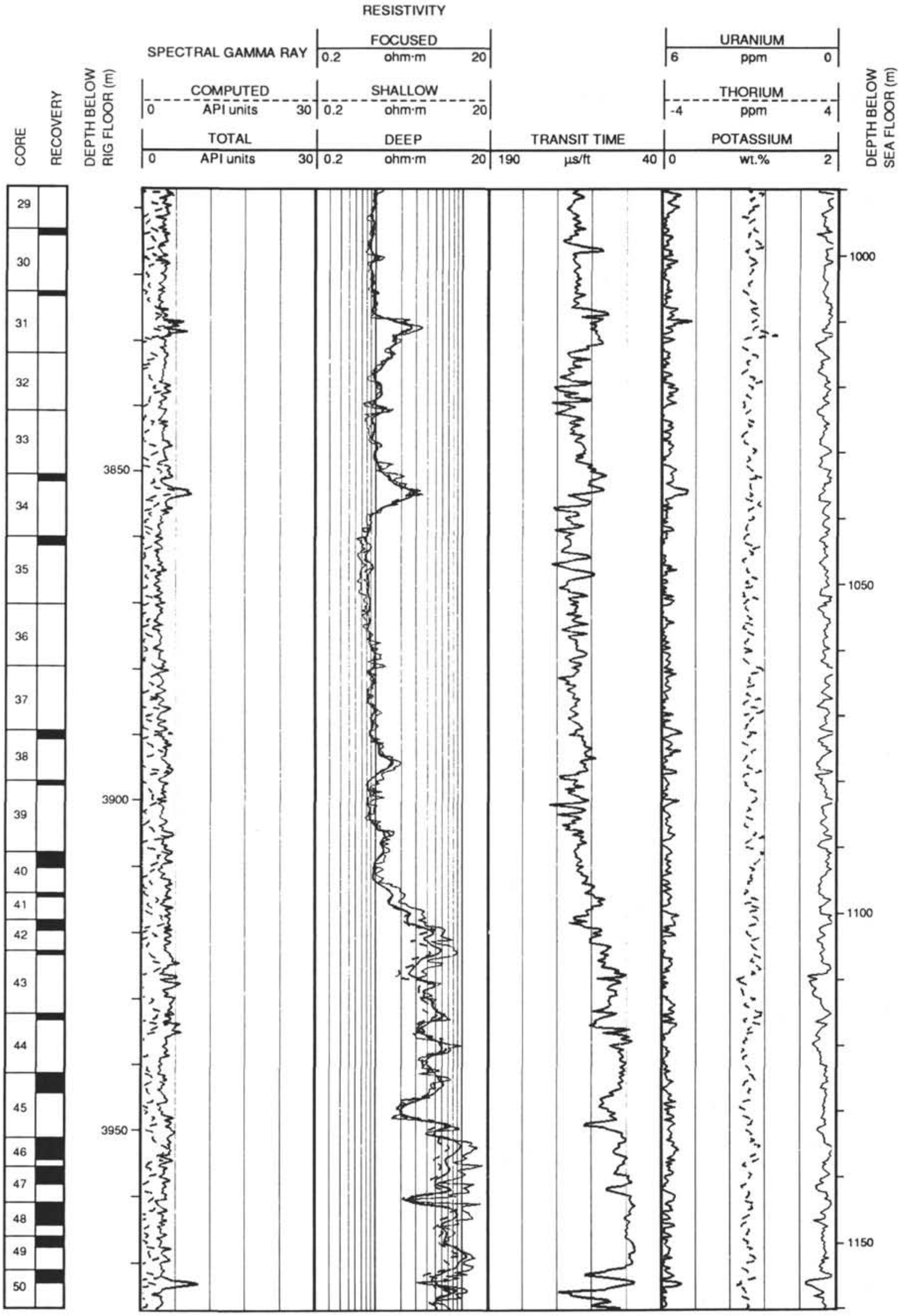

Hole 807C: Resistivity-Sonic-Gamma Ray Log Summary (continued)

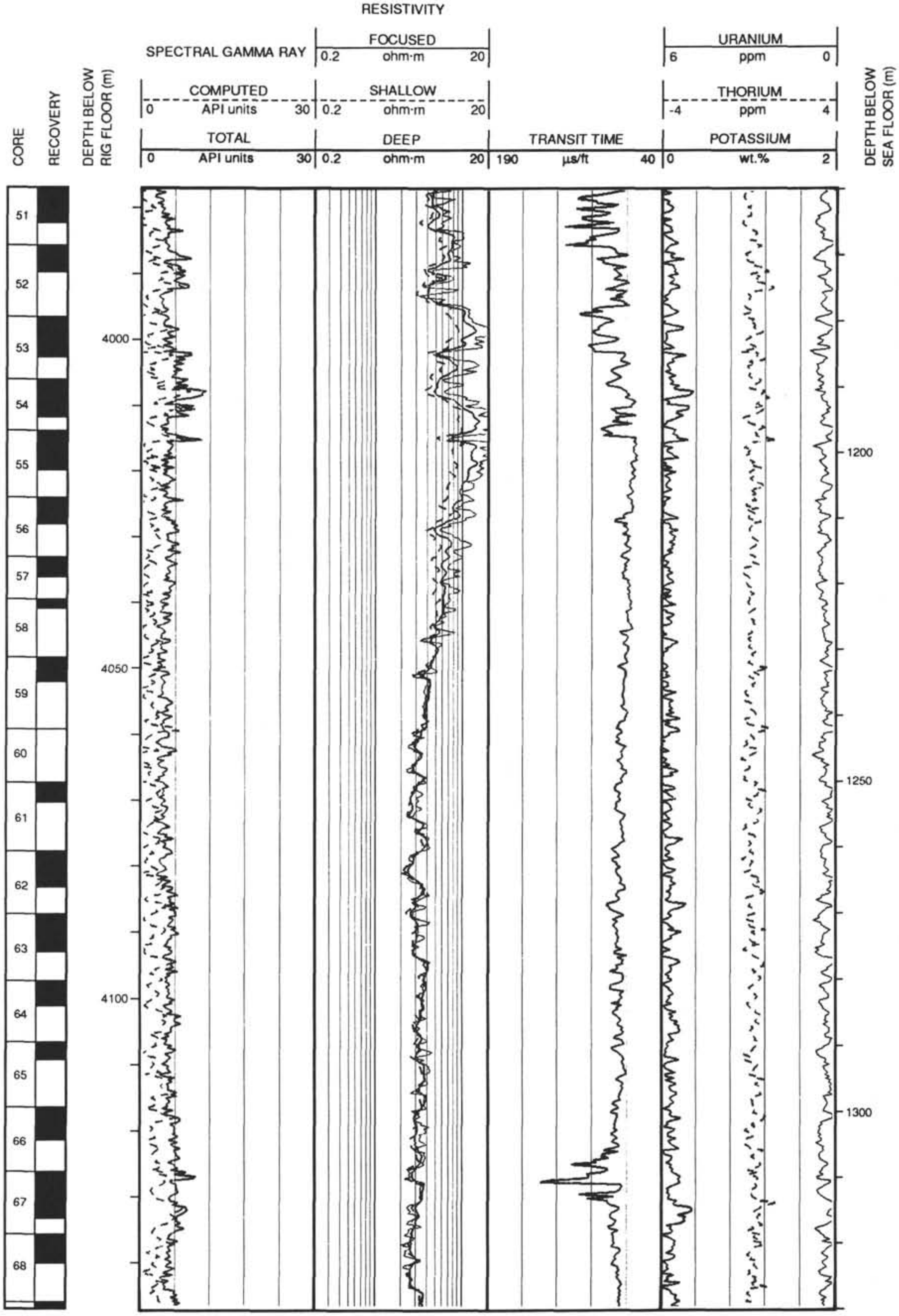

Hole 807C: Resistivity-Sonic-Gamma Ray Log Summary (continued)

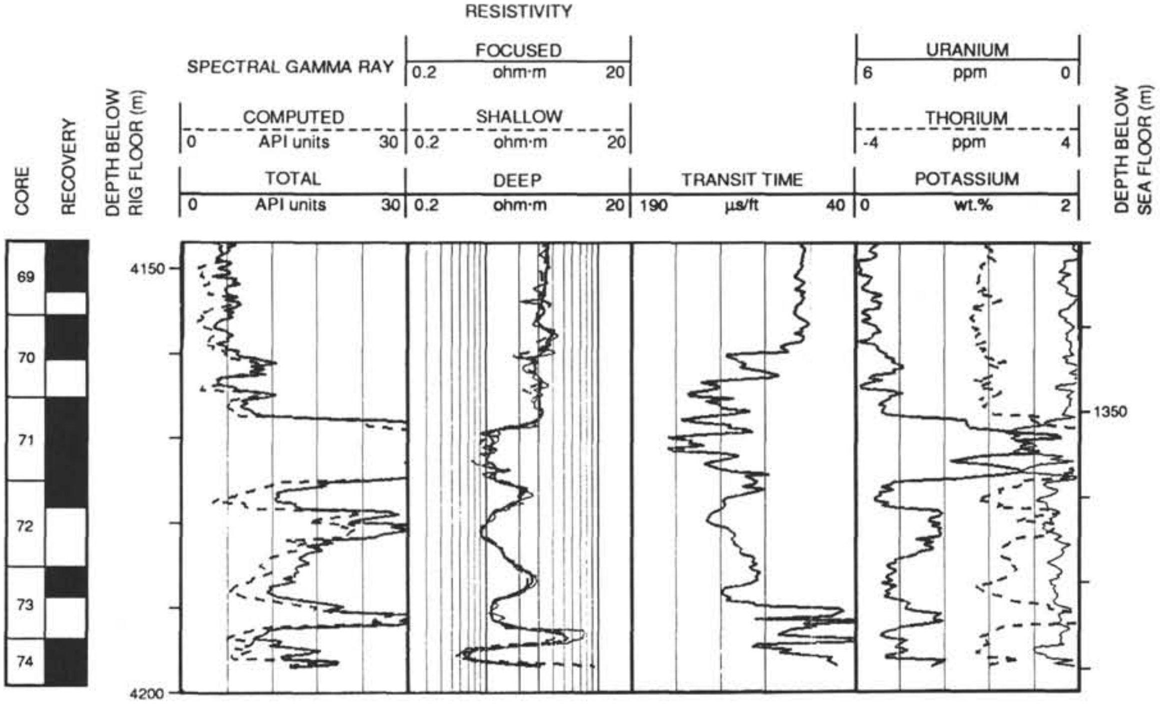

Hole 807C: Resistivity-Sonic-Gamma Ray Log Summary (continued)

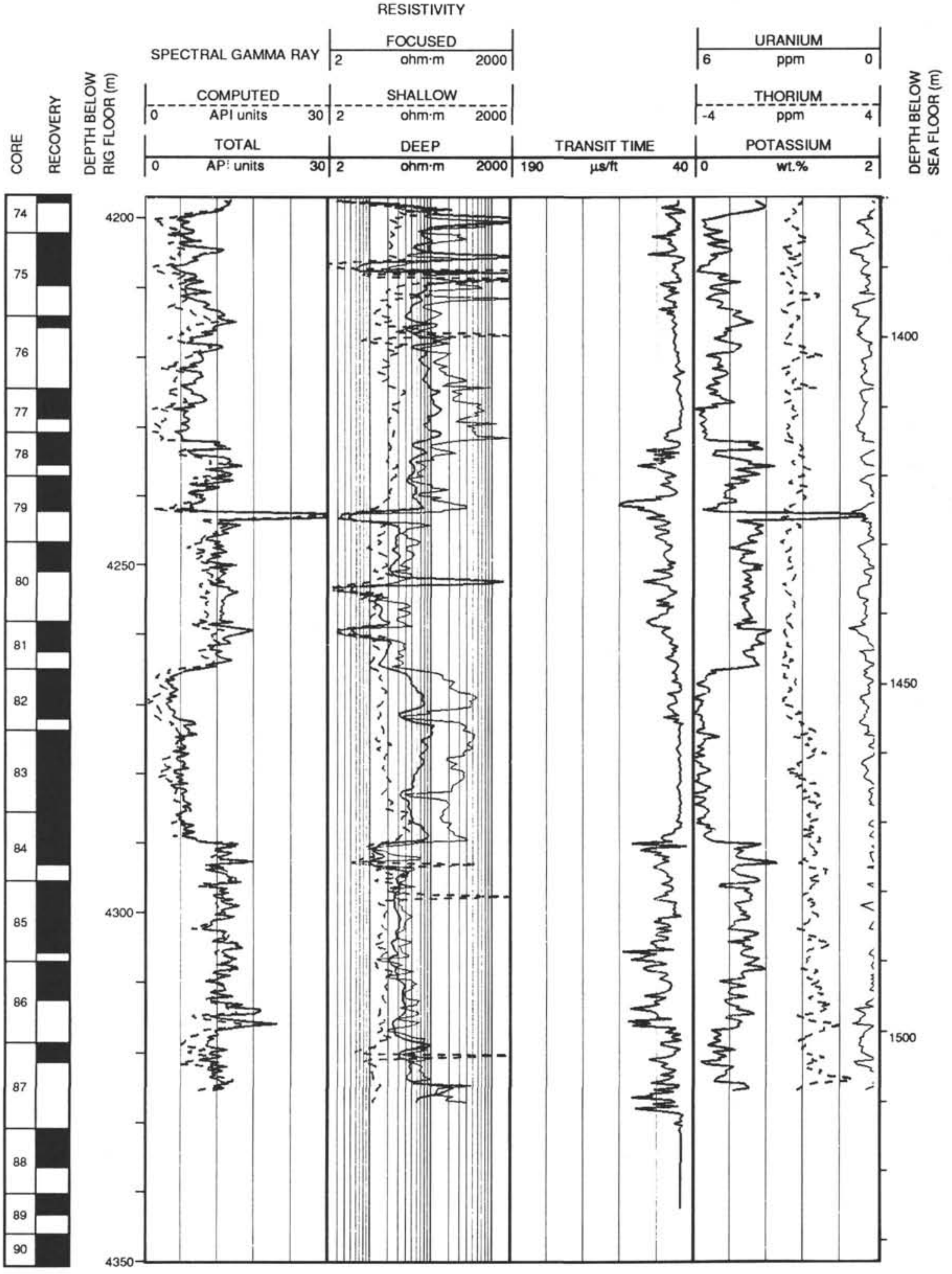

Hole 807C: Density-Gamma Ray-Aluminum Log Summary

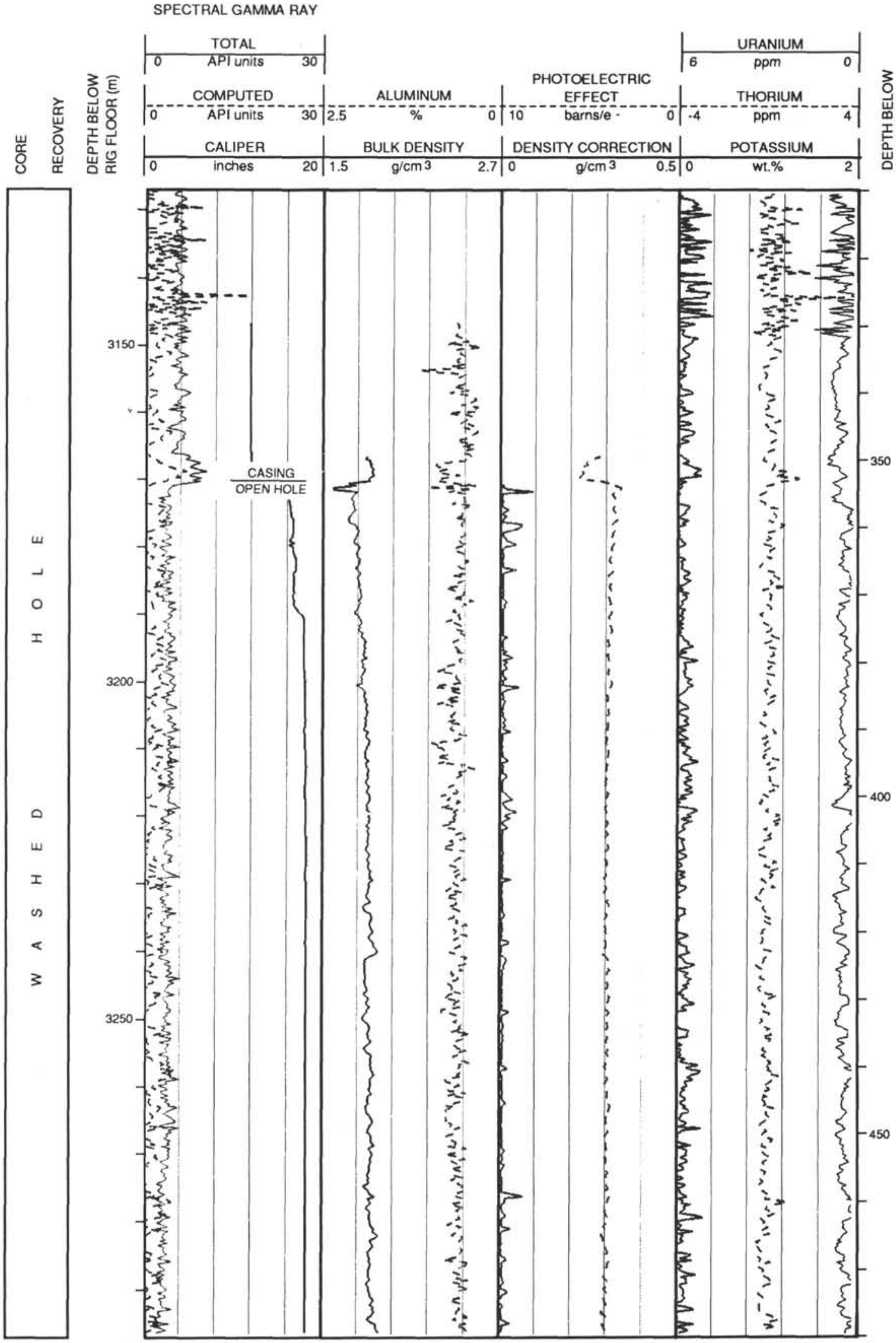

Hole 807C: Density-Gamma Ray-Aluminum Log Summary (continued)

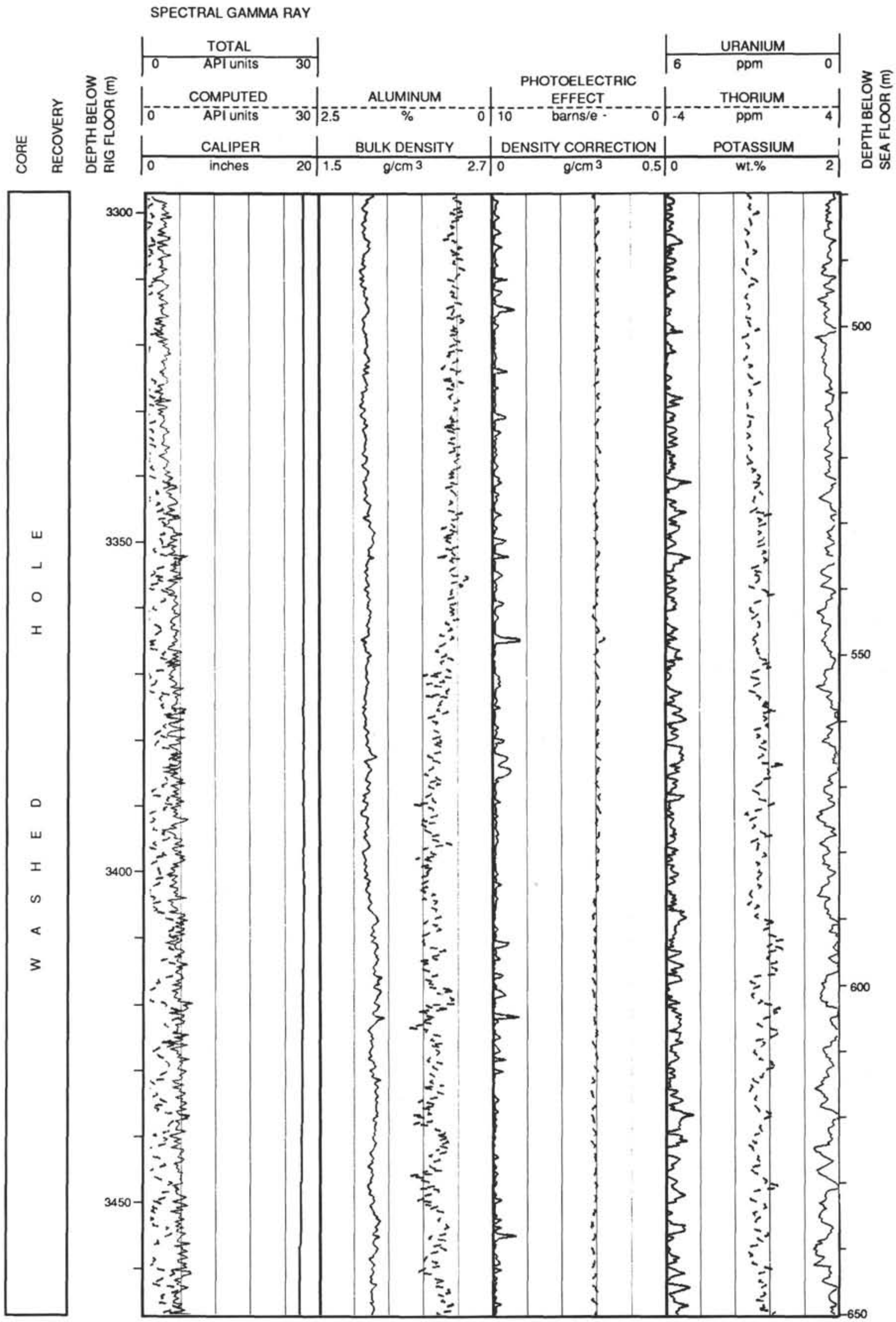

Hole 807C: Density-Gamma Ray-Aluminum Log Summary (continued)

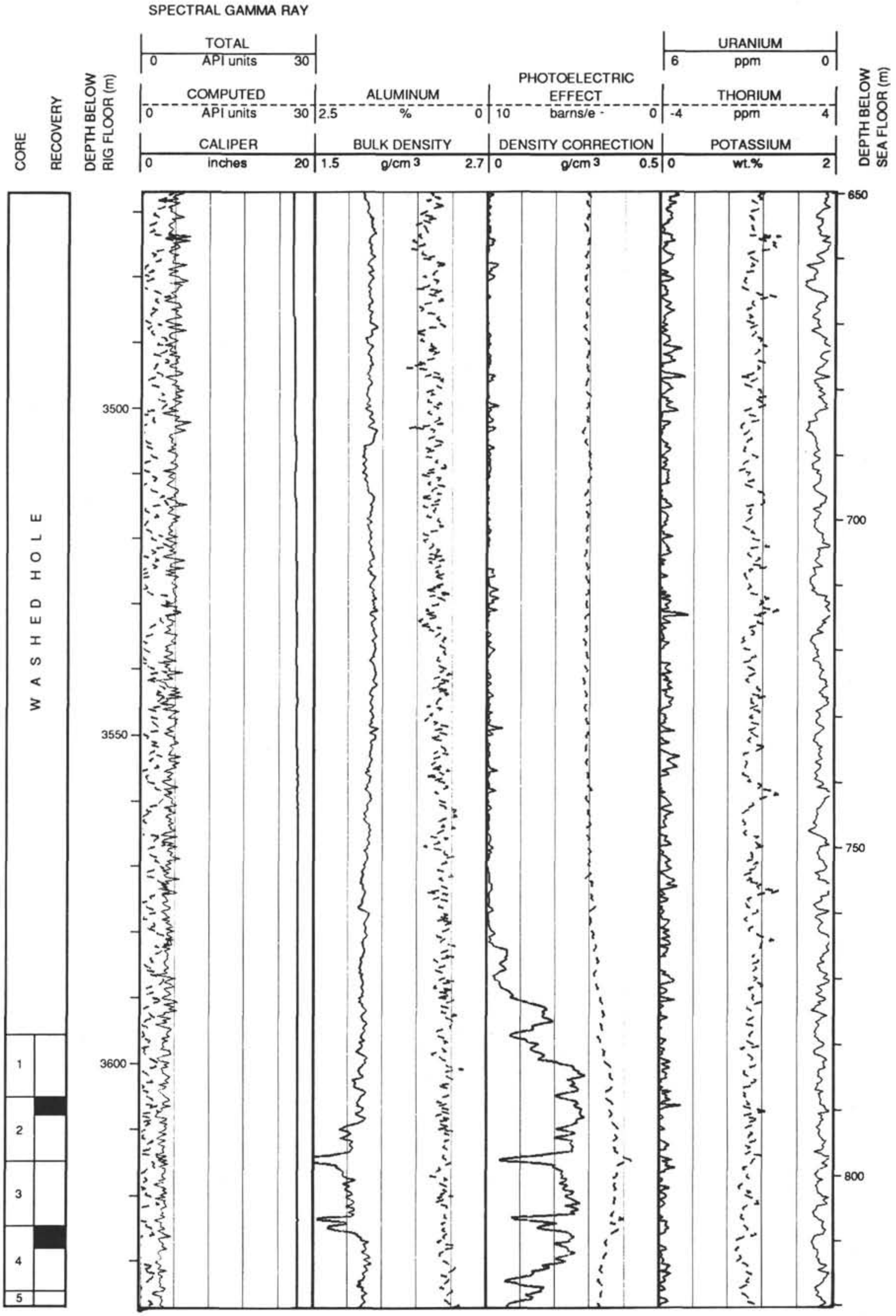

Hole 807C: Density-Gamma Ray-Aluminum Log Summary (continued)

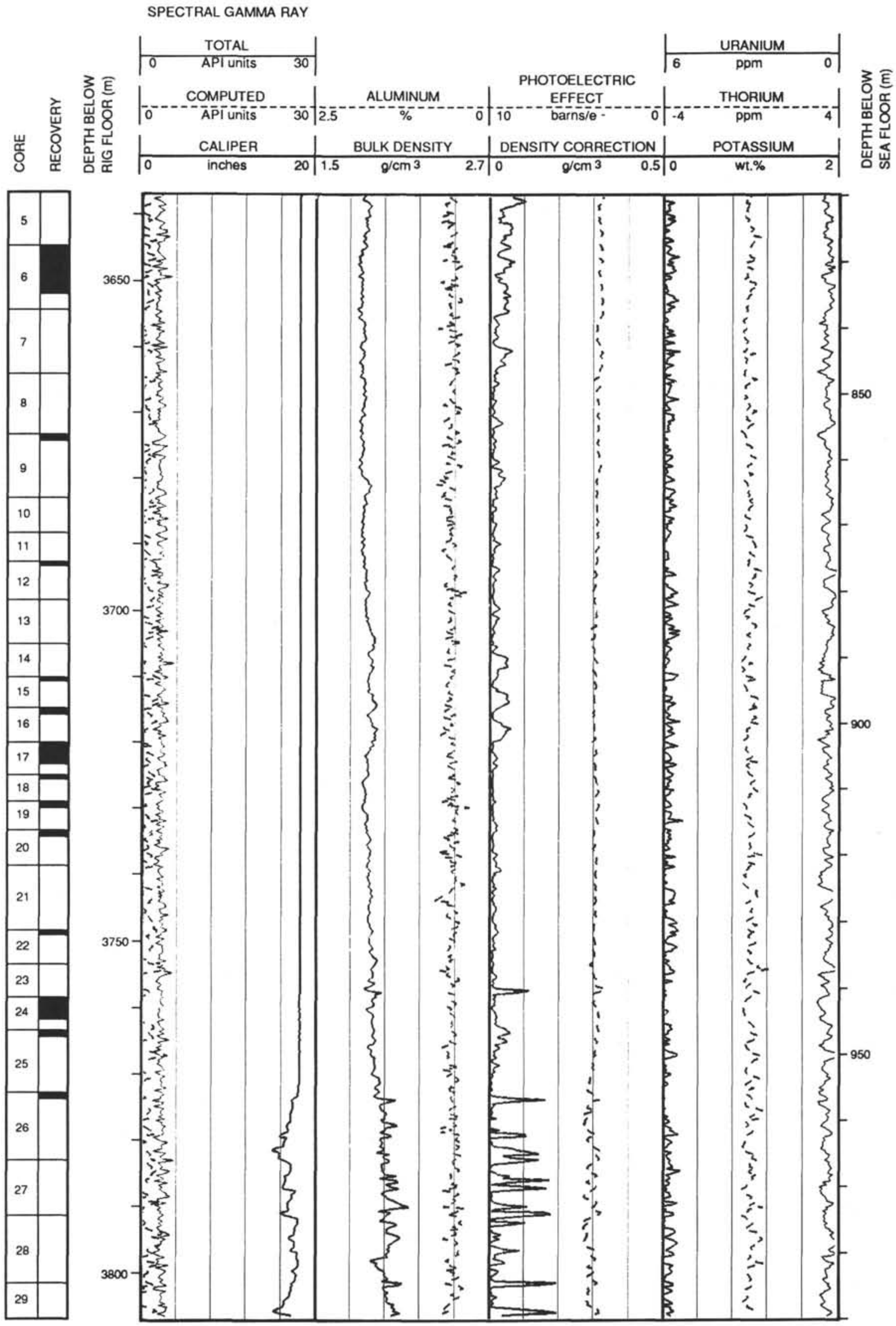

Hole 807C: Density-Gamma Ray-Aluminum Log Summary (continued)

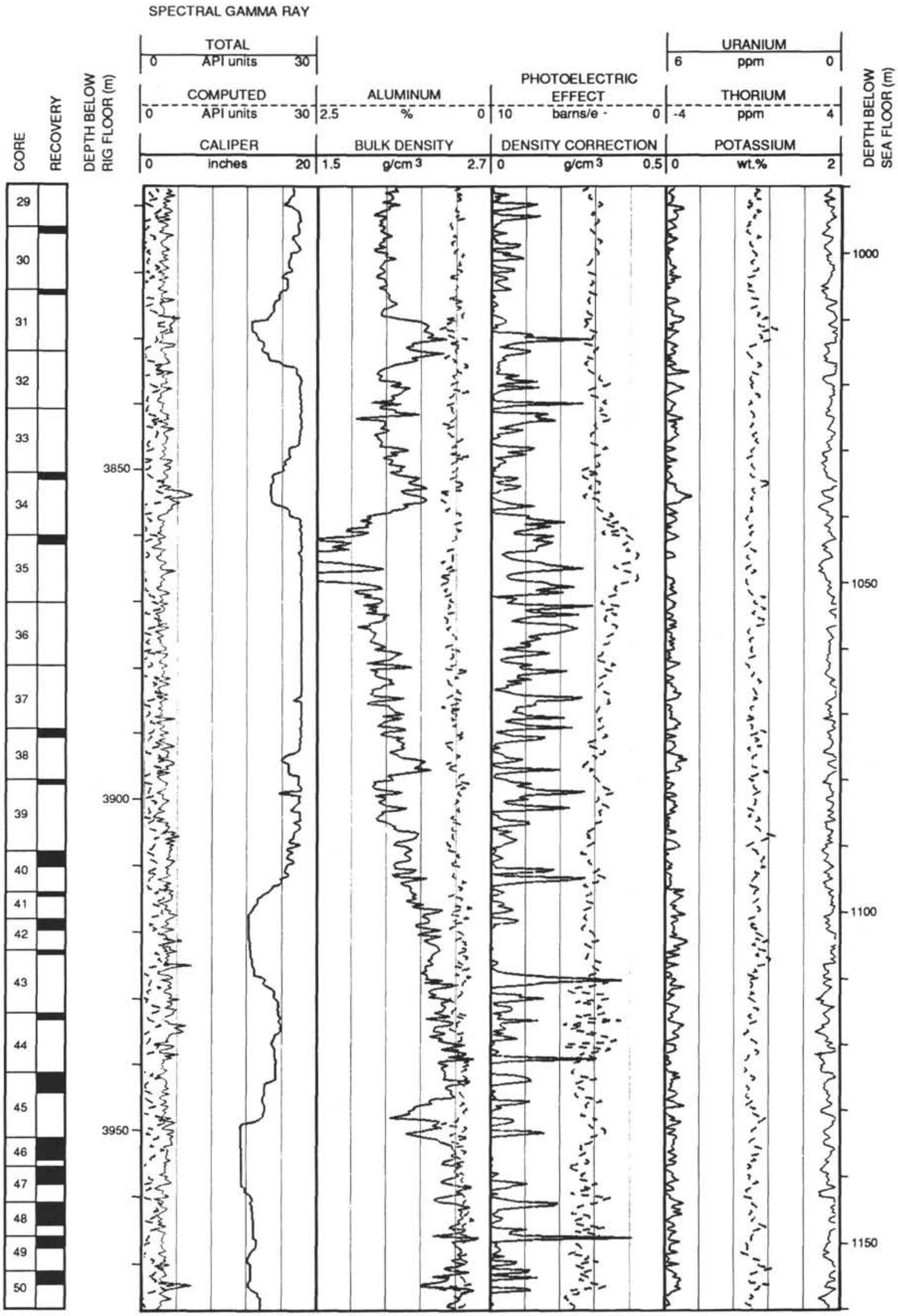

Hole 807C: Density-Gamma Ray-Aluminum Log Summary (continued)

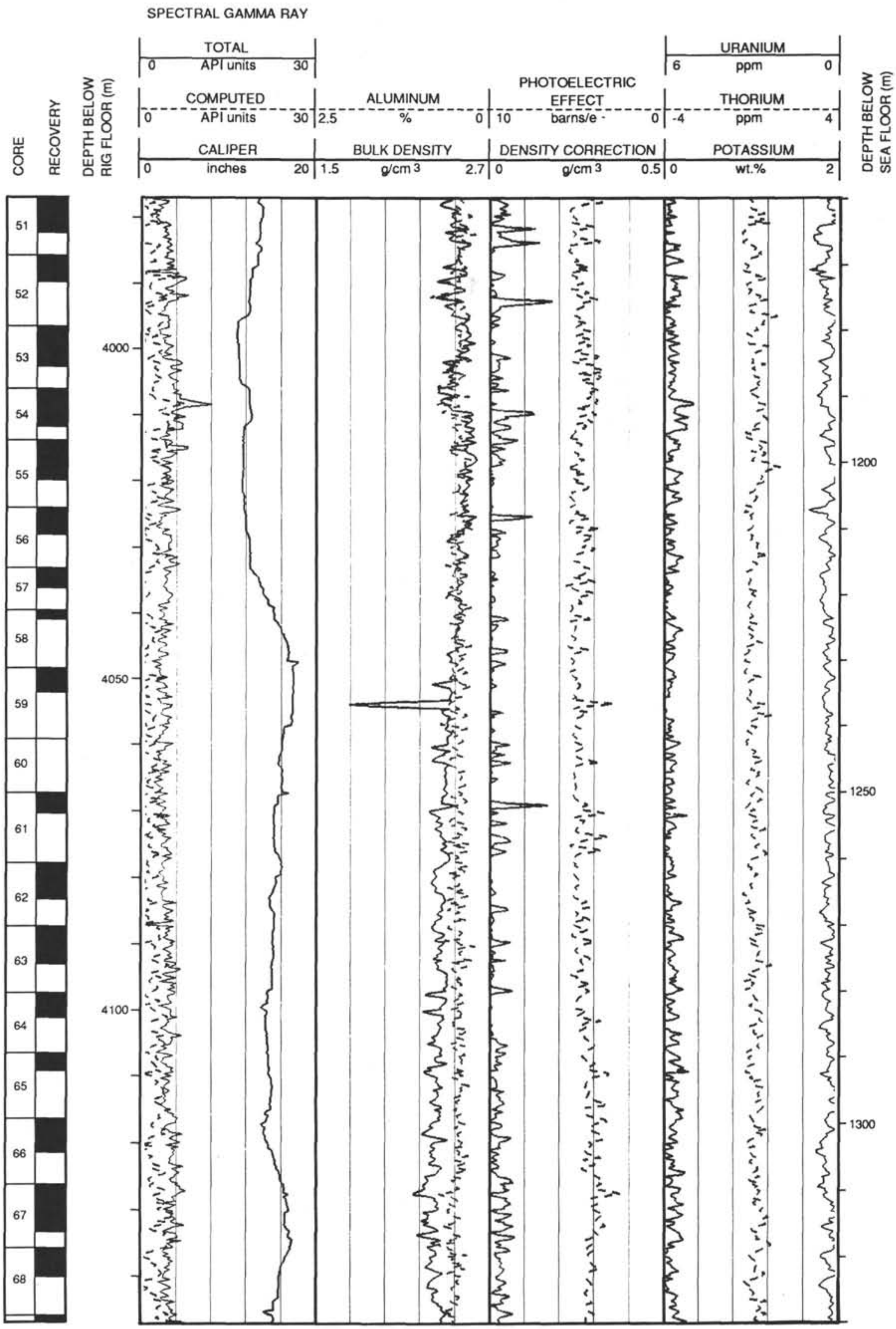

Hole 807C: Density-Gamma Ray-Aluminum Log Summary (continued)

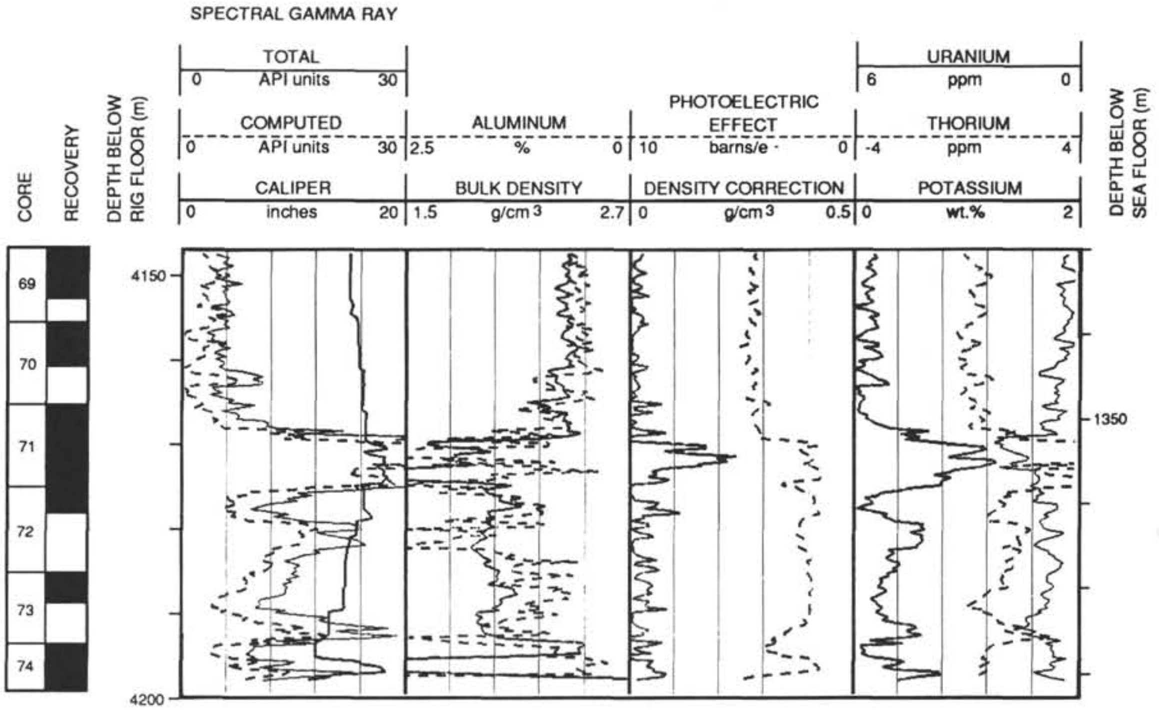

Hole 807C: Density-Gamma Ray-Aluminum Log Summary (continued)